OCS Study
BOEM 2014-669

Measurements in the Yucatan-Campeche Area in Support of the Loop Current Dynamics Study

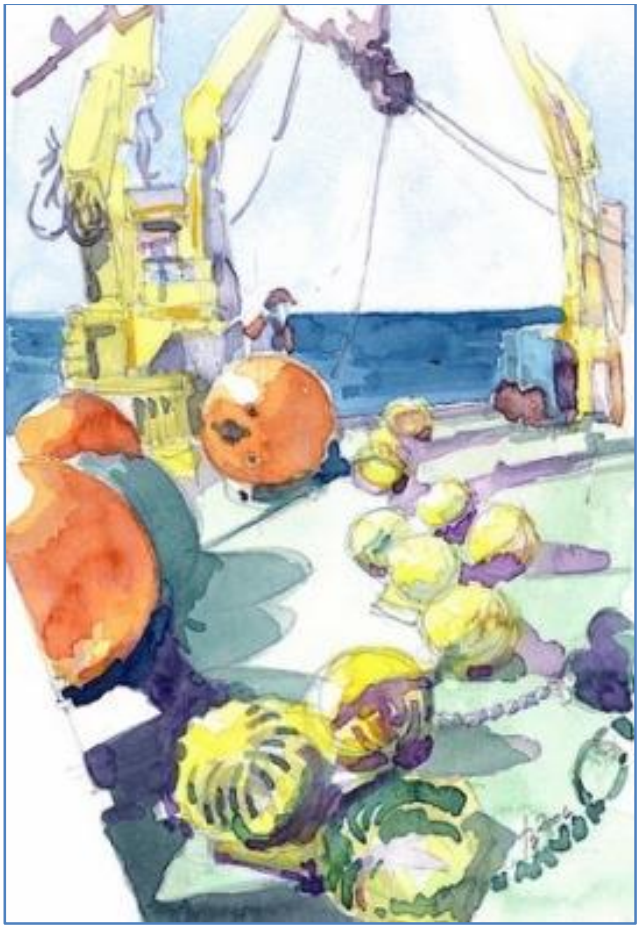

U.S. Department of the Interior
Bureau of Ocean Energy Management
Gulf of Mexico OCS Region

BOEM
Bureau of Ocean Energy Management

OCS Study
BOEM 2014-669

Measurements in the Yucatan-Campeche Area in Support of the Loop Current Dynamics Study

Authors

Gabriela Athie
Julio Sheinbaum
Angelica Romero
Jose Ochoa
Julio Candela

Prepared under BOEM Contract
M09PC00017
by
Centro de Investigación Científica
y Educación Superior de Ensenada
Ensenada, Baja California, México

Published by

U.S. Department of the Interior
Bureau of Ocean Energy Management
Gulf of Mexico OCS Region

New Orleans, LA
November 2014

DISCLAIMER

This report was prepared under contract between the Bureau of Ocean Energy Management (BOEM) and the Centro de Investigación Científica y de Educación Superior de Ensenada (CICESE). This report has been technically reviewed by BOEM, and it has been approved for publication. Approval does not necessarily signify that the contents reflect the views and policies of BOEM, nor does mention of trade names or commercial products constitute endorsement or recommendation for use.

REPORT AVAILABILITY

To download a PDF file of this Gulf of Mexico OCS Region report, go to the U.S. Department of the Interior, Bureau of Ocean Energy Management, Environmental Studies Program Information System website and search on OCS Study BOEM 2014-669.

This report can be viewed at select Federal Depository Libraries. It can also be obtained from the National Technical Information Service; the contact information is below.

U.S. Department of Commerce
National Technical Information Service
5301 Shawnee Rd.
Springfield, Virginia 22312
Phone: (703) 605-6000, 1(800)553-6847
Fax: (703) 605-6900
Website: http://www.ntis.gov/

CITATION

Athie, G., J. Sheinbaum, A. Romero, J. Candela, and J. Ochoa. 2014. Measurements in the Yucatan-Campeche area in support of the Loop Current dynamics study. U.S. Dept. of the Interior, Bureau of Ocean Energy Management, Gulf of Mexico OCS Region, New Orleans, LA. OCS Study BOEM 2014-669. 159 pp.

ABOUT THE COVER

Mooring on the deck of UNAM's R/V *Justo Sierra*. Watercolor by A. Badan. Used by permission. All rights reserved.

ACKNOWLEDGMENTS

Thanks are due to Dr. Alexis Lugo-Fernandez from BOEM and Dr. Peter Hamilton and all the people at LEIDOS, for their generous support throughout the development of the study. We would also like to thank Captain Leobardo Ríos and the crew of R/V *Justo Sierra* for their enthusiastic support at sea. This work would not have been possible without the ample participation of CICESE's technical staff and students, in particular J.I. González, A. Ledo, R. Marquez, D. Piñero, S. Paishao, C. M. Ojeda, B. Pérez, J. García, C. Flores, and administrative support by L. Zuñiga, M.F. Sánchez-Elguera, and M.T. Agüero.

CONTENTS

LIST OF FIGURES

LIST OF TABLES

ABBREVIATIONS AND ACRONYMS

ADCP	Acoustic Doppler Current Profiler
AVISO	Archiving, Validation and Interpretation of Satellite Oceanographic data
BOEM	Bureau of Ocean Energy Management
CERSAT	Centre ERS d'Archivage et de Traitement
CICESE	Centro de Investigación Científica y de Educación Superior de Ensenada
CNES	Centre National d'Etudes Spatiales, France
CRRS	Current meter (Aanderaa or Nortek Aquadopp)
CTD	(or C/T/D) Conductivity/Temperature/Depth
Duacs	Developing Use of Altimetry for Climate Studies
EEZ	Exclusive Economic Zone
EKE	Eddy Kinetic Energy
EOF	Empirical Orthogonal Function
ERS-2	Earth Resources Satellite–2
GDR	Geophysical Data Record
GEOSAT	Geodetic Satellite
GFO	Geosat Follow-On
GMT	Greenwich Mean Time or UTC
GoM	Gulf of Mexico
LC	Loop Current
LCE	Loop Current Eddy
LCFE	Loop Current Frontal Eddies
MADT	Maps of Absolute Dynamic Topography
MMS	Minerals Management Service
NDBC	National Data Buoy Center
NOAA	National Oceanic and Atmospheric Administration
PC	Principal Component
PE	Plataforma Este
PN	Plataforma Norte
PI	Principal Investigator
PIES	Inverted Echo Sounder with Pressure
STD	Standard Deviation
Ssalto	Multi-mission ground segment for altimetry, orbitography and precise localization
SSH	Sea Surface Height
SST	Sea Surface Temperature
Sv	Sverdrups (1Sv equals $10^6 m^3 s^{-1}$)
T	Temperature
WYC	Western Yucatan Channel
YC	Yucatan Channel
YCu	Yucatan Current

ABSTRACT

Three years of direct near-surface to bottom current measurements at the western Yucatan Channel (defined west of 85.6ºW) between 2008 and 2011 capture the main characteristics of the Yucatan Current. Average current structure shows a high degree of consistency over time, with mean near-surface velocities of about 1 m/s, decreasing significantly with depth. The current core position varies between 86.4ºW and 86ºW and the mean current is stronger than the variability. Below 1000m depth, current velocities are below 0.1 m/s and variations and mean flow have similar magnitude. Current velocity near the bottom increases slightly in the center of the channel, which has been shown to be related to the Loop Current dynamics. Further north, the western edge of the Loop Current was monitored with four moorings during 22 months (PE section, June 2009–April 2011); the average current there was lower than that obtained through the Yucatan Channel (0.75 m/s in its core) with variability as strong as the mean current. Five more moorings were deployed over the shelf break and slope north of the Campeche bank (PN section) between March 2008 and May 2011. Current orientation along the Yucatan slope follows the topography with an increased flow near the bottom relative to the flow aloft. This feature observed in the deepest moorings, suggests the presence of Topographic Rossby Waves.

The core of the Yucatan Current and Loop Current was observed to have a more offshore position in summer, moving back westward, toward the shore in winter-spring, suggesting a possible seasonality of the current meanders. Measurements at western Yucatan Channel and PE sections, as well as satellite data, indicate that these current meanders are associated with periods of positive horizontal shear (cyclonic vorticity anomalies) propagating northward from the Caribbean coast of Mexico into the Gulf. An important result of this work is that current meanders are related to Loop Current Eddy detachments, because four of the five Loop Current eddies released between 2008 and 2011 were found to be related to the propagation of negative anomalies of SSH along the Yucatan coast crossing the Yucatan Channel producing intense pulses of eddy kinetic energy in the Loop Current as observed at PE section.

Between May 2010 and May 2011, nine moorings were deployed to measure the whole Yucatan Channel (Yucatan to Cuba), providing relevant information about the total Yucatan transport. Total mean transport during this year was 27.1 ± 0.3 Sv, with a standard deviation of 3.6 Sv, which is 5–6 Sv higher than transport estimated by Canek Project measurements during 1999–2001. An important finding of the present work is that separating the Yucatan Channel into western and eastern sides indicates that transport anomalies at both sides of the channel are of the same order of magnitude (4–5 Sv), and show a remarkable compensation between them over time (observed also for the 1999–2001 period), despite the fact that the western side contributes 90% of the total transport (mean transport of 24.4 Sv at the western side and 2.8 Sv at the eastern side). Moreover, the seasonal cycle shows an asymmetric behavior with maxima in winter-spring and to a lesser extent in summer when only the western Yucatan Channel transport is considered. This semi-annual behavior is absent in the total Yucatan Channel transport series, which depicts a clear maximum only in summer. The wind stress curl over the Cayman Sea has higher correlation with the western Yucatan Channel transport than the total transport. However, even with the western Yucatan Channel transport there are periods when such connection is lost, suggesting that inter-annual variability and forcing at other locations can change conditions enough to break the correlation.

1. INTRODUCTION

The Loop Current (LC) is a western boundary current, which is responsible for the transport of warm waters from the Caribbean Sea into the Gulf of Mexico (GoM), and then to higher latitudes once it crosses the Straits of Florida. The Yucatan Channel (YC) is a key point in this trajectory, since it is the only passage between the Caribbean and the GoM basins. The transport through the YC is considered the principal forcing agent of the circulation in the GoM and its variability has significant implications for the dynamics within the gulf, but also for the circulation in the western Subtropical Atlantic.

The flow through the YC can be thought of as having two layers: an upper and a lower layer. The upper one is characterized by a strong jet on the western side of the channel, known as the Yucatan Current (YCu) that flows into the GoM becoming the LC and exits the GoM through the Straits of Florida over its 700m sill (Maul et al., 1985). This upper layer also includes return flows into the Caribbean: an intermittent near-surface flow close to Cuba known as the Cuban Countercurrent, and a highly variable sub-surface flow over the shallower slope on the Yucatan side. The lower layer lies below the level of the Florida sill, and net exchanges through it are found to be null (Sheinbaum et al., 2002). Lower layer flows at different levels may be related to regional processes that involve water mass transformations and the ventilation of the deep GoM (Maul et al., 1985; Bunge et al., 2002; Rivas et al., 2005; Sturges et al., 2005). These include southward counter-flows near both slopes of the channel, and a deep flow into the GoM over the Yucatan sill. The transport through the YC was measured for nearly two years with a mooring array deployed from August 1999 to June 2001 by the Canek Project. The mean transport observed during that period was 23 Sv, which is about 20% lower than the transport of 28 Sv that had been commonly accepted for this channel and by continuity as that between Cuba and Florida. Besides many other aspects, those two-year Canek measurements revealed the high variability of the currents at the YC and the necessity of continuous and long-term observations to clearly understand its behavior.

Transport and current variability through the YC has important implications downstream, affecting, in particular, the LC dynamics. A characteristic feature of the LC is the detachment of large anti-cyclonic eddies (LCEs) at irregular intervals. The separation process of these warm core eddies is very complicated and usually involves several detachments-reattachments; the reasons why the ultimate eddy release occurs remain unclear and cannot be ascribed to a unique cause. The detachment of LCEs is further described in the following subsection.

Recent studies suggest there are wind-forced seasonal fluctuations in transport at the YC and the Florida Straits (Rousset and Beal, 2011) characterized by a semiannual cycle with maximum transports in summer and winter. The latter appears to be smaller in the numerical experiments of Chang and Oey (2010). The proposed semi-annual cycle has implications for the LC eddy variability, because it is claimed that there is a higher number of eddy releases during summer and winter and less in fall and spring (Chang and Oey, 2012; 2013). These authors suggest the semiannual variations are linked to an out of phase combination of the seasonal intensification

(weakening) of the trade winds over the Caribbean (GoM), resulting in an increase (decrease) of the Yucatan transport which favors an increment (decrement) in the release of LC eddies.

To investigate the flow over the western Yucatan Channel (WYC) and Campeche Bank and its role in the LC dynamics and eddy detachment, an array of moorings was deployed at YC and two other strategic cross-sections farther north over the Campeche Bank where the Yucatan-LC is usually located. This array provides valuable information in support of the high density array of observations deployed by our colleagues from the LC Dynamics Experiment, whose main focus is over the area where LC eddy detachments usually occur. Data recovered from our array document several aspects of the YCu variability and its downstream connection with the LC. In particular, analysis of data from section PE (across the LC, see Figure 1) clarifies some aspects of the anticyclonic eddy releases and their relation to vorticity fluxes from the Northwestern Caribbean into the GoM. Additionally, the four moorings installed north of the Yucatan Peninsula straddling the shelf break and slope, and placed there with the objective to determine the origin of the observed deep southward flow at the YC, revealed other motions of interest, such as short-period velocity fluctuations within the core of the LC, associated with surface intensified Loop Current Frontal Eddies (LCFEs), a process not previously described in detail before.

The present report is organized as follows. Before ending this introduction, a discussion of models and measurements sets the background information. In section 2 we present the location of moorings along descriptions of the recorded data and time series of various data examples. In section 3 Data Analysis, we present the basic statistics of the sub-inertial currents at the WYC, and at sections PE and PN further north along the Campeche bank (see Figure 1). In section 3, also, an empirical orthogonal function analysis of the flow variability at each of the sections is described. Next, in section 4, an analysis of transport through the YC and its connection with the wind forcing and the LC extension is considered. Section 5 is dedicated to the connection between vorticity fluxes through WYC and the release of LC anti-cyclonic eddies. In section 6 we deal with 8–10 days period fluctuations linked to LCFEs and their connection with coastally trapped waves over the GoM. The last section presents the conclusions. A series of appendices include tables and figures of mooring design and mooring statistics.

1.1 BACKGROUND

Transport through the YC, together with the flow from Old Bahama and Northwest Providence Channels, compose the Florida Straits transport at 27°N between Miami and Bimini. This flow has been monitored regularly for more than 40 years (Meinen et al, 2010). By contrast, the YC has been measured less frequently and many questions remain unanswered about the strength and low frequency variability of the flow through this channel. Florida transport estimates from a submarine cable, calibrated by direct current measurements, give a mean and standard deviation of 30.8 Sv ± 3.2 Sv (Larsen, 1992; Baringer and Larsen, 2001); this is about 30% higher than the 23.0 ± 3.2 Sv reported from two years of moored measurements at the YC between 1999 and 2001 by the Canek Project [Sheinbaum et al., 2002; Ochoa et al., 2003]. This last value is also ~20% lower than the 28 Sv estimated for this channel from: i) hydrographic data (Gordon, 1967; Roemmich, 1981), ii) calculations based on the basin-scale mass balance

(Johns et al., 2002), and iii) from the difference between transport measured at Florida and the Old Bahama and Northwest Providence channels (Atkinson et al., 1995; Leaman et al., 1995). These estimates, however, are based on other assumptions than continuous mooring data, such as horizontal levels of no motion or specified transports through other channels (e.g., Windward Passage).

Recent measurements in the YC area and the Florida Straits (between 2001 and 2006) from shipboard ADCP (Rousset and Beal, 2010; 2011, see also Johns et al., 2002), suggest similar transports of about 30 Sv in both passages and a semiannual cycle not detected in the continuous mooring data from Canek (Abascal et al., 2003; Ochoa et al., 2003). These recent measurements, however, eliminate tides using a global tidal model and, although they include several samples, they are not continuous and depend on single ship crossings. The cross-section area of these channels is substantial, making it difficult to estimate transport errors induced by an improper filtering of the tidal signal even if it is of 2–3 cm/sec. The ship-adcp measurements suggest a small contribution (~3 Sv) from Old Bahama and Northwest Providence Channel, but do not agree with recent lower transport estimates for other Caribbean passages (Rousset and Beal, 2011). The complex variability at the YC needs continuous long-term measurements to really grasp the dominant processes at work.

The variability of the flow through the YC is connected with variability downstream of the LC and also the Florida Current. Observations and model studies indicate that shedding events of LCEs are related to transport fluctuations in the YC (Hurlburt and Thompson, 1980; Oey, 1996; Oey et al., 2003; Ezer et al., 2003). However, mechanisms and processes have been proposed to influence ring separation: momentum imbalance (Pichevin and Nof 1997), barotropic and baroclinic instability of the LC (Hulburt 1982; Cherubin et al. 2006), pulses of increased transport through the Florida Straits (Sturges et al. 2010), seasonal modulation by the local wind stress (Chang and Oey 2012), advection of cyclonic vorticity from the Cayman Basin (Candela et al., 2002; Athie et al. 2012), interaction with cyclonic eddies generated locally or LCFEs (Fratantoni et al. 1998; Zavala-Hidalgo et al. 2003; Cherubin et al. 2006; Le Hénnaf et al. 2012; Schmitz, 2005; Leben, 2005), or even remote wind forcing from the Atlantic Ocean (Oey et al., 2003; Chang and Oey, 2010).

Based on numerical modeling, Ezer et al. (2003) show that variability of YCu meanders is related to LC behavior, because the LCE-shedding occurs when the YCu core shifts to the east. However, the number of events in the model was insufficient to conclude a connection between the upstream position of the YCu core and the LCE shedding. Mooring data suggests that potential vorticity fluxes through the YC into the GoM are related to the extension and retraction of the LC, favoring the release of LCE (Candela et al., 2002). However, there is no agreement even on the sign the vorticity anomalies that produce the extension-retreat of the LC (Oey et al., 2003, Cherubin et al. 2006, Candela et al., 2002). Recent work suggests that another factor that can modulate the irregular interval of LC detachments is the fluctuations in transport and vorticity of the YCu, induced by changes in the local wind forcing (Chang and Oey, 2013). Other possible sources of variability are eddies from the Caribbean. Cyclones from the Caribbean may leak through the YC as cyclonic vorticity anomalies and once they pass beyond the Channel's topographic constraint, they can intensify on the Campeche Bank (Schmitz, 2005: its appendix; Athie et al., 2012) and lead to LCE detachment.

The idea that perturbations in the vicinity of the LC can produce LCE-shedding is related to cyclonic eddies along the edge of the LC and/or instability process (e.g., Cochrane, 1969; Fratantoni et al., 1998; Zavala-Hidalgo et al., 2003; Schmitz, 2005). These cyclones, known as LCFEs, have diameters of 50~ 150 km, swirl speeds of 0.30–0.50 ms^{-1} and are generated or grow on both sides of the LC, near 86.5°W and 23.5°N on the Campeche Bank side (Zavala-Hidalgo et al., 2003; Oey et al., 2005) and on the eastern boundary of the LC, at the Tortugas Bank (Fratantoni et al., 1998). LCFE have been observed, either translating from Yucatan towards Florida (Cochrane, 1972; Hurlburt, 1986; Zavala-Hidalgo et al., 2003), from Florida towards Yucatan (Fratantoni et al., 1998), or from both sides at once (Schmitz, 2005), traveling at 15 km/day (Vukovich et al., 1979; Hurlburt, 1986), as a common feature associated with the LCE detachment process.

The model study by Cherubin et al. (2006) provides some evidence in favor of a mixed barotropic-baroclinic instability process as the cause for the formation of LCFEs, pointing out the key role of the cyclonic vorticity belt around the LC in the instability. From infrared images, Vukovich (1988) showed that cyclonic perturbations are intensified on the northwestern sector of the LC. Using a high resolution numerical simulation, Le Hénaf et al. (2012) explained this intensification by a topographic effect: when the LC nears the northeastern Campeche slope, the cyclones aggregate positive potential vorticity anomalies in lower layers which intensify the whole vortex structure.

Zavala-Hidalgo et al. (2003) using along-track altimetry, as well as Le Hénaf et al. (2012) from a high resolution numerical simulation, pointed out the formation of LCFEs on the western side of the LC along the Campeche Bank before a LCE detachment, but do not provide an explanation of the mechanisms involved in the formation of such LCFEs. Some of the issues mentioned above will be addressed in three chapters of the present report: Transport variability at the YC and its seasonality related to wind forcing; the connection between the YCu meandering and LCE releases between 2009 and 2011; and finally, the description of small LCFEs occurring near the Campeche Bank and possible factors controlling their formation and characteristics.

2. DEPLOYMENT SETTING AND DATA CHARACTERISTICS

Three sections of mooring arrays were deployed, nearly perpendicular, to the western edge of YCu and LC flows. A set of 7 moorings were deployed at WYC (Figure 1), designed to adequately sample the distribution of currents from the near-surface to the bottom at each of their locations (Figure 2) YUC2 was deployed around 50 m depth, YUC3 at 100 m, and YUC4 at 500 m. These moorings consisted of Acoustic Doppler Current Profilers (ADCPs) looking toward the surface, 300 KHz ADCPs for YUC2 and YUC3, and a 75 kHz ADCP for YUC4. YUC5, YUC6, and YUC7 were installed at 1200 m, 1800 m and 2020 m, respectively and each had one 75 KHz ADCP deployed around 500 m depth measuring from this depth up to 30–60 m near the surface. YUC6 also had two 300 kHz ADCPs, one at 500 m measuring between this depth and 600 m and the other profiling between 650 m and 750 m depth. Finally, mooring YUC7 additionally had a 300 kHz ADCP sampling downward at 500 m depth. Below 700–750 m down to the bottom, current measurements were taken by 5 or 6 either Aanderaa RCM11 or Nortek Aquadopp current meters, with the deepest instrument measuring at 10 m off the bottom, as shown in Figure 2. The deployment at the YC lasted for over 24 months between June 2009 and May 2011 with a one month gap due to service and redeployment of the moorings (Figure 4 and Table 1 and Table 2). Additional 14-months of data at the YC between March 2008 and May 2009 were also used to complement the transport analysis in Chapter 4.

The LC enters the Gulf of Mexico through the YC with a northeastern predominant direction and then turns slightly to the west, hugging the slope and shelf break of the Yucatan Peninsula. Two mooring sections to the north of YC crossing from the shelf break to depths between 2000–3500 m were deployed on the Campeche bank: section PE ("Plataforma Este" ["Eastern shelf" in Spanish]), consisting of five moorings and section PN ("Platforma Norte" ["Northern shelf" in Spanish]) with four moorings (Figure 3). The slope here is about 150 km wide, with irregular topography joining the slope to the abyss at 3500 m depth (Figure 3). Moorings were designed to efficiently monitor the currents throughout the water column, with 75 kHz ADCPs looking up from 450 m depth in the deep (> 500m) moorings and 300 kHz ADCPs at 100 m depth for the shallow moorings PE1 and PN1. Currents in the surface layer were recorded with 16 m depth bins on the 75kHz ADCPs and 8 m bins on the 300 kHz ADCPs. A second 75 kHz ADCP at 1000 m depth was installed on moorings PE4, PE5 and PN4 recording in the same fashion sampling between 1000 m and about 550 m depth. Intermediate depths not sampled by the ADCPs were monitored with Aanderaa RCM11 or Nortek Aquadopp current meters at intervals of 300 m to 500 m, with the last device recording currents from 10 m off the bottom, as shown in Figure 3. The deployment at sections PE and PN lasted over 22 months, from June 2009 to April 2011. There was previous data collected at section PN, starting on March 2008; therefore, this section has observations for 36 months like the Yucatan section.

In the three sections most of the instruments worked as expected except for some mishaps which consisted in battery failure before recovery on the ADCP deployed at 740 m for YUC6 and the ADCP deployed at 472 m for PE4 (Figure 4). Important failures that lasted almost the entire first period of measurements were the current-meters at 1155 m depth on mooring YUC7, and the top ADCPs of moorings PN4 and PE1. During the second period, it was the ADCP at YUC4 that failed. These instruments, factory delivered before deployment, had problems related

to faulty seals around the transducer heads that lead to partial water leakages into the instruments' electronics shortly after deployment, with the consequence of complete data loss. There were also problems with the firmware which caused some instruments to stop recording.

Objective mapping of the velocity data (sections 4.1 and 5) was carried out considering all functional instruments at each time-step including those with short time series. Tests to check the impact of missing data in the mapped fields showed no significant difference whether those data were included or not. 65% of the pressure sensors worked correctly. Most of the moorings had small vertical excursions (10–20 m), with a maximum down-draft of 90 m. Similarly, 85% of the temperature sensors deployed during the two periods operated adequately.

Table 1. Location and deployment depth of the 16 moorings between July 2009 and March 2010 (Canek 20).

Mooring	Longitude W(°)	Latitude N (°)	Depth (m)
YUCN	86.34	21.69	488
YUC2	86.49	21.54	58
YUC3	86.45	21.57	112
YUC4	86.36	21.57	485
YUC5	86.23	21.60	1189
YUC6	85.99	21.65	1870
YUC7	85.73	21.65	2018
PE1	87.01	22.38	118
PE2	86.64	22.84	490
PE3	86.43	23.06	989
PE4	86.29	23.25	1983
PE5	86.03	23.61	3342
PEN	86.79	23.07	496
PN1	87.92	23.76	118
PN2	87.58	24.21	490
PN3	87.42	24.40	1195
PN4	87.12	24.96	3352

Table 2. Location and deployment depth of the 16 moorings between May 2010 and May 2011 (Canek 23).

Mooring	Longitude W(°)	Latitude N (°)	Depth (m)
YUC2	86.49	21.54	58
YUC3	86.45	21.57	112
YUC5	86.23	21.60	1189
YUC6	85.99	21.65	1870
YUC7	85.73	21.65	2018
PE1	87.01	22.38	118
PE2	86.64	22.84	490
PE3	86.43	23.06	989
PE4	86.43	23.06	1983
PE5	86.03	23.61	3342
PEN	86.79	23.07	496
PN1	87.92	23.76	118
PN2	87.58	24.21	490
PN3	87.42	24.40	1195
PN4	87.12	24.96	3352

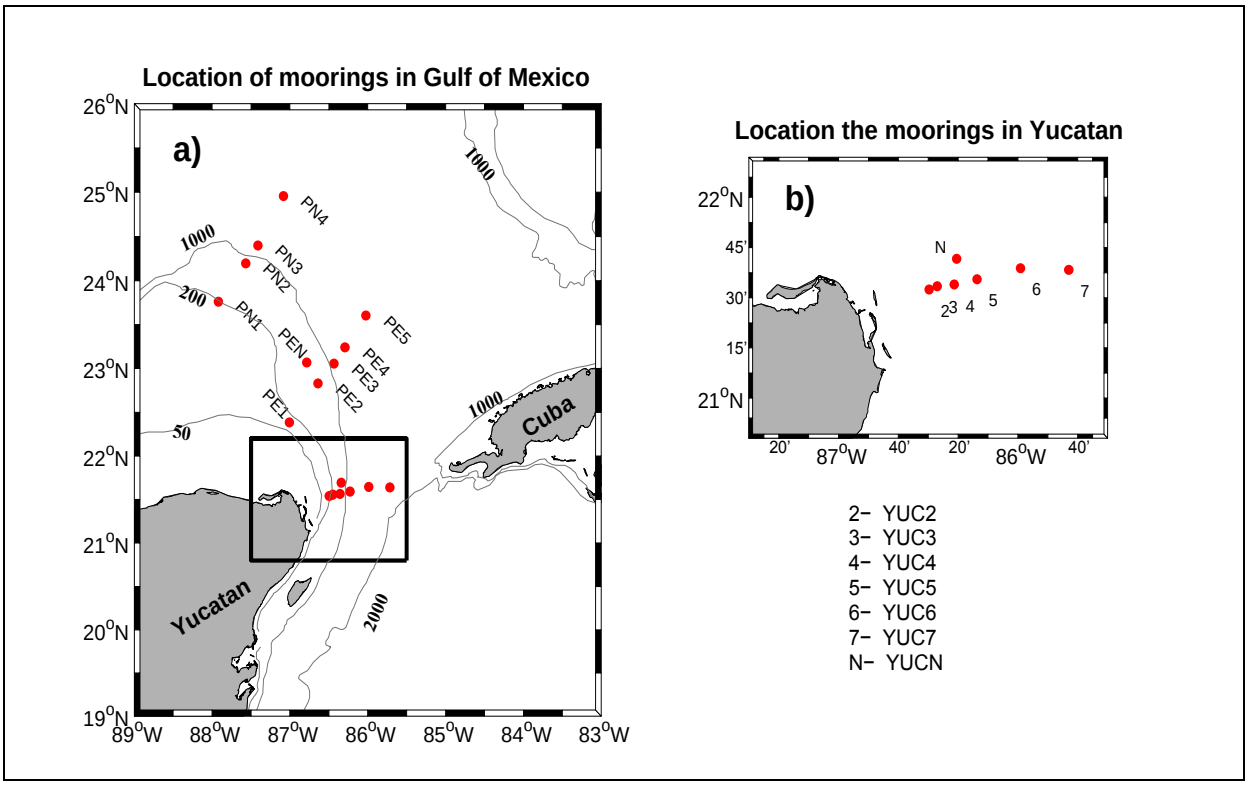

Figure 1. (a) Location and labels of the Canek moorings along the Yucatan Peninsula. The rectangle in (a) marks the area shown in (b) for moorings over YC. Depth contours are in meters.

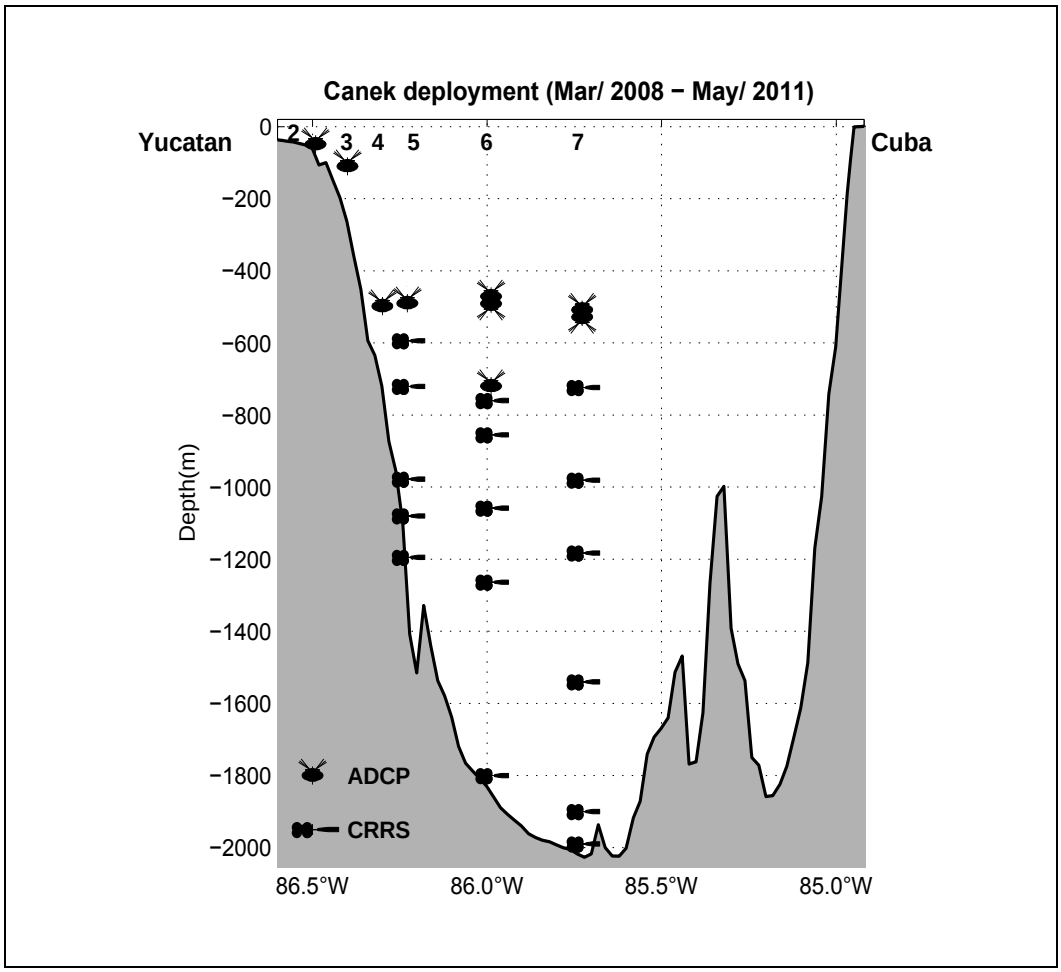

Figure 2. Vertical distribution of instruments on the moorings deployed at YC between March 2008 and May 2011.

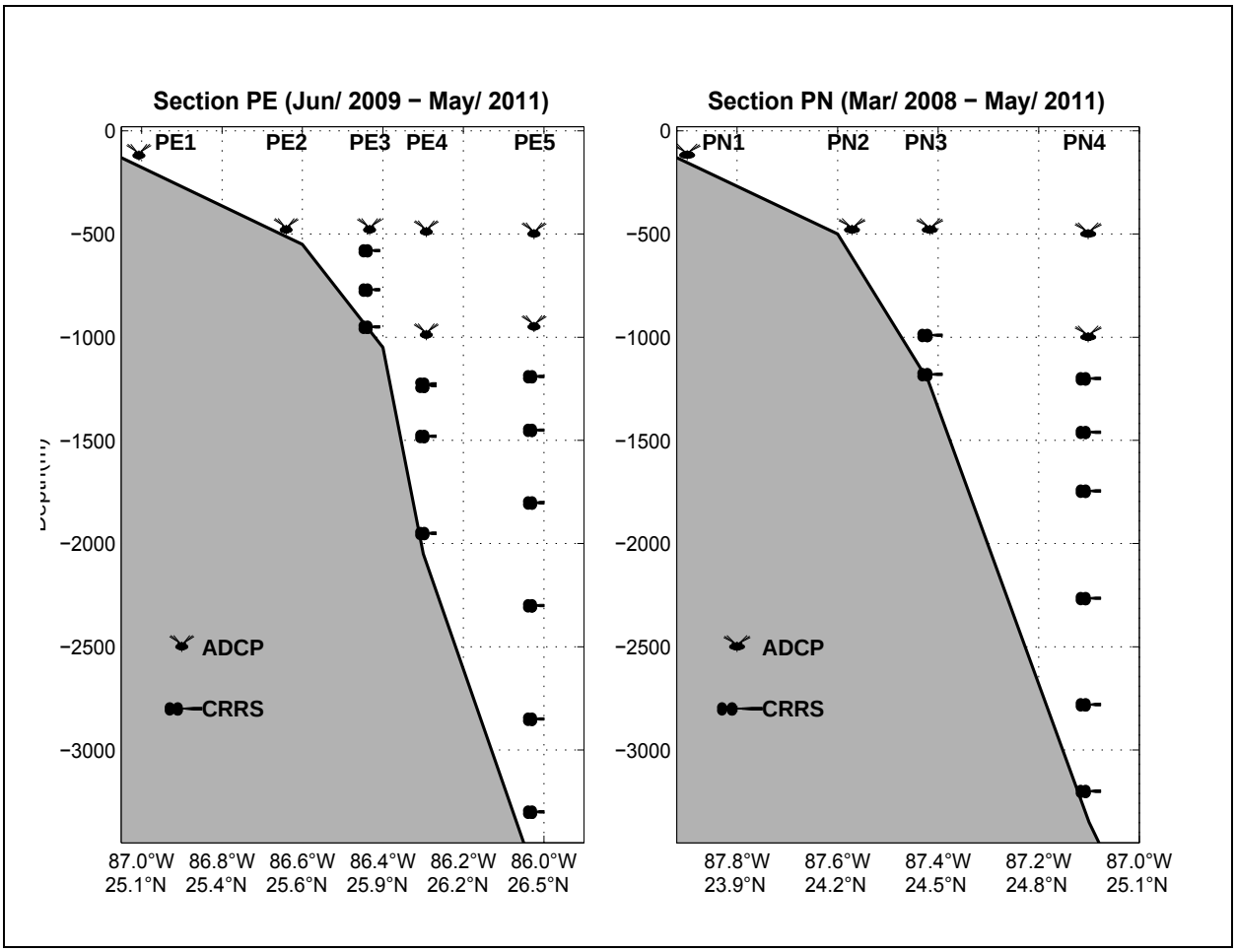

Figure 3. Vertical distribution of instruments over the PE and PN sections.

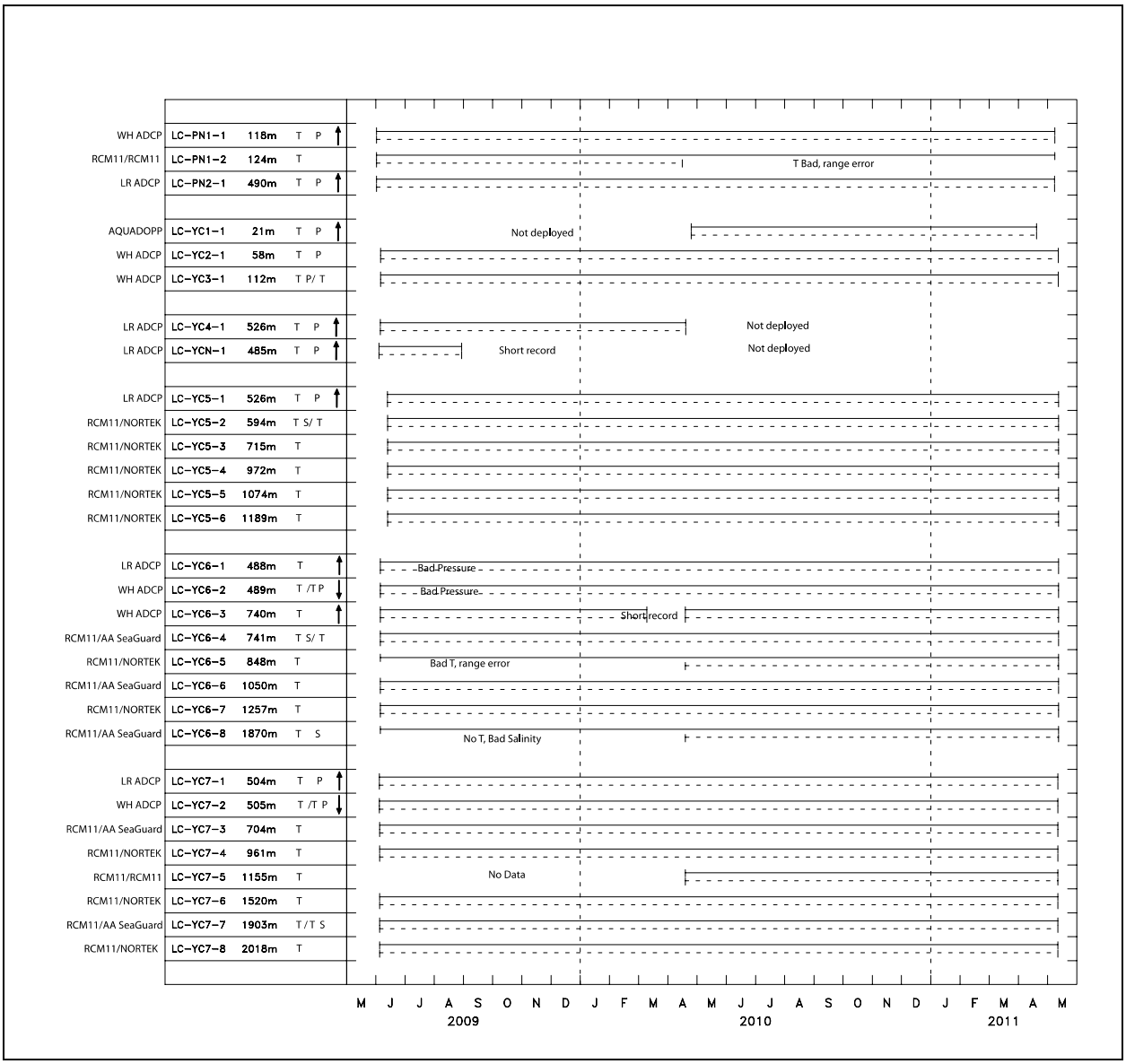

Figure 4. Data record history for the instruments in each mooring.

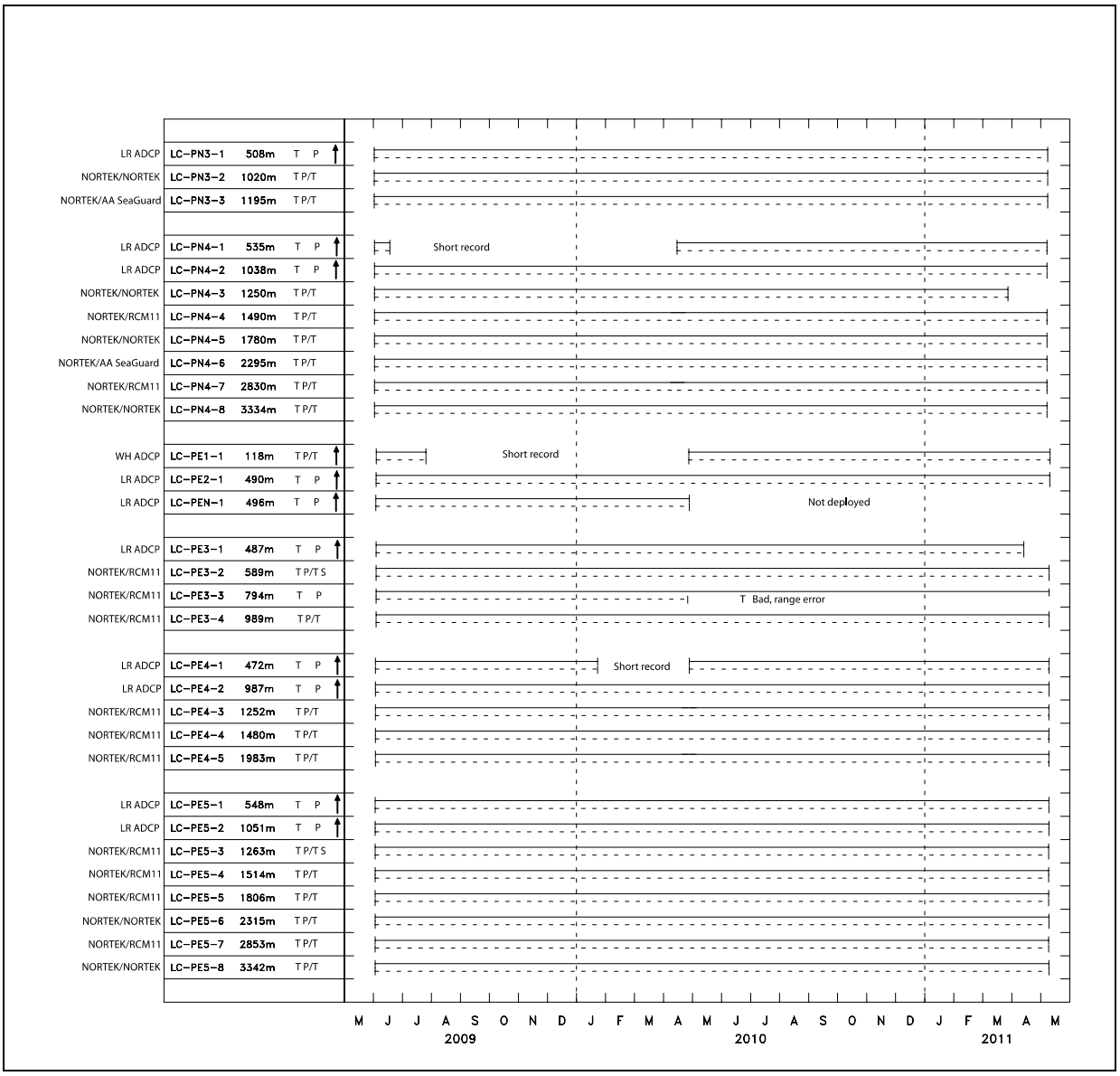

Figure 4. Data record history for the instruments in each mooring (continued).

In what follows, we present some examples of time-series from the different mooring sections. The raw data was filtered and processed independently by both CICESE and Leidos research teams. As a consistency check, we show that both processing methods produce very similar results, so either processed data can be used for the analysis.

Figure 5 shows a comparison between data processed by CICESE and Leidos from a single ADCP instrument for each of the mooring sections. Data were processed slightly differently (applied filters to suppress noise or to obtain de-tided low frequency time-series are different, filling of data gaps is done by Leidos). Panels in Figure 5 show either the component of the horizontal velocity along the section (u), which is eastward to northeastward or perpendicular to

the section (*v*), which is northward to northwestward. Both data series show very similar results. For example, on YC (Figure 5), the ADCP located at 100m depth on mooring YUC3, shows more energy in the *v*-component, which is expected due to the presence of the YCu, with some high-frequency variability (~one week), particularly intense in the winter season. There are four events of high energy in both velocity components in May, September, and December 2010, as well as in February 2011, which are clearly represented by the two processed versions.

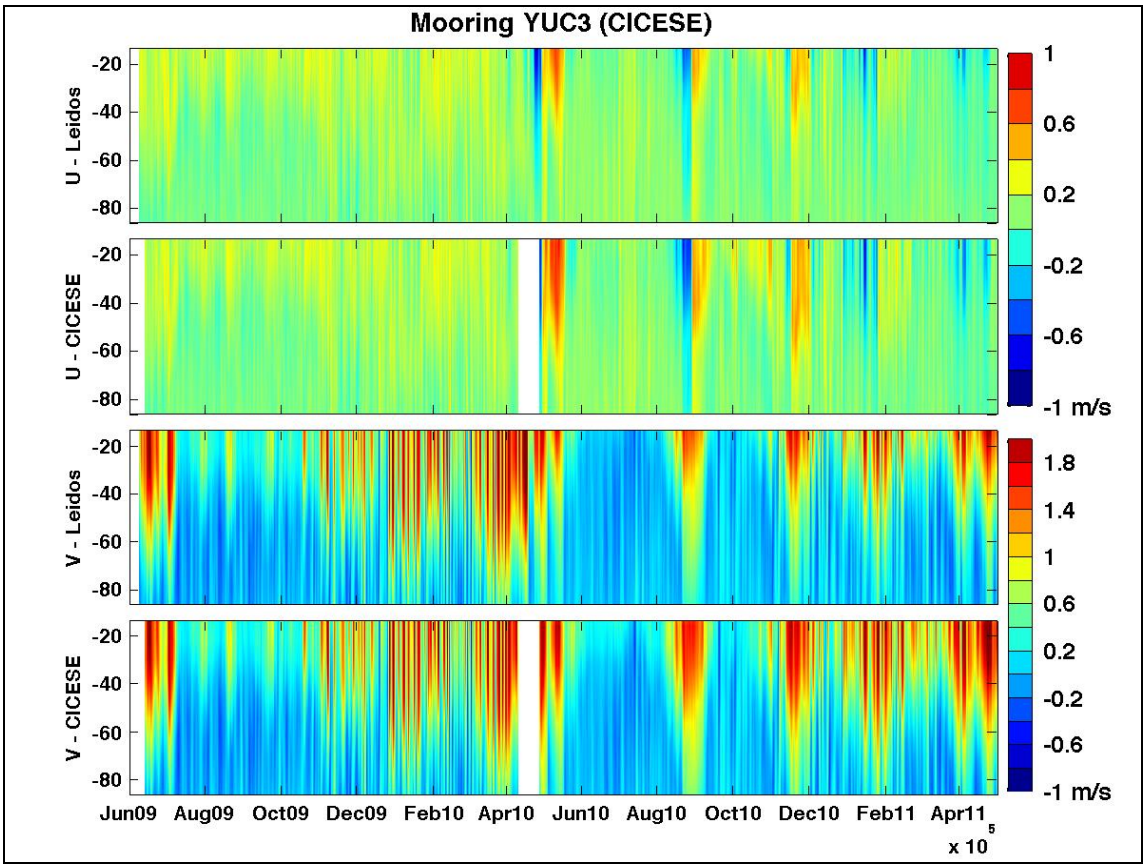

Figure 5. Time-depth diagrams from ADCP instruments located on YUC3. The plots compare the zonal (top two panels) and meridional (two lower panels) components of the velocity (in m/s) using Leidos-processed data (first and third panels) and CICESE-processed data (second and fourth panels). Leidos processing fills the data gaps using an in-house method and CICESE leaves gaps intact. Filters are slightly different in their frequency transfer function.

Velocity variations on section PE (Figure 1) are shown considering *u* and *v* components of an instrument located on mooring PE3 at 500 m (Figure 6). As previously stated, the *v* series is of the velocity component perpendicular to the section and its maxima (positive) at PE can be interpreted as periods when the LC core is detected by the ADCP (northwest current direction) whereas negative values indicate presence of a cyclone and/or absence of the LC core (southeast current direction). This variability will be discussed in more detail in chapter 5. Current at section PN is mostly in the southeast direction, but some events are detected where current intensifies in the Northwest direction (see Figure 1 for moorings alignment and panels of Figure 7 with PN1 data); during August–September 2009, June 2010 and September–November 2010.

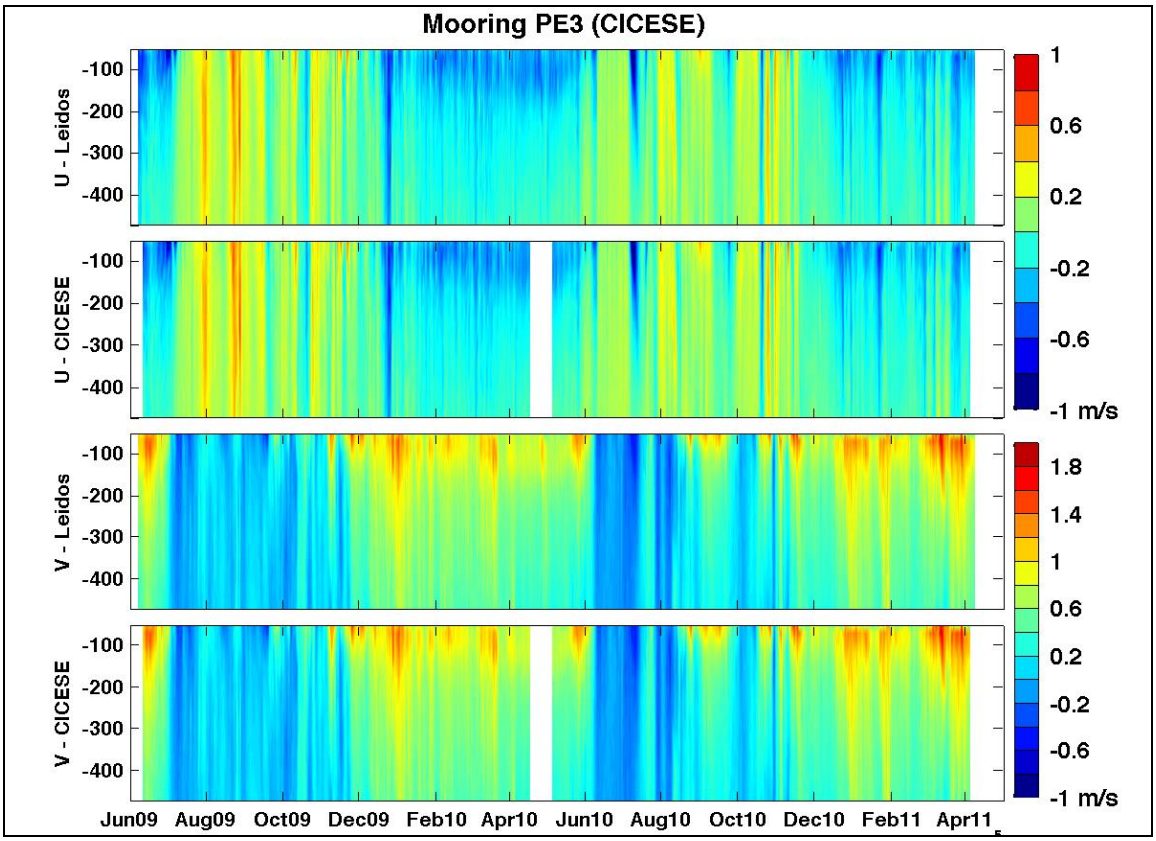

Figure 6. As in Figure 5, for ADCP instrument at 500 m depth on mooring PE3.

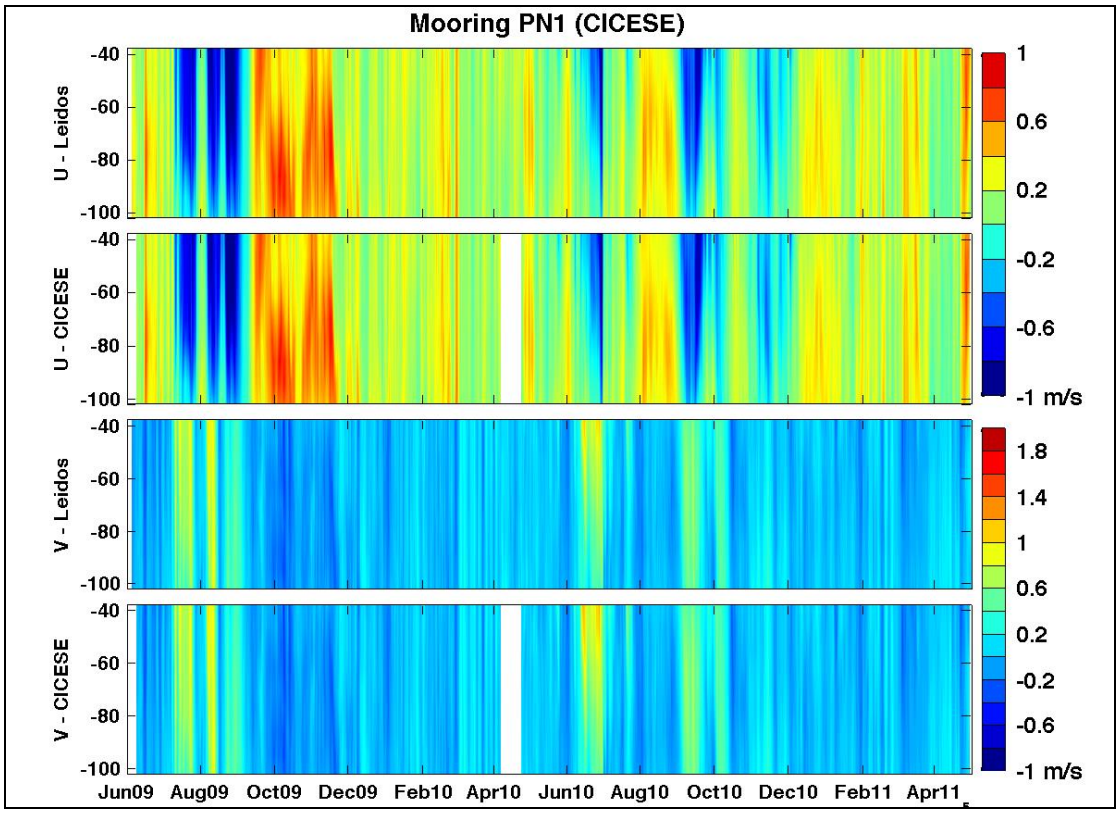

Figure 7. As in Figure 5, for ADCP instrument at 100 m depth on mooring PN1.

Data processed by CICESE and Leidos are also in good agreement for the two velocity components at the deepest current meter of each section. For YUC7 at 2018 m (Figure 8), the standard deviation of *v* is around 10 cm/s and a maximum value of 36 cm/s. The *u*-component at this depth has a maximum of 16 cm/s with standard deviation of 4 cm/s and the difference between the two versions does not exceed 3 cm/s. For PE5 at 3342 m depth (Figure 9), the difference between datasets is also smaller than 3 cm/s, while the standard deviation is ~6 cm/s for both components. For PN4 at 3334 m (Figure 10) the difference between the two datasets is slightly higher, exceeding several times 5 cm/s. Intense pulses are observed in the *v*-component at PN4, reaching 20 cm/s, while the standard deviation is 7 cm/s. The high differences between both versions occur when the intense pulses are present. The maximum intensity of the *u*-component at this depth is 35 cm/s with standard deviation of 11 cm/s. During April 2010, the moorings were not deployed due to maintenance and rotation of the equipment. The Leidos-processed version interpolates this gap, while CICESE-processed data does not.

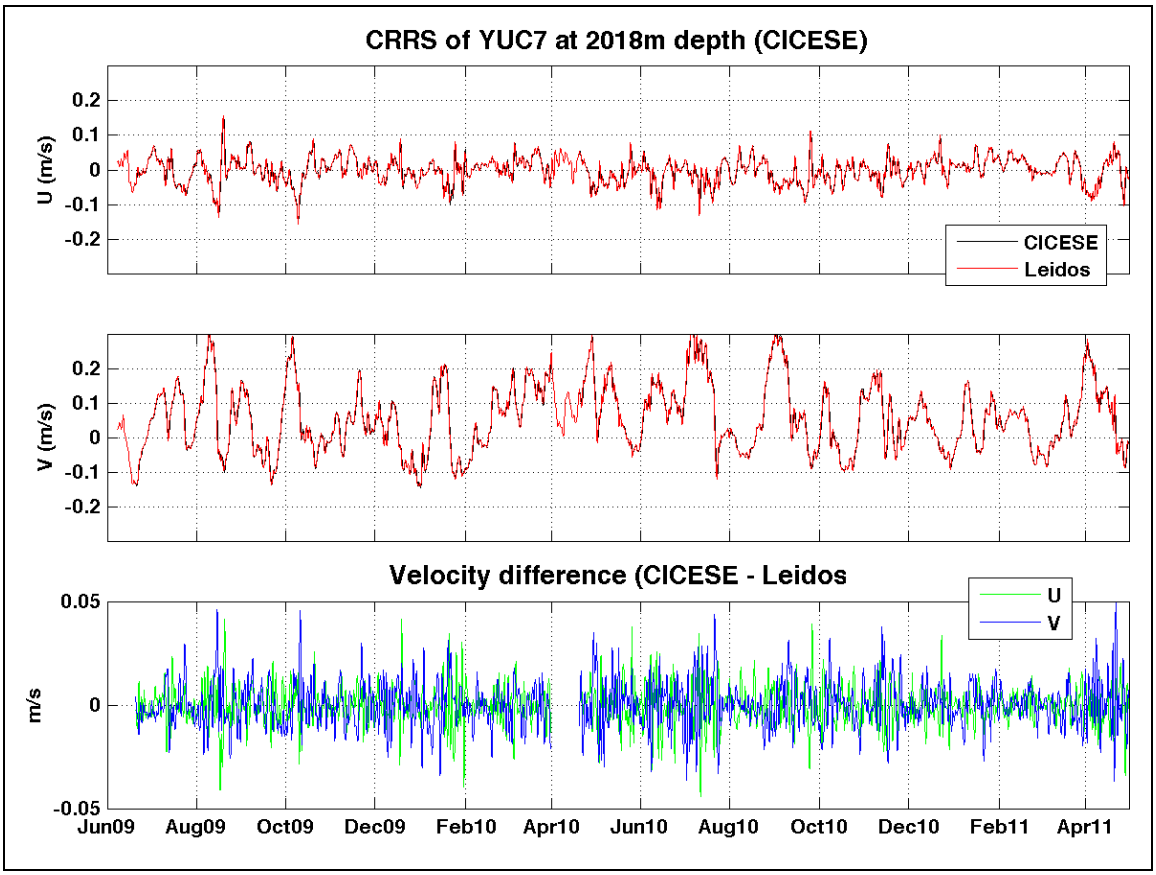

Figure 8. Zonal (top panel) and meridional (middle panel) components of velocity (in m/s) of the deepest current meter of Yucatan section. Comparison between Leidos-processed data (red line) and Canek-processed data (black line). The difference between both versions is shown in the lower panel for each velocity component.

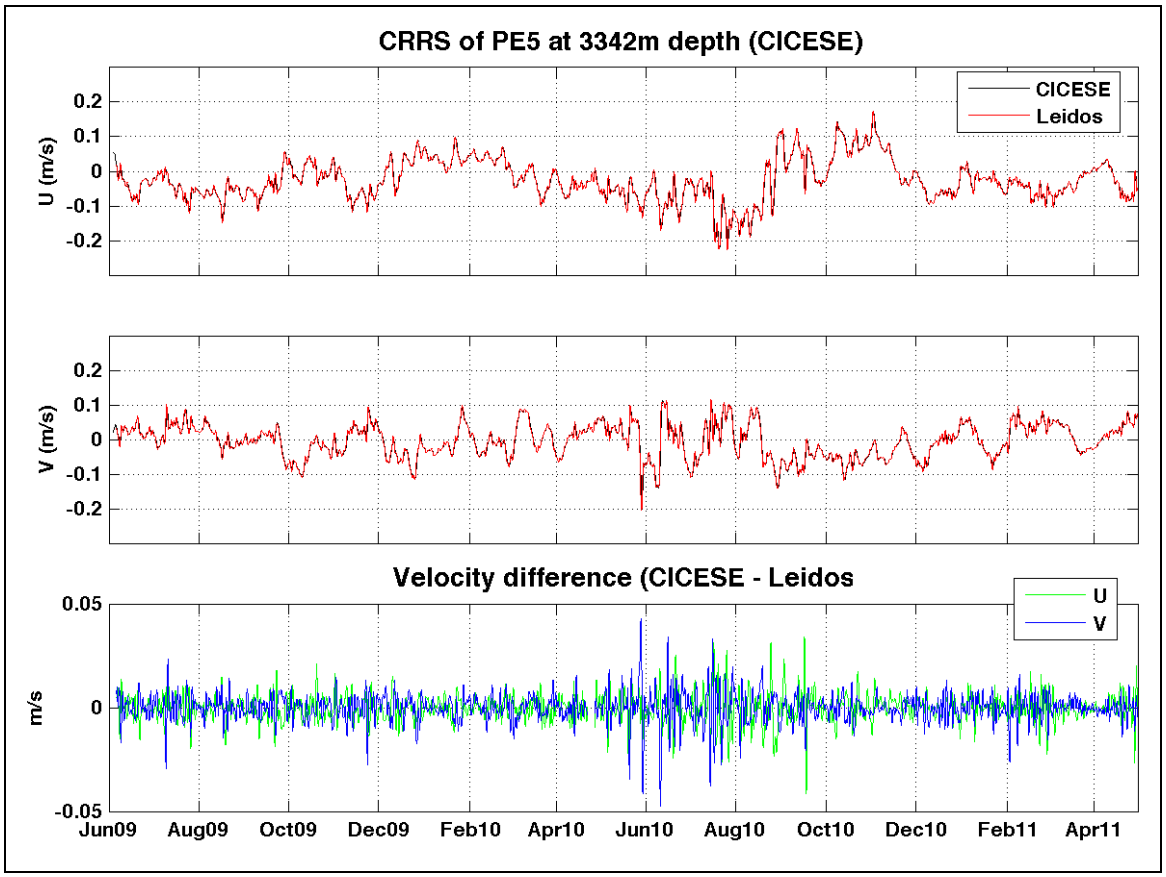

Figure 9. As in Figure 8, for PE section.

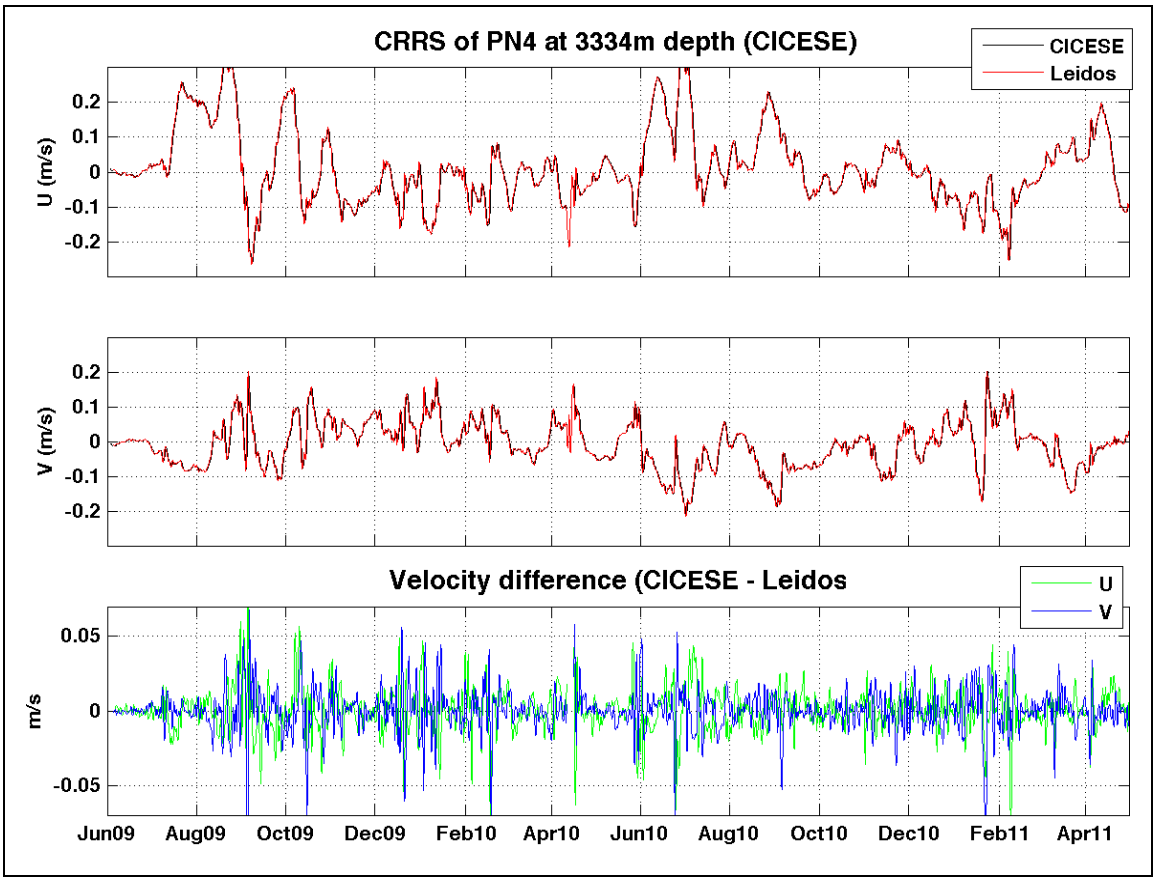

Figure 10. As in Figure 8 for PN section.

3. DATA ANALYSIS

3.1 MEAN CURRENT PROFILES AND BASIC STATISTICS

Figure 11, 13, and 17 show show the vertical profiles of speed of mean current (left panels), root mean square variability (STD, middle panels) and the ratio of sub-inertial velocity variance to total variance (right panels) for three moorings at the YC, calculated separately from June 2009 to March 2010 (top panels) and from May 2010 to May 2011 (bottom panels). Mean currents are intense near the surface with values higher than 100 cm/s at moorings YUC5 and YUC6, and a standard deviation of 25 cm/s. Further east, at YUC7, the mean near surface current reduces to about 50 cm/s with STD of 20 cm/s; this indicates that the highest speeds are found mainly in the region of moorings YUC4, YUC5 and YUC6. This is confirmed by the mean current vector profiles for each mooring at the YC shown in Figure 19. The principal direction is to the north, from the surface down to 500–1000 m depth (depending on the mooring depth) with the most intense currents observed between YUC4 and YUC6 for both periods. Interestingly, the mean current at YUC7 decreases from the surface, down to 1000 m with a minimum magnitude of 3 cm/s and then increases slightly, from this depth down to the bottom at 2020 m to 5–10 cm/s, with a nearly constant north-northeast direction throughout the water column. Similar behavior was observed on moorings YUC5 and YUC6, but there, the current decreases from the surface down to 750 m depth with values less than 5 cm/s of magnitude and STD of less than 10 cm/s. Below those depths, the current changes its northward direction (above 1000 m) to a southwest direction (below 1000 m, (Figure 19) intensifying near the bottom to over ~8 cm/s on mooring YUC6.

The sub-inertial currents dominate the observed variability representing more than 60 % of the total variance from the surface to the mid-water near 1000m depth on the three moorings at Yucatan. Near 700 m depth, the ratio of sub-inertial to total variance starts to decrease and can get as low as 25% between 1000 m and 1200 m (Figure 13, mooring YUC7). It is worth noticing is the fact that there is a general tendency for high frequency variations to increase their importance relative to sub-inertial motions after 700–800 m depth, having their largest impact around 1000–1200 meters. For both periods in YUC7, the sub-inertial currents dominate again below 1500 m where an increase of the mean current was observed near the bottom. This increased in mean current, as well as in flow variability near the bottom through the center of the YC, can be related with deep flow variability, below the 6°C isotherm, which has been associated with changes in the LC extension at time-periods larger than 20 days (Maul et al., 1985 and Bunge et al., 2002). Also interesting is the relative increase of high frequency variability near the surface and near the bottom on mooring YUC5 (Figure 11).

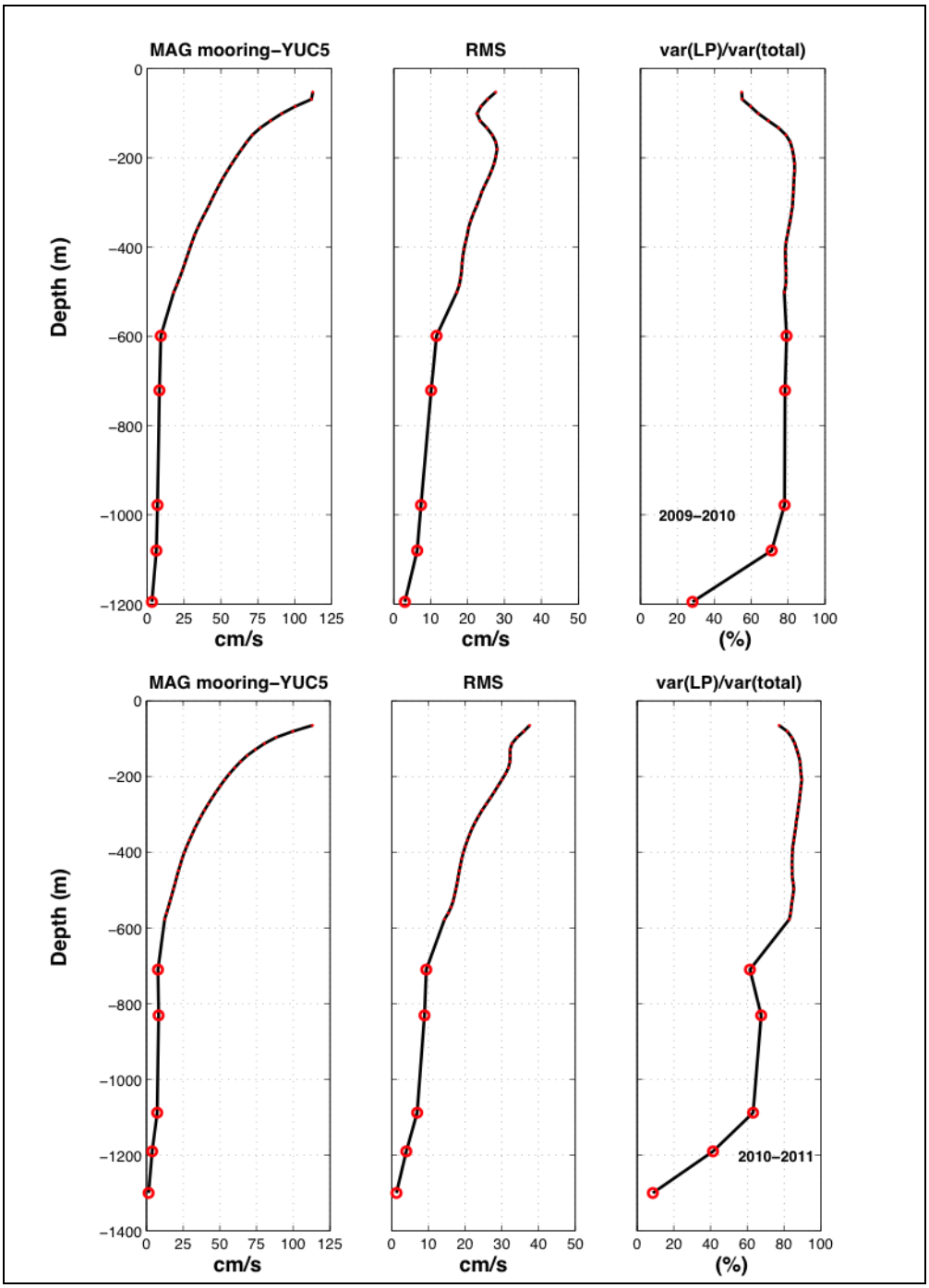

Figure 11. Speed of mean current profile, standard deviation (STD) profile, and ratio of subinertial to total current variance measured by the instruments on YUC5 at the YC. Red dots indicate the specific depth of measurements with the ADCPs and current meters.

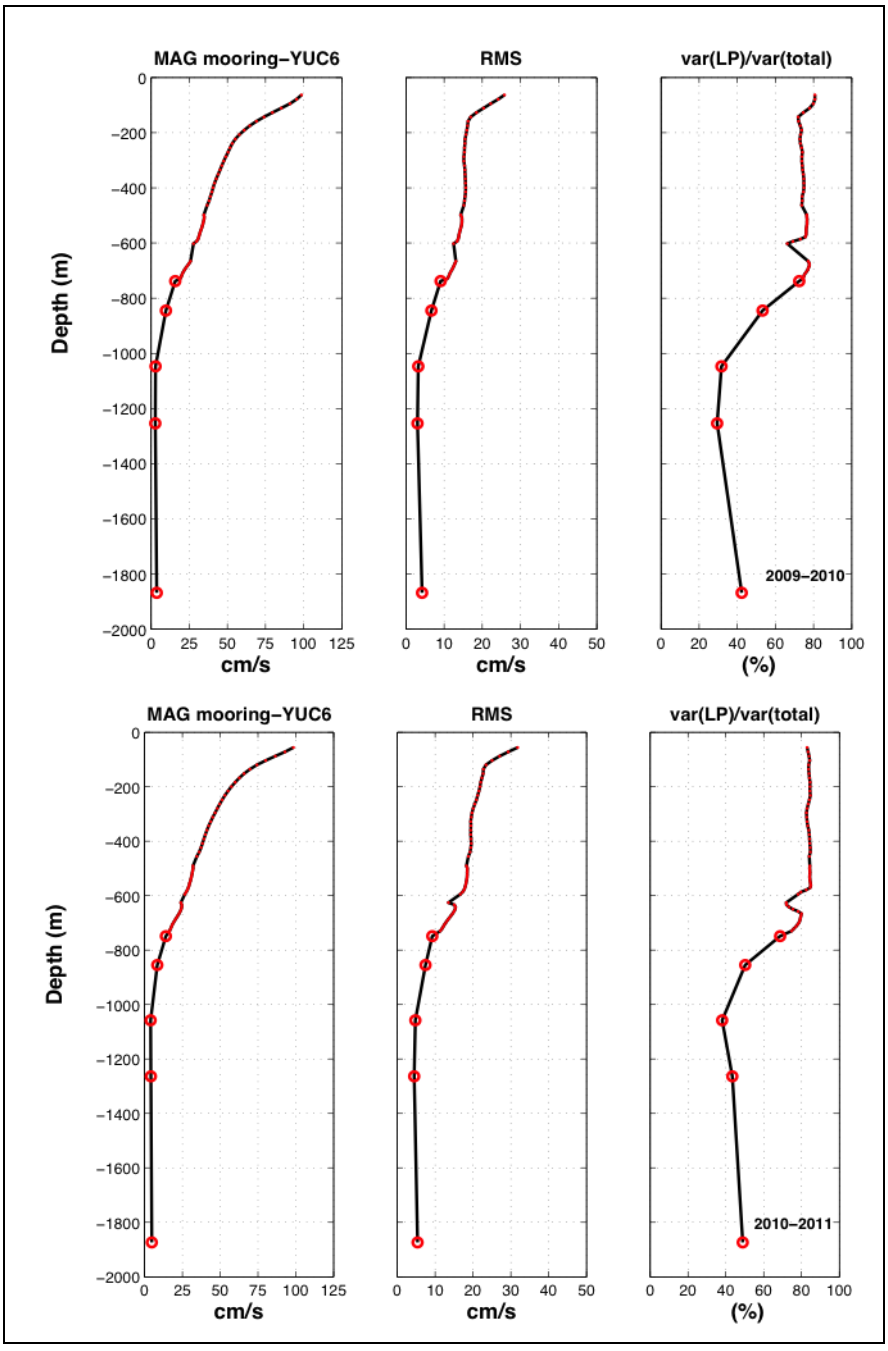

Figure 12. As in Figure 11 for mooring YUC6 at the YC.

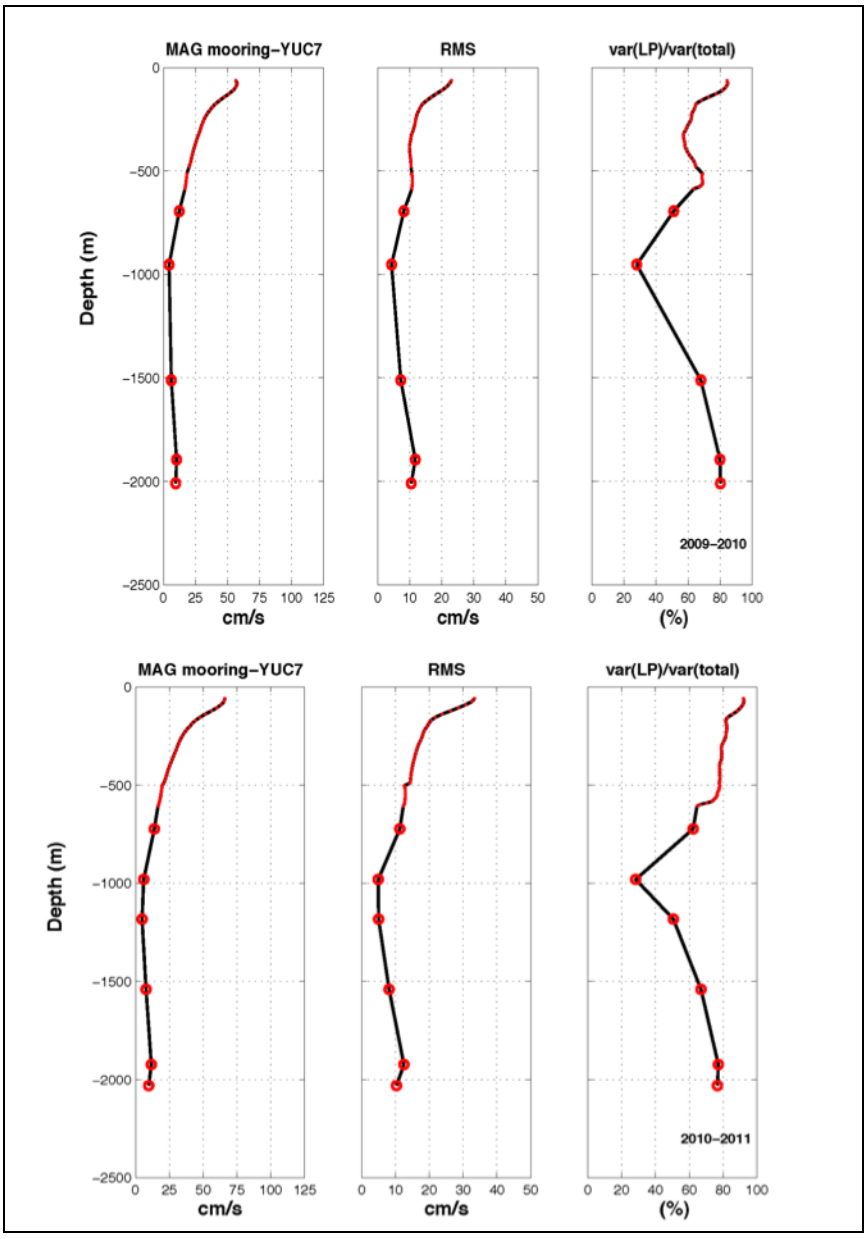

Figure 13. As in Figure 11 for mooring YUC7 at the YC.

Section PE is located further north of the YC and principally measures the western edge of the LC. Figure 14 shows vertical profiles of mean current speed, STD value and ratio of sub-inertial velocity variance to total variance for this section; just as Figure 11 but for different section. The highest mean velocities are observed on moorings PE2, PE3 (not shown), PE4 (Figure 15) and slightly lower on PE5 (Figure 16); it varies between 50 and 70 cm/s, which is lower than the mean current at YC. The STD is of the same order of magnitude as the mean speed (~50 cm/s), and both gradually decrease until 1000 m depth, where current speed is a bit lower than 10 cm/s and is nearly constant down to the bottom (2000 m to PE4) with a slight increase (15 cm/s) at 3500m in PE5. The mean direction of the current at moorings PE2, PE3 and PE4 is northwest and remains the same in the whole water column for PE2 and PE3 (Figure 11). However, current direction at PE5 is mainly to the northeast in the upper layers changing direction below 1200m, a change also observed on mooring PE4.

Sub-inertial current variability accounts for 80% of the total variability from near surface to 800 m depth at PE4 and PE5; below this depth, the ratio of sub-inertial to total variance starts to decrease down to 20% at 1200 m, showing different behavior on moorings PE4 and PE5. On PE4, high frequency current dominates variability between 1200 m and the bottom, whereas on PE5 variability is similar to the one found on YUC7, with a minimum value of sub-inertial to total variance ratio at 1200 m (~20%) that increases again down to the bottom, where sub-inertial current represents 80% of the variability between 1700 m and 3500 m depth. Over the shelf break, mooring PE1 shows a different behavior compared with moorings further offshore: mean current magnitude is ~20 cm/s at the surface, decreasing with depth to values below 10 cm/s near the bottom at 110 m depth. STD values show similar behavior and magnitude as the mean current throughout the water column, but surface mean current direction is to the southwest, rotating in a spiral to the bottom (Figure 11). Sub-inertial current accounts for 60% of the variance between the surface and 75 m depth, decreasing to 40% near the bottom.

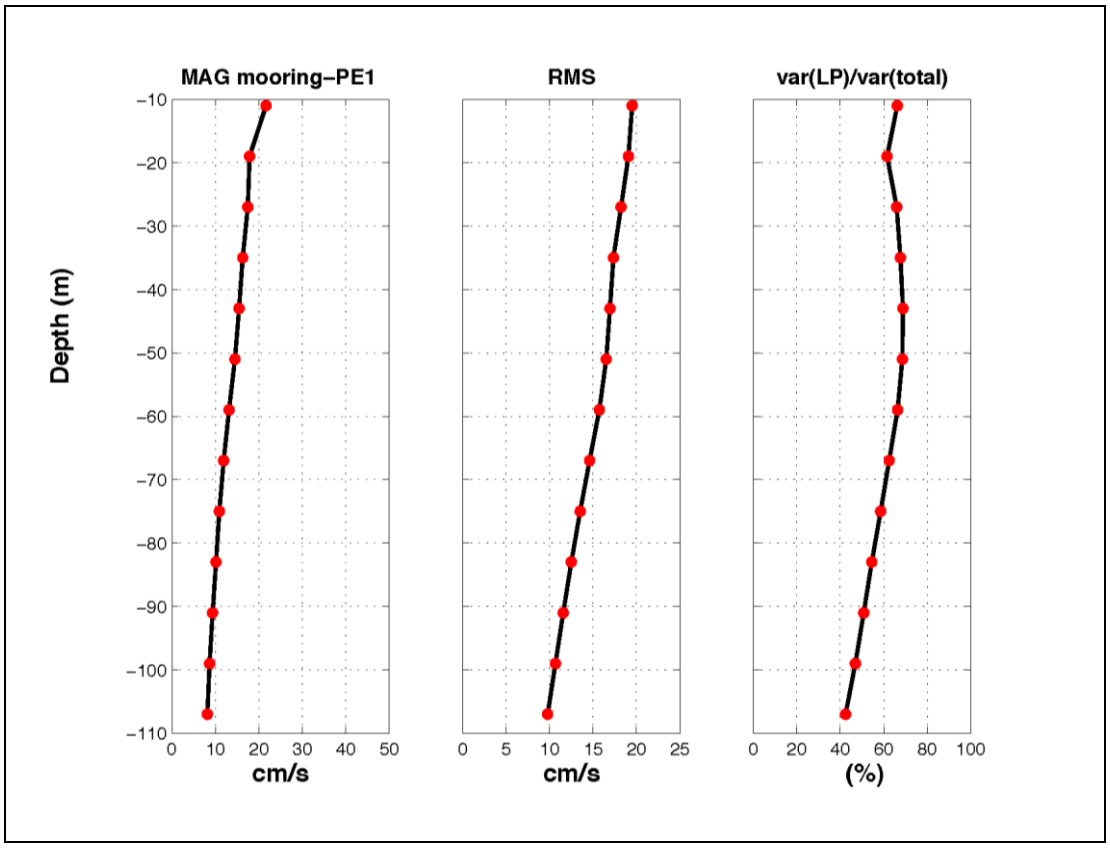

Figure 14. As in Figure 11, for mooring PE1.

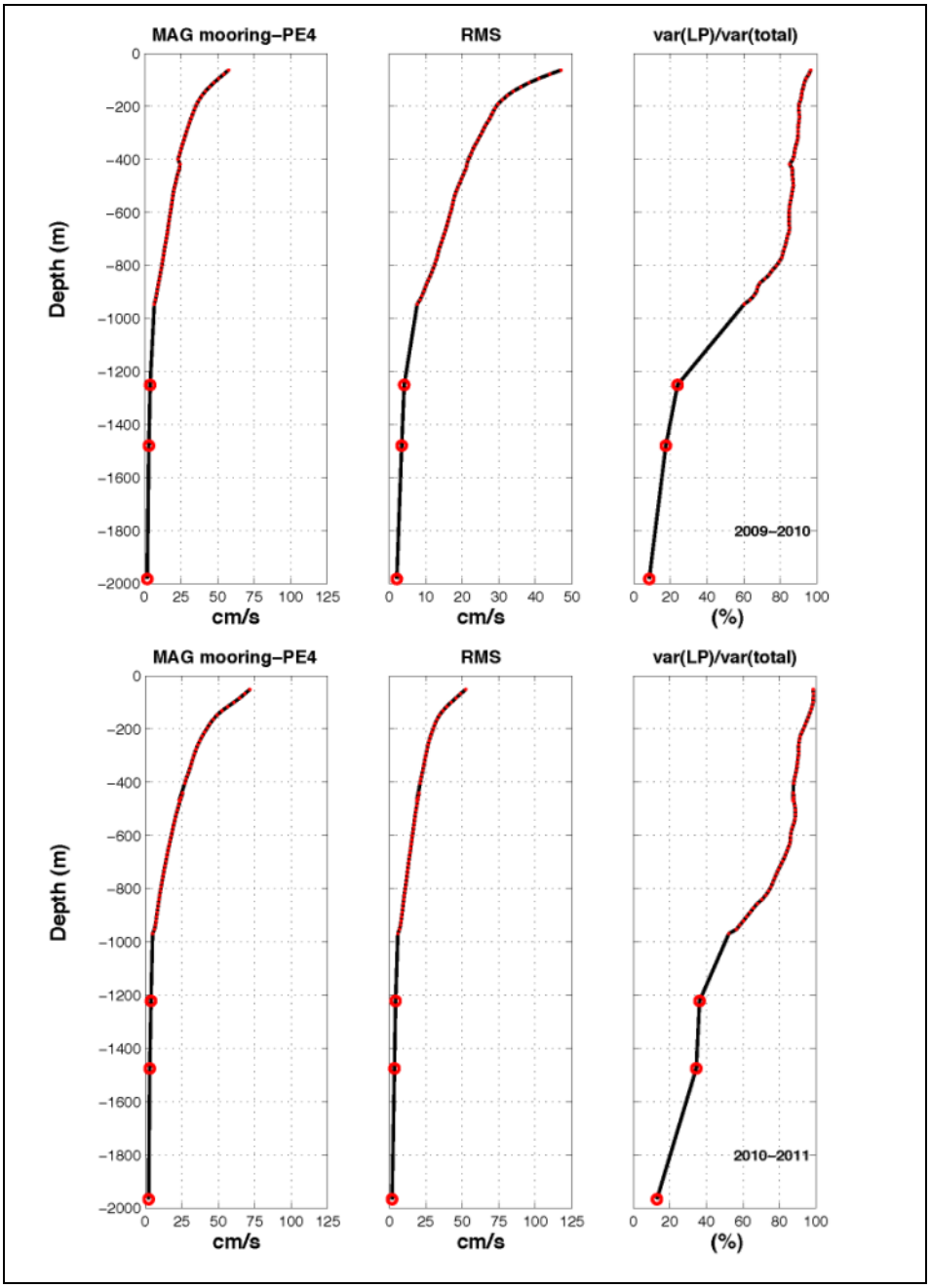

Figure 15. As in Figure 11, for mooring PE4.

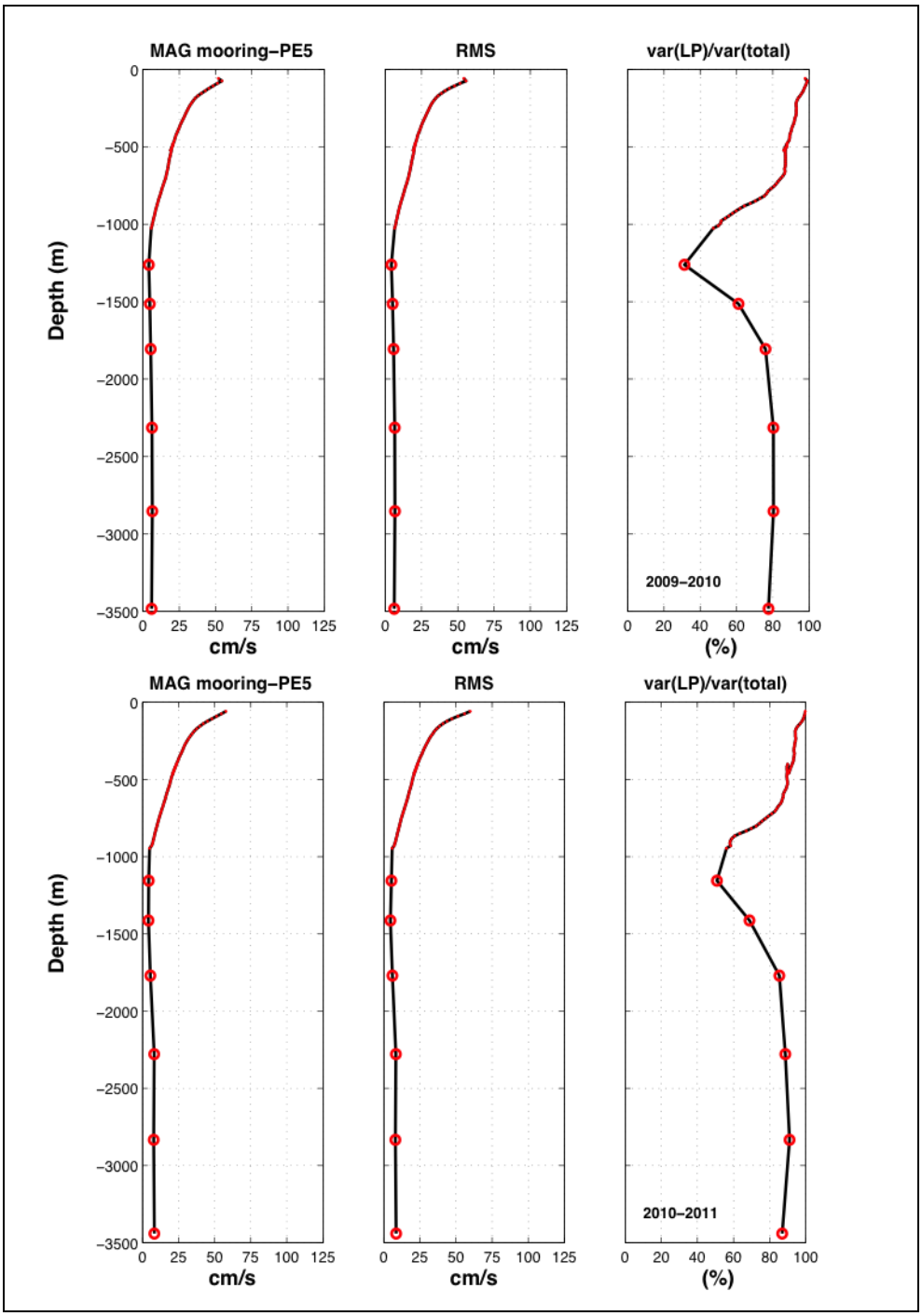

Figure 16. As in Figure 11, for mooring PE5.

Moving on to section PN, we see that the highest mean current speds are observed on moornings PN2 and PN3, with a magnitude of 75 cm/s near the surface (Figure 17) and with a northwest mean direction (Figure 21). A change in current direction is observed at mid-water depth in almost all moorings of this section, together with a relative current intensification near the bottom. This shift in direction is observed at 60–80 m on PN1, at 400 m on PN2 and at 1200 m on PN4 (on PN3 this depth cannot be accurately detected due to instrument failure at depths between 500 and 1000m). Mean speed near the surface is lower than 10 cm/s on PN1 and about 20 cm/s on PN4. STD values on moorings PN3 and PN4 (Figure 17 and Figure 18, respectively), show that the fluctuations of the current are as intense as the mean speed values and both decrease at a similar rate from the surface down to the bottom. The variance is dominated by sub-inertial currents from the surface to 3500m depth on PN4 and from the surface to 1000 m depth on PN3. In the latter the ratio of sub-inertial to total current variance reduces to 20% near the bottom (1200 m depth). For completeness and reference, a set of 17 tables for each measuring period containing the basic statistics (mean, standard deviation, maxima, and minima) of the horizontal velocity components is included in Appendix A.

The vector plots of the mean velocity profile from the moorings show general agreement and similarity of the profiles between the two deployment periods (Figure 19, 20, 21). It is worth mentioning that the ADCP measurements between 500–600 m depth on mooring YUC6 appear to be faulty in current direction. The jump in current direction is observed in both periods, but was measured with different ADCPs (300 kHz workhorse) in each period and is not continuous with the measurements above or below.

Figure 23 and Figure 24 show variability ellipses and also depict the mean current vectors at different depths for the three sections. The YCu is detected by the high mean velocities at moorings YUC4, YUC5, YUC6 and to a lesser extent at YUC7 with an average speed around 100 cm/s, which is clearly higher than current fluctuations . The variability in this area is mainly oriented across the Yucatan Channel, while further west at YUC2 and YUC3, ellipses are oriented along the channel with higher magnitude than the mean vectors. At 450m the current speed diminishes rapidly to about 20–25 cm/s for YUC4 to YUC7, the variability is almost of the same order of magnitude as the average, oriented in the along channel direction.

Current fluctuations at sections PE and PN are of magnitude similar to the mean values, close to 70 cm/s near the surface and 20 cm/s at 450 m depth. Variability ellipses are oriented prevalently along the topography over the slope from the surface to the bottom, but going from parallel at PE2, PE3, PN1, PN2, and PN3 to almost perpendicular to the isobaths at PE5; at PN4 the variability intensifies being higher than the mean current of 20 cm/s and without dominant orientation.

It is found that the fluctuations over the slope are oriented along the topography from Yucatan to section PN practically throughout the water column, but showing two different directions of the mean current as function of depth; near the surface the mean current direction is northwest, while near the bottom (at 500m for PN1, 1000 m for YUC5, PE3, PN3, as well as ~2000m depth for YUC6 and PE3, Figure 24) the mean current is to the south following the 1000 m contour of the topography toward the Caribbean. Further down at depth, the mean

current direction varies with depth at 1000, 2300 and 2800 m, suggesting a possible spiral turn, which was also observed in the mean profiles (Figure 20 and Figure 21); variability there, is largely higher than the mean current.

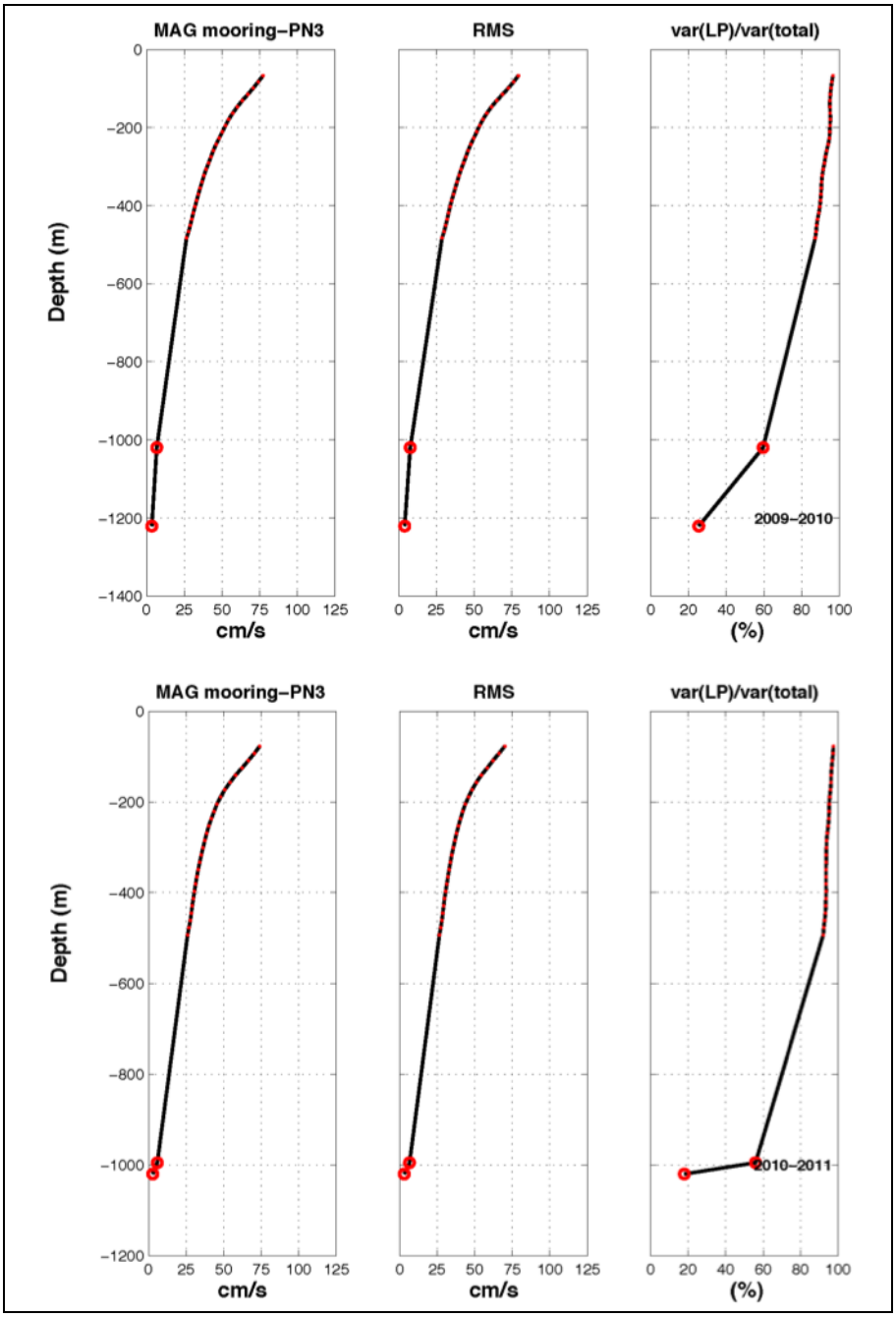

Figure 17. As in Figure 11, for moorings PN3.

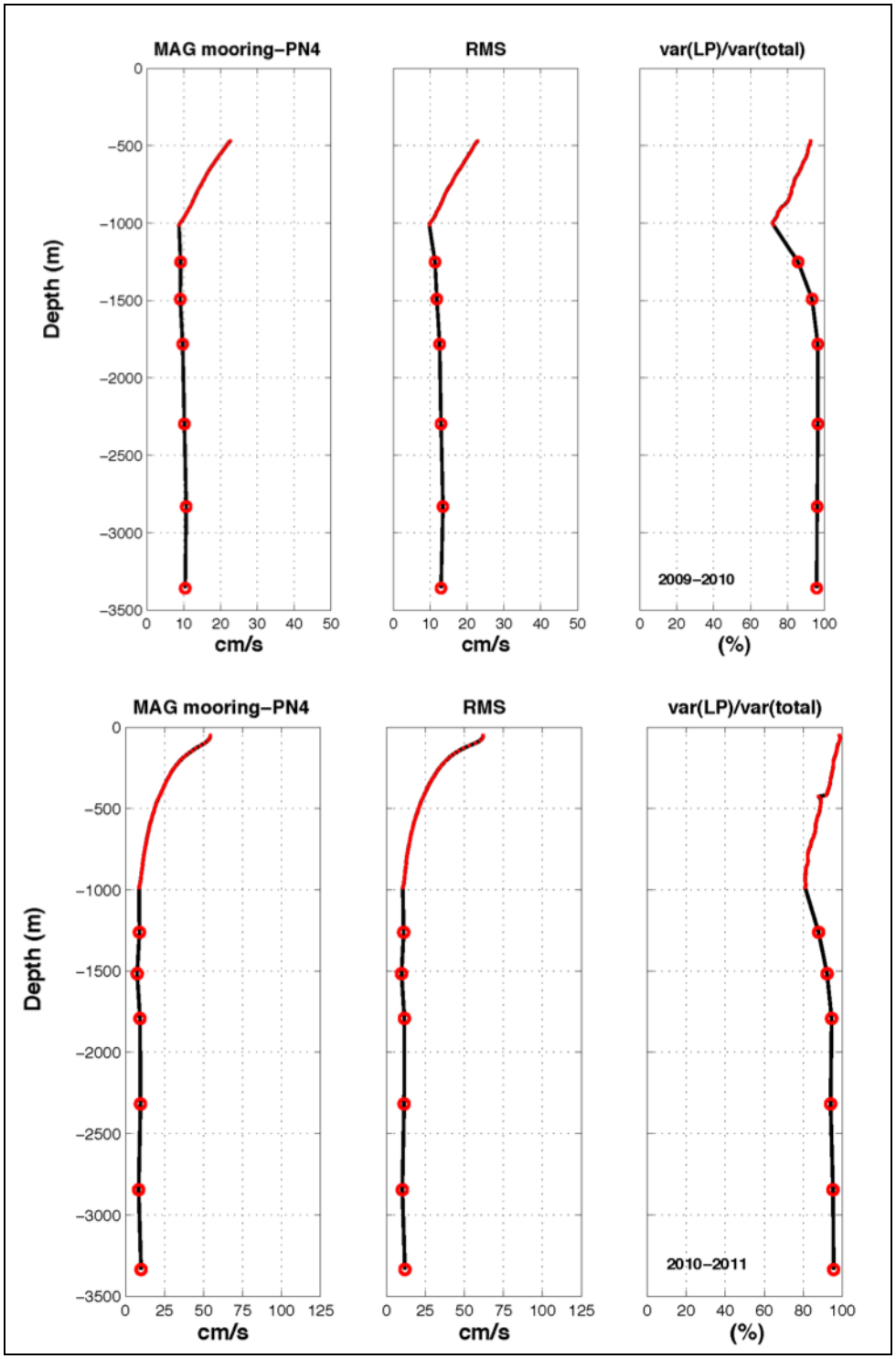

Figure 18. As in Figure 11, for moorings PN4.

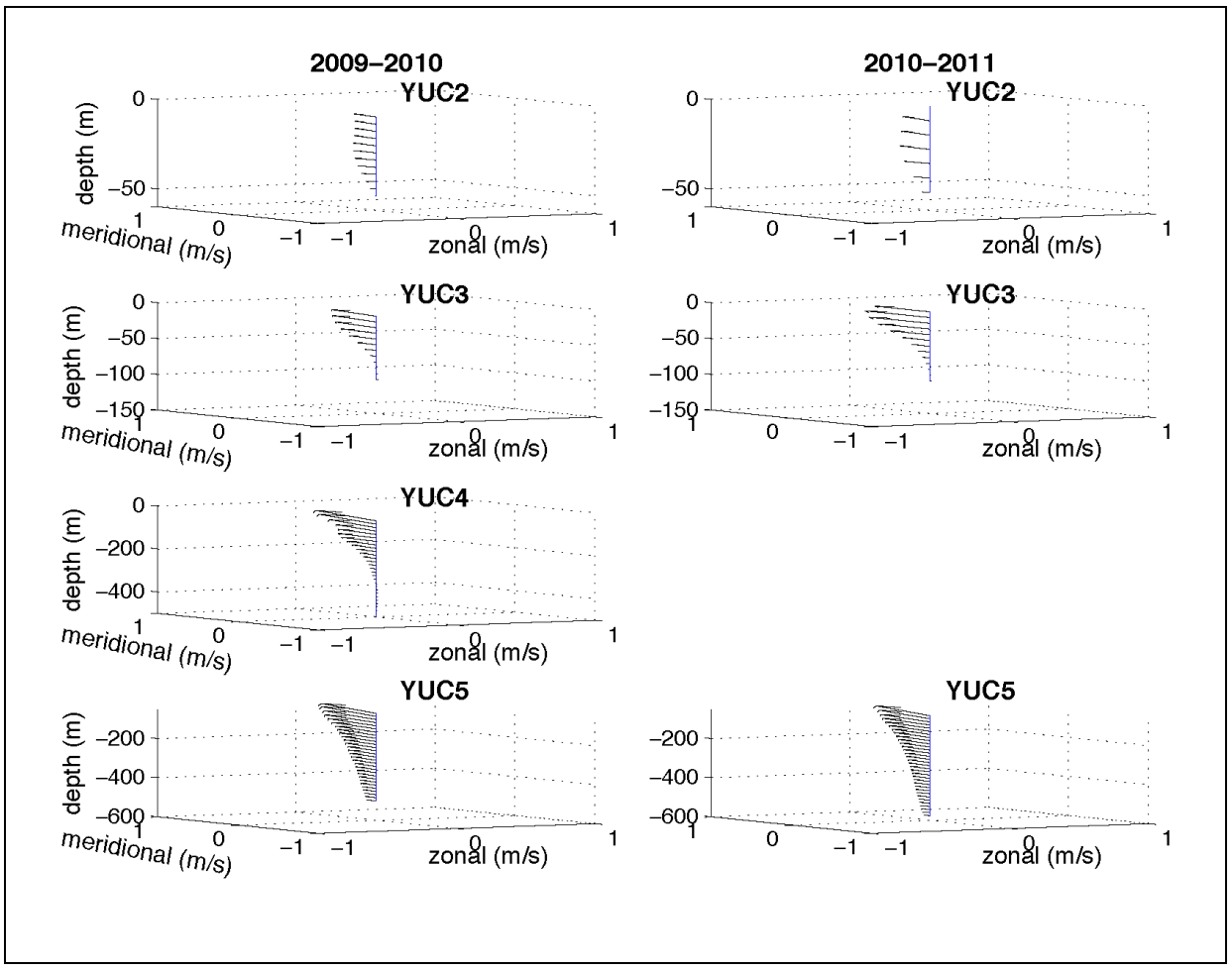

Figure 19. Mean horizontal current profile (vectors in 3-D space) observed at each of the six moorings at the YC. The left panels show the profile averaged between July 2009 and March 2010, and the right panels averaged between May 2010 and May 2011. The east-west/north-south components are in the abscissa/ordinate directions with each vector starting at its corresponding depth.

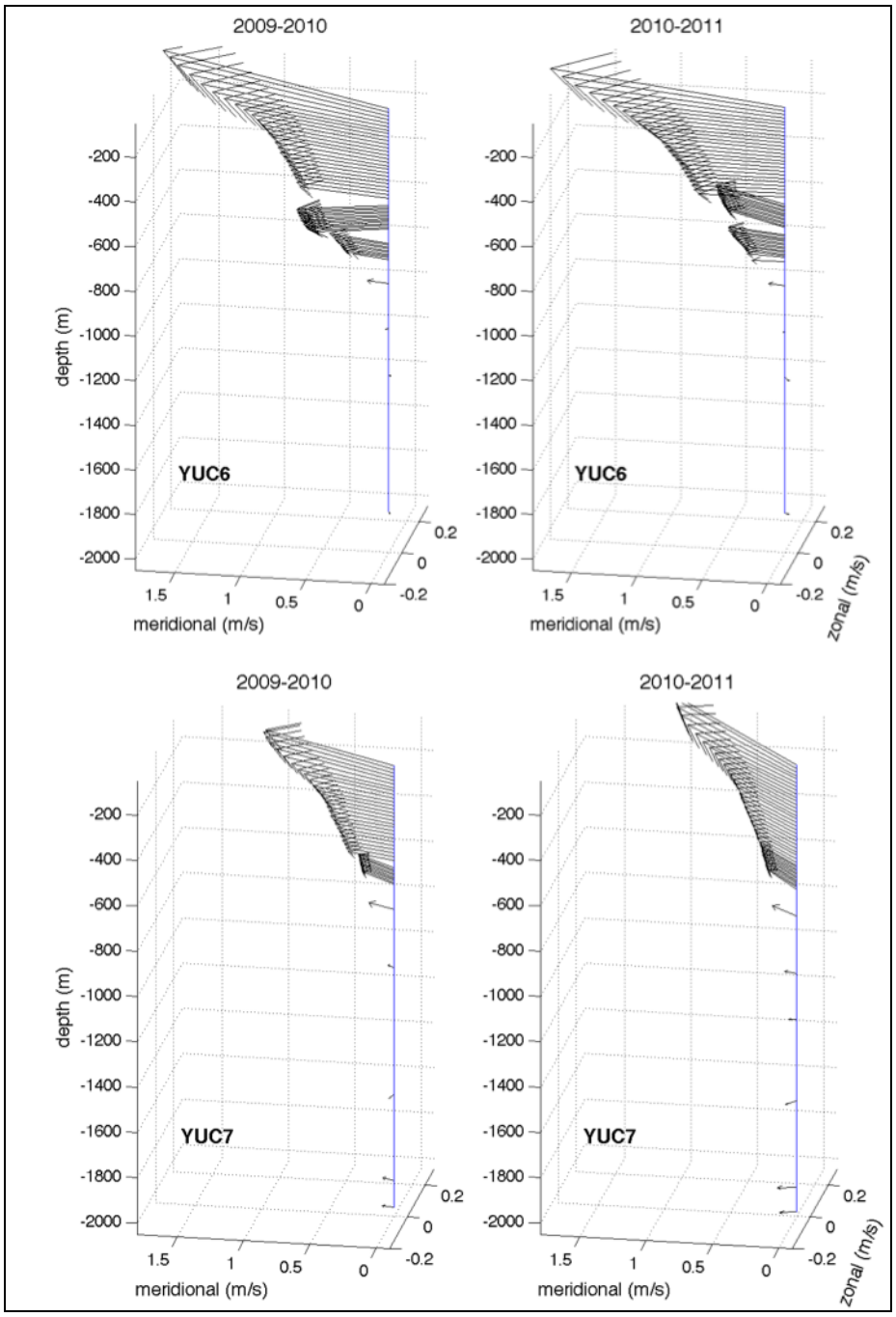

Figure 19. Continues.

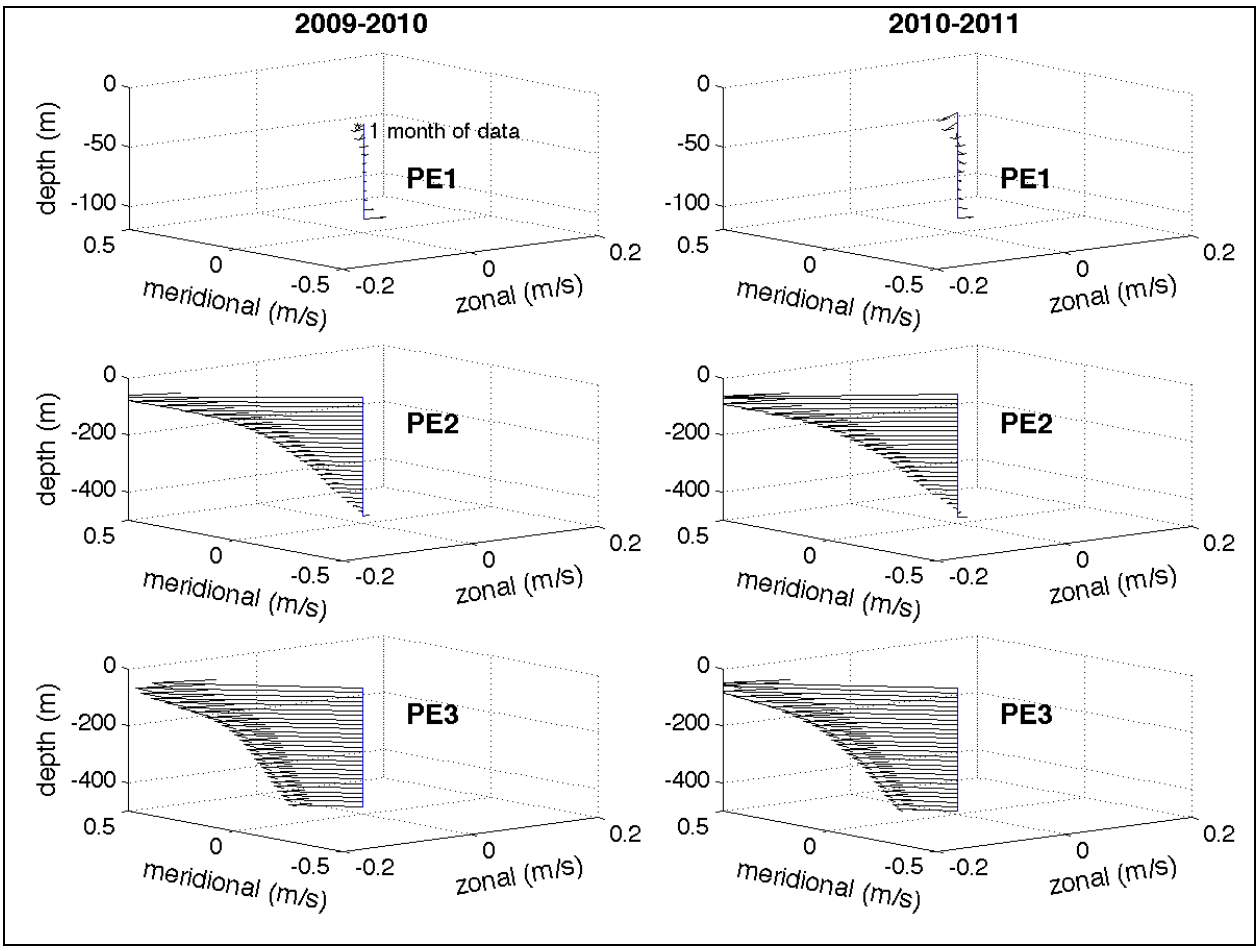

Figure 20. As in Figure 19, for moorings on section PE. For the exception of the upper left panel the average is for only the month of July 2009.

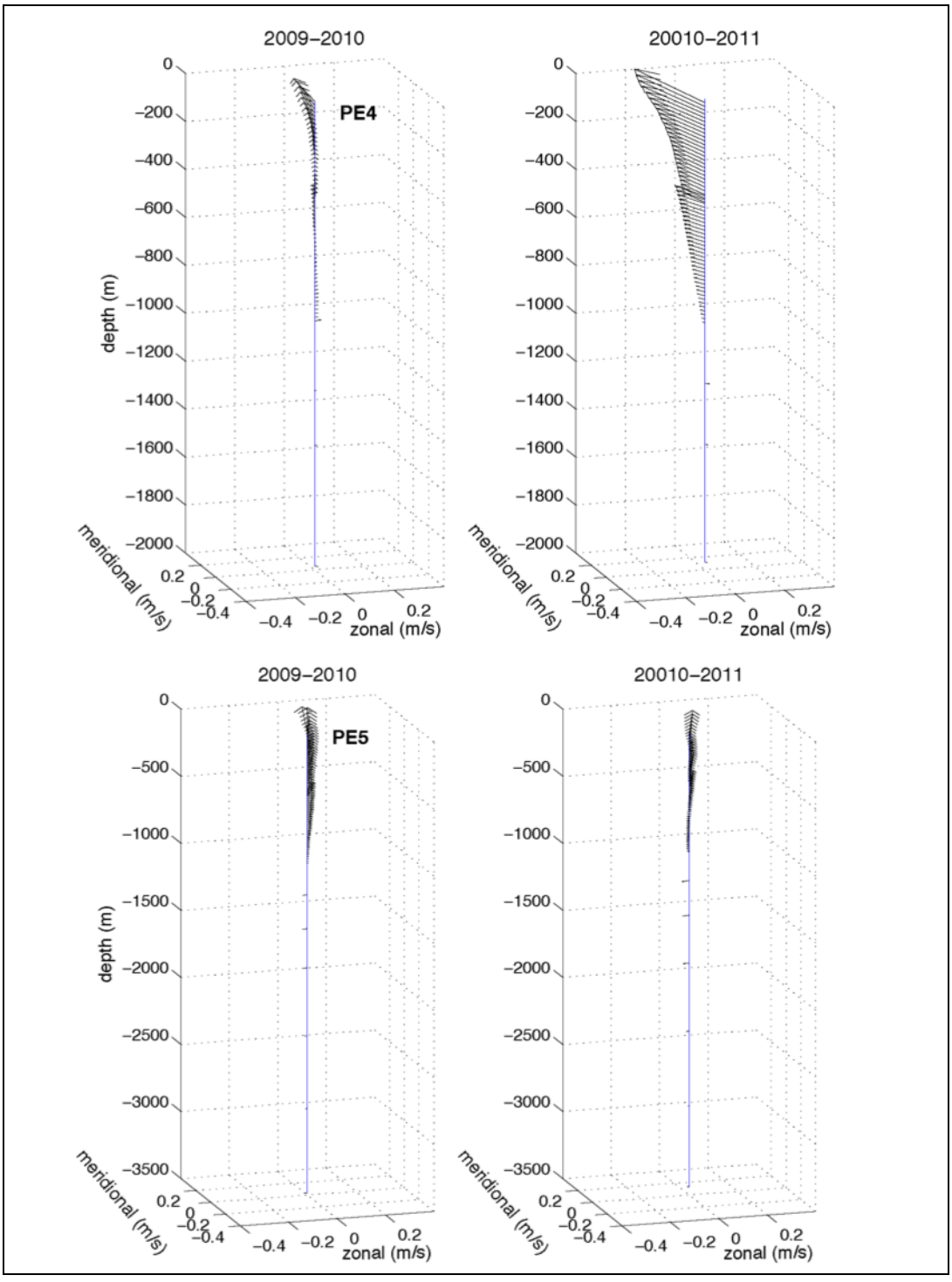

Figure 20. Continues.

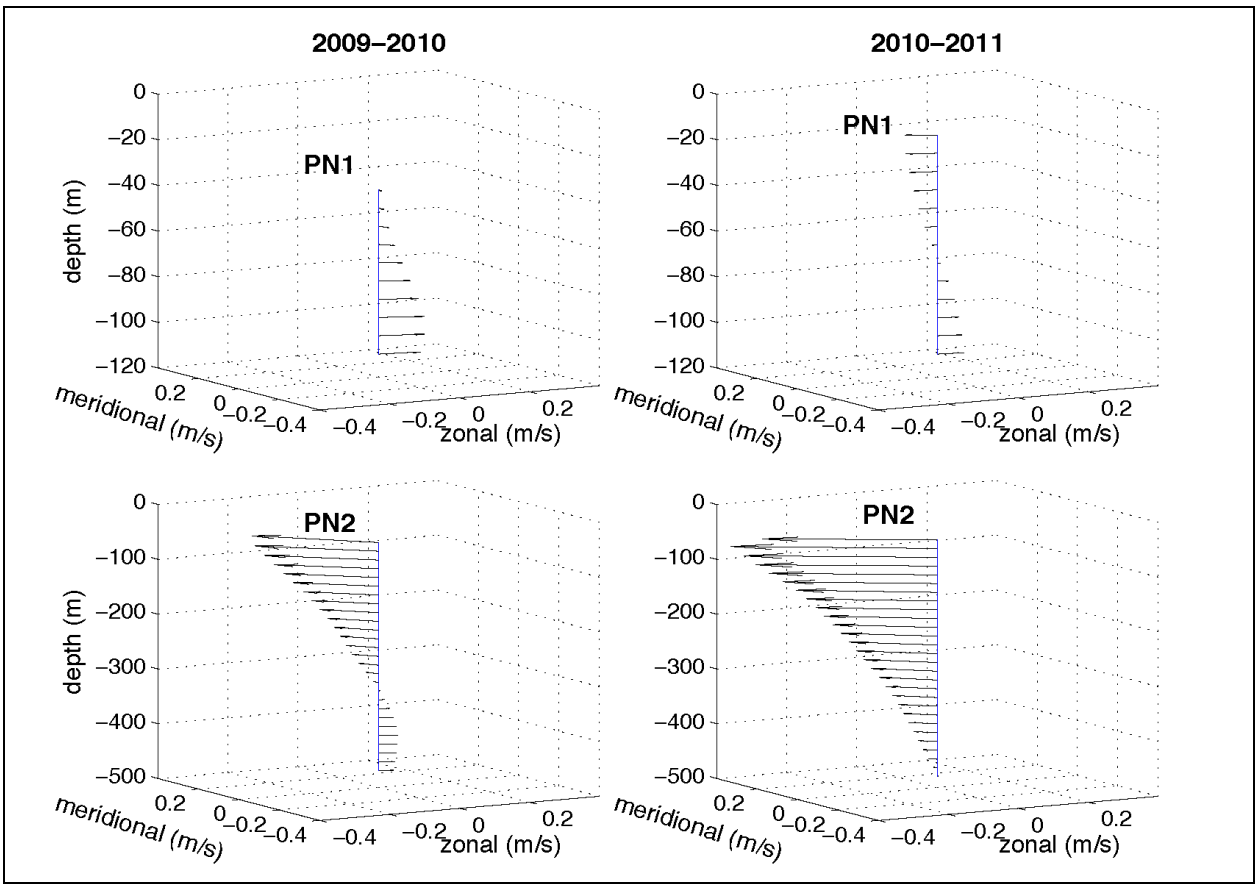

Figure 21. As in Figures 19 and 20, for moorings on section PN.

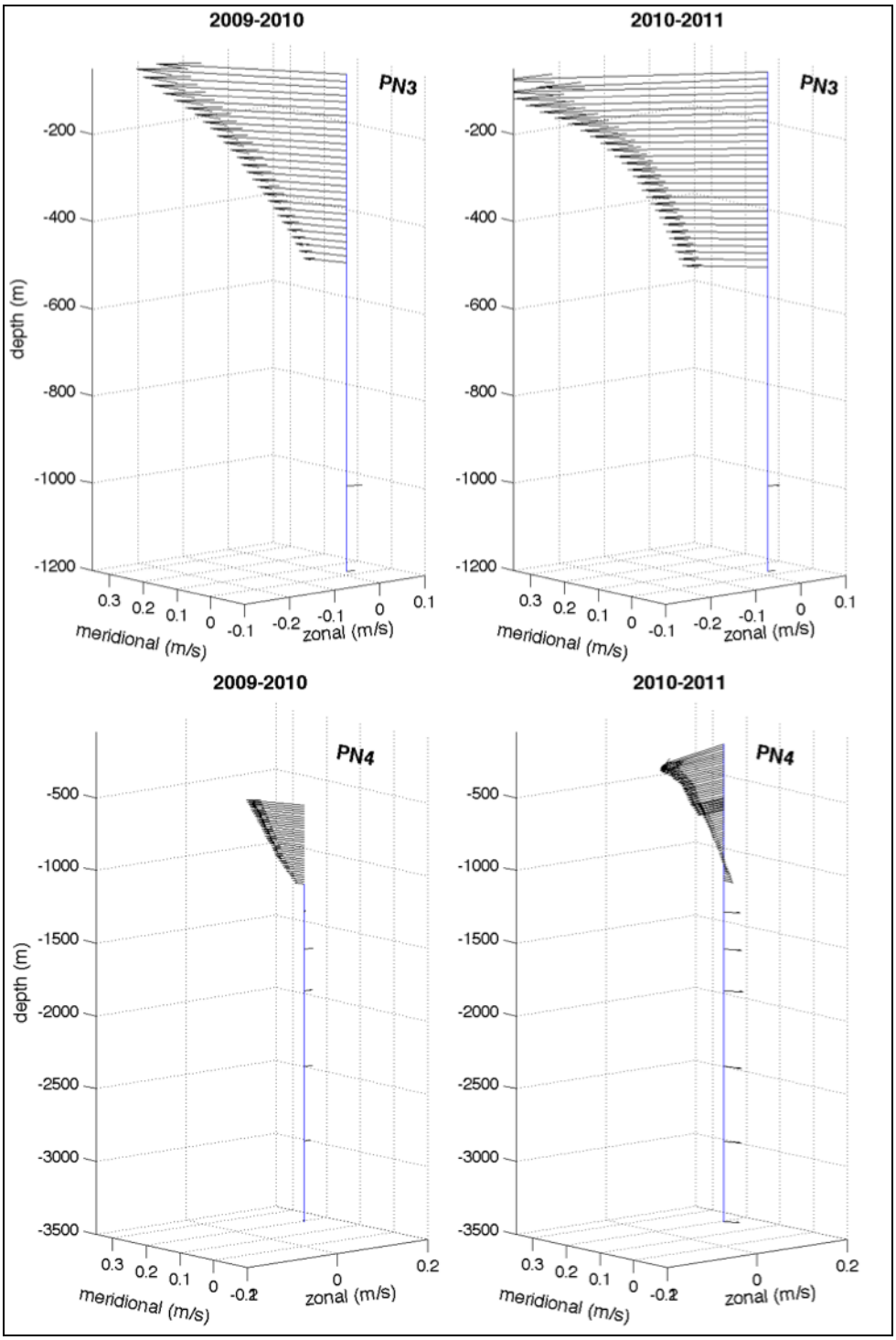

Figure 21. Continues.

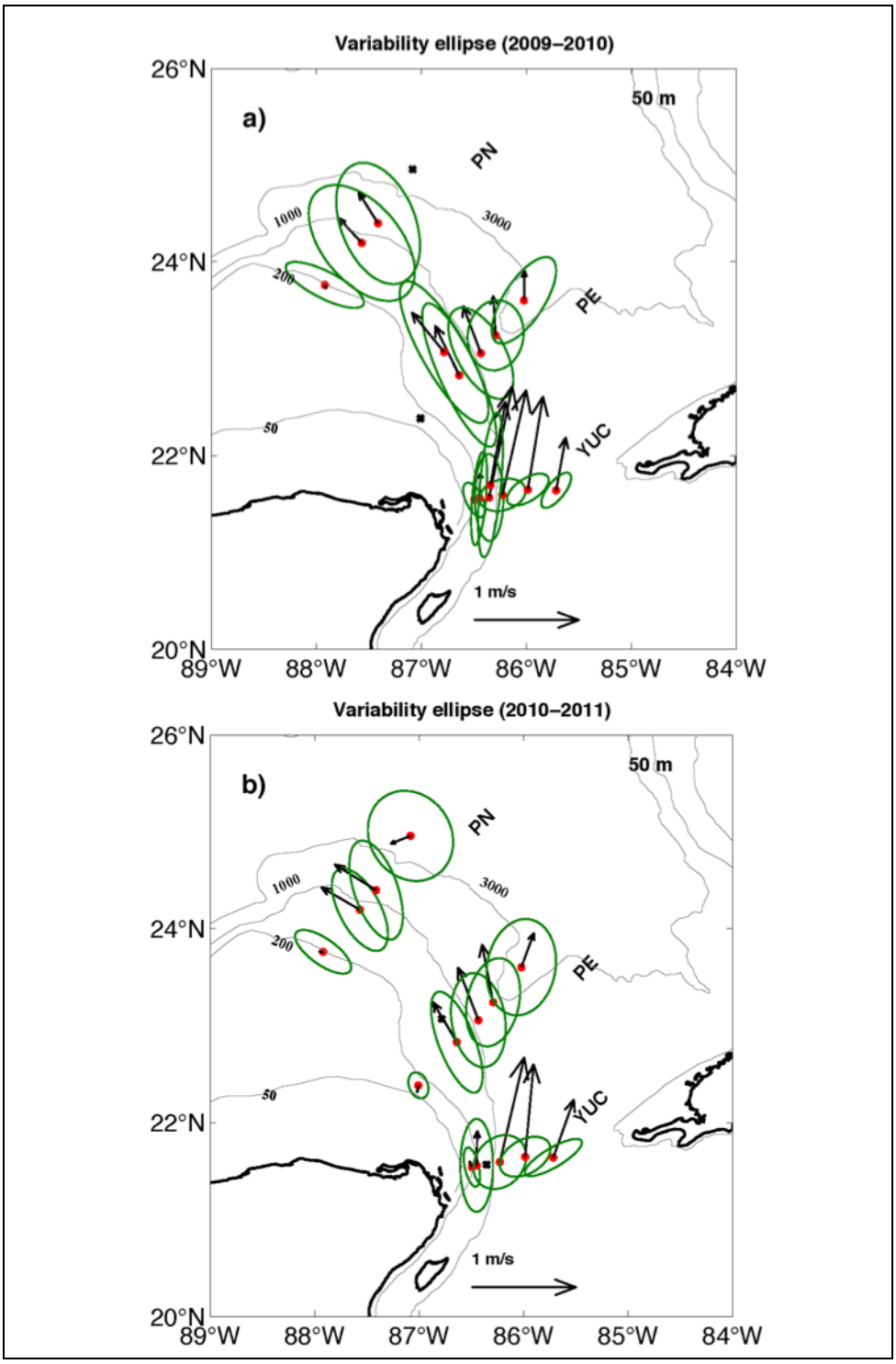

Figure 22. Mean and variability ellipses of the measured currents at 50m depth.

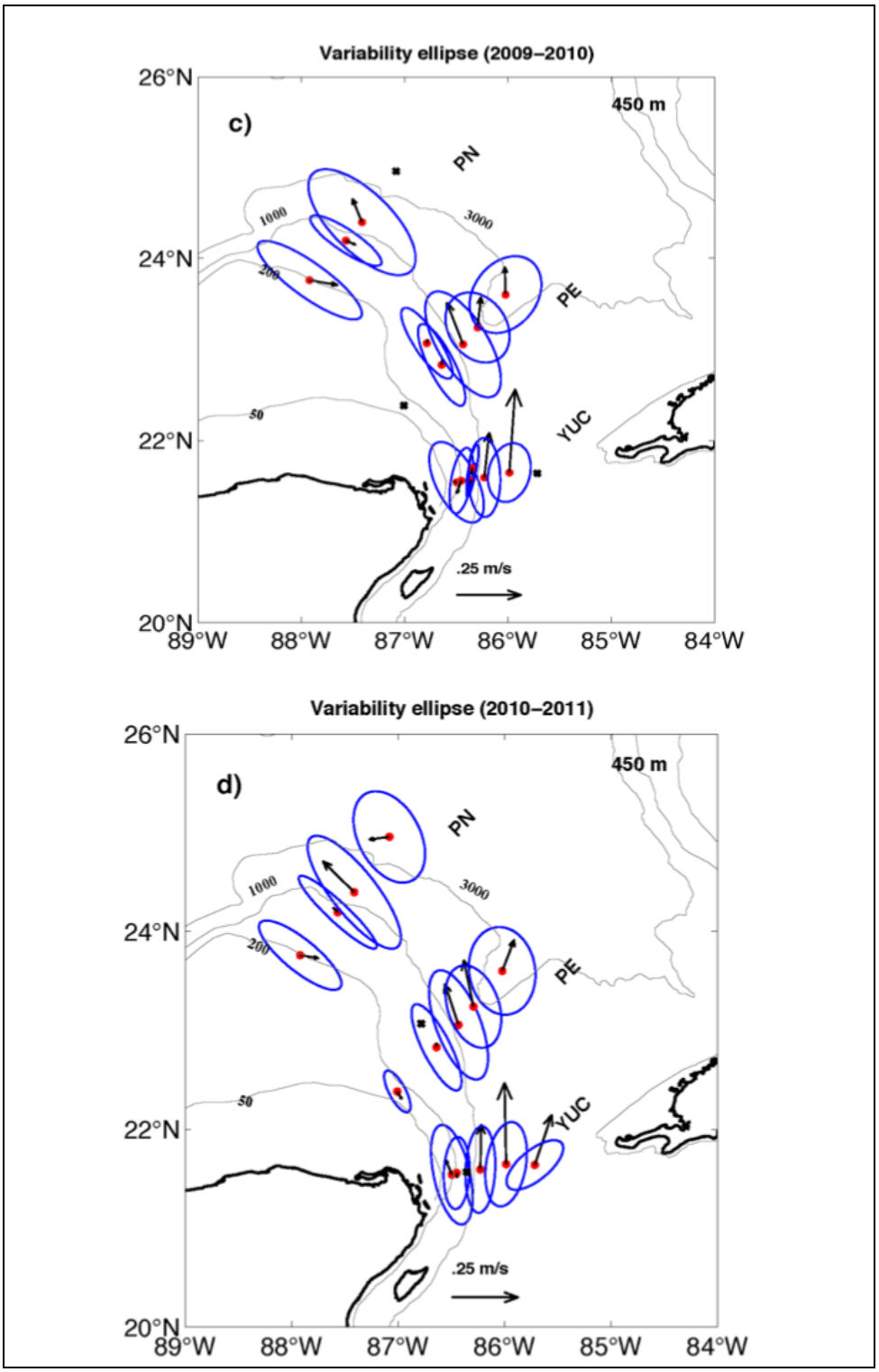

Figure 23. Mean and variability ellipses of the measured currents at 450 m depth.

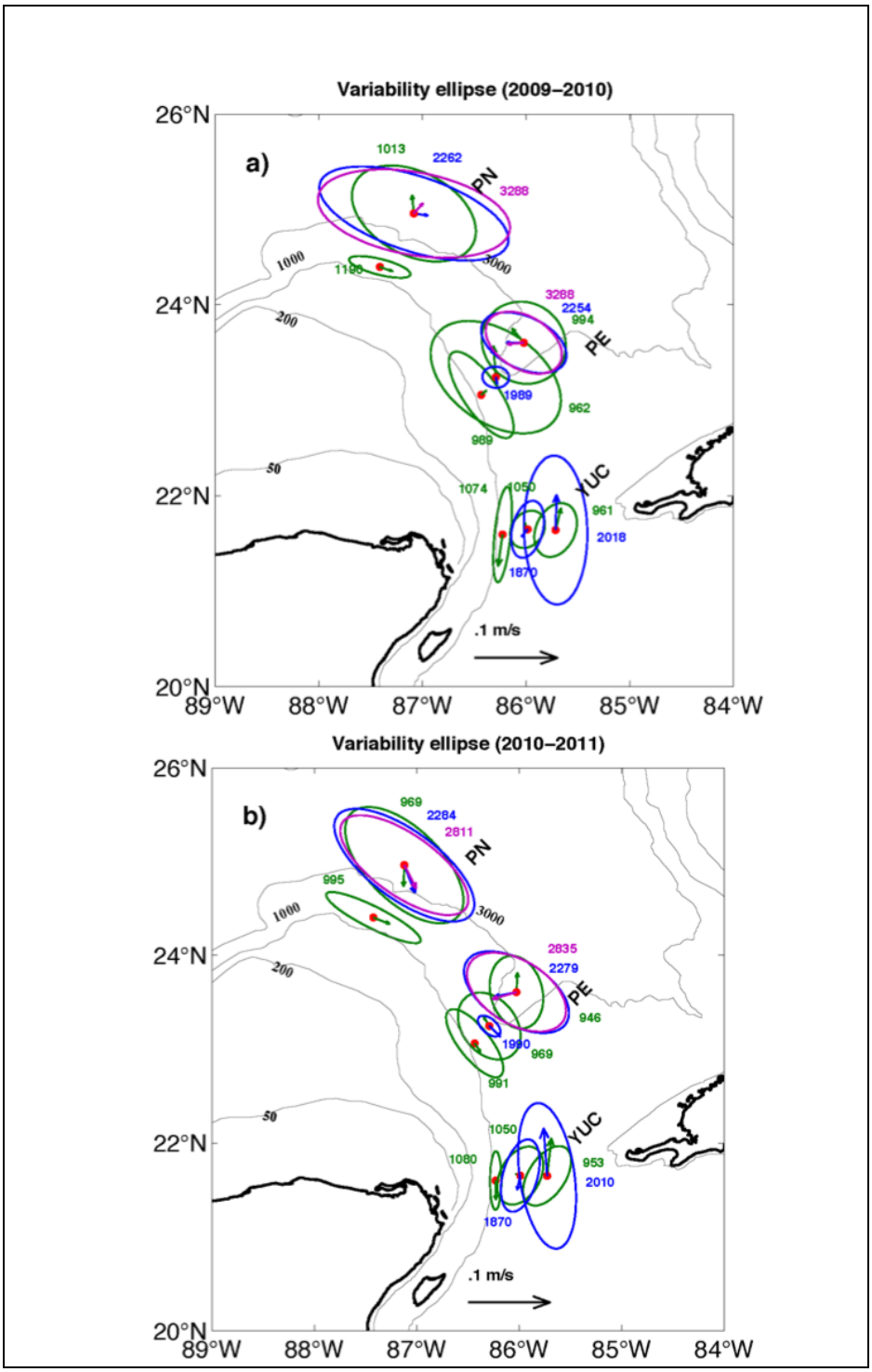

Figure 24. Mean and variability ellipses of the measured currents at the indicated depths (numbers are indicated with colors).

The vector time series of low-pass subinertial currents at several depths in moorings YUC2 and YUC3 (Figure 25 and Figure 26), over the shelf (at 60 m and 100 m, respectively), show a dominant current to the north (into the Gulf). There are some episodes of southward flow, which are present at both moorings; interestingly, the duration of these episodes increases with depth, being slightly detectable near the surface and more evident from ~30 m depth down to bottom. The first event lasts from July to September 2009, while a second long-lasting southward flow event was observed from April to October 2010 interrupted by an intense northward flow of about three weeks in July. At YUC3, the signature of the first event was observed at 30 m and 46 m depth, as northward-southward pulses with periods of ~15 days; It is noteworthy that these two events are also detected at mooring YUC5 at 150 and 300 m depth (Figure 27), which is located quite to the center of the channel but still over the shelf edge (see Figure 2). Further north, these two southward events are observed on the shelf break, at PE2 and PE3 throughout the water column (Figure 30 and Figure 31). Over the shelf at PE1 (Figure 29) and PN1 (Figure 34), variability appears to be from a different origin; northwest-southeast oscillations reaching the 50 cm/s are observed at PE1; while at PN1 southward flow dominates with lower magnitude ~30cm/s and only few events of higher current events (~50 cm/s) with northwestern direction.

In the center of the YC (from mooring YUC5 to YUC7, Figure 27 and Figure 28) the flow appears to be divided in two main layers, with the upper levels dominated by the strong current (>70 cm/s) with direction mainly to the north varying slightly to the northeast; only at YUC7, and with no southward flows detected between 50 and 500 m depth. Below that level, reversals of the current are frequent; however the variability between YUC5 and YUC7 is apparently not connected; below 590 m depth. Fortnightly fluctuations O (25–50 cm/s) are observed at ~600 m and ~700m depth at YUC5, from where the current decreases rapidly down to the bottom (< 10 cm/s at 1189 m). In the deepest part of the YC at YUC7, current fluctuations have no clear periodicity varying north-south below 1000 m and intensifying near the bottom at 2020 m. As mentioned before, this intensification is also observed in the deepest moorings of the downstream sections (PE5 and PN4) near 3300 m (see Figure 33 and Figure 36) and may indicate the presence of topographic Rossby waves (Hamilton, 1990, 2007).

A flow divided into two layers seems to be a feature also for sections PE and PN. Above 1000 m depth, the intense current (reaching ~100 cm/s) from northwest to northeast varies with some reversals during June 2009 and April 2010 (see Figure 33 and Figure 36). A strong northward/southward current (>1m/s) in the upper layer here, is likely to be associated with the passage of cyclonic/anticyclonic eddies. Likewise, episodes of weak currents seem to be related with eastwards shifts of the LC off the section, particularly at PE5 (Athie et al., 2012). Due to the highly variable path of the LC, it is not necessarily expected that the signals at PE and PN are correlated, which is the case here.

One important feature on the deep slope at moorings PN4 and PN3 (Figure 35 and Figure 36) are the intense current pulses (>15 cm/s) across the section (or the topography), with direction northwest-southeast, observed in current meters at 1500, 2800, and 3300 m depth. From model analysis, the northern topographic slope of Campeche Bank has been identified as a preferred site for deep cyclogenesis by Oey (2007), right in the area where section PN is located, which could be related to these observations.

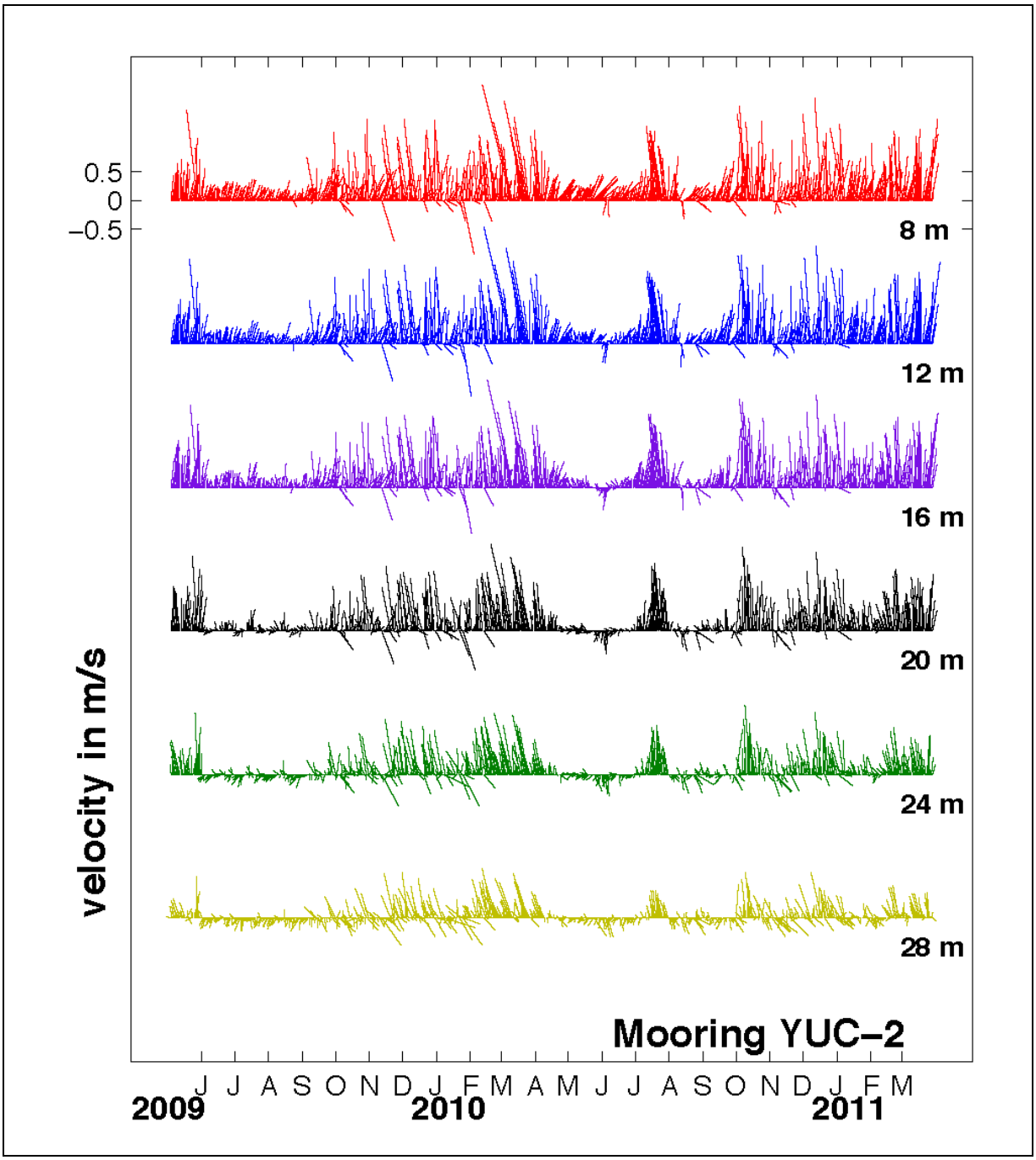

Figure 25. Vector time series from mooring YUC2 at the YC; different depths are indicated.

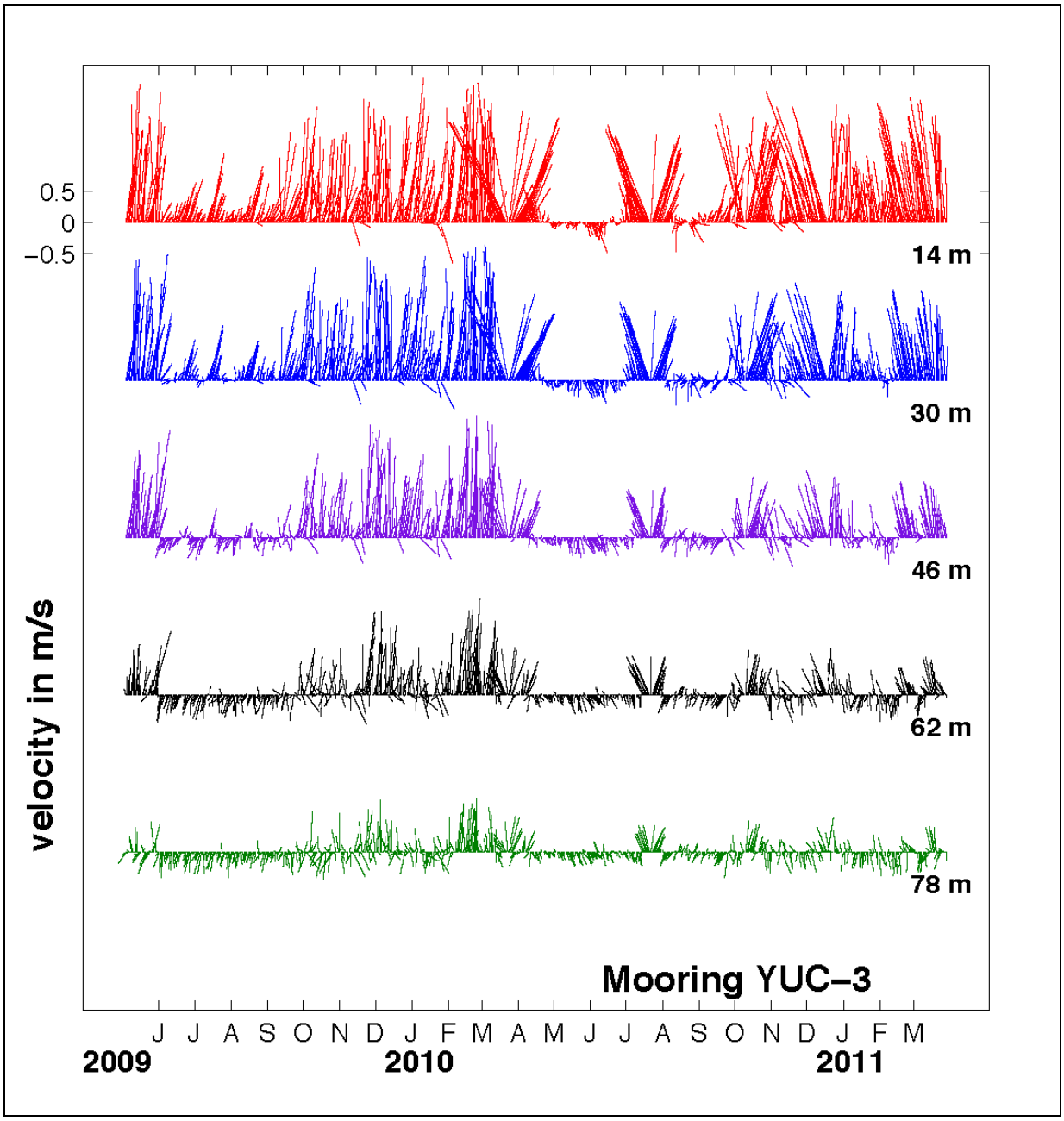

Figure 26. As in Figure 25 from mooring YUC3 at the YC.

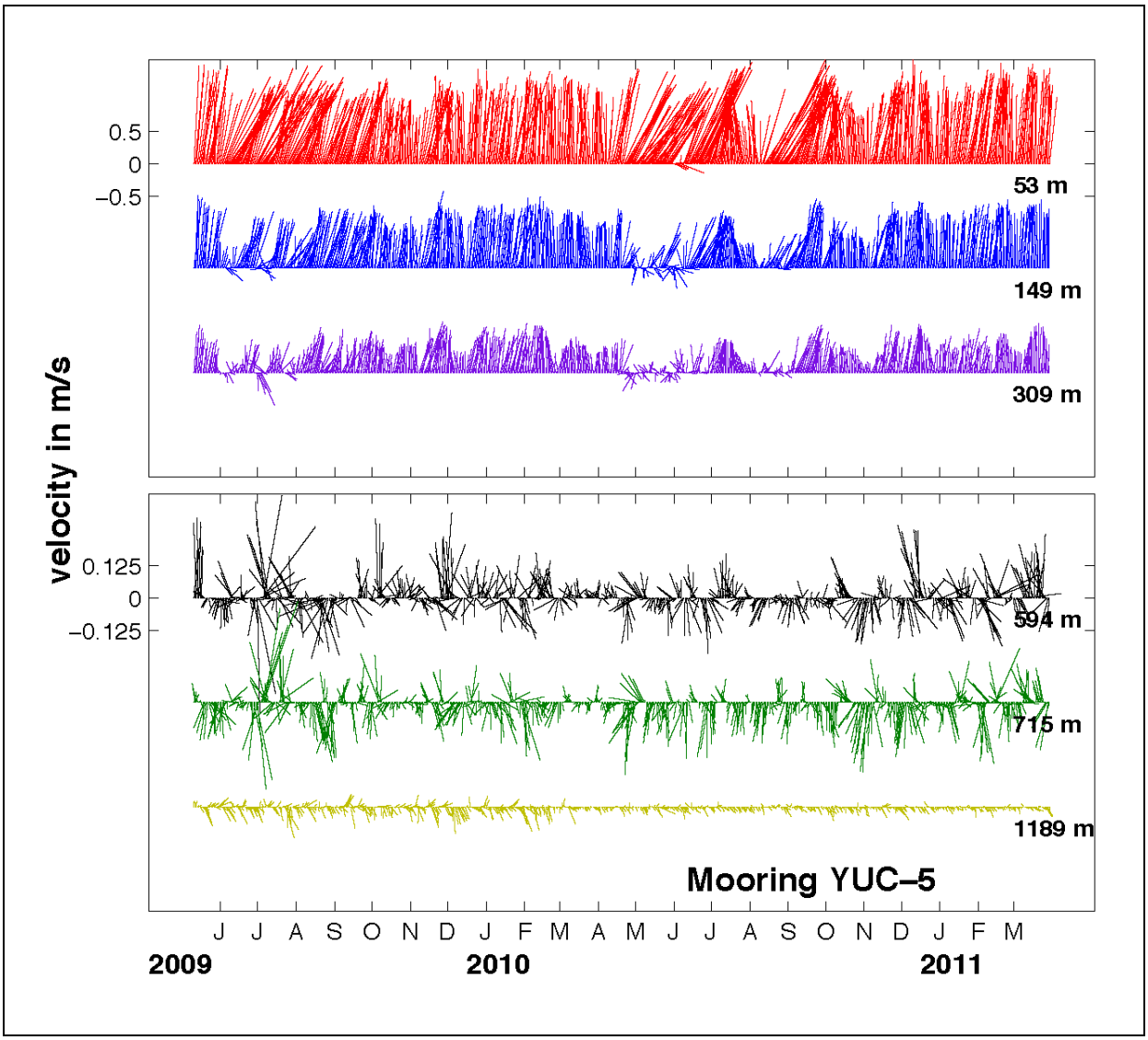

Figure 27. As in Figure 25 from mooring YUC5 at the YC.

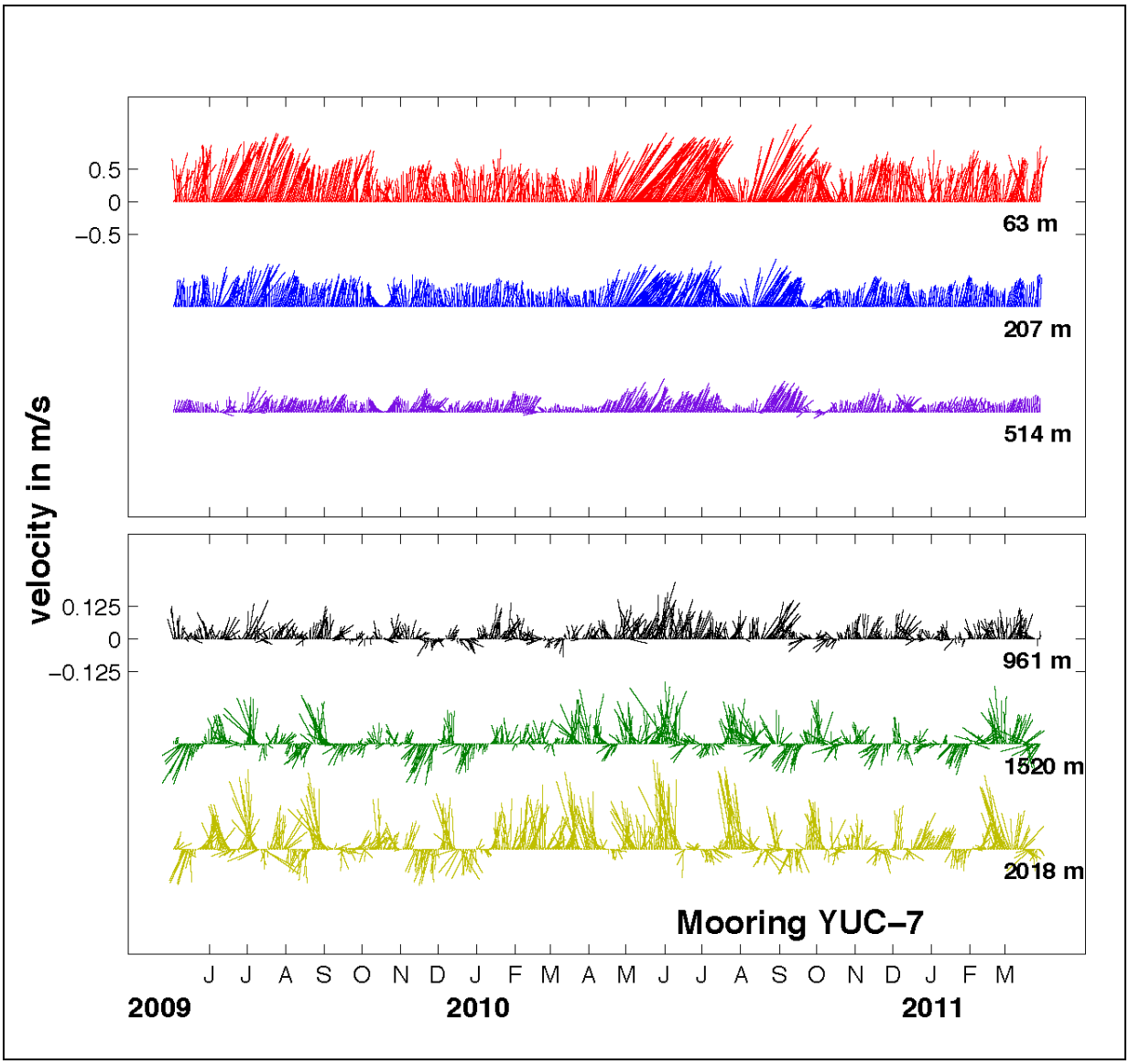

Figure 28. As in Figure 25 from mooring YUC7 at the YC.

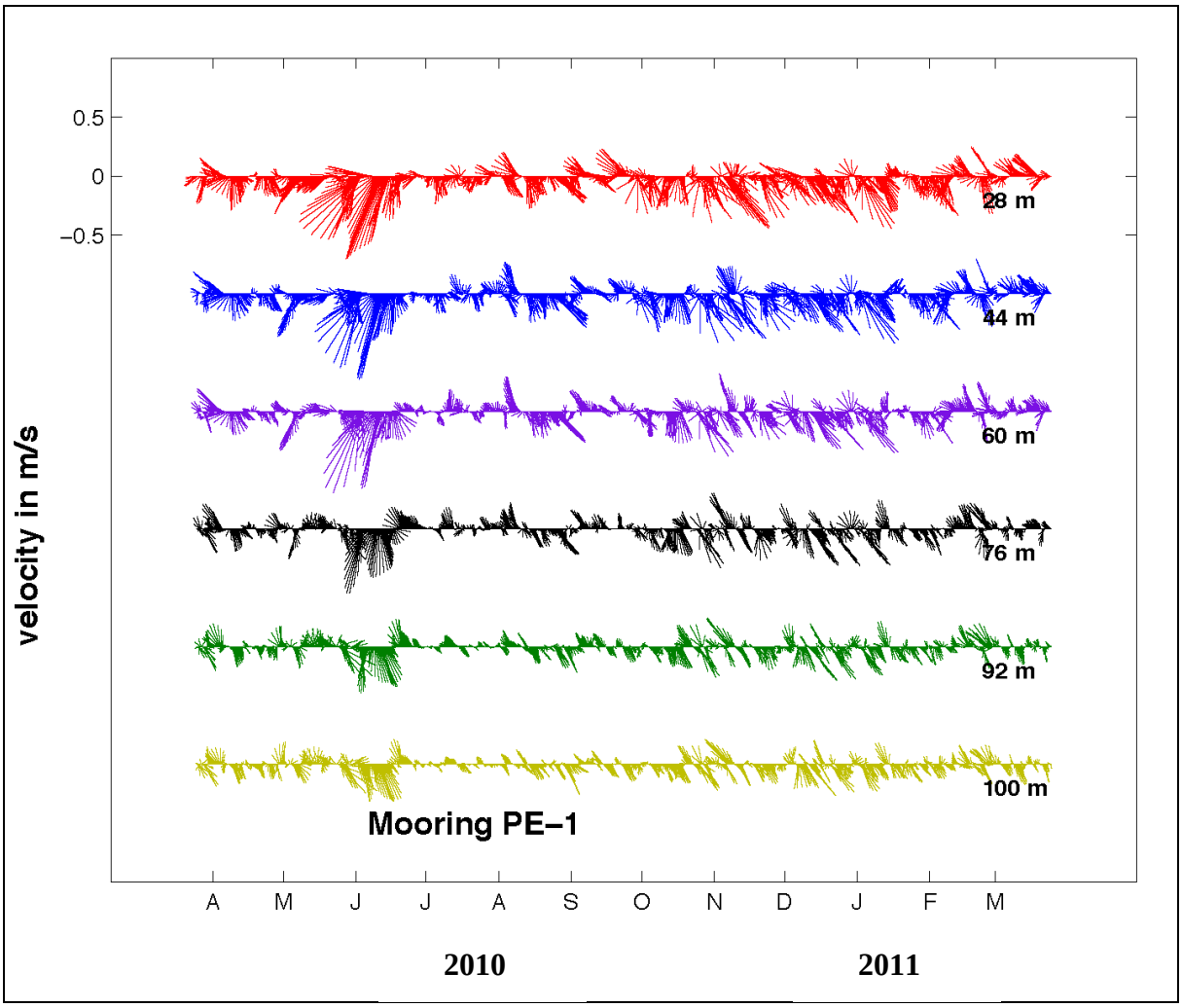

Figure 29. Vector time series from mooring PE1; different depths are indicated.

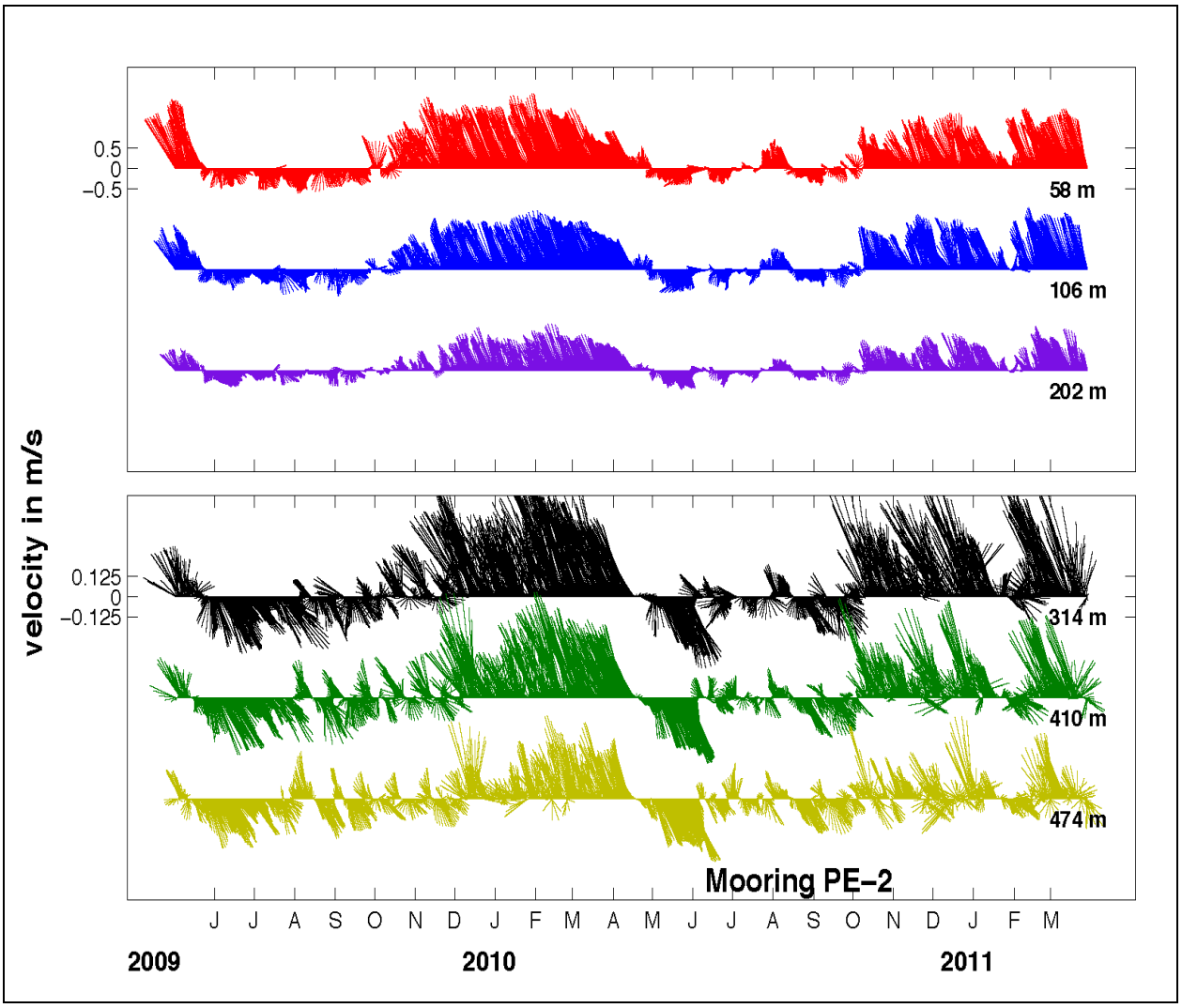

Figure 30. As in Figure 29 from mooring PE2. Note the change in the velocity scale.

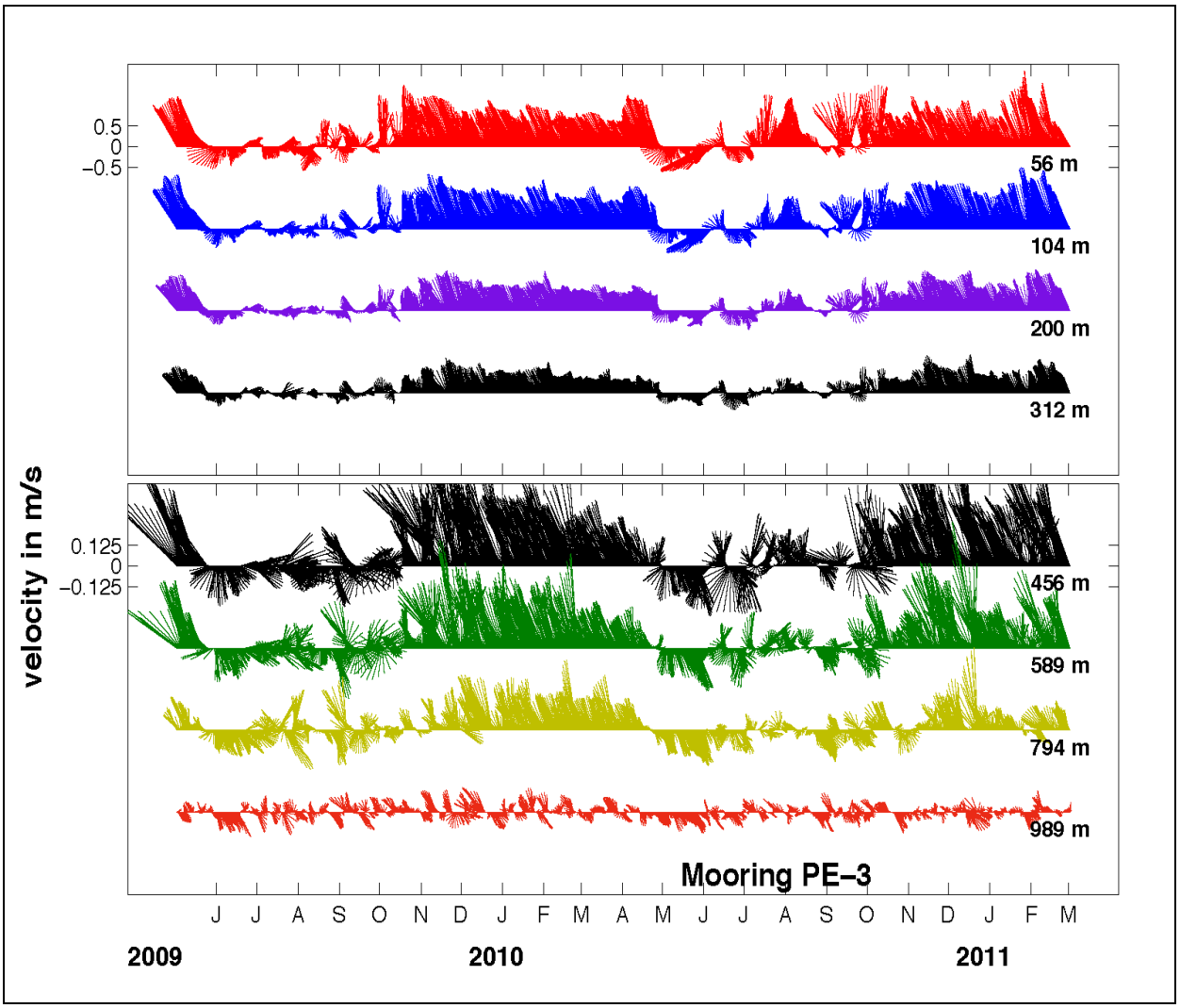

Figure 31. As in Figure 29 from mooring PE3. Note the change in the velocity scale.

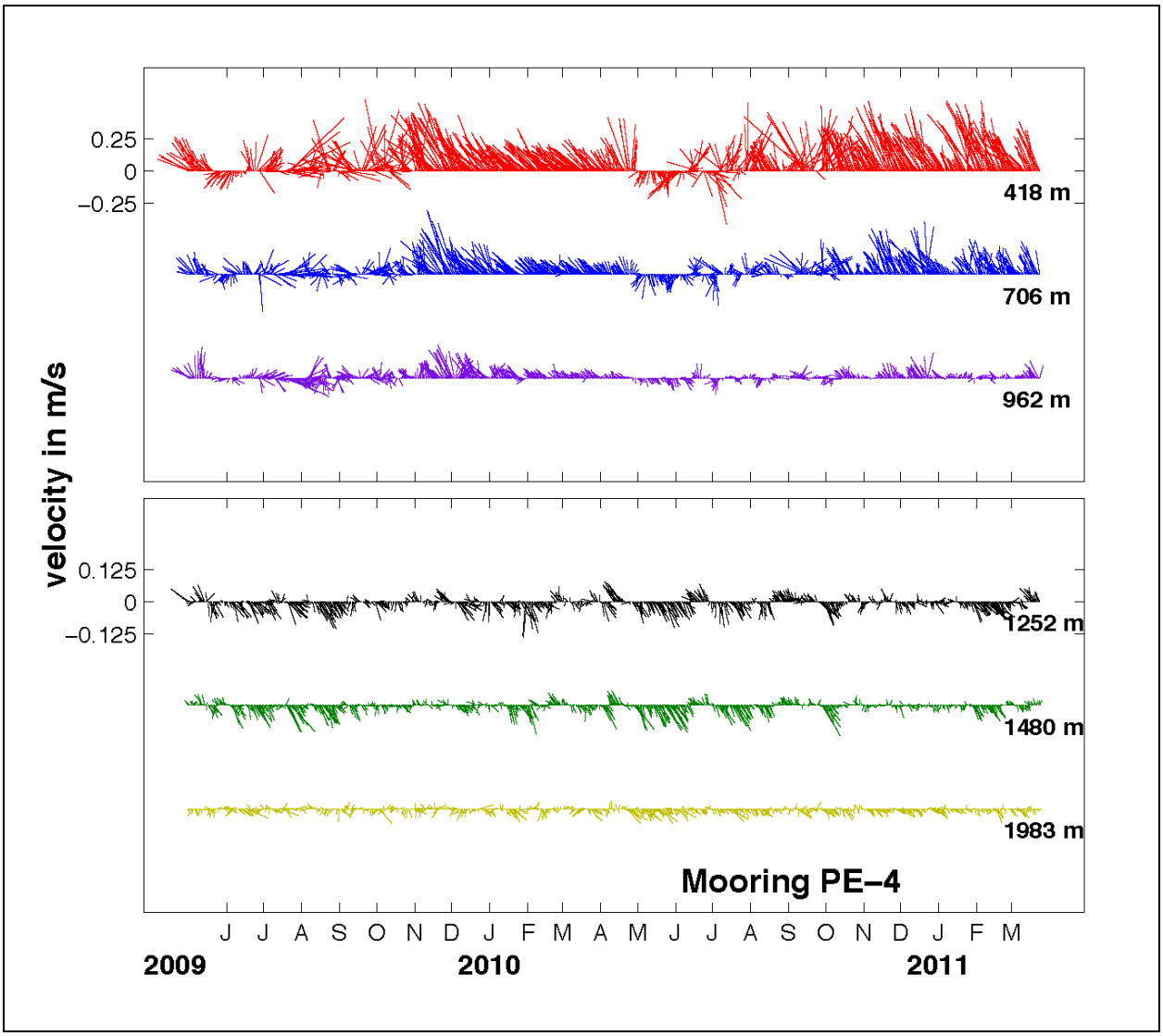

Figure 32. As in Figure 29 from mooring PE4. Note the change in the velocity scale.

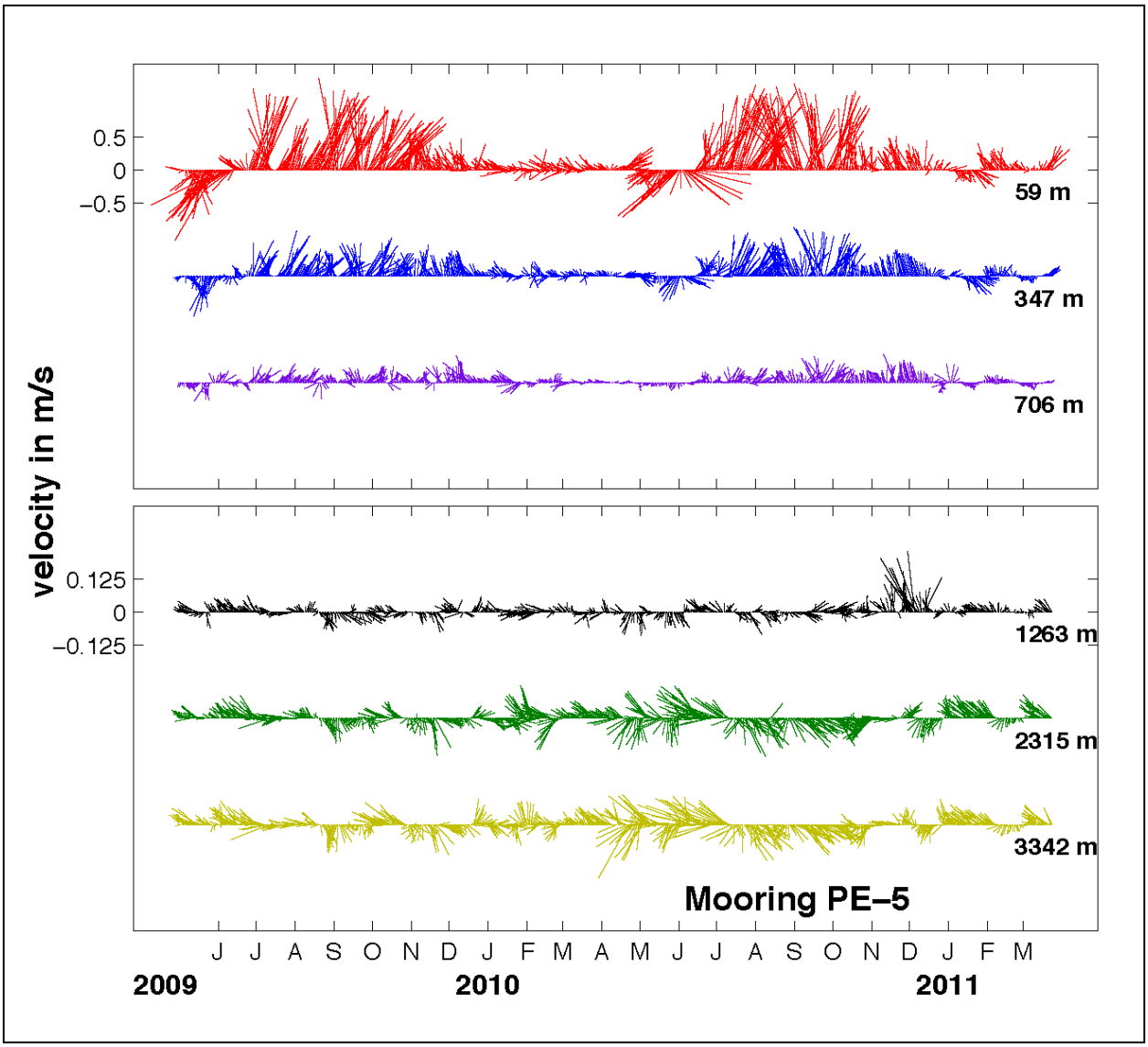

Figure 33. As in Figure 29 from mooring PE5. Note the change in the velocity scale.

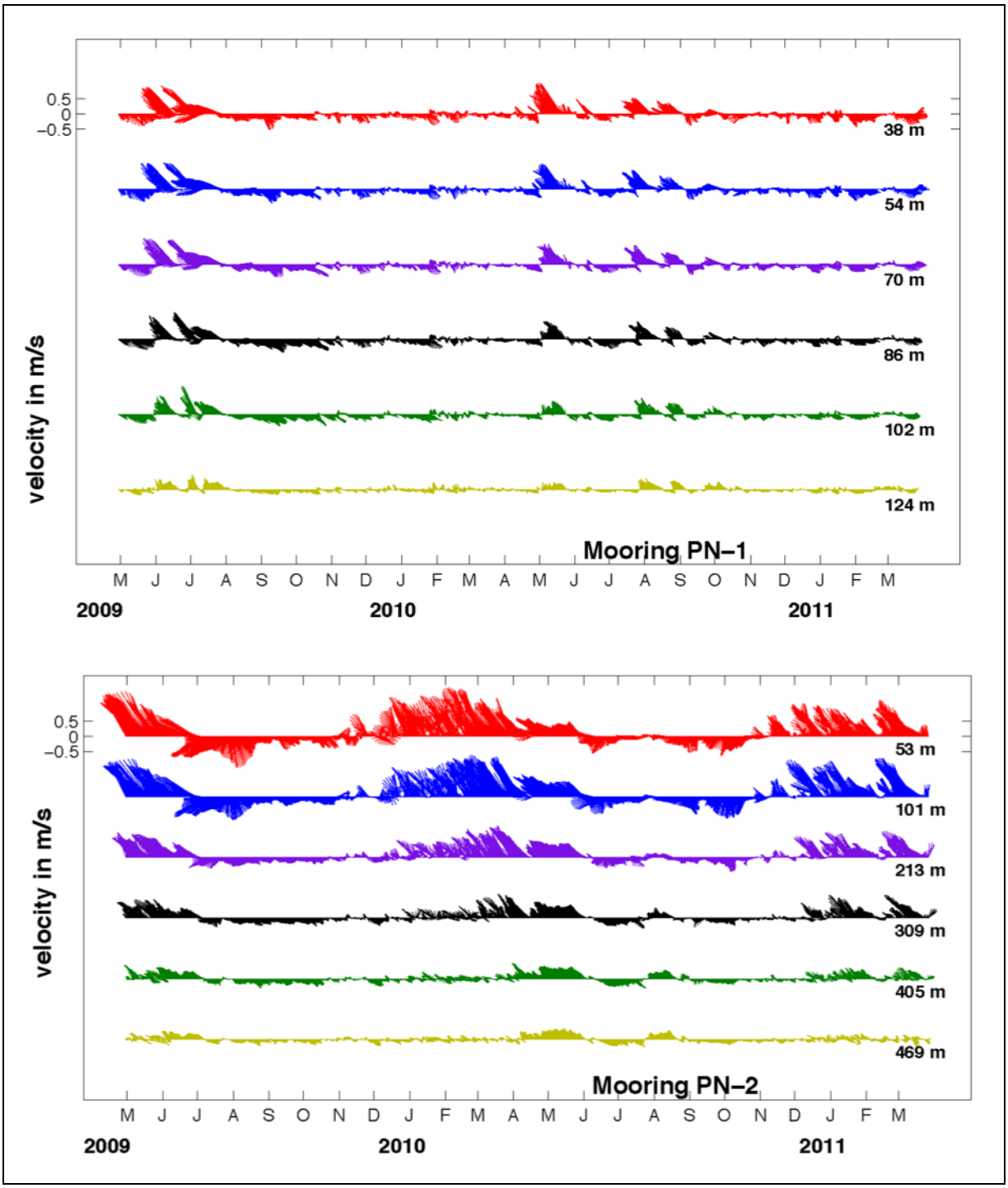

Figure 34. Vector time series from moorings PN1 and PN2, different depths are indicated.

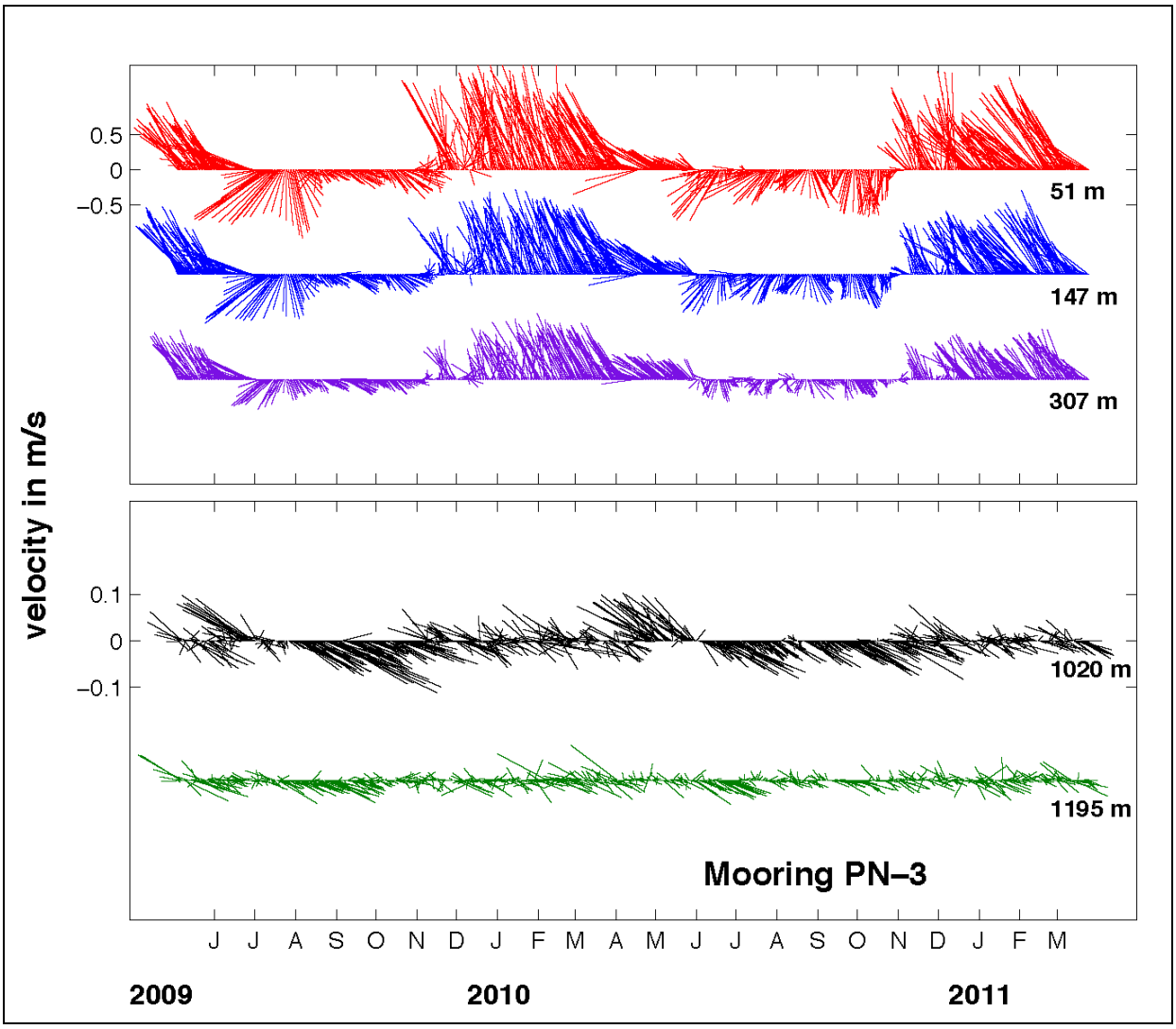

Figure 35. As in Figure 34, from mooring PN3. Note the change in the velocity scale.

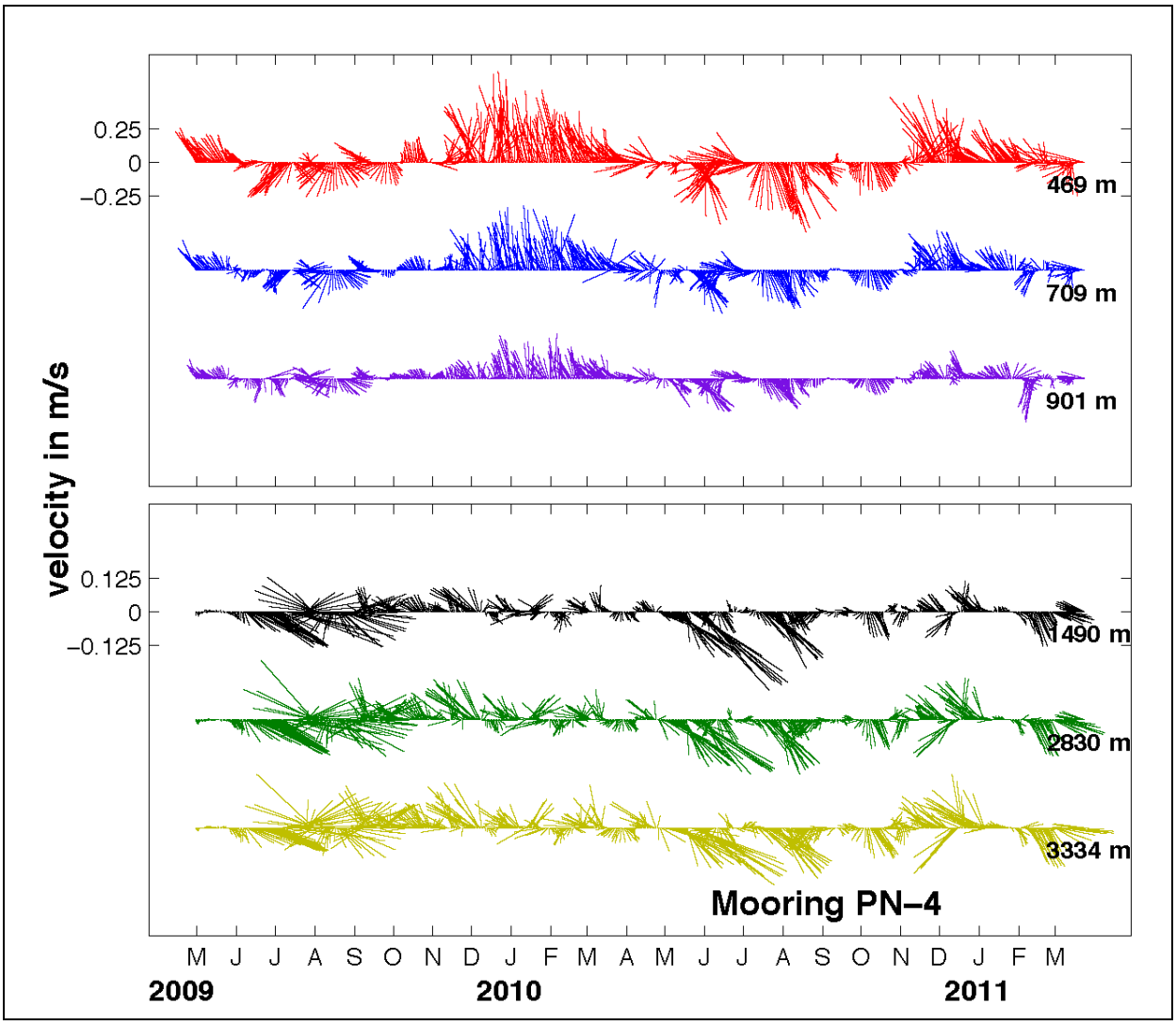

Figure 36. As in Figure 34, from mooring PN4. Note the change in the velocity scale.

3.2 EMPIRICAL ORTHOGONAL FUNCTION ANALYSIS

Using Empirical Orthogonal Function (EOF) analysis of the currents in each mooring, one can decompose the variance of the currents into vertically coherent patterns that can help understand the behavior of the variability observed on each mooring. Depending on the degree of polarization of the current data being analyzed, one can either arrange the data along independent components (zonal and meridional), maintaining the analysis in the real domain, as done here, or combine the horizontal currents into a complex vector. For the case when the observed currents are not well polarized, the complex arrangement usually results in a more compact and clear representation of the patterns. In our present case, the EOF analysis was computed for each mooring independently, also to evenly weight current observations in the vertical and to take into account the longest measurement interval, currents were linearly interpolated to nominal depths (20 m) using only the longest common time series in each mooring.

The first two modes of the subinertial currents were grouped in a map showing the spatial structure of the average vector, considering the vectors above 500 m depth of both modes for all the moorings; although the EOF analyses were processed separately for each mooring and considering all the data throughout the water column (Figure 37). The first mode usually represents more than about 60% of the variability of the currents in the vertical profile at each mooring, for the second mode the percentage of explained variance varies around 10–30%. In the central channel, where variability-ellipse analysis indicates the mean current is larger than the variability, YUC5, YUC6, and YUC7 show a common spatial behavior, as well as the vertical structure of EOF1, which are mainly oriented in the along-channel direction, while EOF2 shows rather a cross-channel orientation. The EOF time series are also called Principal Components (PC). From PC1 series it can be observed that between July and October, current on the central channel is more intense (positive anomalies), while currents over the western side have negative anomalies, indicating a slower flow (Figure 38). In the western channel, the fist EOF of moorings YUC2 and YUC3 represents high-frequency variability (see PCs of Figure 38), which are highly correlated (Table 3). Variability in YUC7 has an inverse behavior relative to the western side of the channel (YUC2, YUC3 and YUC5), but does not show this high-frequency variability.

Table 3. Correlation values between principal components of moorings at the YC (upper half of the table), considering only the first EOF mode over the 500 m depth; 95% significant (not significant) values are indicate in black (gray). Blue values represent the effective degrees of freedom, calculated from the expression given by Chelton (1983), which considers the cross-covariance between the series.

Moorings	YUC2	YUC3	YUC5	YUC6	YUC7
YUC2		0.82	0.35	-0.19	-0.5
YUC3	56		0.49	-0.19	-0.58
YUC5	68	32		0.39	-0.56
YUC6	91	73	59		0.24
YUC7	51	34	25	48	

The EOF analysis unveiled an interesting behavior of currents at sections PE and PN (Figure 37). In all the moorings, vectors of the first mode are oriented parallel to the bathymetry, with variability exceeding 0.5m/s, especially in moorings over the slope and diminishing in intensity toward higher depths. The EOF2 vectors are all oriented perpendicular to the bathymetry and with a similar intensity of about 0.3 m/s. Mooring PE5, however, shows different orientations in both modes compared to moorings over the slope. This is probably caused by a change in the bathymetry at this position, so even if different from the others, EOF1 (EOF2) vectors at PE5 remain oriented parallel (perpendicular) to the bathymetry. The PC1 corresponding to the first mode at mooring PE1 is the only one of this section that shows high frequency variability in winter, similar to the one observed in the near-coast moorings in Yucatan Figure 40). The PC1 of modes at PE2 and PE3 (over the slope) have, in general, an inverse behavior than the PC1 of PE5, with PE4 showing a less coherent anti-correlation (a sort of transition). That is, positive (northward) anomalies at PE5 indicating intensification of the LC there are associated with negative anomalies over the shallower slope at moorings PE2 and PE3. This suggests an off-shore movement of the LC core. In contrast to section PE where most of the high frequency variability is contained in the second mode PC2 (Figure 41), the first mode at section PN (Figure 42), shows high frequency variations particularly between January and May, 2010, along the slope, i.e., at moorings PN2 and PN3. High frequency variability (in this first mode), is weaker during the winter of the second period.

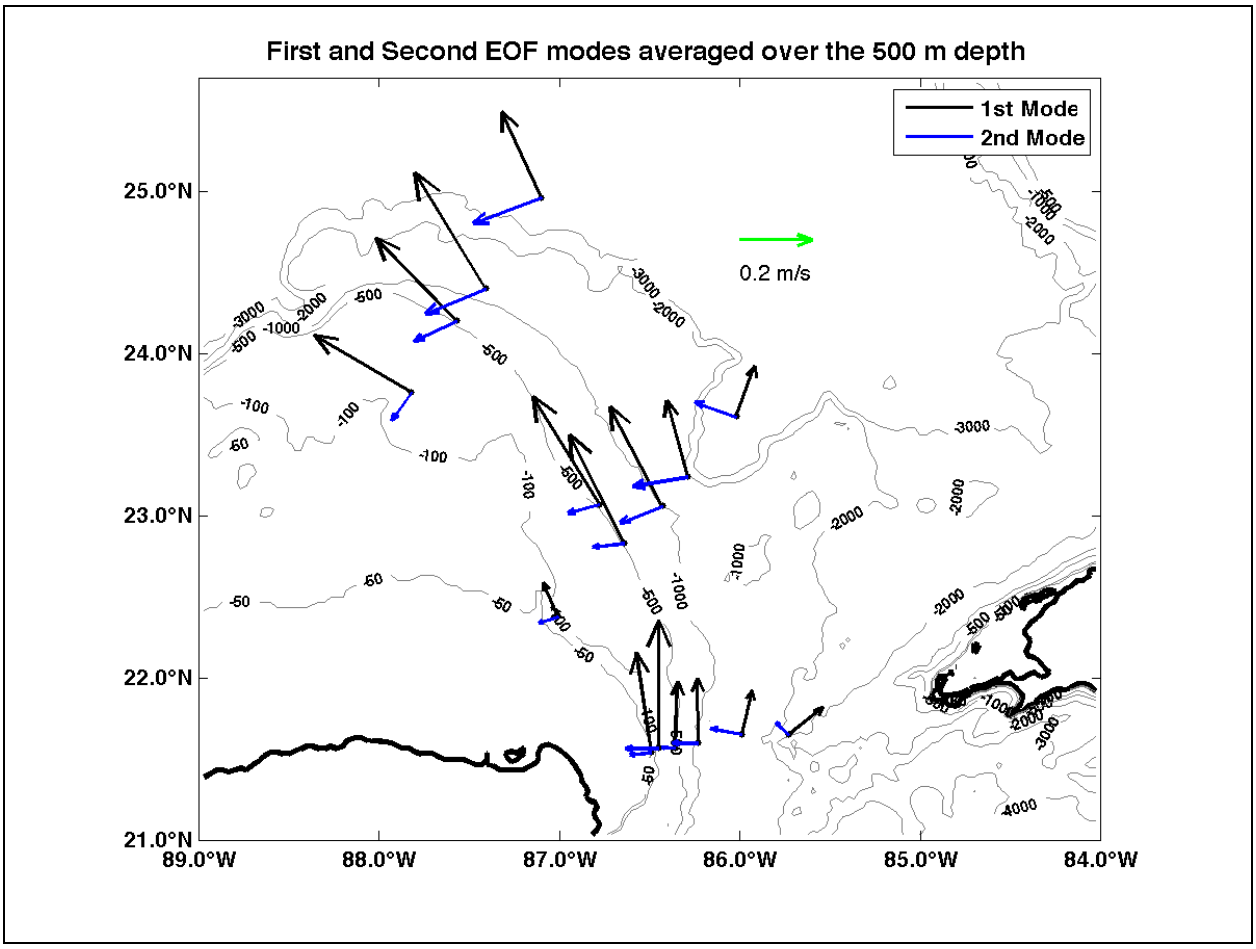

Figure 37. Map of the spatial structure averaged over the 500m depth of the first (black arrows) and second (blue arrows) EOF modes, calculated for each mooring individually.

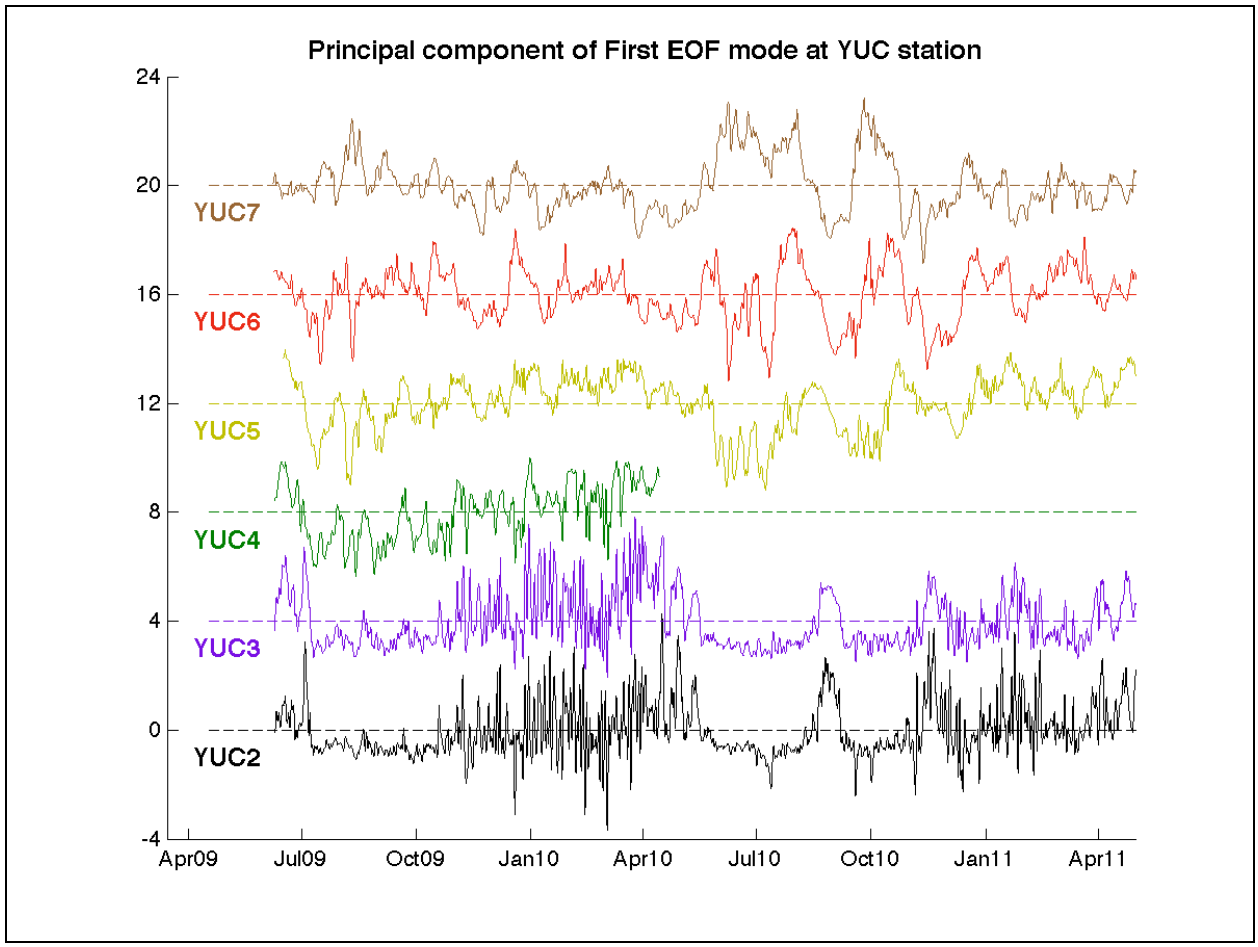

Figure 38. Time series (also called principal components) of the first EOF modes at the YC; time series are lagged by 4 for clarity.

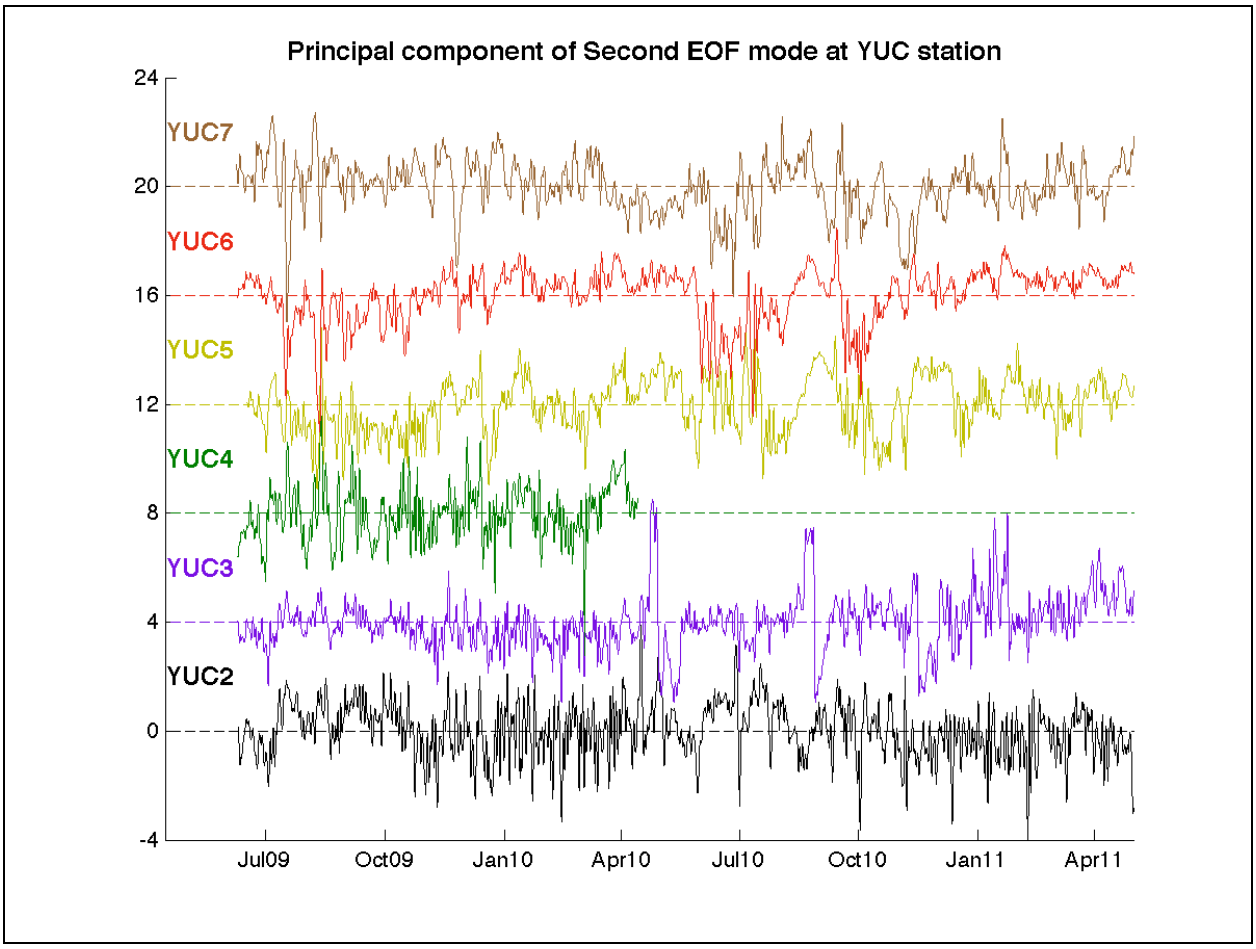

Figure 39. As Figure 38, of the second EOF modes at the YC.

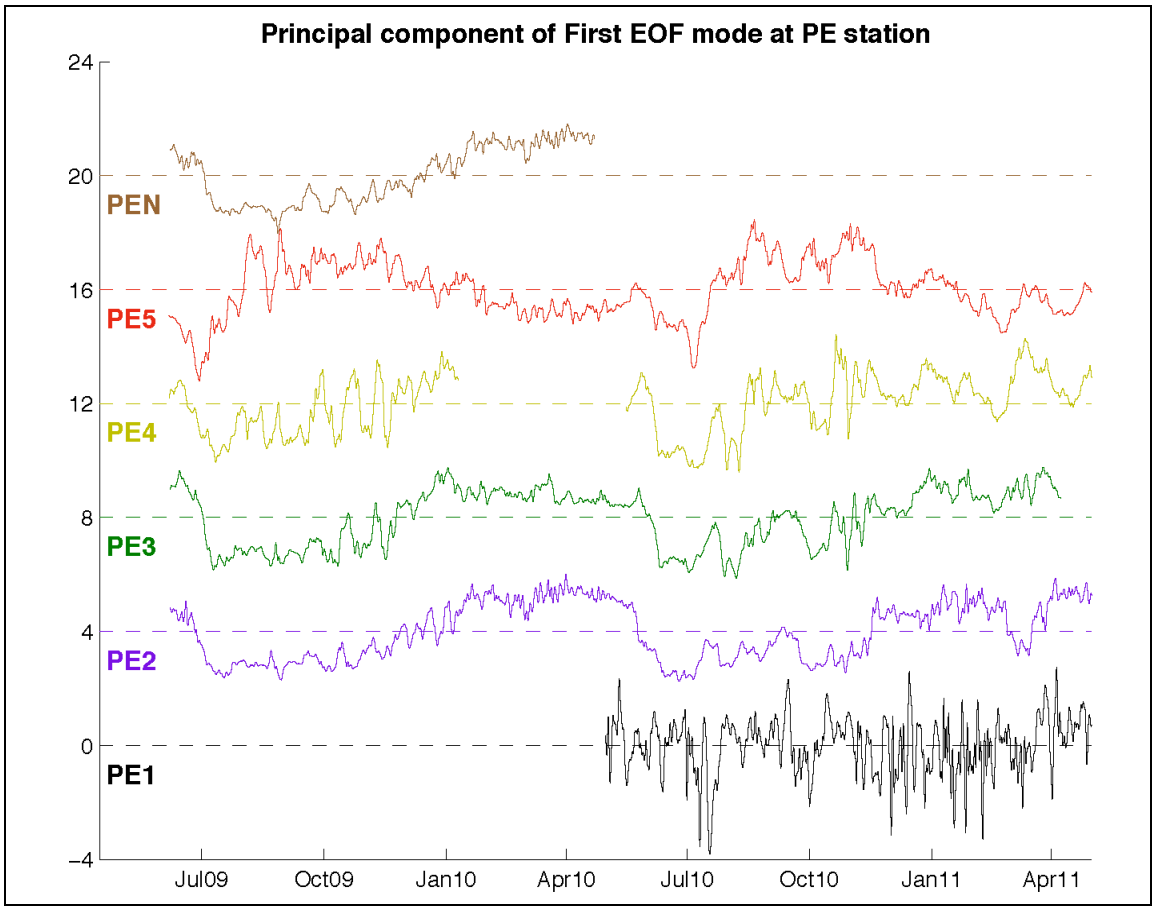

Figure 40. Time series (also called principal components) of the first and EOF mode for section PE. Vertical axis is shifted 4 units for each time-series for clarity.

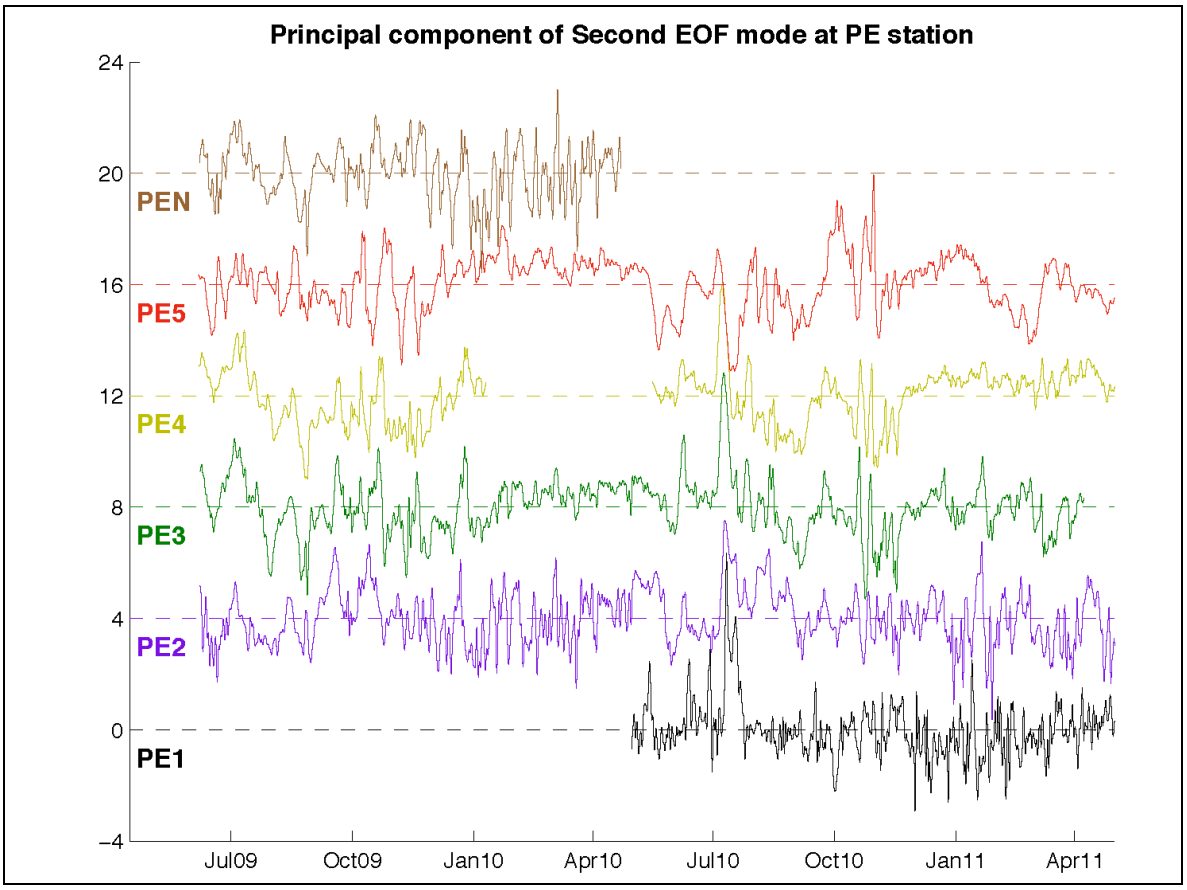

Figure 41. As Figure 40, of the second EOF mode for section PE.

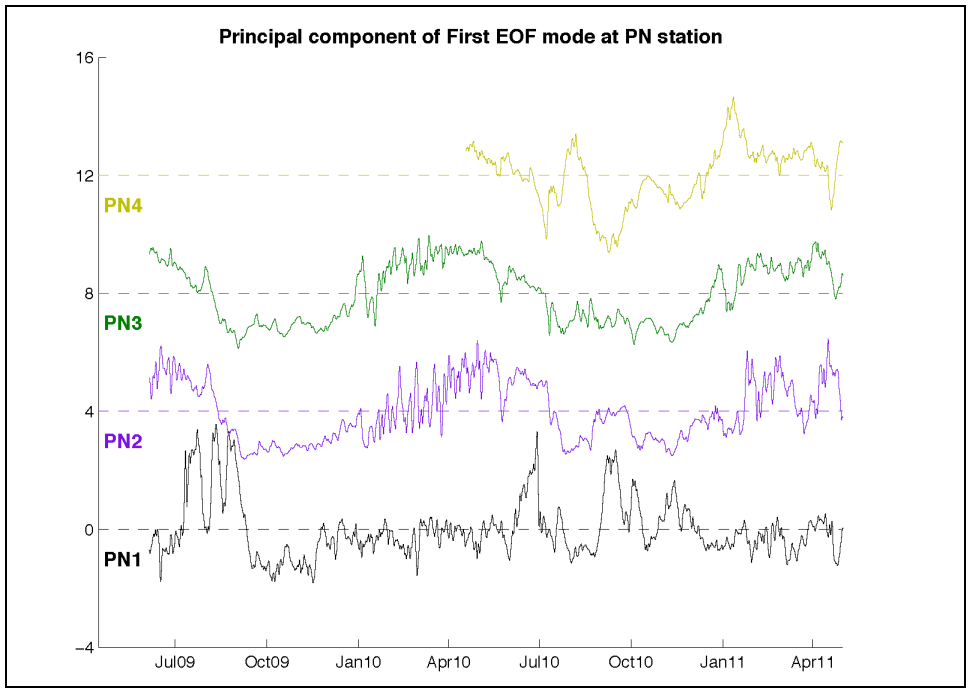

Figure 42. Time series (also called principal components) of the first EOF mode for section PN. Vertical axis is shifted 4 units for each time-series for clarity.

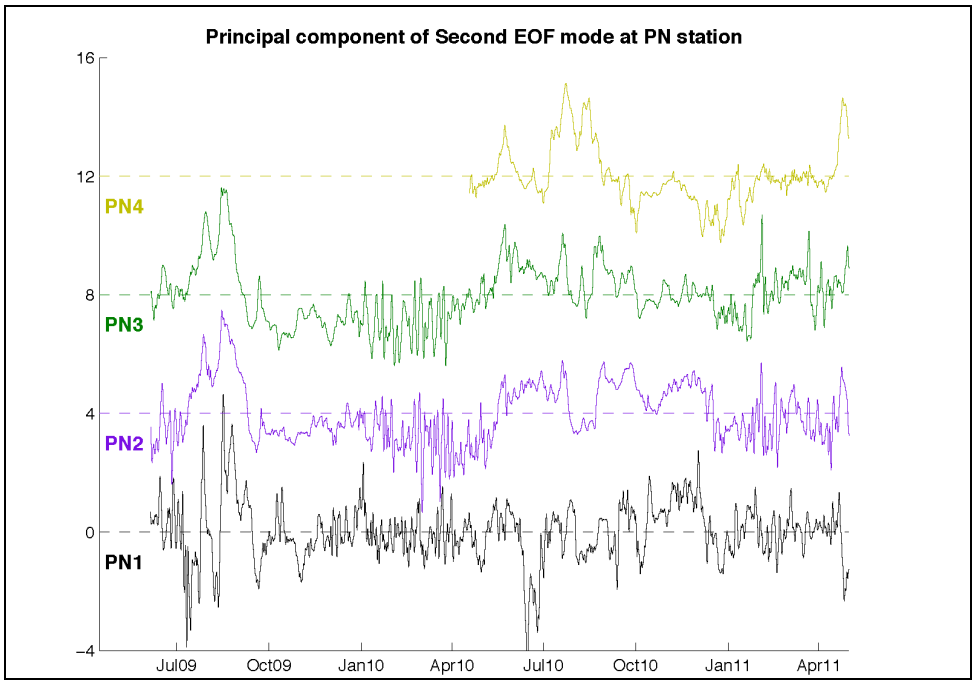

Figure 43. As Figure 42, of the second EOF mode for section PN.

The variance presented by the second mode is of higher frequency than the first mode with PC2 series showing, in occasions, events consisting of strong (high amplitude) pulses that appear to propagate in the mooring arrays, particularly on sections PE and PN. Notice the small lag between the timing of the pulses on moorings over the slope with respect to the one in the deep moorings, width the pulses appearing first in the shallower moorings. These pulses do not show a clear seasonal preference (see Figure 41 and Figure 43).

Figure 44 to Figure 58 shows the vertical structure of the first two EOFs at each mooring as well as their principal components. Current anomalies represented by the first mode are generally unidirectional with current speed decreasing with depth. Over the Yucatan slope (YUC3, YUC4, and YUC5), a change in direction is observed in the second mode of variability suggestive of a first baroclinic mode structure (see Figure 44 and Figure 45).

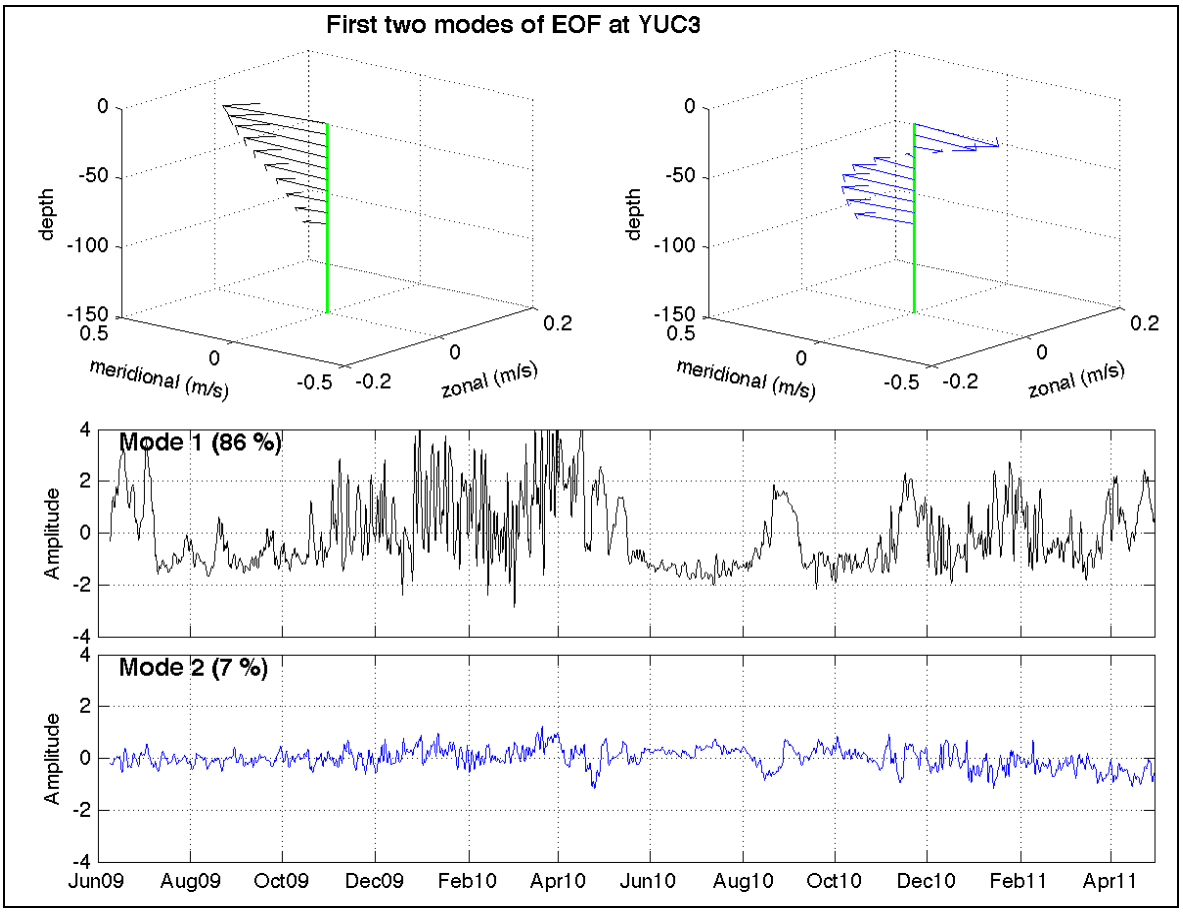

Figure 44. First two EOF modes for the observed subinertial current calculated for mooring YUC3 at the YC. Spatial structure and its principal component are indicated for the first (black) and second (blue) modes.

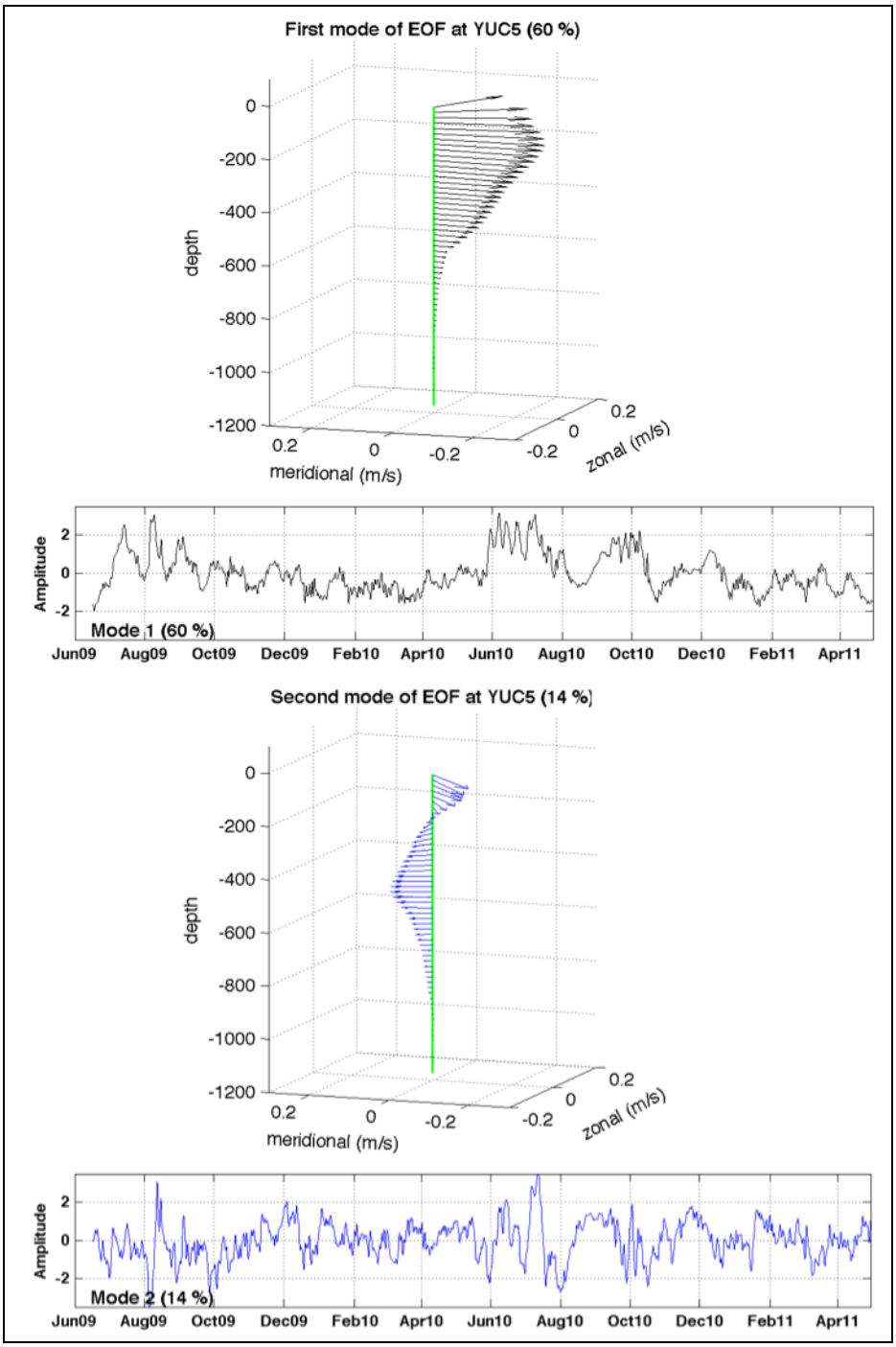

Figure 45. As in Figure 44, for mooring YUC5 at the YC.

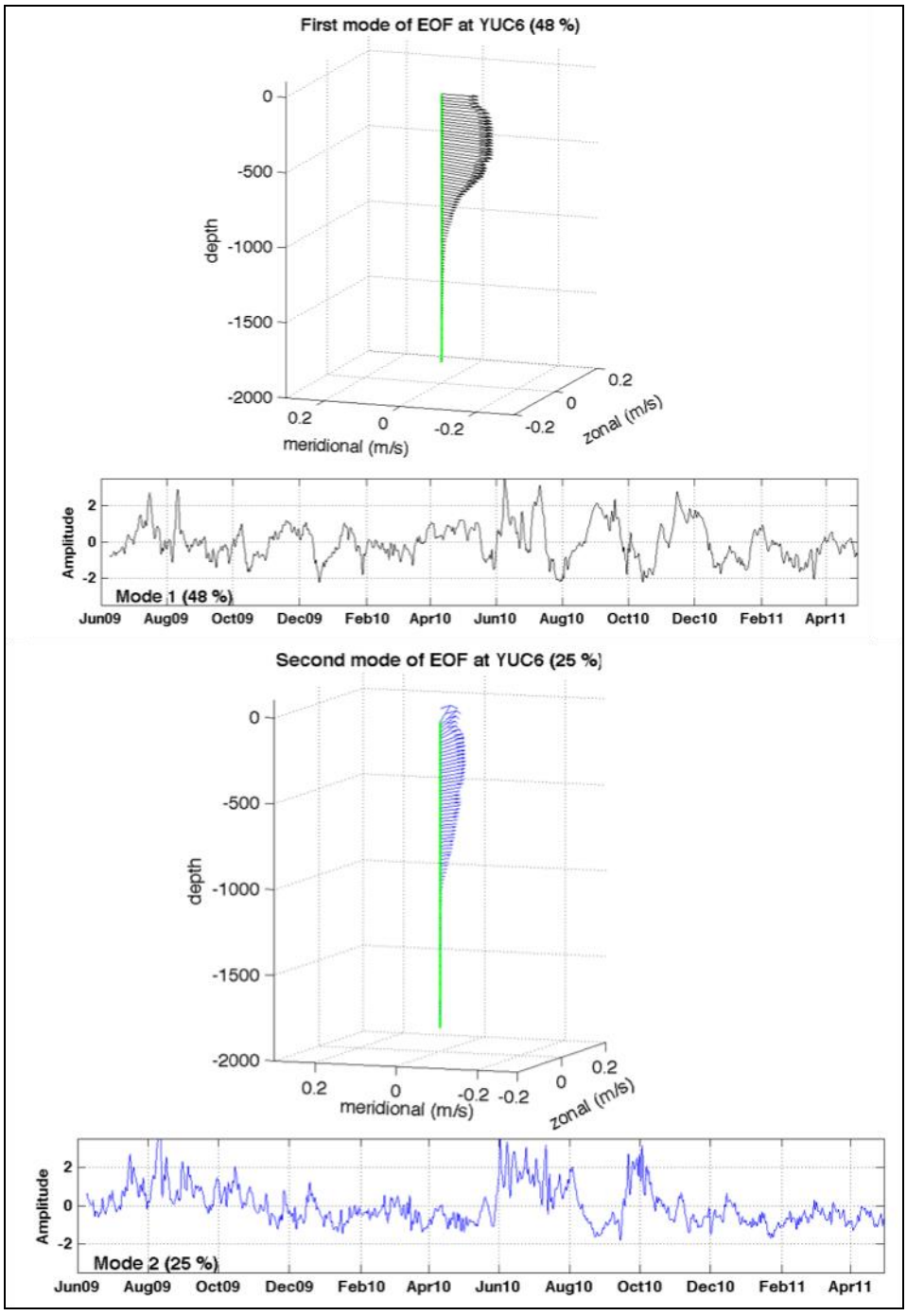

Figure 46. As in Figure 44, for mooring YUC6 at the YC.

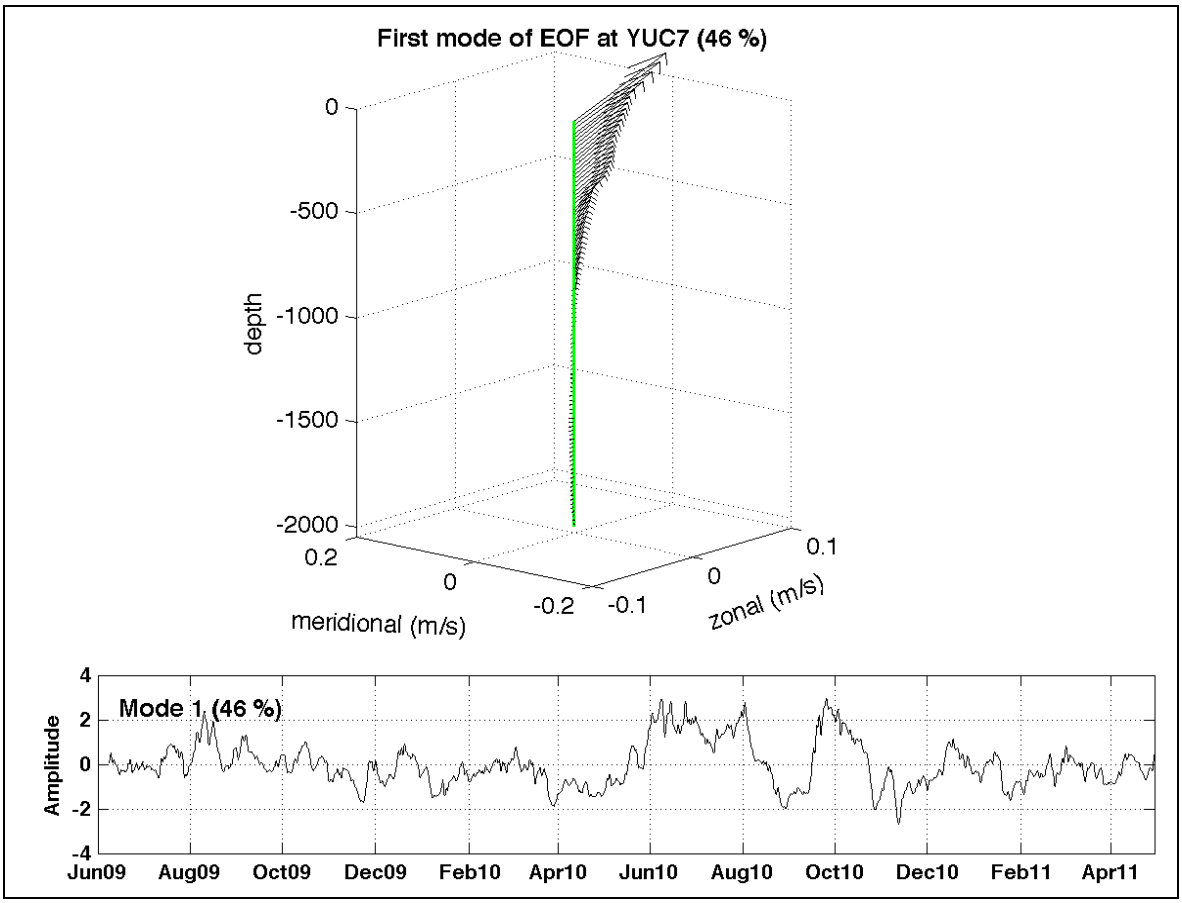

Figure 47. As in Figure 44, for mooring YUC7 at the YC.

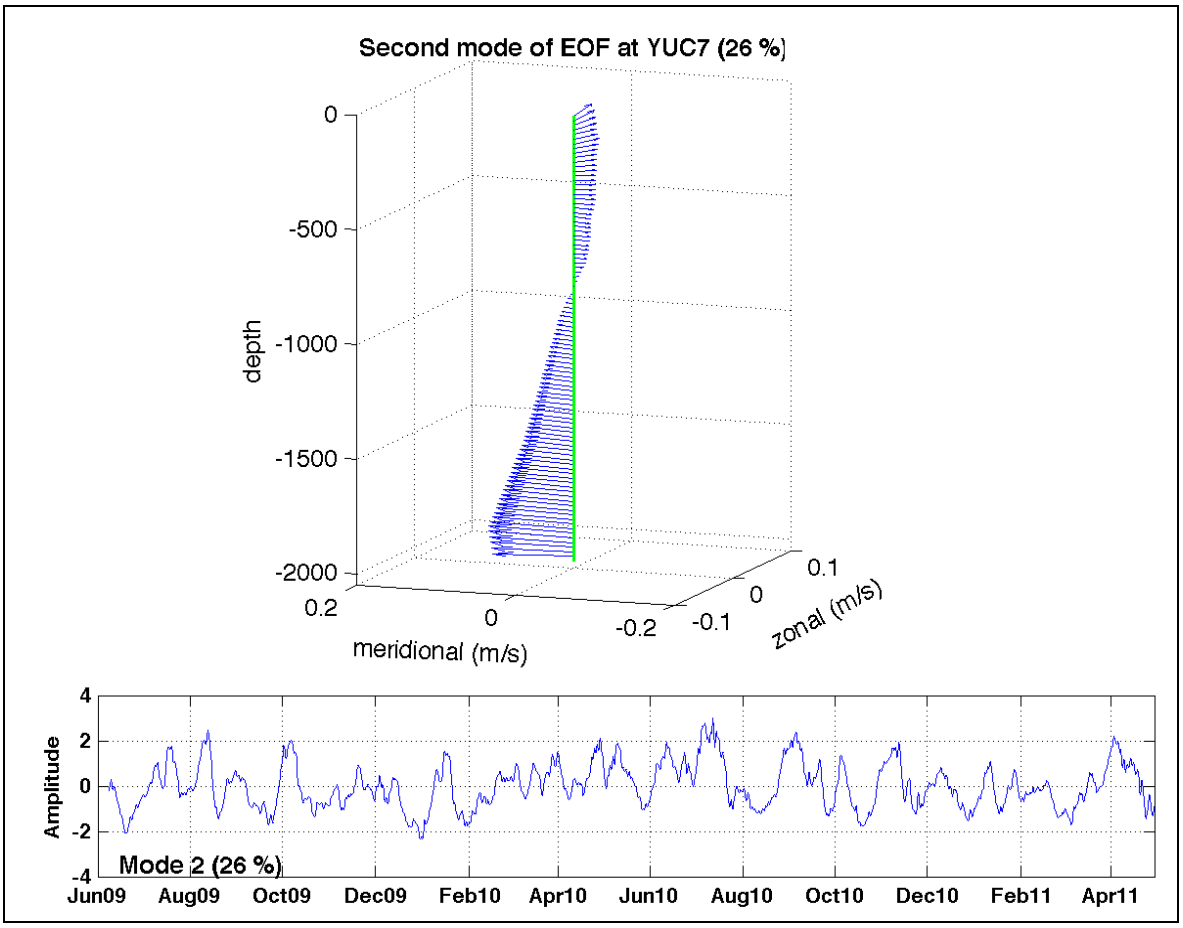

Figure 47.Continues.

EOF analysis was performed individually to velocity time series of current meters, for moorings YUC6 and YUC7 at different depths, to evaluate the correlation of the principal components in the central deep portion of the YC. Current PCs at YUC6 (Figure 48) show high-frequency variability that is correlated below 1000 m depth (correlation values are significant at 95% confidence level). Interestingly, variability between ~1000 and ~1900m are significantly correlated (r= 0.47). For YUC7 (Figure 49), variability below 1500m depth are highly correlated (r > 0.9), showing pulses of the same amplitude throughout this part of column, down to ~2000 m depth. PC at 961 m have lower correlation with the deepest flow, but still significant (r= 0.48), suggesting a different variability at this depth and below 1500 m depth. Correlation of PCs between YUC6 and YUC7 were not significant.

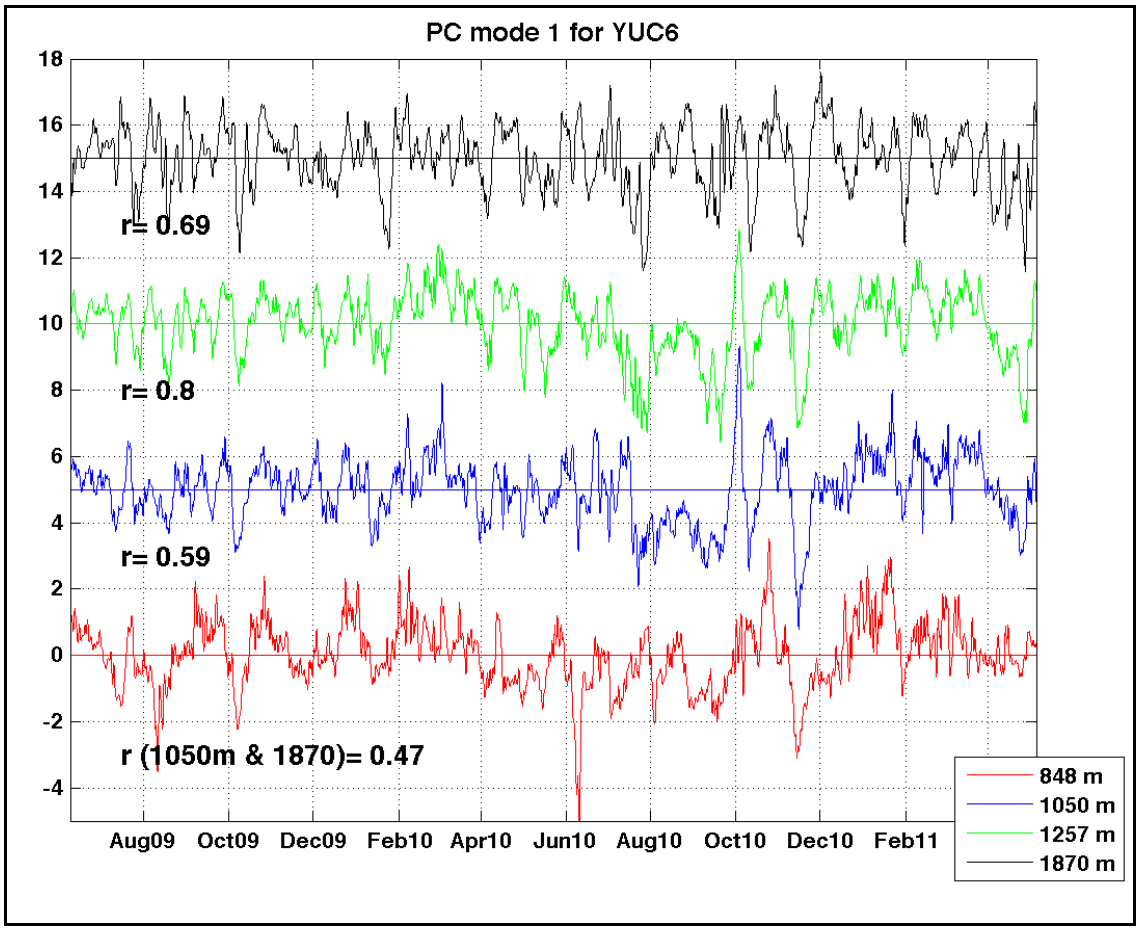

Figure 48. Principal components of the first mode EOF performed to currents time series below 800m depth for mooring YUC6, individually. Time series are offset by 5 units for clarity. Correlations values between contiguous series are indicated between them.

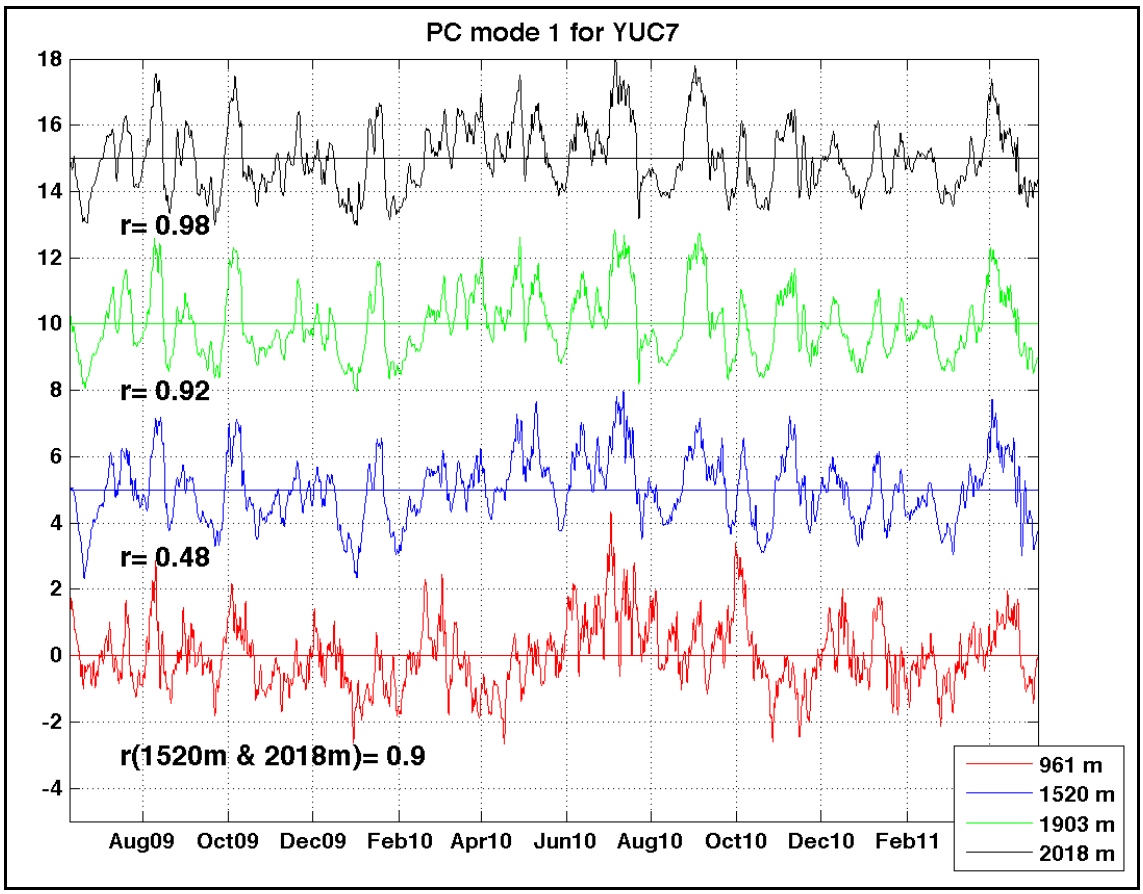

Figure 49. Principal components of the first mode EOF performed to currents time series below 800m depth for mooring YUC7, individually. Vertical axis is shifted 5 units for each time-series for clarity. Correlations values between contiguous series are indicated between them.

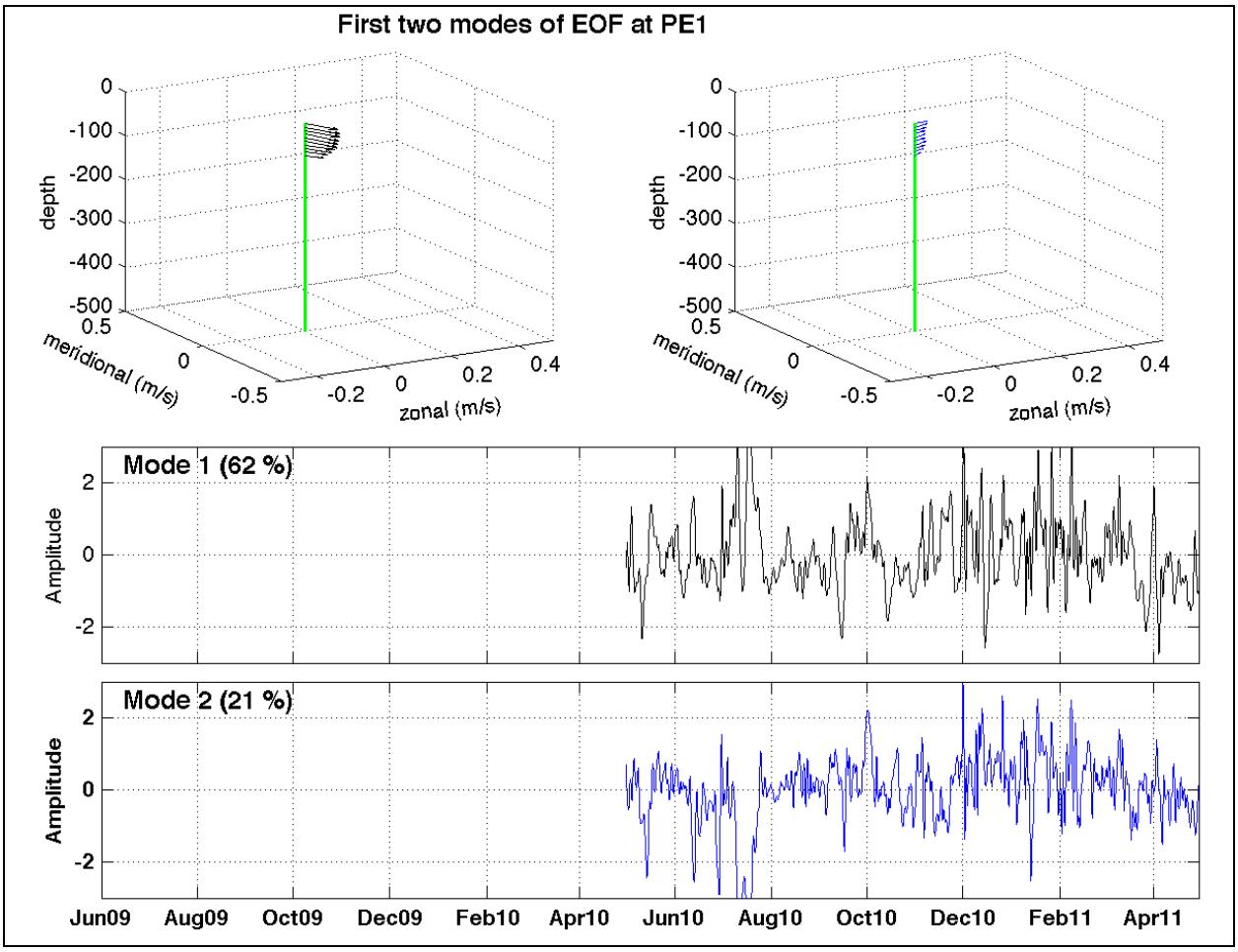

Figure 50. First two EOF modes for the observed subinertial current calculated for mooring PE1. Spatial structure and its principal component are indicated for the first (black) and second (blue) modes.

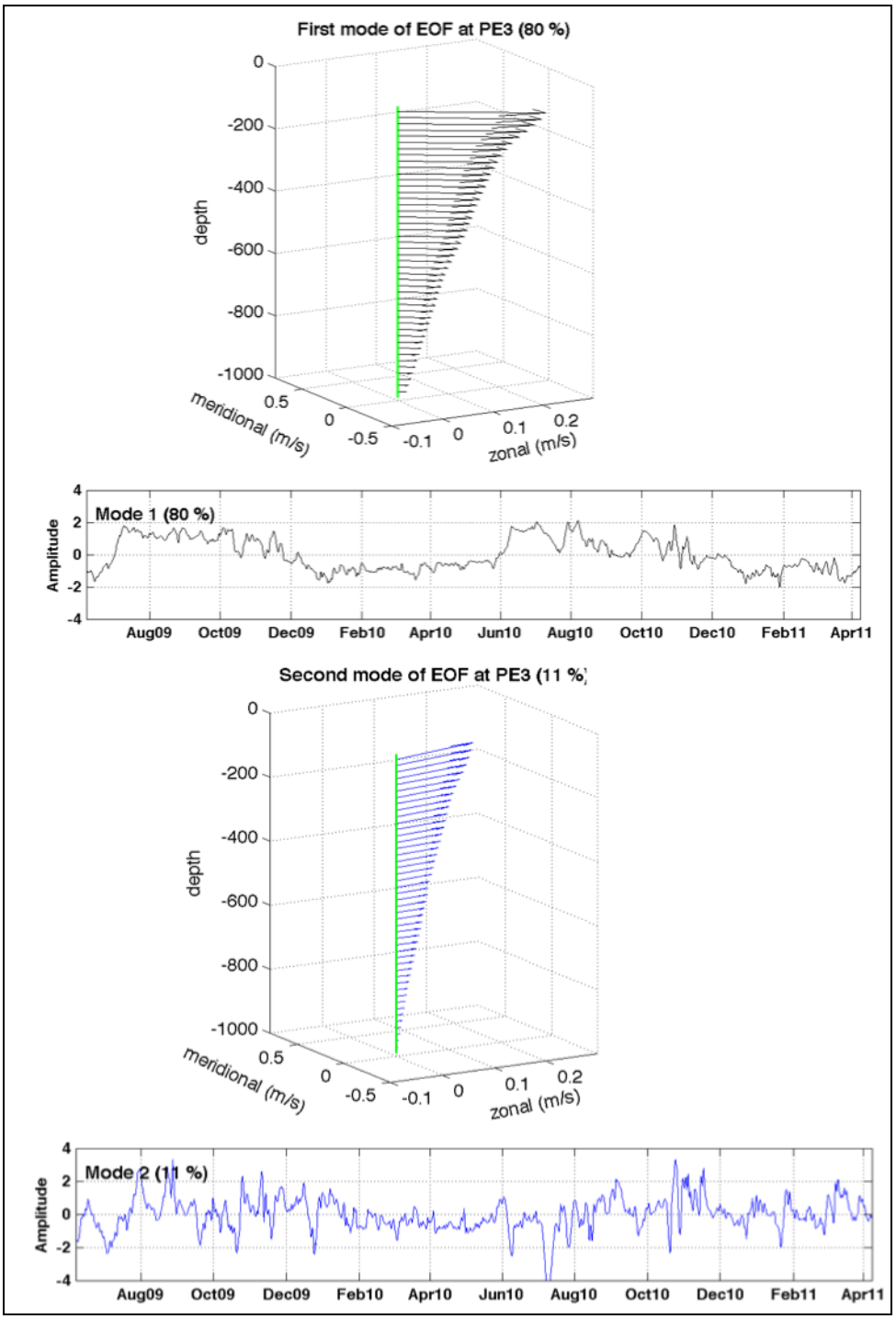

Figure 51. As in Figure 50, for mooring PE3.

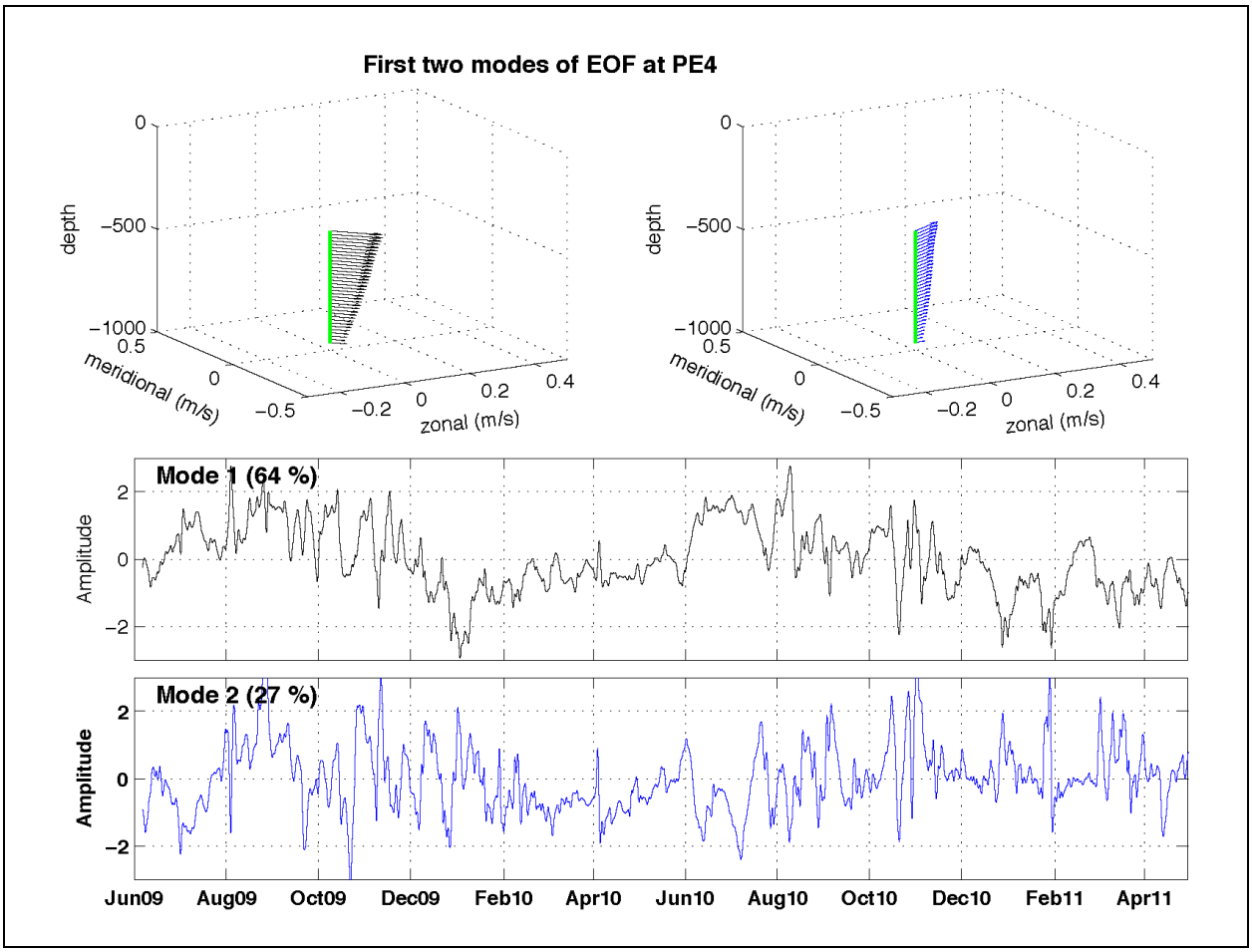

Figure 52. As in Figure 50, for ADCP installed at 1000 m depth at mooring PE4.

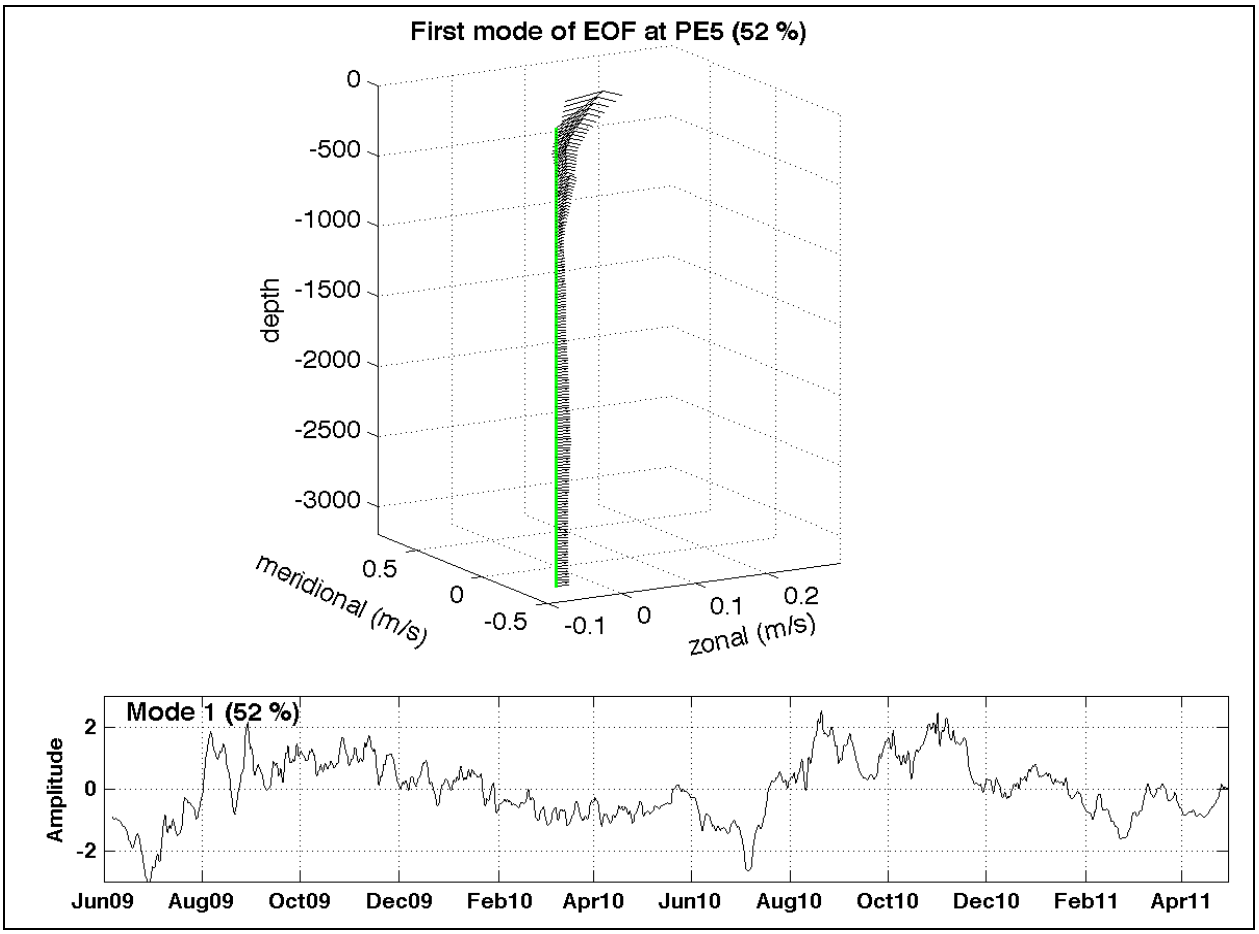

Figure 53. As in Figure 50, for mooring PE5.

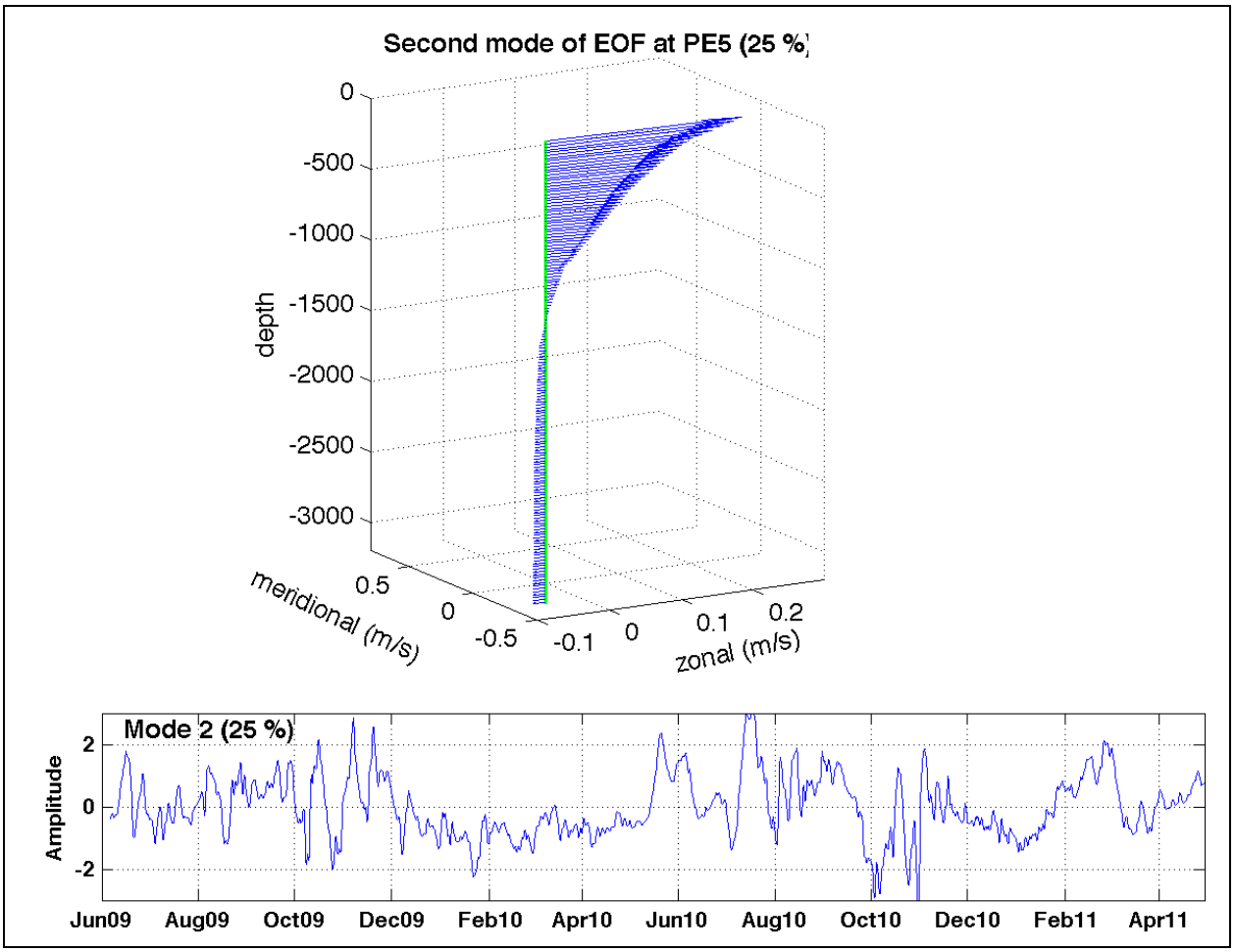

Figure 53. Continues.

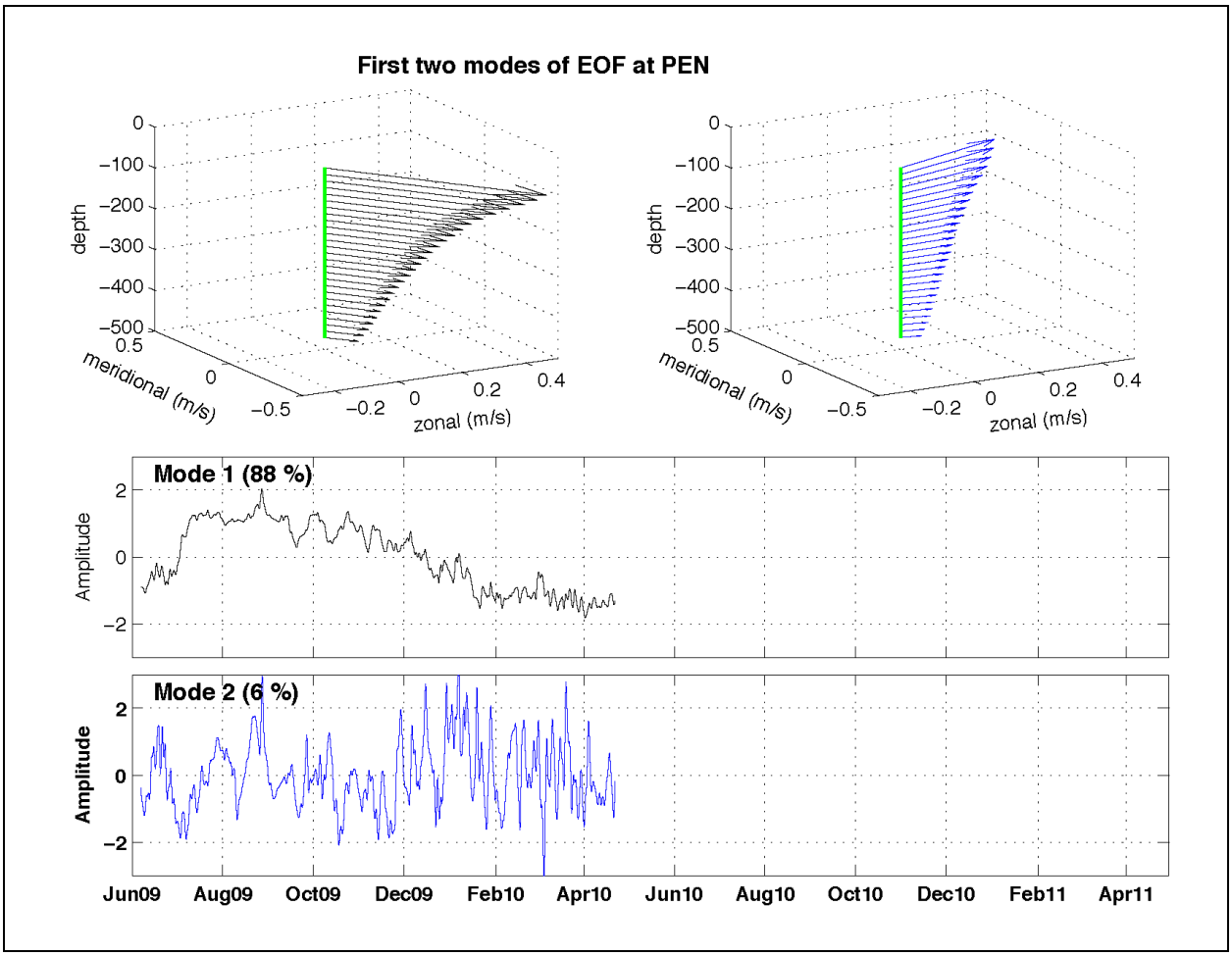

Figure 54**.** As in Figure 50, for mooring PEN.

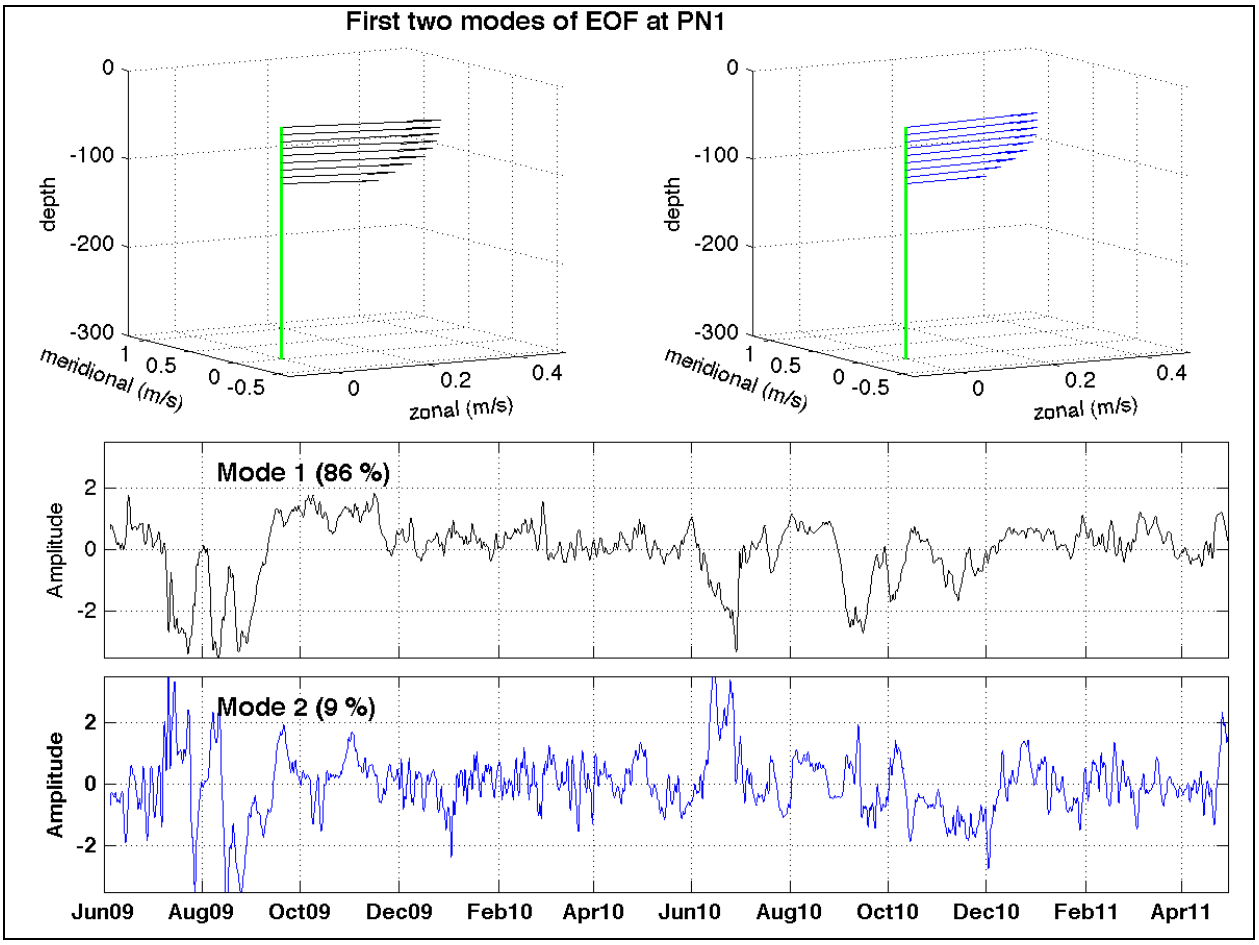

Figure 55. First two EOF modes for the observed subinertial current calculated for mooring PN1. Spatial structure and its principal component are indicated for the first (black) and second (blue) modes.

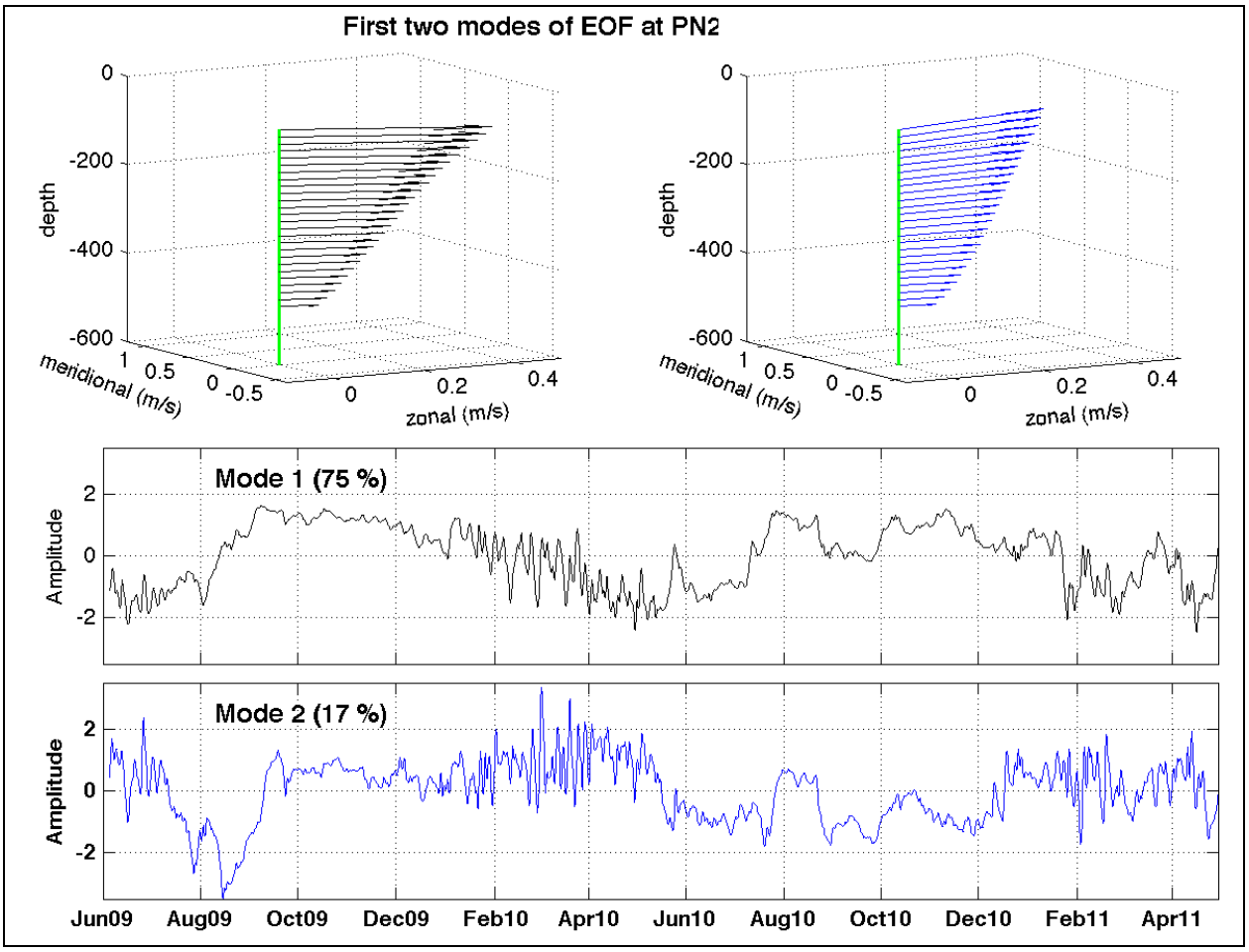

Figure 56. As in Figure 55, for mooring PN2.

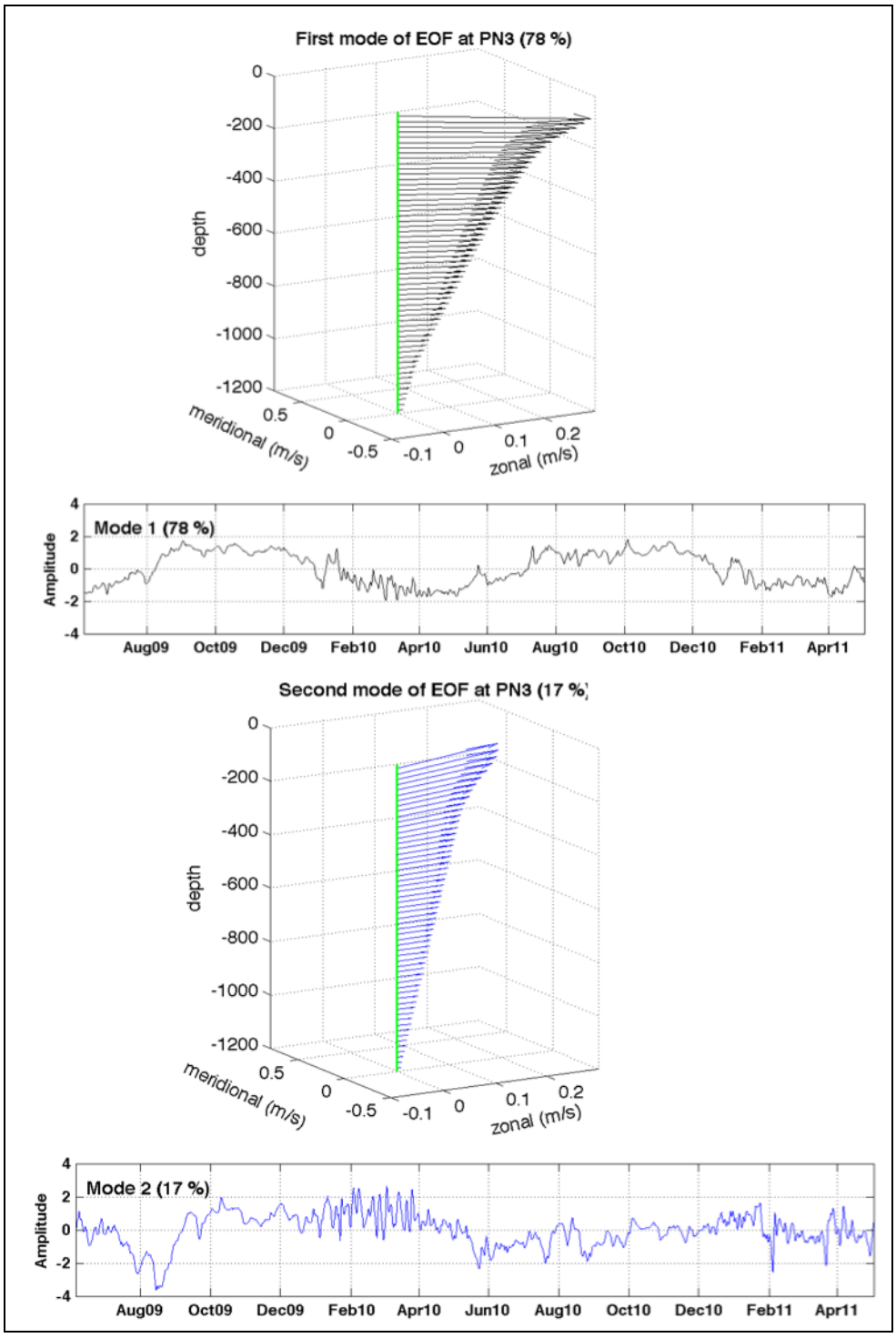

Figure 57. As in Figure 55, for mooring PN3.

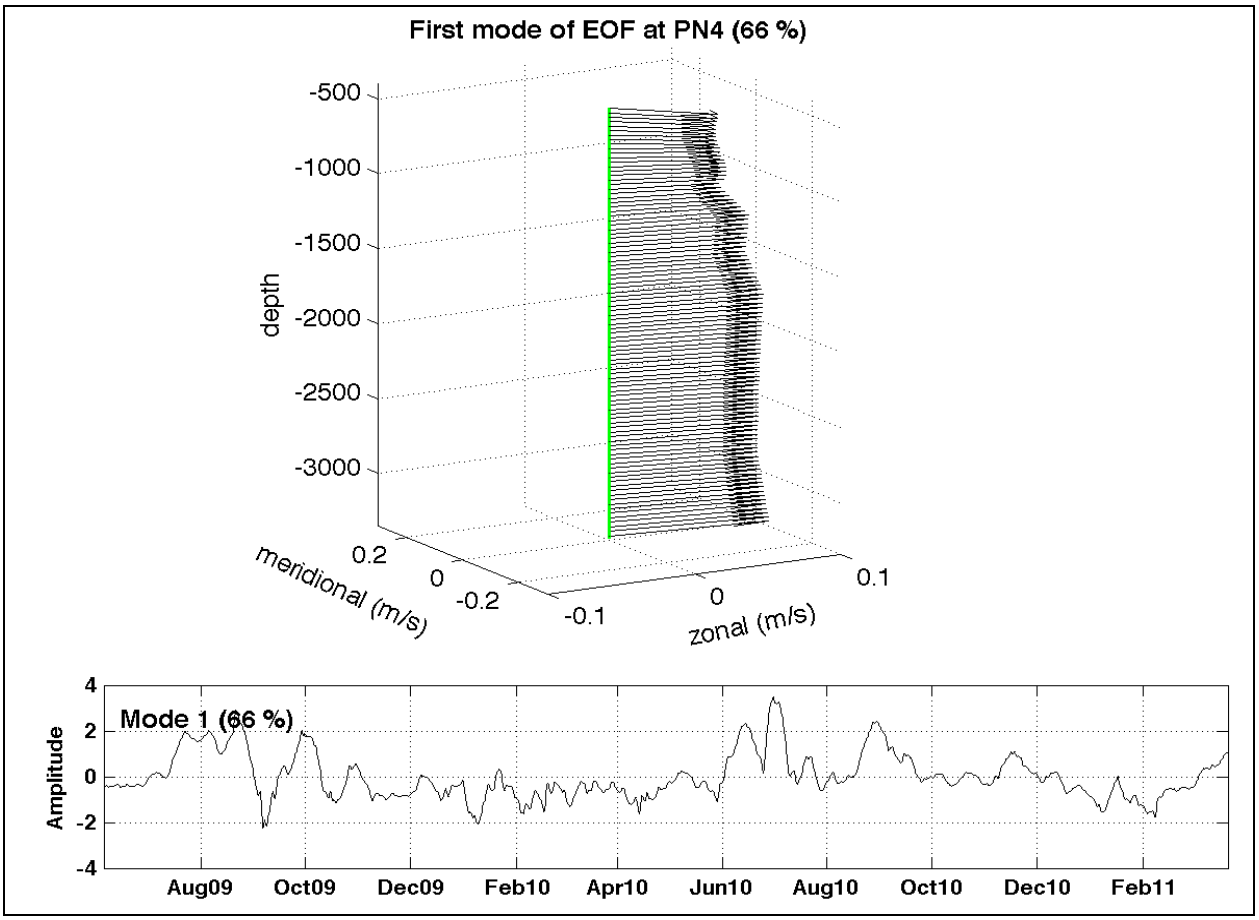

Figure 58. As in Figure 55, for mooring PN4.

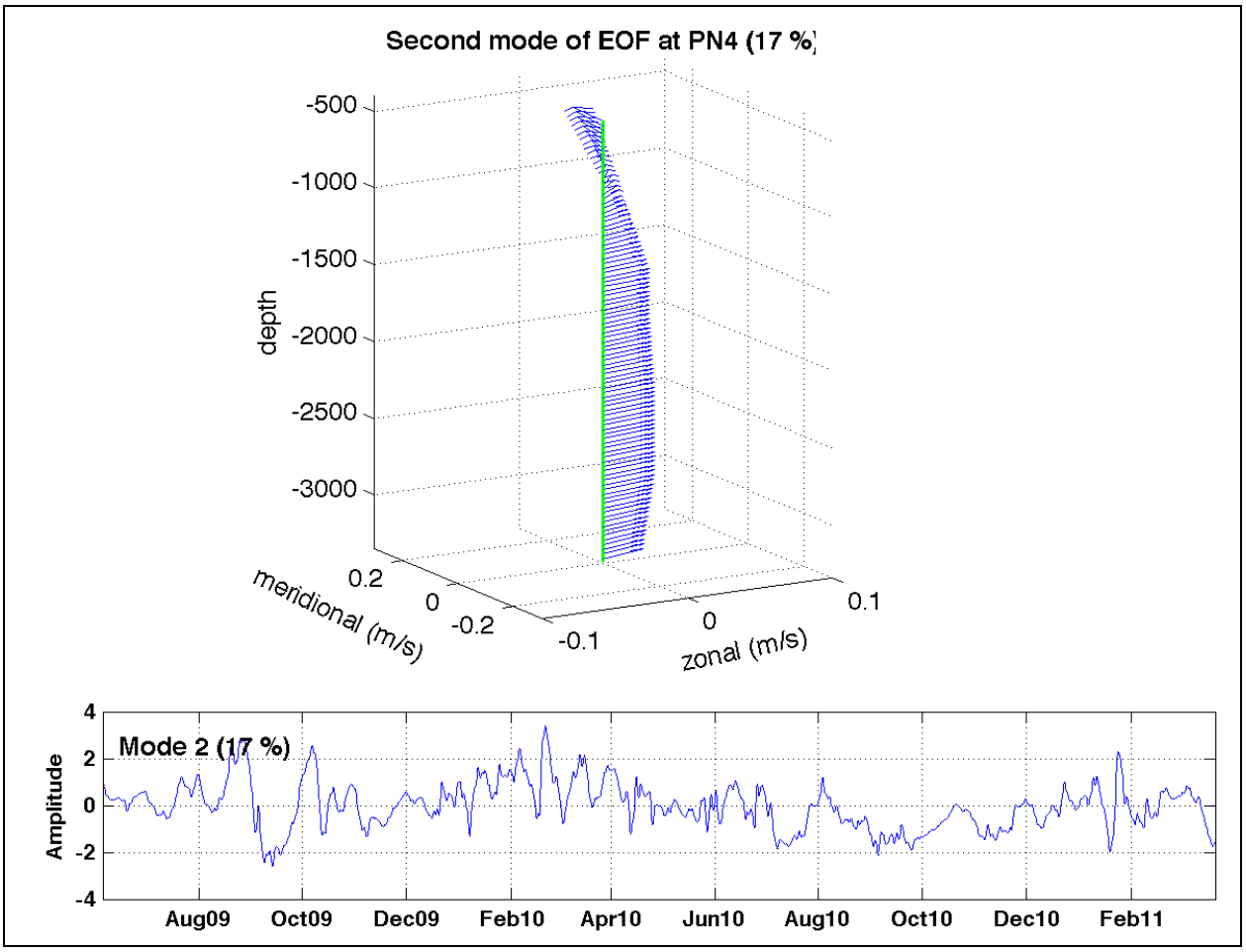

Figure 58. Continues.

4. SEASONALITY OF THE YUCATAN CURRENT

Two years of continuous measurements of the flow through the YC (Sep., 1999 to May, 2001) revealed a mean transport of 23.1 Sv (Sheinbaum et al., 2002; Ochoa et al., 2003). This value was 20% smaller than transport of 28 Sv previously estimated for this channel (Johns et al., 2002), and also smaller than the 32 Sv estimated from long-term cable measurements monitoring transports at the Florida Straits (Larsen, 1992, Baringer and Larsen, 2002). Moreover, recent measurements (between 2001 and 2006) from shipboard ADCP, indicate a similar transport of around 30 Sv through YC and Florida Straits, and suggest that both transports are linked at seasonal time scales (Rousset and Beal, 2010; 2011, see also Johns et al., 2002). The new measurements of currents at the YC from the Canek Project, give new evidence of the YCu variability. Unfortunately, only the western side of the channel (west of 85.6°W) was measured between March, 2008 and May, 2010. This new 3-year velocity time-series from Canek data is analyzed and compared with the transports estimated by the Canek group during 1999–2001 (Sheinbaum et al., 2002), the results reported by Explorer of the Seas (Rousset and Beal, 2010, 2011), as well as the seasonality of the YCu, recently studied by Chang and Oey (2013) in their numerical models.

4.1 TRANSPORT VARIABILITY AT THE YUCATAN CHANNEL

The objective mapping method described in Ochoa et al. (2003) was used to interpolate the data to a regular grid and then calculate the mean profiles through the WYC and their standard deviation for each period of measurements (Figure 59). Each mean profile and its standard deviation are in good agreement with the average profiles previously reported from observations (Sheinbaum et al., 2002; Candela et al., 2002; Rousset and Beal, 2010) and estimated from numerical models (e.g. Ezer et al., 2003). YCu is observed west of 85.5°W between the surface and 800m depth, with a mean velocity of 1.2 m/s in its core. It is noteworthy that the moorings installed in the western side of YC, practically covered the whole YCu (see also Figure 2), as well as their changes over the time. The highest standard deviation was observed at the surface on the western side of the channel (~0.3 m/s), due to counter-flows present in the most western side of the channel (see also Figure 25). Below 800 m depth, the mean flow at the center of the channel is into the Gulf direction; while at the edges of the channel the flow direction is southward (see also Figure 19), with features such as the current into the GoM, near the bottom at YUC7 and current out of the GoM over the shelf break in the deepest current meters of YUC5 and YUC6. In general, results over the five years (1999–2001 and 2008–2011) show a very stable average profile.

On the western side of the YC, the mean transport for the three consecutive years (March 2008 to May 2011) was 24.4 Sv with standard deviation of 4.1 Sv, which is around 2 Sv higher than the 22.3 Sv estimated at the western side during 1999-2001 (Figure 60). Note that average transport values were quite stable between 2008 and 2011 (Table 4). It is also worth mentioning that mean transport estimated for the whole YC in the 2010-2011 period was 27.1 ± 0.3 Sv, with a standard deviation of 3.6 Sv. This value is 4–5 Sv higher than the transport estimated by Canek Project

during the 1999–2001 period and more in agreement with the 28 Sv previously reported for this channel (Johns et al., 2002), as well as the 30.5 Sv measured by Explorer of the Seas (Rousset and Beal, 2011). Interestingly, transport on the eastern side (east of 85.6°W) was 2.8 Sv between 2010 and 2011, which is also ~2 Sv higher than the 0.6 Sv measured between 1999 and 2001. These results suggest that the southward flow on the eastern side was more intense in the 1999–2001 period indicative of a stronger Cuban Countercurrent. Inter-annual variability of the currents, particularly on the eastern side of the YC is currently investigated using altimetry data, but such results are beyond the scope of the present report.

Table 4. Mean transport and its standard deviation (in Sverdrups: 1Sv= 10^6 m^3/s), estimated for the whole YC (total), and divided in two parts: west of 85.6°W (western) and east of this longitude (eastern). Standard error with a 95% confidence level, are also indicated for the total transports. The calculation was made for each period of continuous measurements of Canek Project.

Period	Transport (Sv)			Standard deviation	
	Total	Western	Eastern	Total	Western
Sep/1999–Jun/2000	23.8± 0.3	23.1	0.7	3.2	
Jul/2000–May/2001	22.1± 0.2	21.5	0.6	3.1	
Mar/2008–May/2009	----	24.2 ± 0.5	----	----	3.9
Jul/2009–Mar/2010	----	24.8 ± 0.6	----	----	3.6
May/2010–May/2011	27.1 ± 0.3	24.3	2.8	3.6	

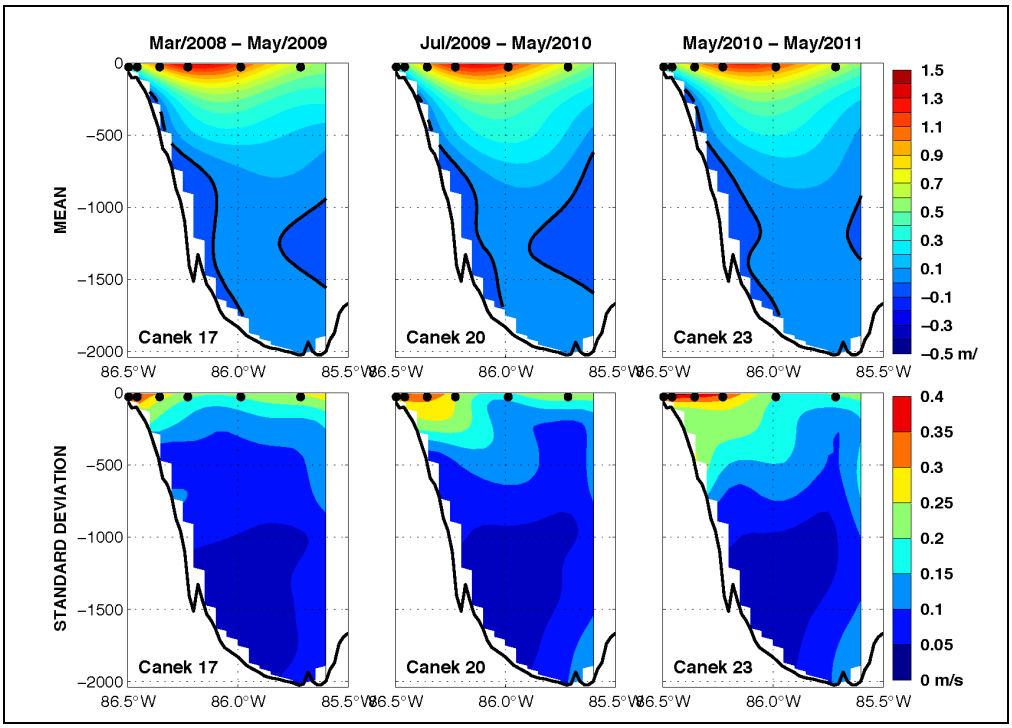

Figure 59. Mean along-channel velocity from objective mapped current observations at the WYC (top panels, black line indicates the cero velocity contour). Standard deviation of velocity fields (bottom panels). Calculations were performed separately for each period of Canek measurements.

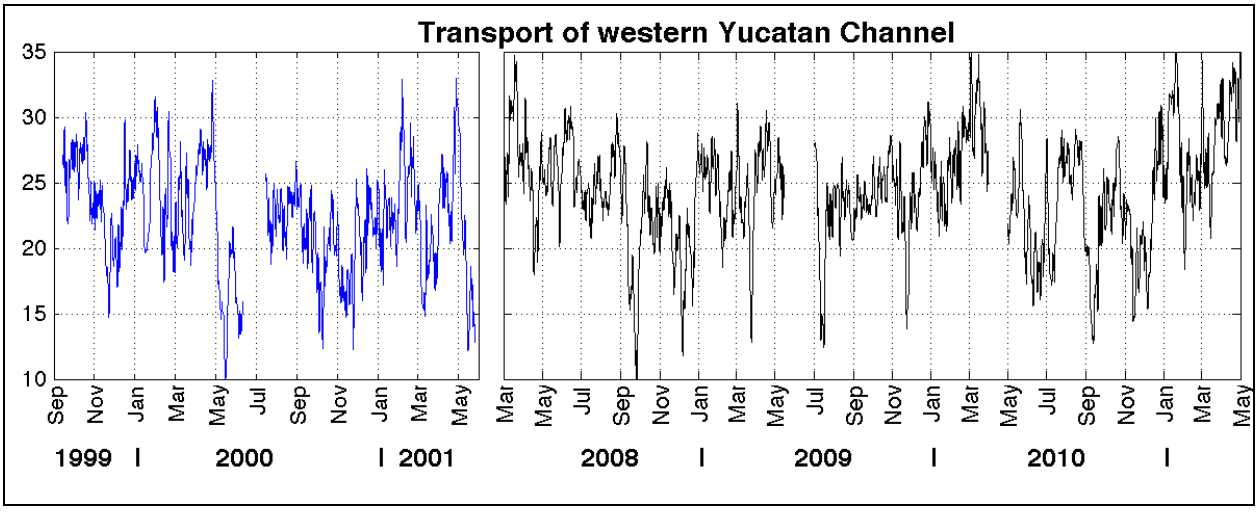

Figure 60. Time evolution of transport through the WYC (west of 85.6°W). Left panel: Canek measurements between September 1999 and May 2001, showed for reference. Right panel: Canek measurements between March 2008 and May 2011.

Empirical orthogonal functions of the along-channel velocity (velocity perpendicular to the mooring section) data were computed to provide a compact description of its spatial and temporal variability. Usually, most of the variance of the spatially distributed time series falls in the first few empirical orthogonal functions. A singular value decomposition of the data matrix was used to obtain eigenvalues, eigenvectors and time varying amplitudes (principal components) of the sample covariance matrix of velocity in the YC. The first and second modes represent 36% and 24% of the variance, respectively. The spatial structure of the first mode (EOF1, Figure 61) shows that the flow anomalies at the center of the channel are 180° out of phase with those of the western side; the change of sign at about 86.0°W. The western core has higher amplitude with velocity anomalies reaching 0.9 m/s. Below 1000 m, the flow in the whole western channel is in the same direction as the central near-surface core, although magnitudes are smaller there. The temporal evolution of this mode (PC1) shows some seasonality or slope in the series, with negative phases between May and September, that means intensified current (positive anomalies) in the central channel, with weaker currents (negative anomalies) on the western side. The positive phase with most intense currents at the western side of the channel is observed between November and April. Notice, however, that higher frequency (60–100 days) variability appears to be stronger than the seasonal signal. The EOF1 can be interpreted as representing horizontal movements (meanders) of the YCu with the positive anomalies marking the core of this current. The highest amplitude of this mode seems to occur during the negative phases, i.e. when the YCu core is away from the coast (in the central channel), with current anomalies reaching -0.9 m/s on the western side and +0.5 m/s over the central channel, with maxima in July 2009 and July 2010.

These results are partially in agreement with the EOF1 calculated from the first mooring deployment of Canek (1999–2000) and reported by Abascal et al. (2003), who interpreted the EOF1 also as indicating current meanders, with maximum velocity on the western channel in November and in the central channel in September–October. However, those seasonal phases are not that clear in the second period of the Canek deployment (2000–2001, Candela et al., 2003).

The spatial structure of the second mode of variability (EOF2, Figure 62) shows flow anomalies centered at 85.9°W over 1000m depth and weaker anomalies with opposite sign over the Yucatan slope. Further at depth, there is a small flow intensified towards the bottom in the center of the channel, with opposite sign to the near-surface flow, which can be associated with intensified variability observed near the bottom at mooring YUC7 and described in section 3.1.

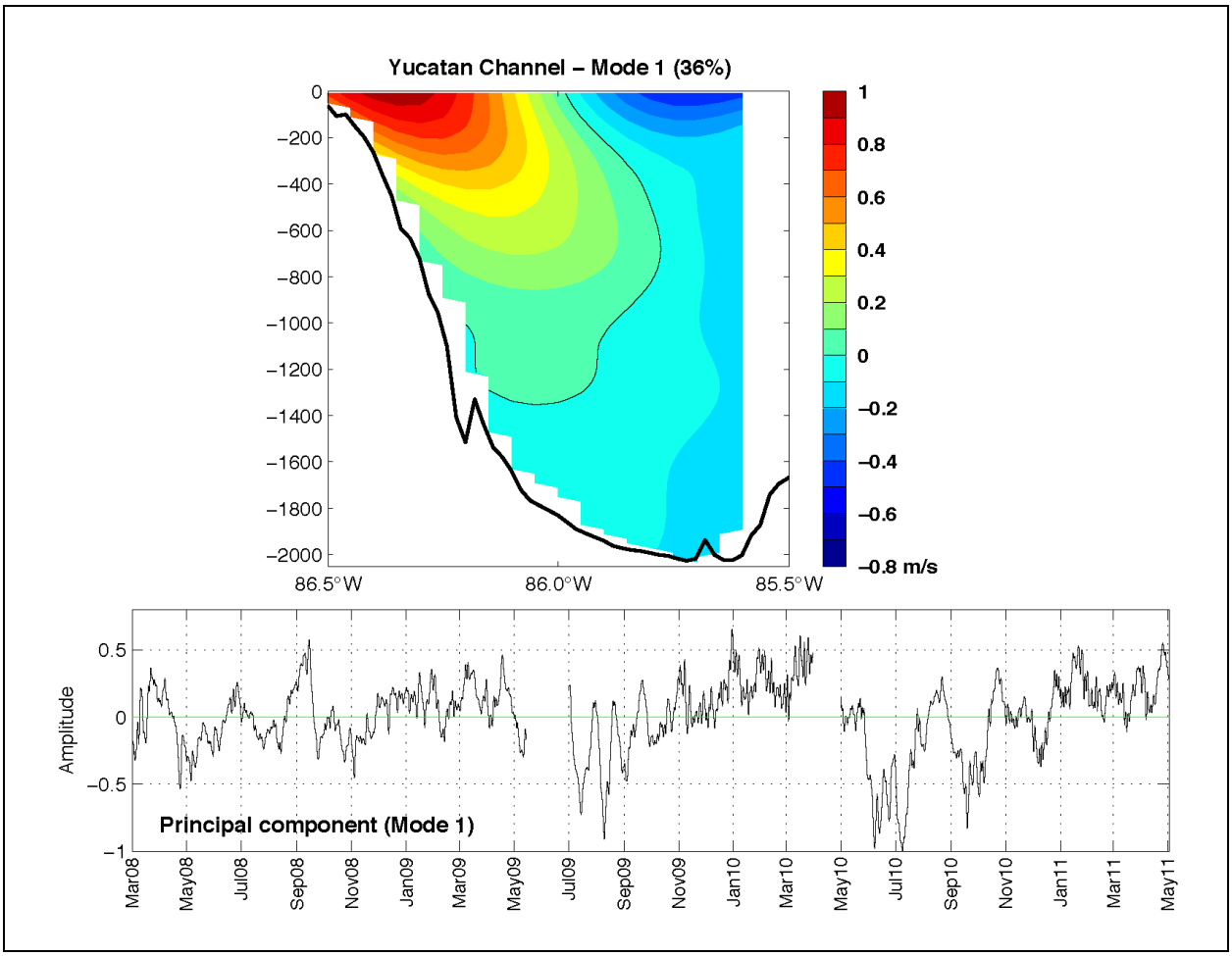

Figure 61. Spatial structure of the first EOF mode (top panel, black line indicates the zero contour) at the YC. Time evolution (principal component) of the first EOF mode.

The time-series of the second mode (PC2) does not show a "slope" as PC1 does, but rather, oscillates around zero between positive-negative phases, with a period around 60–80 days. This behavior could be interpreted as increase-decrease pulses of the YCu, or even meanders of the current. PC1 also shows this 60–80 days variability and both principal components appear to be out of phase with PC2 leading PC1 by 15 days. This is particularly noticeable during the second and third deployments (July 2009–May 2011); although between March 2008 and May 2009, the 60–80-day variability is also observed, there are some periods without any connection between PC1 and PC2 (November–May 2009). Low-pass transport series also show these 60–80 days pulses, however high amplitude events in the series are not explained by a single mode but rather seem to agree with the sum of the two modes, since depending on the date, the transport pulses are in phase either with PC1 or PC2 (Figure 63).

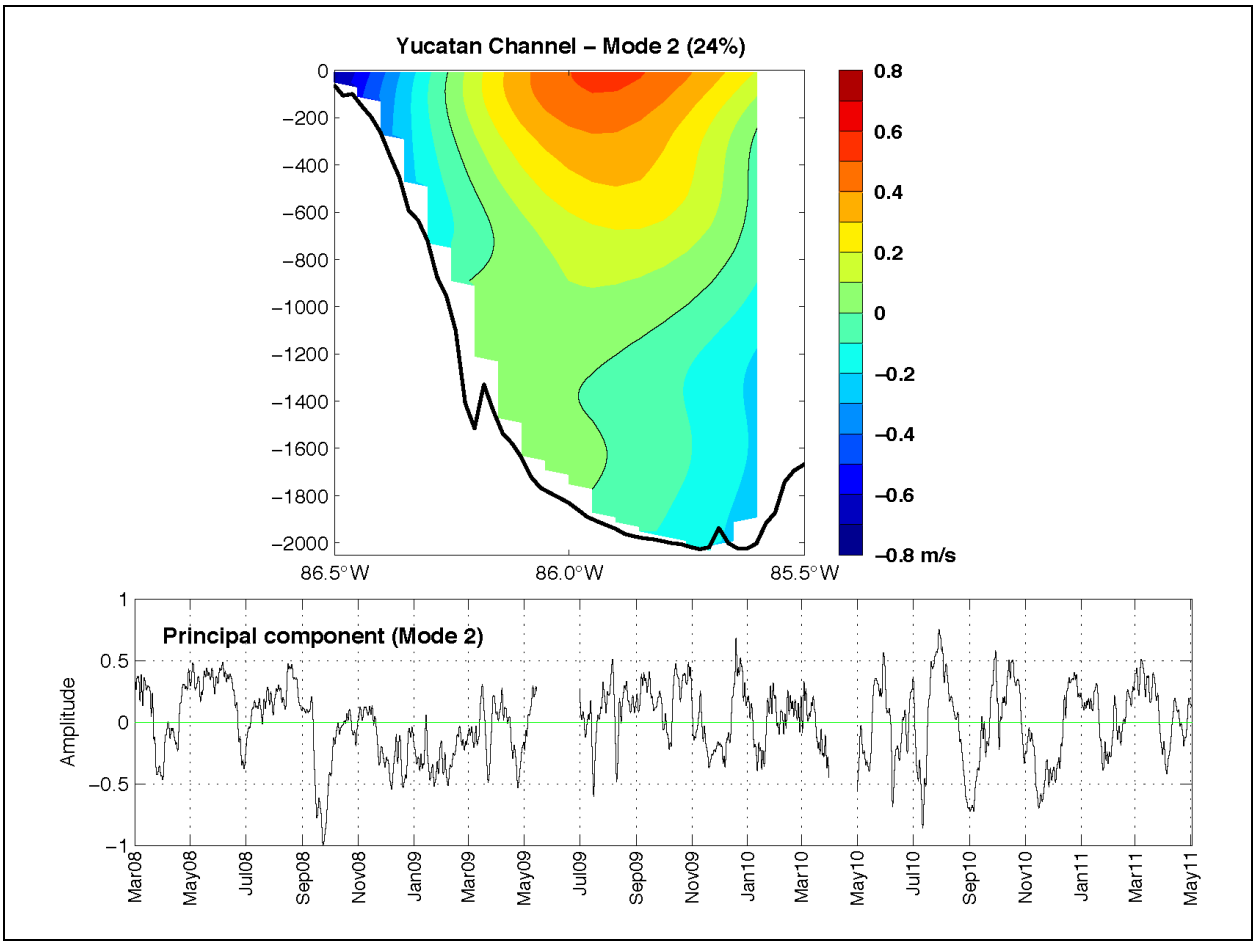

Figure 62. As in Figure 61, for the second EOF mode at YC.

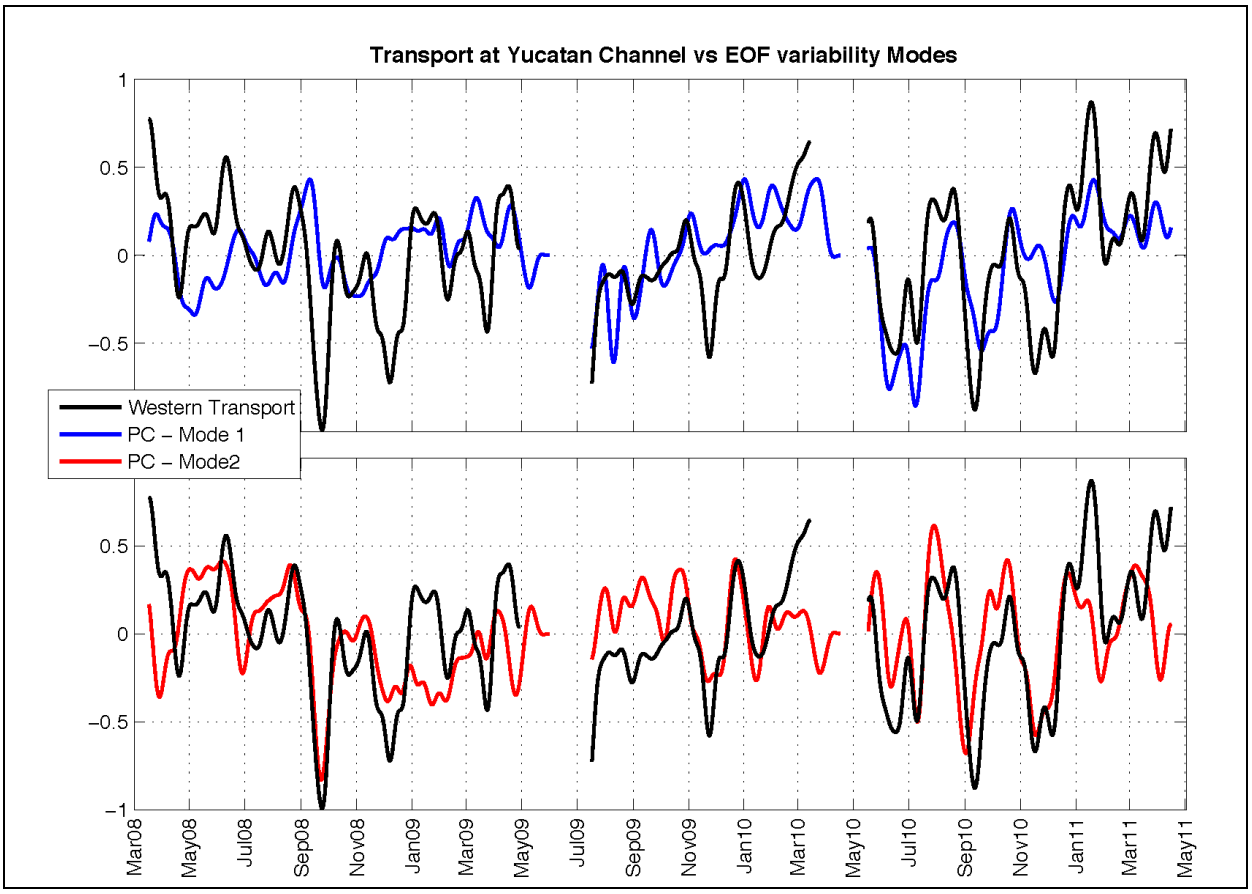

Figure 63. Standardized anomalies of the low-pass transport series from the WYC (black line), compared with the principal components of the first (blue line, top panel) and second (red line, bottom panel) EOF modes at the YC.

4.2 SEASONAL VARIATIONS OF THE YUCATAN CURRENT AND LOOP CURRENT

Seasonality of the flow through the YCu and the LC has been the focus of many publications, and is associated in many cases with the seasonal variations of the wind (e.g. Molinari et al., 1978; Sturges and Evans, 1983; Rousset and Beal, 2011; Chang and Oey, 2012). However, some other studies did not observe strong seasonal variations of the YC transport, although the time-series were short, (e.g. Sheinbaum et al., 2002; Candela et al., 2003; Abascal et al., 2003.). The main objective of this chapter is to determine whether there is a significant seasonal cycle in the YCu and/or transport, using the three consecutive years of observations between April 2008 and May 2011 in the WYC. Earlier observations from September 1999 to May 2001 were also used to complement the analysis. It is important to note that monthly time-series for seasonal cycle calculations were made considering the whole YCu transport in the periods September 1999–May 2001 and May 2010–May 2011, when data for the whole YC were available. We also computed seasonal cycles considering only the WYC with data from April 2008–May 2011, sometimes taking into account the 1999–2001 data. The periods used in a particular analysis are indicated in the text and figures.

Seasonal cycle of full YC transport (Figure 64) shows an annual maximum (positive anomaly) in summer (June–August) and another weaker relative maximum during January which is difficult to defend as significant (based on the number of degrees of freedom). This behavior differs from the semiannual cycle calculated by Rousset and Beal (2011), from 2001-2006 non-continuous measurements of shipboard ADCP observations, with two similar maxima in summer and late winter. When the total YC transport is divided in its western and eastern channel contributions (Figure 65), it is quite clear there is inverse behavior between both sides of the channel (see also Figure 67) and a substantial compensation if anomalies are added up. The biannual cycle, according to Rousset and Beal (2011), has maxima in April and August. Our WYC data show a clear maximum in April and a weaker one in August. Seasonal variations on both sides of the YC are around 4–5 Sv, while those of total YC transport are O(1–2 Sv), which reflect the compensation in variability between the eastern and western sides of the YC. A similar WYC cycle is observed not only in the 1999–2001 and 2010–2011 Canek measurement periods, but also from the three years of consecutive observations between 2008 and 2011 (Figure 66).

Chang and Oey (2012, 2013) carried out numerical model simulations spanning 20 years and analyzed also altimetry data. They propose an asymmetric semiannual cycle in YC transport with a strong maximum in summer and a weaker one in late winter. They suggest the cycle is related to the seasonal Trade wind intensification in the western Caribbean (Cayman Sea). To explore this issue and see if our directly measured transport data bear some connection with the regional wind forcing, European Centre for Medium-Range Weather Forecasts (ECMWF) ERA-Interim reanalysis winds were used to calculate the wind-stress (τ_x, τ_y) and the wind stress curl ($\nabla \times \boldsymbol{\tau}$) inside the areas indicated in Figure 68, i.e. the Cayman Sea and the GoM. For this calculation, only WYC transport variability was compared to wind forcing anomalies for the periods (September 1999–May 2001 and April 2008–December 2010, Figure 69). The transport time-series was ended on December 31, 2010 to match the wind time-series of high resolution

data we had available. The transports as well as the wind series were filtered with a 40-day low-pass Lanczos filter.

Mean values for τ_X were -0.05 Nm^{-2} for the Cayman Sea and 0.02 Nm^{-2} for the GoM with average $\nabla \times \bar{\tau}$ values of 1.6 x 10^{-8} Nm^{-3} and 2.8 x 10^{-8} Nm^{-3} in the Cayman Sea and the GoM, respectively. In the Cayman Sea, the easterlies (negative τ_X) intensify with equal magnitude in February and June–July, while wind from the east in the GoM decreases. Stronger easterly winds and wind-stress τ_X are observed in the GoM during April–June, while, at the same time, easterlies reduce their magnitude in the Cayman Sea. The $\nabla \times \bar{\tau}$ also shows a semi-annual cycle, but asymmetric, with anticyclonic anomalies (negative values) in February and to a lesser extent in July. These precede transport increases that occur one or two months later in April and August on the WYC (Figure 69). From May to June, wind from the east in the GoM intensifies and the $\nabla \times \bar{\tau}$ is predominantly anti-cyclonic while the transport and westward wind in the Cayman Sea are at its minimum (Figure 69).

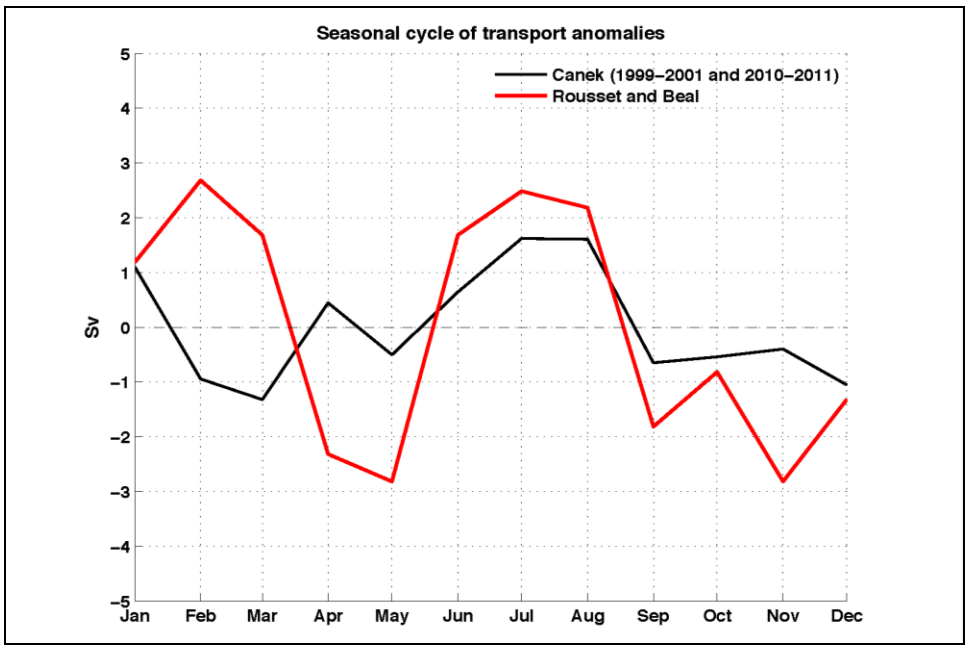

Figure 64. Seasonal cycle of transport through the YC (total transport anomalies indicated with black line), calculated between September 1999–May 2001 and May 2010–May 2011. The YC seasonal cycle from Rosset and Beal (2011) is indicated (red line).

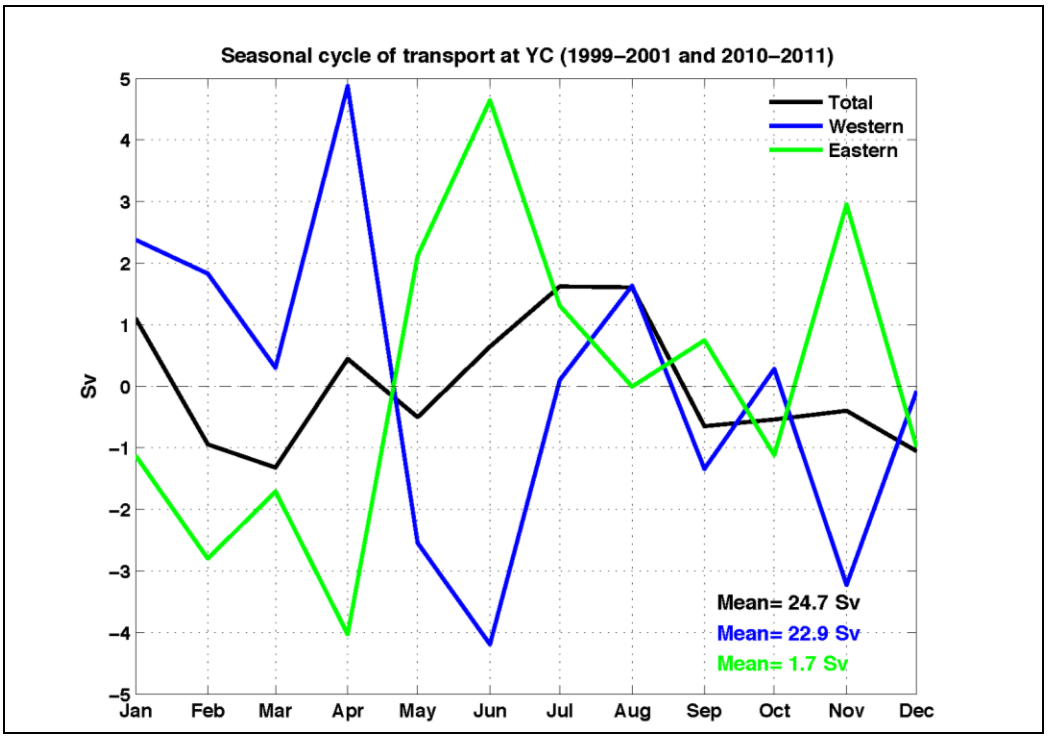

Figure 65. Seasonal cycle of transport anomalies through the YC calculated between September 1999–May 2001 and May 2010–May 2011. Seasonal cycles were calculated separately for total YC transport (black line) and through the east (green line) and west (blue line) of 85.6ºW.

Chang and Oey (2013) relate the Trade wind intensification to their model semi-annual transport signal, which in turn, they suggest, reflects on the LC dynamics and eddy shedding period. Summarizing: total transport estimates presented here show weak annual and possible semi-annual cycles different from those of Rousset and Beal (2011) and Chang and Oey (2013). Transport anomalies separated in western and eastern contributions indicate large compensations with WYC anomalies depicting a strong positive peak in March–April and weaker relative maxima in January and July. Positive (negative) WYC transport anomalies generally coincide with negative (positive) wind stress curl anomalies over the Cayman Sea (Figure 69). It is interesting that the long-term (40-year, not shown) seasonal cycle of the wind stress and wind stress curl does have its stronger negative signal in summer; however, the seasonal cycle of the periods 1999–2001 and 2008–2010 have a more intense westward wind and anticyclonic $\nabla \times \bar{\tau}$ during winter-spring rather than summer, suggesting the importance of inter-annual variability.

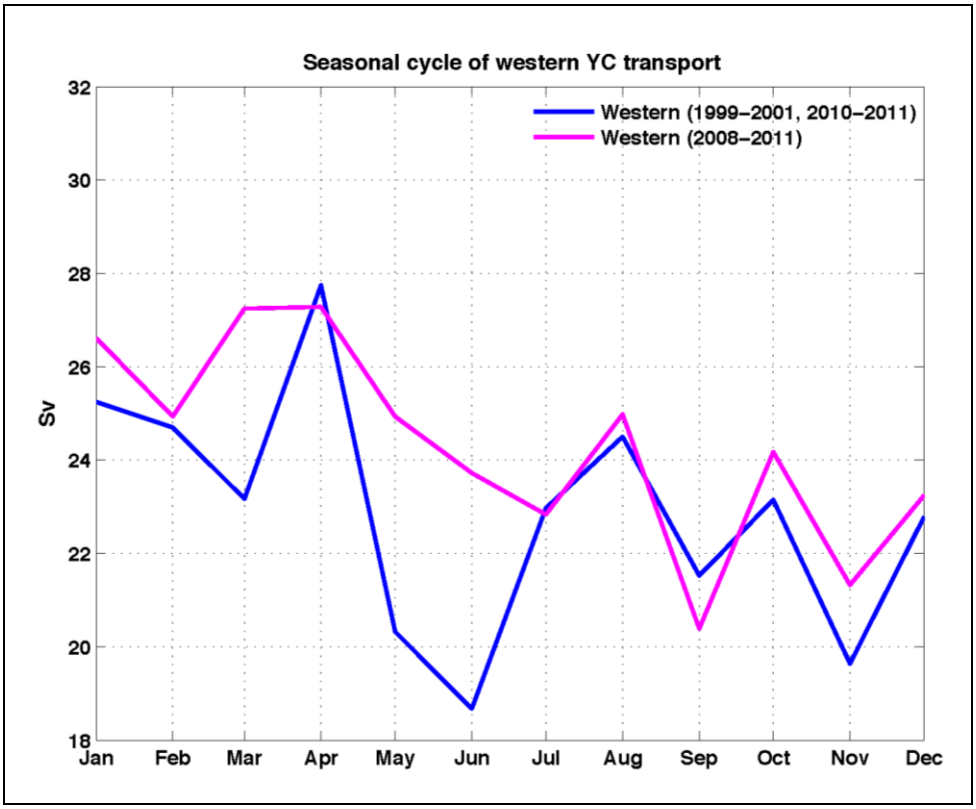

Figure 66. Seasonal cycle of transport through the WYC (west of 85.6ºW); calculated between September 1999–May 2001 and May 2010–May 2011 (blue line) and between April 2008–May 2011 (magenta line).

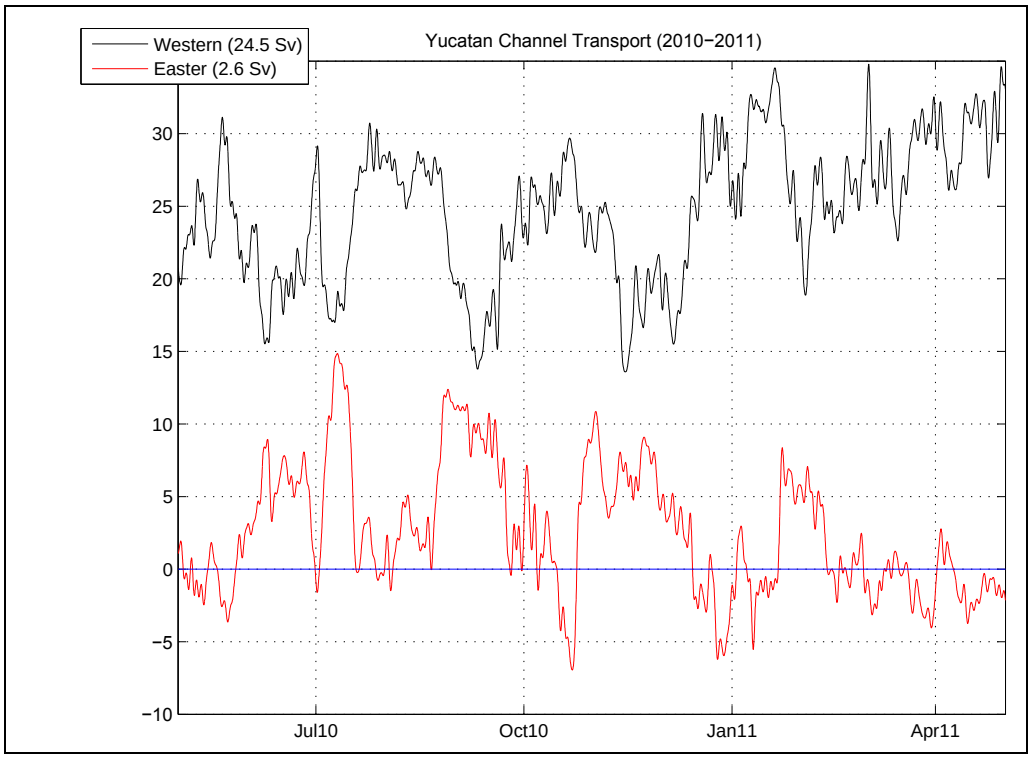

Figure 67. Time-evolution of the YC transport calculated for the western (black line) and eastern (red line) YC between May 2010 and May 2011.

The connection between wind and WYC transport is perhaps clearer and easier to understand looking at the wind stress curl rather than the wind-stress. Between September and December, anomalies of $\nabla \times \bar{\tau}$ and τ_X are positive over both the Cayman Sea and GoM basins and coincide with a decrease in WYC transport. The origin of the drop to zero in transport anomaly in October is not clear, but coincides with a simultaneous or previous (one month) drop in the positive anomalies of the wind-stress curl over the GoM (see Figure 69 and Figure 70).

To investigate if the anti-correlation between transport and wind-stress curl anomalies remains during different periods, monthly series of $\nabla \times \bar{\tau}$ in the Cayman Sea and GoM, as well as WYC transport were calculated independently for the two periods of Canek measurements (September 1999–May 2001 and April 2008–December 2010 (Figure 70). Most important differences between both periods are: i) the winter intensification of easterlies occurs one month later (February) in 1999–2001 than in 2008–2010 (January), the stronger anomaly in WYC transport occurs in March for the 2008–2010 period, and one month later (April) in 1999–2001, with apparently a two-month lag between wind and transport maxima. ii) In 1999–2001, the summer anticyclonic $\nabla \times \bar{\tau}$ lasted for three months (June, July, August), whereas in 2008–2010 only lasted one month (July). A similar (delayed) response was observed in WYC transport, which increased one month later during July, August, September, October in 1999-2001 but only increased in August during 2008–2010). In 2008–2010 the seasonal cycle in the ($\nabla \times \bar{\tau}$) is

strongly annual with anticyclonic behavior between January and July and cyclonic behavior the rest of the year. It is not always possible to establish a one month lag between wind-stress curl anomalies over the Cayman basin and WYC transport anomalies, although on average, such a delay appears to remain (see below). Our analysis suggests there is a connection between transport and winds, but the physics of it remains uncertain. One must also remember that being an integral part of the subtropical gyre, the YCu can respond to both local and remote forcing at these time-scales.

Figure 71 shows the temporal evolution of monthly-averaged WYC transport and wind-stress curl for the Caribbean and the GoM. Figure 72 is a similar plot but for the zonal stress τ_X. Both figures now separate all measurement periods individually, with the purpose to corroborate if every year the inverse behavior between WYC transport and $(\nabla\times\bar{\tau})$, as well as τ_X remains valid. In general, one can say there is indeed an opposite relation in the curl-transport series but there are also occasions when such relation is not valid. Even if there is inter-annual variability in the timing and strength of the wind-stress curl anomalies, the anti-correlation between WYC transports and Cayman wind-stress curl anomalies remains. The semi-annual signal in $\nabla\times\bar{\tau}$ generally present with anticyclonic anomalies in January–February and July–August varies however, since the highest anomaly is not always in summer. For example, during 2001 and 2010 negative anomalies of $\nabla\times\bar{\tau}$ occur in winter which are, at least, as intense as the anomalies of summer (2008). In a similar way, there are years (2000 and 2009) where the anomalies of WYC transport do not seem to be inversely correlated with $\nabla\times\bar{\tau}$ over the Cayman Sea. Cross-correlation was performed between the spatial mean of $\nabla\times\bar{\tau}$ or $<\nabla\times\bar{\tau}>$ and WYC transport and between the spatial mean of t_X and the WYC transport, for each Canek measurement period individually (Figure 73). The $\nabla\times\bar{\tau}$ precedes transport with a mean lag of 28 days (varying between 6 and 65 days) and t_X precedes transport with a lag of 24 days (varying between 7 and 39 days). The time-lag of one month between wind and transport is consistent with time difference observed in the seasonal cycles between the negative peak in wind variables ($\nabla\times\bar{\tau}$ and t_X) and the positive peak in transport during late winter and summer.

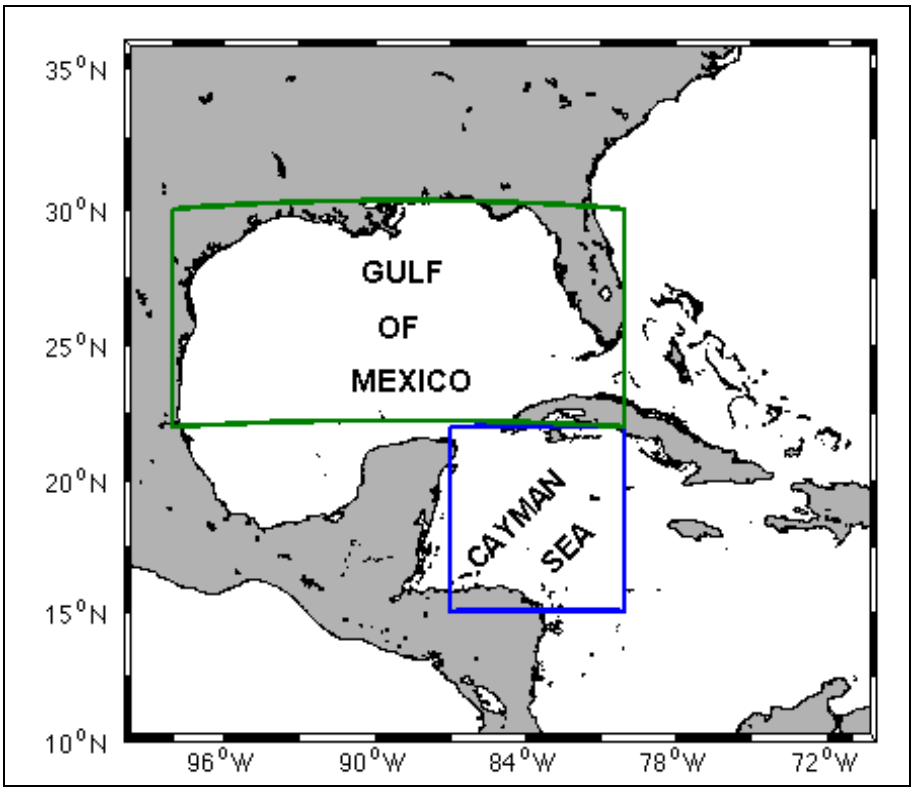

Figure 68. Map of the Caribbean Sea–Gulf the Mexico system, showing the areas where τ_X, t_Y and $\nabla \times \bar{\tau}$ were estimated from the ERA-interim data. The Cayman Sea (blue square) is the same region chosen by Chang and Oey (2012, 2013).

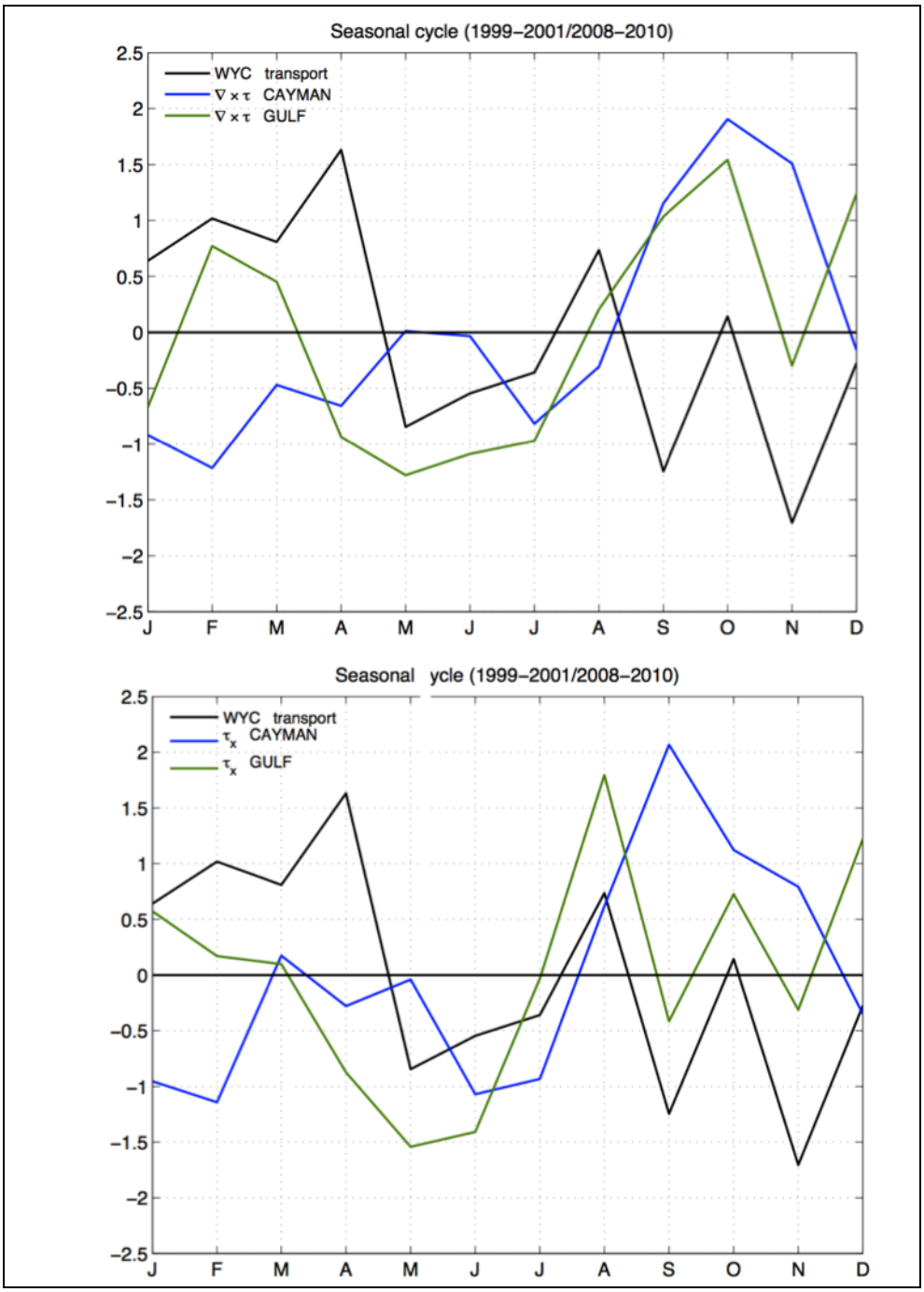

Figure 69. Seasonal cycle of the WYC transport (black line) compared with the zonal wind stress curl (upper panel) and the wind stress (lower panel) for the Cayman Sea (blue line) and the Gulf of Mexico (green line, areas are indicated in Figure 68) between September 1999–May 2001 and April 2008–December 2010. All the series are 40-days low-pass filtered and showed in standarized anomalies.

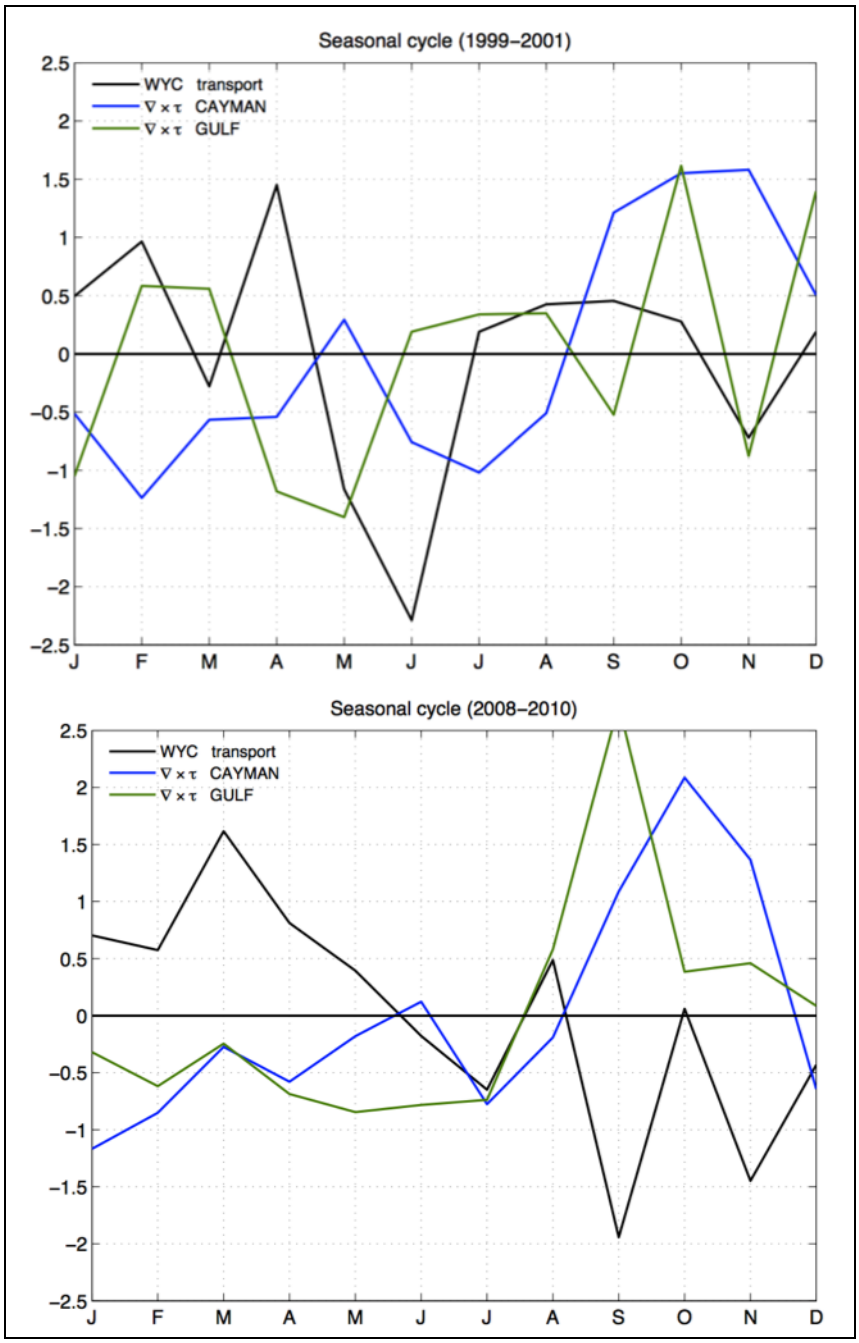

Figure 70. Seasonal cycle of the WYC transport (black line) compared with the zonal winds tress curl for the Cayman Sea (blue line) and the Gulf of Mexico (green line, areas are indicated in Figure 68) separated by periods: September 1999–May 2001 (upper panel) and April 2008–December 2010 (lower panel). All the series are 40-days low-pass filtered and showed in standarized anomalies.

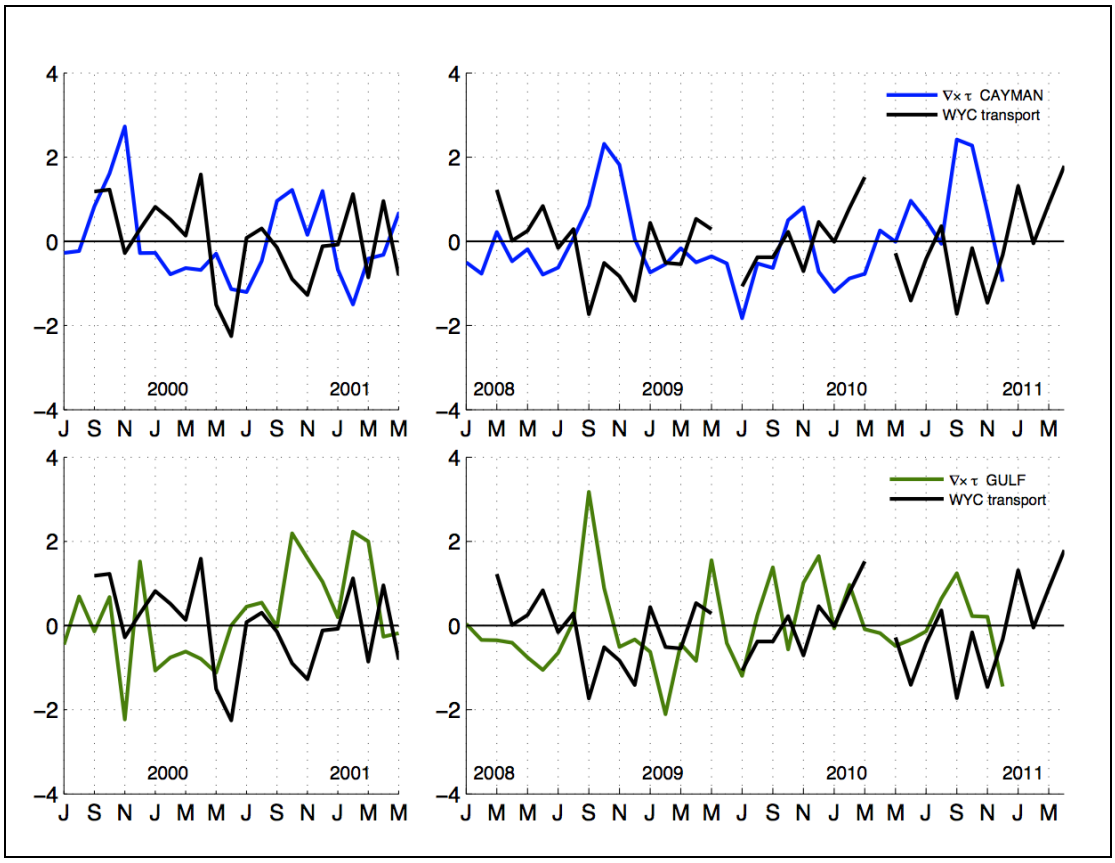

Figure 71. Monthly averaged time series of the WYC transport (black line) compared with the winds stress curl for the Cayman Sea (upper panels) and the Gulf of Mexico (bottom panels), areas are indicated in Figure 68 for the two periods of Canek measurements. All the series are 40-days low-pass filtered and showed in standarized anomalies.

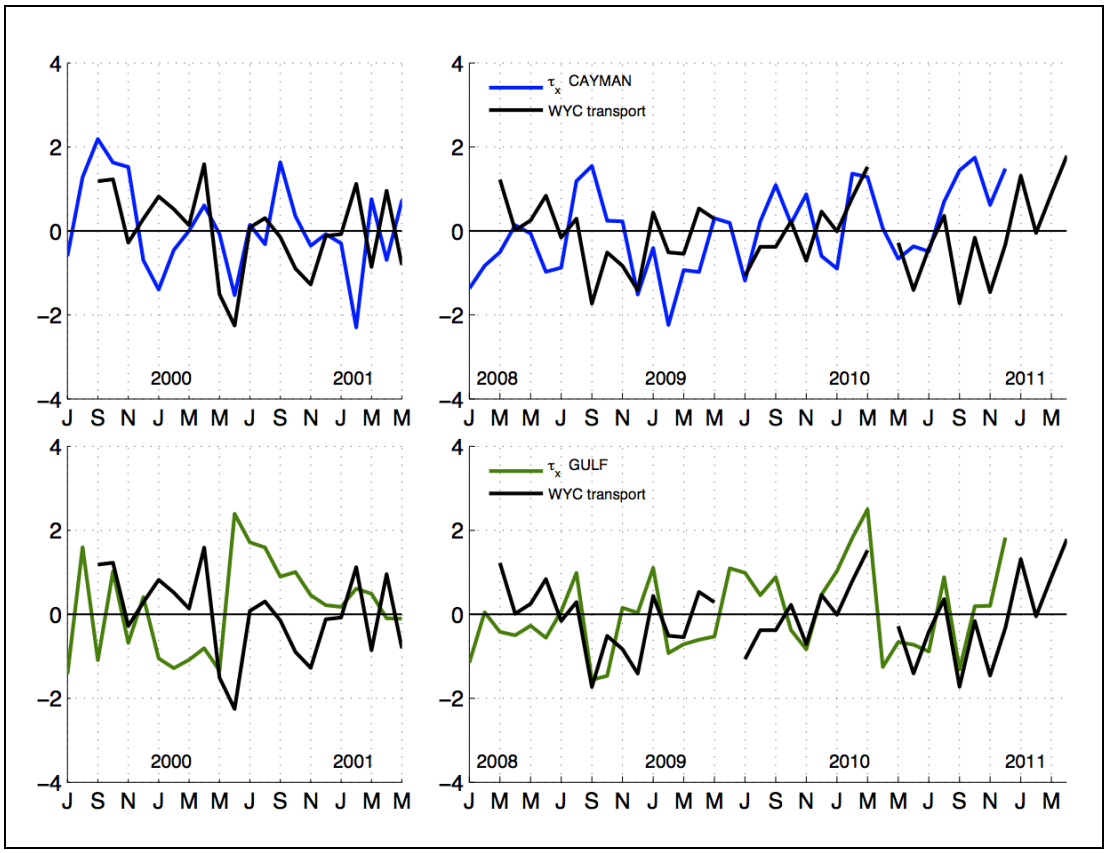

Figure 72. Monthly averaged time series of the WYC transport (black line) compared with the zonal winds stress for the Cayman Sea (upper panels) and the Gulf of Mexico (bottom panels, areas are indicated in Figure 68) for the two periods of Canek measurements. All the series are 40-days low-pass filtered and showed in standarized anomalies.

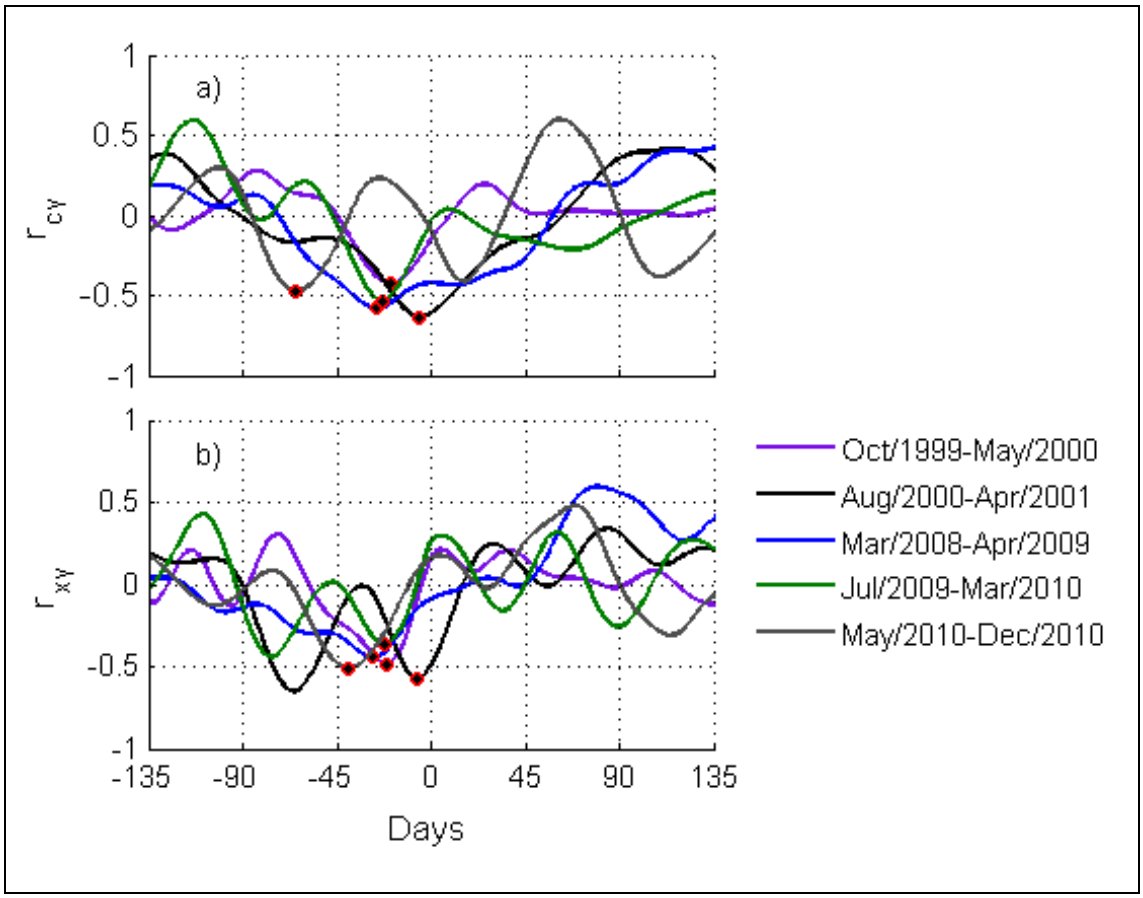

Figure 73. Cross-correlation between wind stress curl and WYC transport (r_{cy} upper panel) and between zonal wind stress and WYC transport ($r_{xy,}$ bottom panel) calculated separately for each Canek campaign. The maxima correlation time-lag (negative) is indicated by the red dot.

Some observations and model studies indicate that the LC dynamics, particularly the LC northern extension and LCE release rate, are related to transport fluctuations in the YC (e.g., Hurlburt and Thompson, 1980; Oey et al., 2003; Candela et al., 2002; Chang and Oey, 2013). These studies however provide different–even contradicting–views of the relation between LC dynamics and eddy shedding with other dynamical variables such as vorticity, LC strength and extension, to mention a few. Specifically, Chang and Oey, 2013 suggest that an increased velocity of the YCu leads to higher YC transport and LC extension and a very strong positive correlation between vorticity anomalies and LC northward extension. To investigate how these relations appear in the mooring data, vorticity through the YC was estimated in a "Lagrangian" way from the difference between the maximum velocity of the YCu (regardless of its zonal position) and the velocity at the fixed point located at 86.45W, divided by their distance (which varies in time). Figure 74 (left panel) is a longitude-time plot of the along-channel velocity at the YC showing the maximum velocity position (black line) and the 86.4°W longitude position used for the vorticity computation (yellow line). The position of the YCu core is not directly

correlated with its value, i.e., a western shift of the current core does not necessarily imply an increase in velocity (Figure 74 right panel).

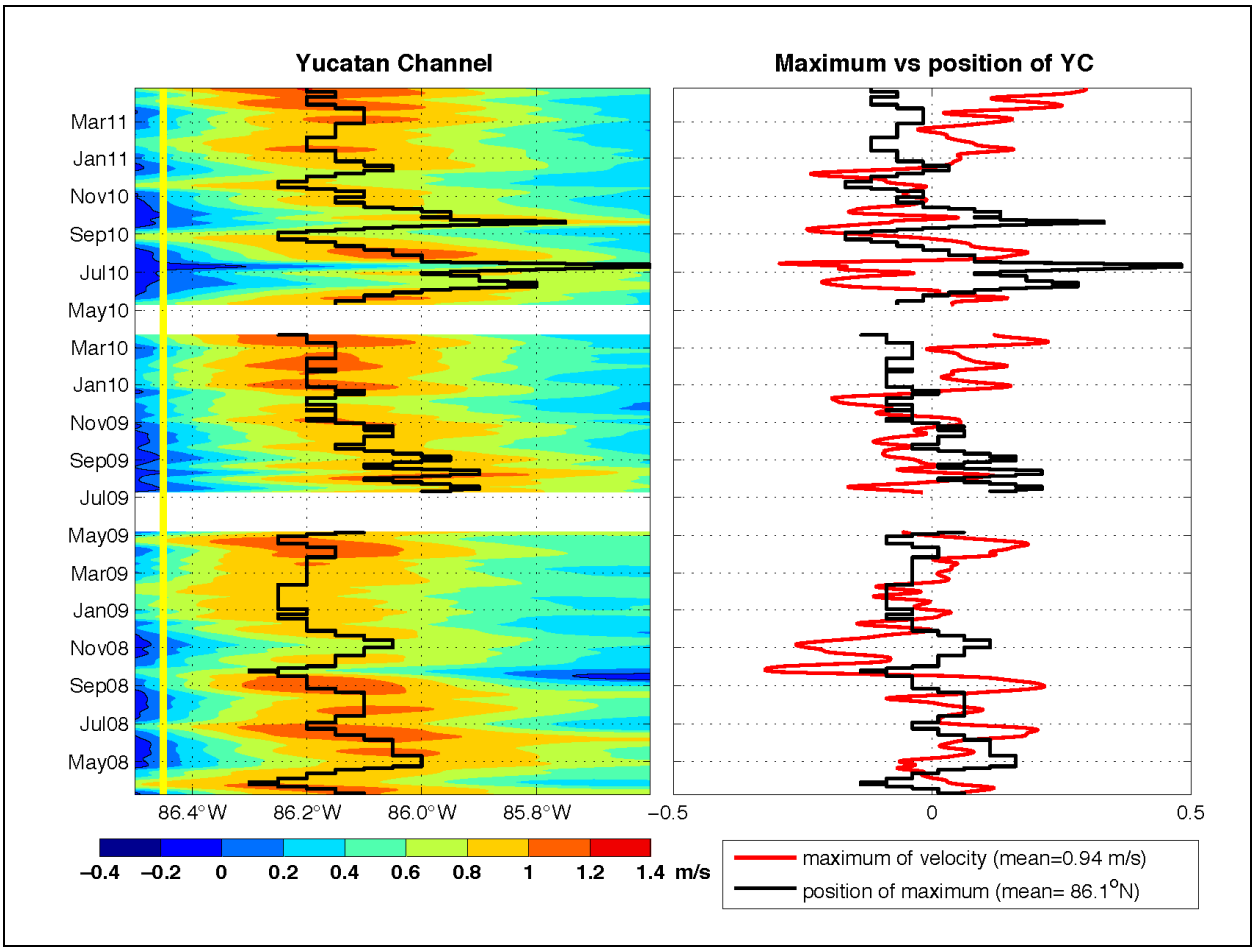

Figure 74. Longitude-time diagram of the along-channel velocity through YC (left panel); the maximum value of the YCu is indicated by the black line and the yellow line indicates the 86.4W fixed longitude. Time series of the maximum value of velocity from YCu anomalies (black line) and of the position in longitude anomalies of this maximum value (red line).

Figure 75 shows the seasonal cycle (monthly means) of LC northern extension, YCu vorticity (as defined above) and WYC transport for the Canek observation period 2008–2011; the LC northern extension was determined using AVISO data and the metric developed by Leben (2005), consisting on tracking the 50-cm contour of SSH, which is used as an approximation for the high velocity core of the LC. Transport and LC extension series depict positive anomalies from February to June and negative afterwards. Vorticity has a similar tendency but has more variability. Peaks in March and August in the transport and vorticity series precede LC extension peaks occurring one month later (April and September). Figure 76 shows times series of WYC transport, vorticity and LC extension. There is significant correlation between vorticity and transport (upper panel) of YCu between March 2009 and March 2011, but this is not true for May 2008 to May 2009, where the correlation is 0.3. The relation between these two variables and the LC extension is not so obvious (middle and bottom panels) since large LC extension happen both with positive and negative transport and vorticity anomalies. Nevertheless, there are periods when LC extension increments coincide with positive vorticity and more clearly transport also increase (e.g., March–July 2009, November–May 2010, and September 2010–March 2011). Consistently with the transport–vorticity relation, before March 2009, LC extension does not seem to have any relation with vorticity nor transport of the YCu. To better appreciate the fluxes of vorticity, its time-integral was compared with the LC extension (Figure 77), confirming that the connection between variability of YCu is not always strong throughout time. The regression of monthly averages for the LC with WYC transport anomalies (Figure 78) shows a slight relation between lower (higher) LC latitudinal extension and negative (positive) transport anomalies (r=0.4). Colors in Figure 78 represent the different years of measurements; the correlation appears stronger in 2009 and 2010, even for the regression of LC extension and vorticity, which does not show any correlation considering the whole period. The correlation between LC extension and transport anomalies increases to 0.6 when the whole seasonal cycle is considered (calculated between 2008 and 2011, (Figure 79), suggesting that these two variables are better correlated on seasonal scales. However, the analysis indicates that the connection between YCu and LC dynamics is complex even at seasonal scales and inter-annual variability plays an important role that needs further investigation.

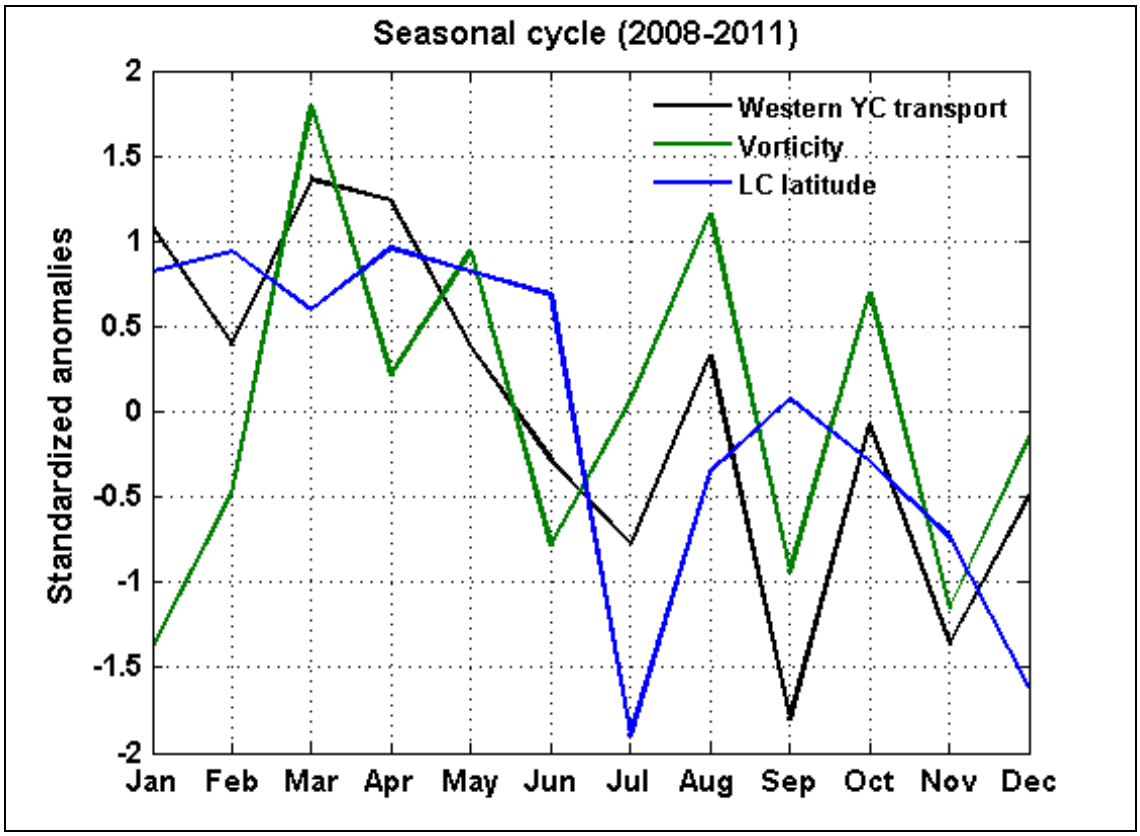

Figure 75. Seasonal cycle of the WYC (black line), vorticity of the YCu (green line), and the LC northern extension in latitude (blue line); values are indicated in standardized anomalies calculated between March 2008 and May 2011.

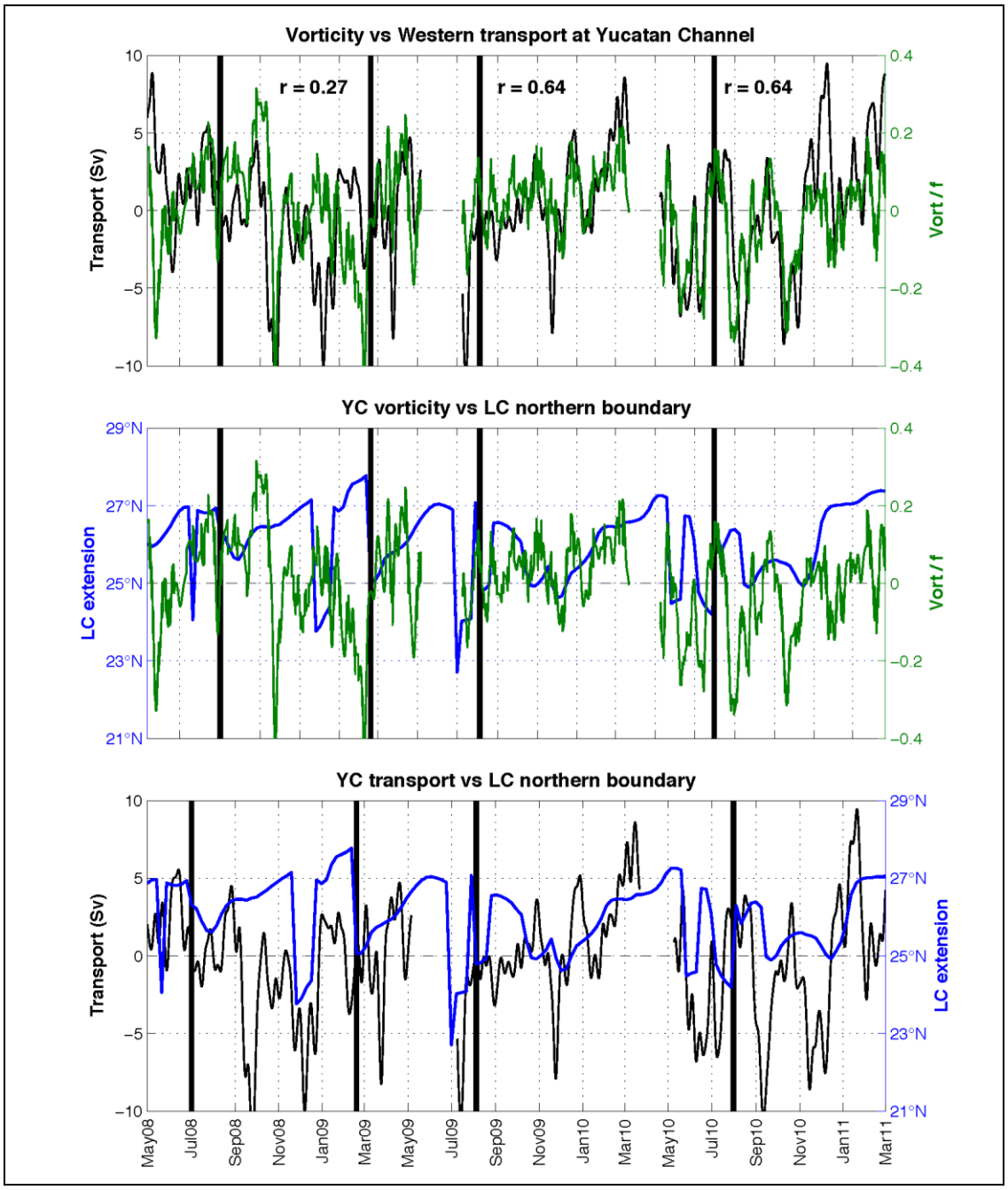

Figure 76. Vorticity of the YCu (green line) compared with the WYC transport (black line, upper panel) and with the LC northern extension (blue line, middle panel); WYC transport and the LC extension are also compared (bottom panel).

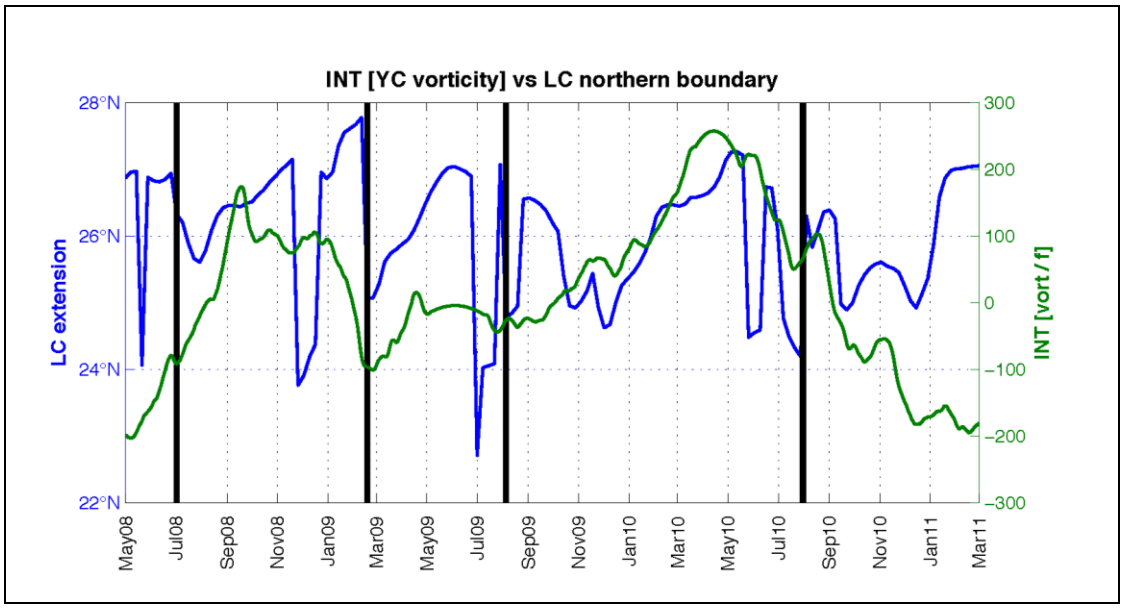

Figure 77. Detrended time integral of vorticity of the YCu (green line) and the LC northern extension (blue line).

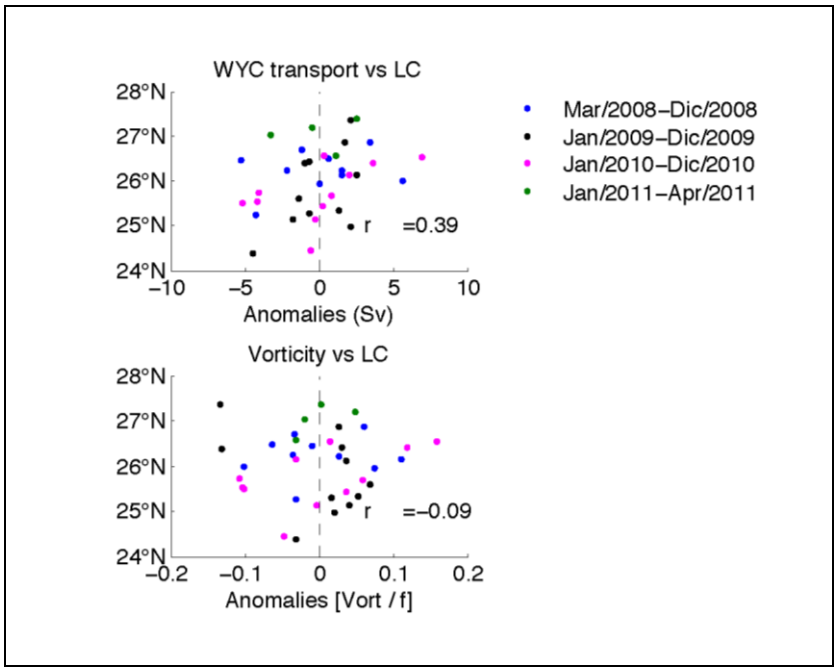

Figure 78. Regression performed year by year using available Canek data between the LC northern extension and WYC transport anomalies (upper panel) and between the LC northern boundary and vorticity anomalies (bottom panel; note that vorticity is divided by Coriolis parameter *f*).

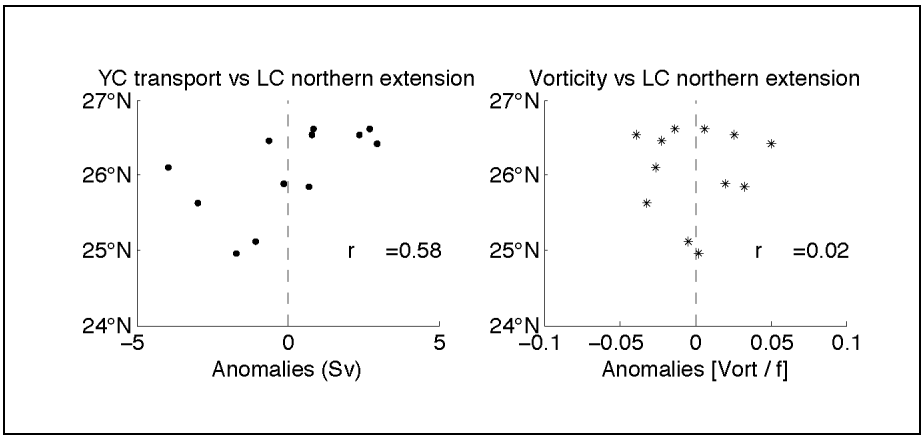

Figure 79. Regression of the seasonal cycle calculated from March 2008 to April 2011 between the LC northern extension and WYC transport anomalies (left panel) and between the LC northern extension and vorticity of the YCu anomalies (right panel, vorticity divided by *f*).

5. ON THE LOOP CURRENT EDDY RELEASES

The LC wraps around over itself and sheds large warm, anticyclonic eddies that extend several hundred meters in depth and propagate in a west-southwest direction across the GoM (see the monograph edited by Sturges and Lugo-Fernandez, 2005, for a comprehensive review). This is a slow and complex process that often involves several detachments-reattachments of the anticyclonic eddy within the same shedding event. Understanding of this complex dynamics is one of the main purposes of the observations and modeling carried out in this project.

Eddies are conveniently detected from satellite altimetry data, for which we use the maps of absolute dynamic topography (MADT) and geostrophic velocities derived from it using a multiplatform product that includes data from the Topex-Poseidon, Jason-1, and GFO satellites, as offered by AVISO (the altimeter products are produced by Ssalto/Duacs and distributed by AVISO, with support from CNES). This information has a 1/3 of a degree spatial resolution, and seven days temporal resolution. From these data, we determined that four LCE were released during the time our instruments were deployed and serve to illustrate the behavior of currents and eddies as they separate from the LC. The moorings installed at the YC and PE section then serve to document the behavior of the YCu as well as at the western edge of the LC from the surface to the bottom. The current pulsations as well as the zonal migration of the YCu in the YC can be clearly identified in AVISO data. For a thorough comparison and validation of AVISO data using mooring observations near the coast, see Athie et al. (2012). The criterion used to identify each detachment, including the pinching point, is the same as that used in section 4.20, described by Leben (2005). For the purpose of this section, we will consider only the total LCE release, which means the last and final detachment of each LCE before moving into the GoM.

The four LCE releases that will be analyzed are: LCE1 on July 2, 2008; LCE2 on February 18, 2009; LCE3 on August 5, 2009 and LCE4 on August 11, 2010. Figure 46 shows that the four eddies were detached farther north from the location of the section PE (north of 24ºN). The release process for each LCE is illustrated in Figure 81. In all cases, the LCE detachment is preceded by a low sea surface height upstream at the northwestern Caribbean, suggesting a cyclonic eddy, followed by the eastward shift of the YCu; shortly after, inside the GoM the cyclone located west of the LC increases in intensity (at LCE1, LCE3 and LCE4), leading to an LCE, final, release. This mechanism that suggests the northward propagation of cyclonic anomalies along the Caribbean coast of Mexico into the gulf has been described for sixteen of twenty-one detachments (partial and total releases) observed between January 2005 and July 2009 by Athie et al. (2012). In this chapter mooring data will be analyzed after this date to study this mechanism in subsequent eddies.

Geostrophic velocities from AVISO were interpolated to WYC (Figure 82) and to the position of section PE (see Figure 83 for Canek data and Figure 84 for AVISO data). The YCu core is clearly observed with the Canek data (Figure 82), as a higher along-channel velocity. Although, AVISO velocities show lower magnitude throughout the study period, usually, the current core in the satellite and mooring data is equally located west of 85.8°W and intensity variations also

coincide in time; however, at the western side of the channel, the return flow is not well represented by AVISO data. The horizontal movements of the current core are also in good agreement in both datasets, remarking how the current axis is gradually moving to the east before each of the three releases (LCE1, LCE3, LCE4 and, to a lesser extent, for LCE2). This is most noticeable with satellite data, due to the high variability detected by mooring measurements; however, the time evolution of the longitude-averaged current confirms also an increase (~0.2 m/s) of the velocity before each LCE detachment of equal magnitude in both datasets. The eastward shift of current before a release is also observed further north, at PE section, in the along-section velocity from both, Canek (Figure 83) and satellite (Figure 84) datasets; moreover, a strong pulse of negative cross-section velocity preceding the releases is also observed. Note that in the PE section analysis, only LCE2, LCE3 and LCE4 are considered in satellite data and only LCE3 and LCE4 in mooring data, because of the length of the time series at this position.

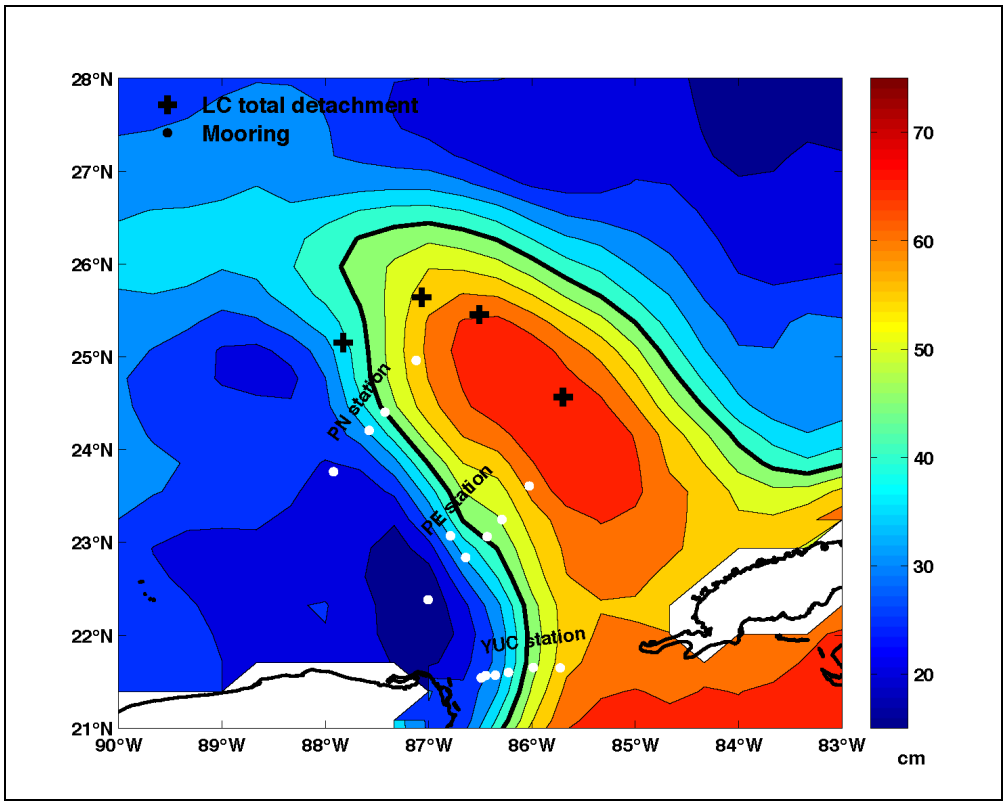

Figure 80. Averaged sea surface height (contours) and horizontal distribution of the detachments (crosses) occurred between July 2008 and August 2010. The 45 cm mean contour of sea surface height (black line) and the mooring positions (white dots) are indicated.

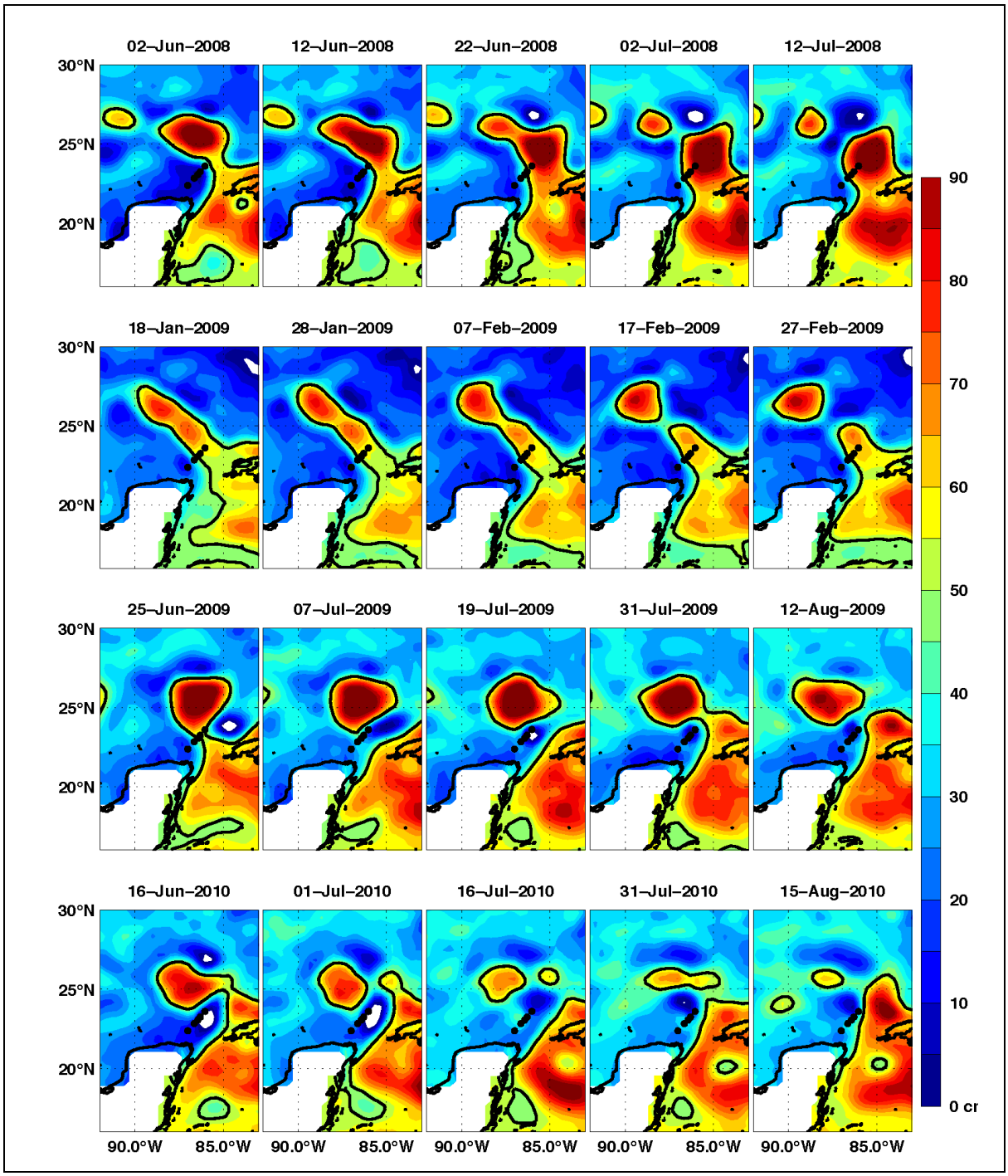

Figure 81. Snapshots of absolute sea surface height from AVISO showing the evolution of the four detachments documented: July 2, 2008 (top panels); February 18, 2009 (middle top panels); August 5, 2009 (middle bottom panels); August 11, 2010 (bottom panels). Detachment dates are determinate by the date that the 45 cm contour separated from the LC.

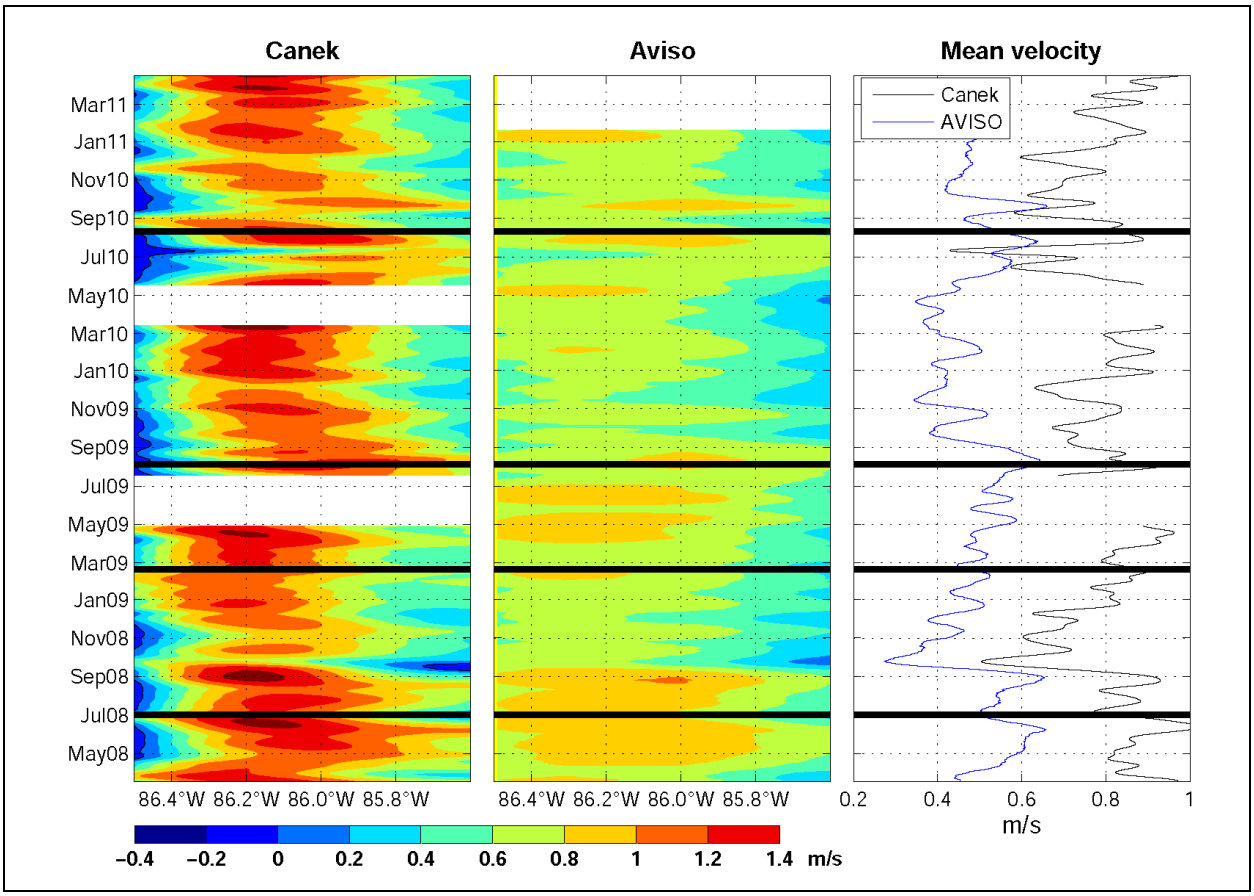

Figure 82. Longitude-time plot of the along-channel velocity for the WYC for Canek data (left panel) and geostrophic velocities from AVISO (middle panel). Along-channel velocity was averaged in longitude (right panel) for Canek data (black line) and AVISO data (blue line). Black lines indicate the dates of the LCE detachments.

In order to evaluate the horizontal current shear of the YCu during the LCE release events, the difference between the velocity at the current core (maximum velocity) and velocity at 86.4°W (the western edge YCu) was calculated (Figure 85), as an indicator of possible vorticity fluxes. There is a clear increase of the current shear (>.3 m/s for Canek and >0.05 m/s for AVISO), during three of the four release events (PE1, PE3 and PE4); this is confirmed by the time-integral of the current shear (lower panel of Figure 85), in which the four releases take place during or after a period of positive horizontal shear. During the release of LCE2, the current shifts to the east (Figure 81) without any clear increase of the positive horizontal shear, this may be due to a small increase in the current intensity (Figure 84); unfortunately, there is no mooring data available at this time at PE section.

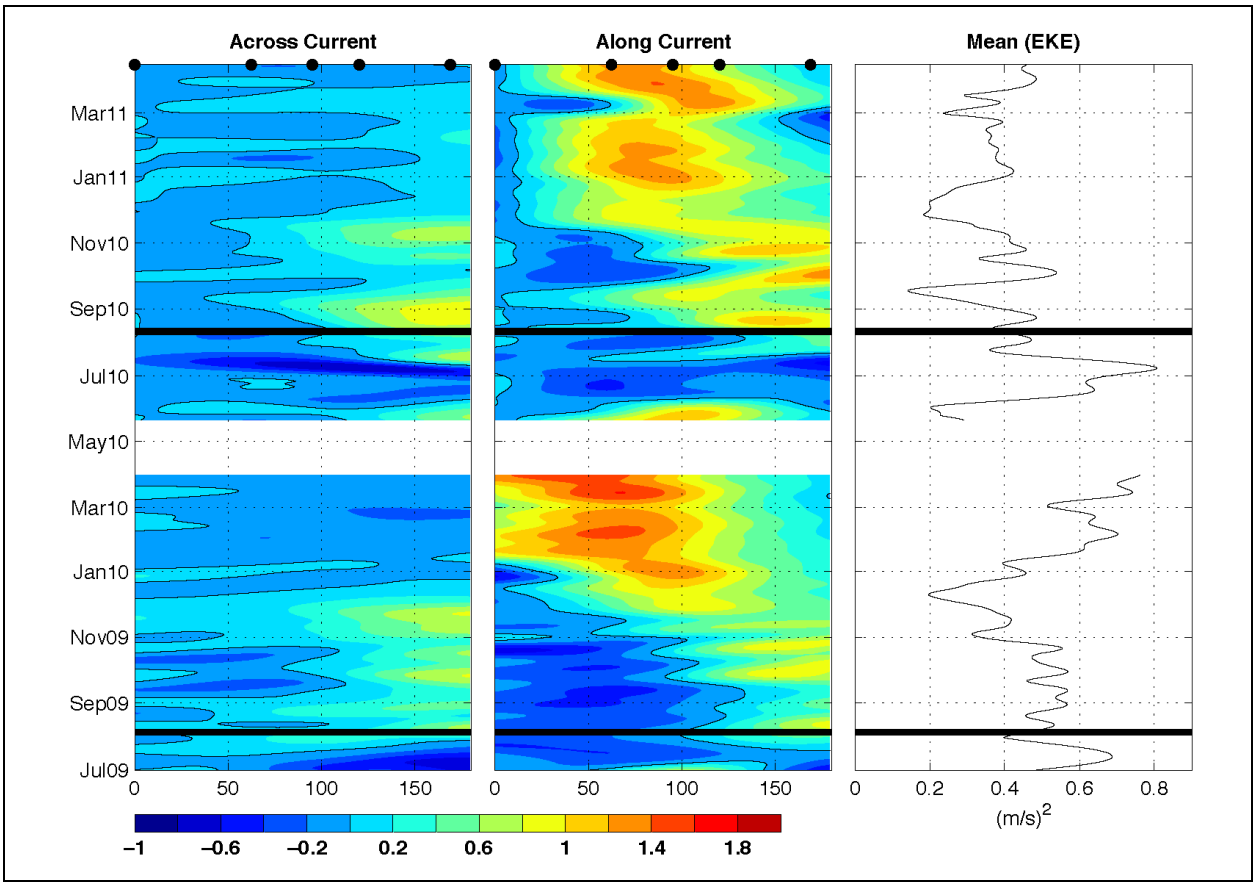

Figure 83. Longitude-time plot of the Canek data velocity components: parallel to section PE (left panel) and perpendicular to section PE (middle panel). Eddy kinetic energy is shown in the right panel. Black lines indicate the dates of the LCE3 and LCE4 detachments occurred between July 2009 and April 2011.

The sea surface height (SSH) anomalies were interpolated along the Western Caribbean, passing through the YC into the central and eastern part of the GoM, to visualize the time evolution of the variability from the YCu to the western side of LC (along the line in Figure 86). Based on the SSH anomalies diagram (Figure 86), a succession of positive-negative anomalies propagate from the northwestern Caribbean into the YC. Between January 2009 and January 2011, three of these anomalies propagate through YC into the GoM (~22°N). It is noteworthy that the three LCE detachments match the three arrival of corresponding negative SSH anomalies at the PE section. Current shear between along-section velocities of moorings PE5 and PE2 was calculated at 50 m depth (Figure 85, upper panel). Three of the four LCE releases observed during this time period (LCE1, LCE3, and LCE4), occurred after the increase of current horizontal shear (positive vorticity). The detrended time integral of the horizontal shear confirms that LCE1 and LCE4 releases occurred just after the positive shear of current turns negative, and LCE3 during a period of positive vorticity.

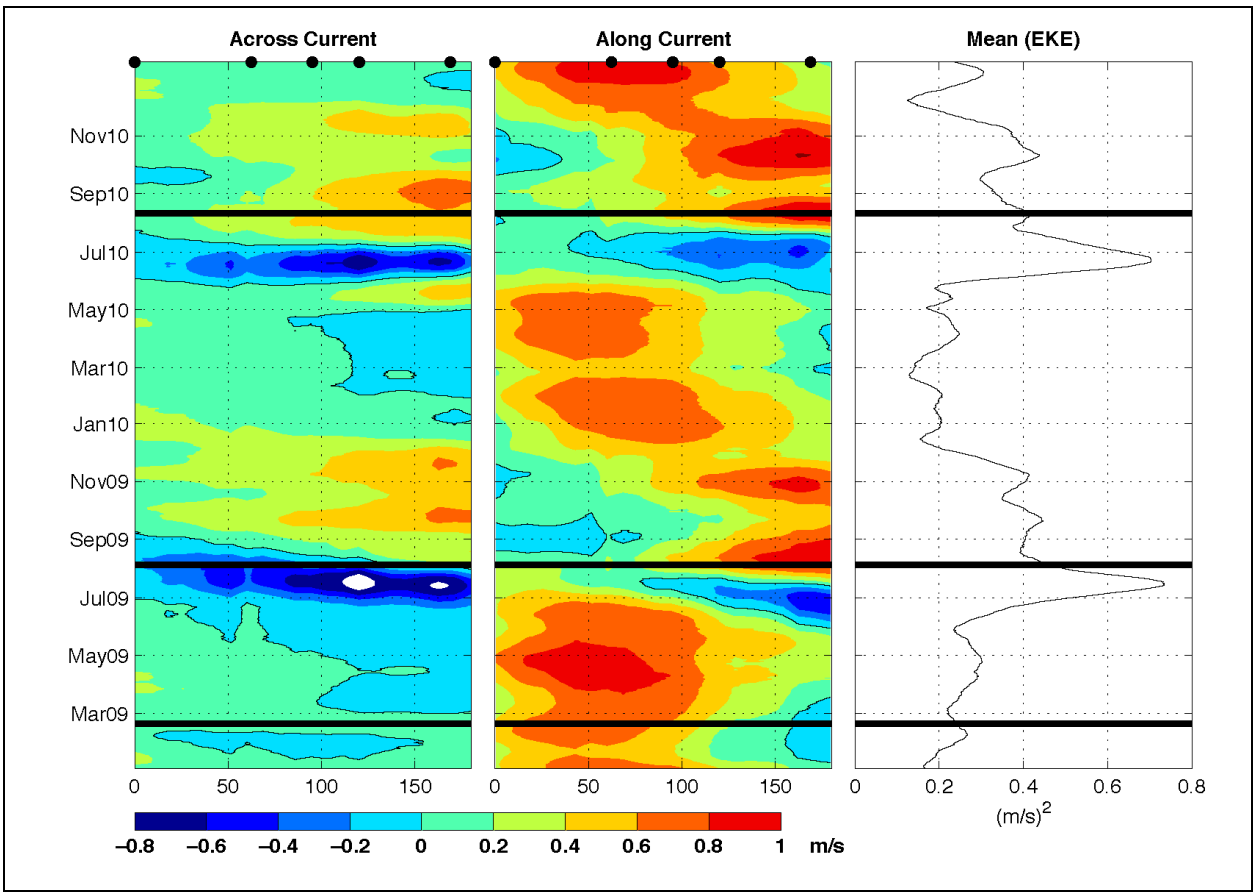

Figure 84. Longitude-time plot of the geostrophic velocity components deduced from AVISO sea surface height: parallel to section PE (left panel) perpendicular to section PE (middle panel). Eddy kinetic energy is shown in the right panel. Black lines indicate the dates of the LCE2, LCE3, and LCE4 detachments occurred between April 2009 and December 2010.

The connection between the eastern shifts of the YCu core and the eddy shedding events by the LC, have already been recognized in a numerical model (Ezer et al., 2003); after that, it was demonstrated from 3-years of mooring and satellite observations, between 2006 and 2009 (Athie et al., 2012), that release periods are associated with an eastward shift of the current core and cumulative positive horizontal shear for both, the YCu and the LC. In this chapter the same connection was demonstrated for the subsequent period between 2009 and 2011.

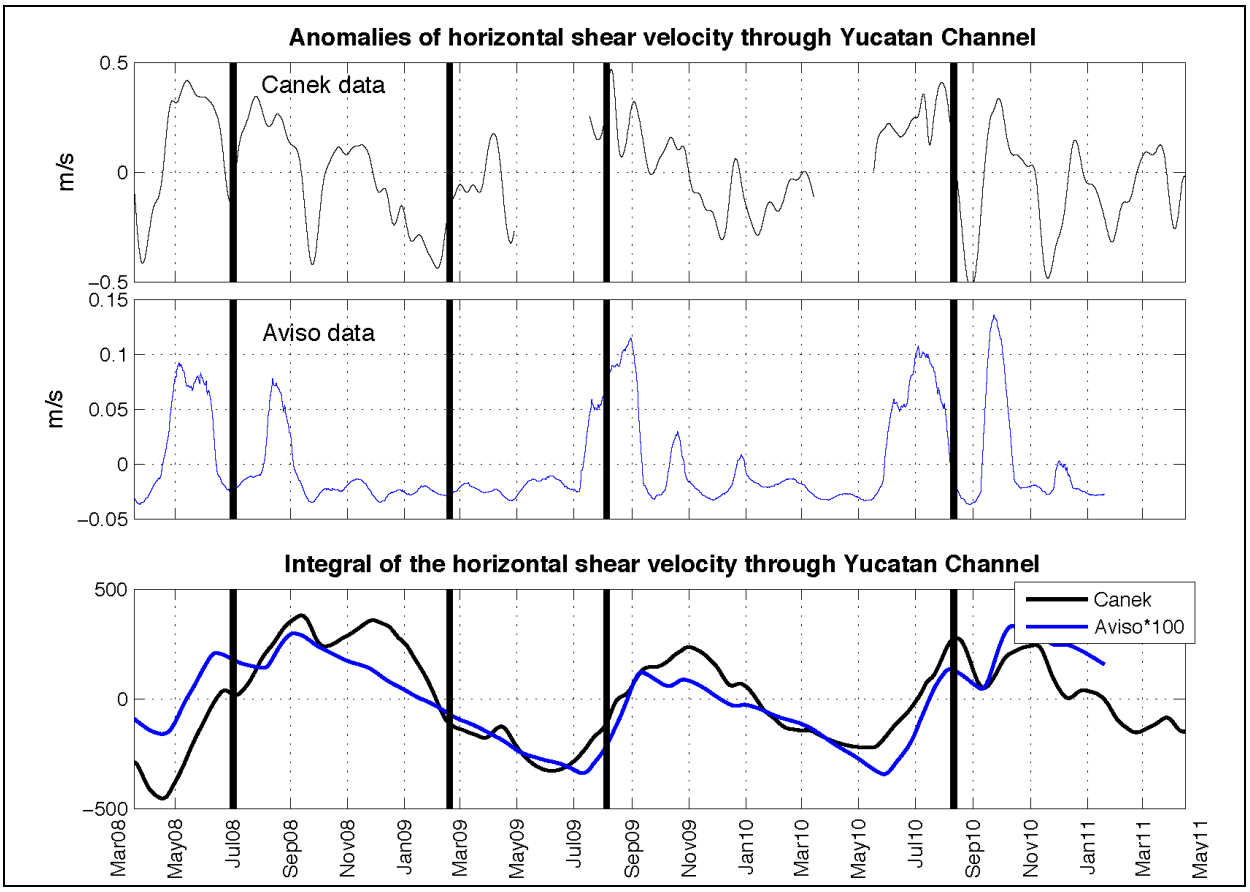

Figure 85. Horizontal shear at the WYC from mooring data (top panel) and AVISO geostrophic velocities (middle panel). Horizontal shear was calculated from the anomalies of the difference between the highest velocity of the YCu and the velocity at 86.4°W. Detrended time integrals of horizontal shear velocities were estimated (bottom panel).

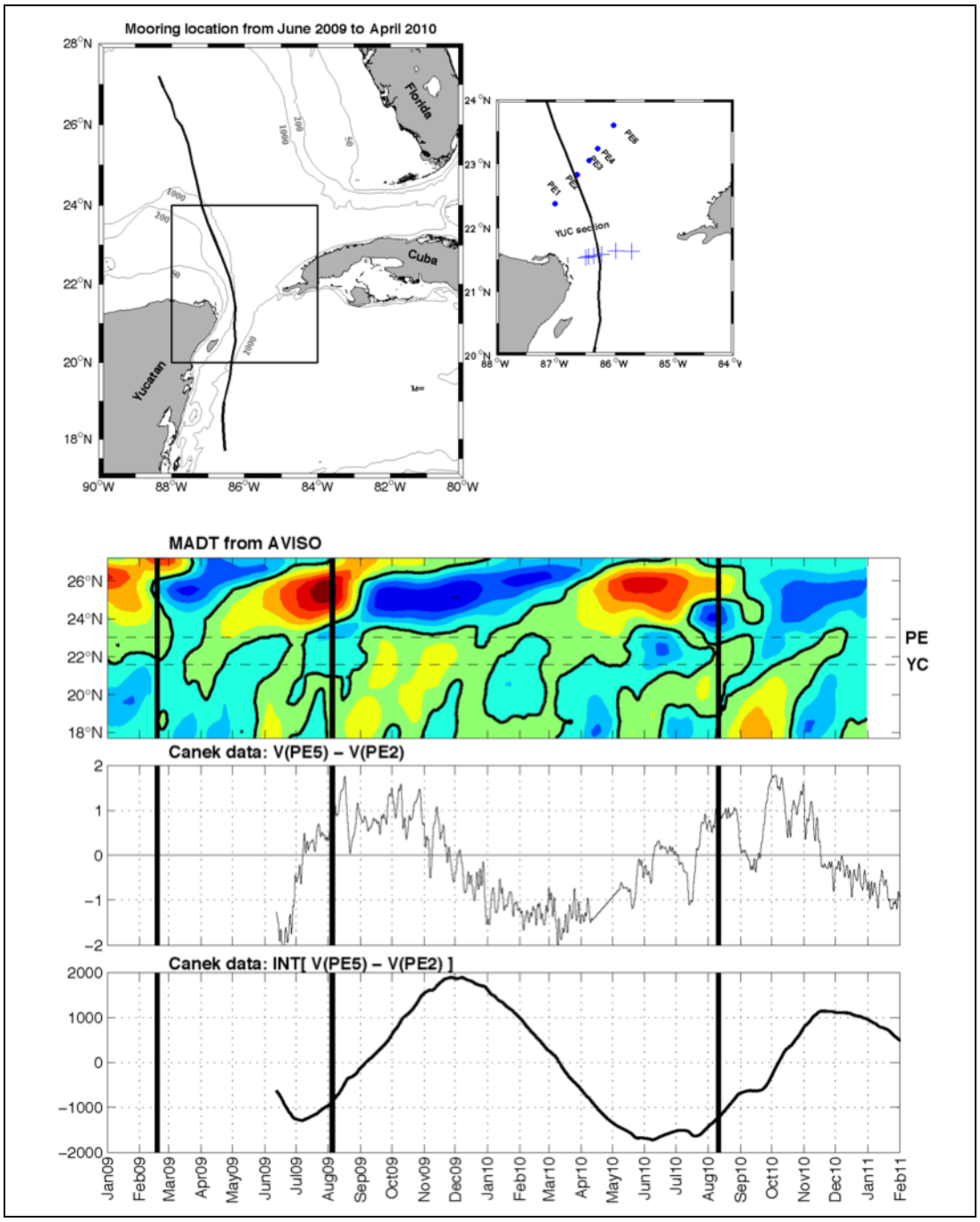

Figure 86. Time-latitude diagram of the sea surface height anomalies interpolated along the black trace of the map at the top. Anomalies of the horizontal shear velocity along the PE section calculated between moorings PE5 and PE2 (middle panel). Detrended time integral of the horizontal shear velocity at PE station (bottom panel). Time span only covers LCE2, LCE3, and LCE4.

6. SUMMARY AND CONCLUSIONS

The mooring array installed at the WYC (west of 85.6ºW) between March 2008 and May 2011 revealed a high degree of consistency in the yearly-averaged current structure over time, compared with the first detailed current measurements at YC between August 1999 and June 2001 (Sheinbaum et al., 2002). Additionally, two more sections installed along the shelf break from 150 m to over 3000m depth provided valuable information downstream in the western edge of LC (PE section) and northeast of the Campeche Bank (PN section). In the WYC, current structure is characterized by the intense flow of YCu with mean velocities around 1 m/s in its core, whose position varied between moorings YUC4, YUC5, and YUC6 although unfrequently up to YUC7, with mean current dominating over the variability. Current decreases considerably from the surface to 1000 m depth, where mean speeds are below 0.1 m/s with variations of the same order. Further north, the position of the current core varies between moorings PE2 and PE4, and between PN2 and PN3, but here the mean current velocity near the surface is lower than through the YC (0.75 m/s). The variability at PE is of the same order than the mean current, and at section PN variability exceeds the magnitude of the mean currents.

Empirical Orthogonal Function analysis of the velocity anomalies carried out at each mooring of the YC, PE, and PN sections showed that the first two modes explained nearly 90% of the variability (see Section 3.2). The first mode, that represents between 62% and 86% of the variance, shows that the mean orientation of currents are along the YC, and along the topography for the northern sections over the shelf. The second mode explains 7–25% of the variability with a structure basically across the YC and perpendicular to the topography at PE and PN. The principal component of this second mode shows intense pulses propagating from the shelf to the deep slope (Figure 41), without any apparent seasonally.

The vertical structure in almost all moorings has the highest velocity current near the surface and decreasing with depth, until 1000m depth, where the minimum of velocity is observed; this zone is also characterized by a minimum of the ratio of sub-inertial velocity variance to total variance, which diminishes below 40% at this depth. For the deepest moorings (YUC7, PE5, and PN4), this value increases again over 70% and is also associated with a slight increase of current velocity at depth. The increase near the bottom at the YC (YUC7) are due mostly, to deeper flows entering and exiting the GoM near the bottom, which have been proved related with the LC dynamics (Maul et al., 1985; Bunge et al., 2002). On the other hand, the southward, bottom-intensified, along-slope flows observed in deep moorings of sections PE and PN, suggest the presence of strong topographic Rossby waves seen in other areas of the GoM along the slope (e.g., Hamilton, 2007, Oey and Lee, 2002, Kolodziejczyk et al. 2012).

The ellipses of variability together with vector time series and the individual mooring EOF decomposition, show that the current meanders (zonal variations of the current core position) are of greater magnitude in PE and PN stations than in the YC with a seasonal trend: current core was observed offshore, i.e. shifts eastward in summer, between June and September and westward, toward the shelf, in winter–spring (between November to April). Moreover, three of

the four LCE releases observed between July 2008 and June 2011 occurred in summer. However, the shifts of the current core or current meanders are a common feature observed in the YCu and the LC. An important result is that current meanders are related to the LCE releases. These new measurements prove that four LCE releases observed between 2008 and 2011 were preceded by an intense pulse in along-channel velocity at the WYC, as well as by an EKE pulse in the LC (PE section). Furthermore, LCEs' releases are simultaneous with the eastward shift of the YCu, together with periods of positive horizontal shear (cyclonic vorticity) along the YC and PE section. This relation is very clear in three of the four LCE releases (July 2008, August 2009, and August 2010). Additionally, this seasonality represents a significant proportion of the variability; it is captured in the first EOF mode of variability. At PE section the first EOF represents 61% of the variance (Figure 87) and the spatial mode presents negative (positive) anomalies of the flow near the shelf between June–November (December–May), which are in good agreement with the horizontal shear of the LC at PE (also indicated in the figure).

The altimetry, and eddies detected by it, provide a clear framework to interpret the mooring observations and allows to explain the connection between observed currents at different locations. MADT allowed to have a clear vision of the process involved; in the four LCE releases, the meander of the current or the eastward shift of the YCu was observed just before the arrival of a cyclone to the northwestern Caribbean and just before the LCE detachment; Figure 86 confirms the propagation of SSH anomalies along the Yucatan shelf from the Caribbean into the GoM, with negative anomalies just before each LCE release. These findings were already discussed by Athie et al. (2012), considering an earlier period of observations (between January, 2005 and July, 2008); however, there are other processes that could contribute to the increase of cyclonic vorticity through the YCu. Huang et al. (2013) using a numerical model, show that the passage of anticyclonic eddies from the Caribbean into the GoM, not in the western side but in the central YC, is also related to EKE pulses and a shift of the YCu, which in turn contribute to the LCFE increase inside the GoM. However, a clear connection between the passages of anticyclonic eddies through the YC and the LCEs releases could not be established.

Regarding seasonality, one important result is the remarkable compensation between variability at western and eastern sides of the YC (west and east from 85.6°W). Transport anomalies at both sides of the channel are of the same order of amplitude (4–5 Sv) and show a compensating behavior (negative correlation around 0.7 to 0.8); consequently, significant changes in the total transport variability with respect to the transport only at the western side of the channel (YCu transport) are observed, even if the mean transport in the WYC represents about the 90% of the total mean transport. Then, variability of the total transport cannot be accounted with only the western side, as it is modified, not only in the high frequency but also in its seasonal cycle, by the contribution of the eastern side. The time evolution of the monthly-averaged transport between May 2010 and May 2011 for total and WYC (Figure 88) shows two maxima of equal magnitude in August and January, but considering only the WYC the maximum in winter increases over the summer. It is important to mention that using a longer time-series, the total YC transport appears to have a stronger annual cycle, whilst the YCu transport shows a hint of a semi-annual signal with asymmetric maxima in summer and winter–spring (with higher transport in winter–spring) for the period analyzed (not shown here).

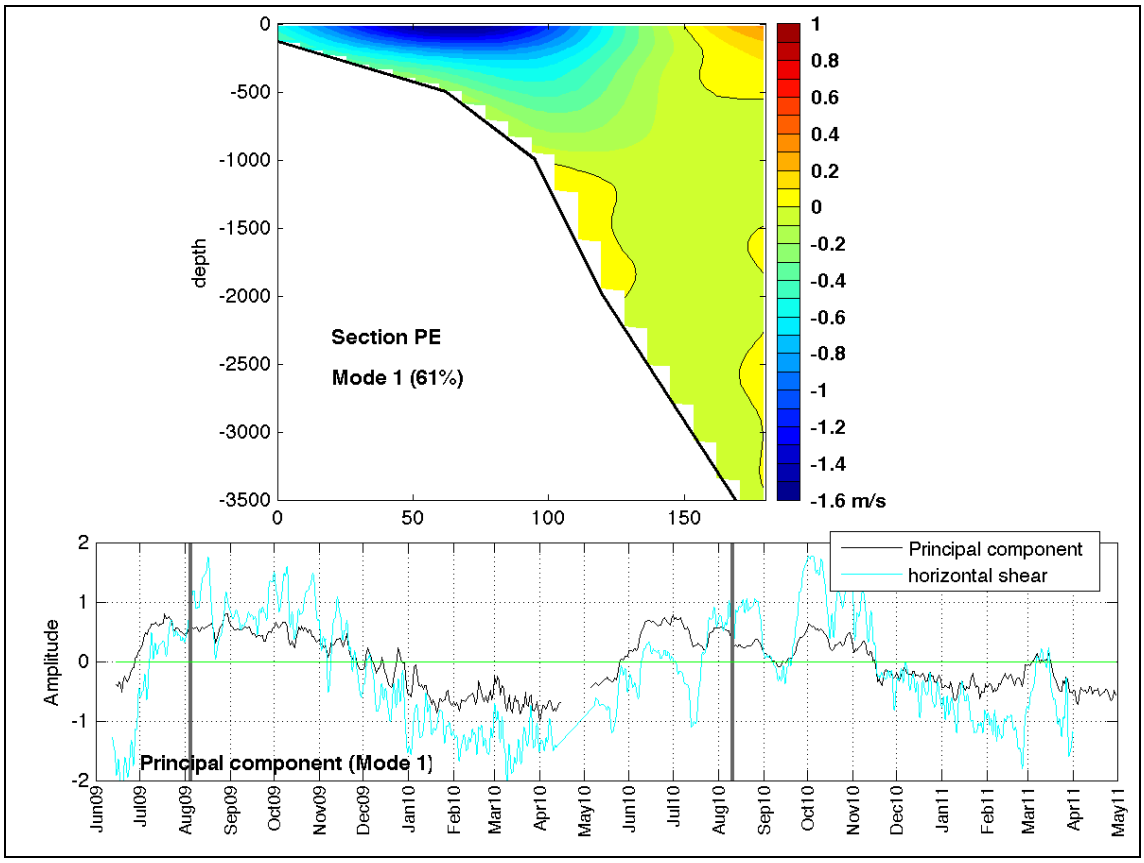

Figure 87**.** Fist EOF mode of variability for the section PE, which represents the western side of the LC. Temporal evolution or principal component of the mode (lower panel, black line) with anomalies of the horizontal shear velocity along PE section calculated between moorings PE5 and PE2 (cyan line). LCE releases dates are indicated (vertical black lines).

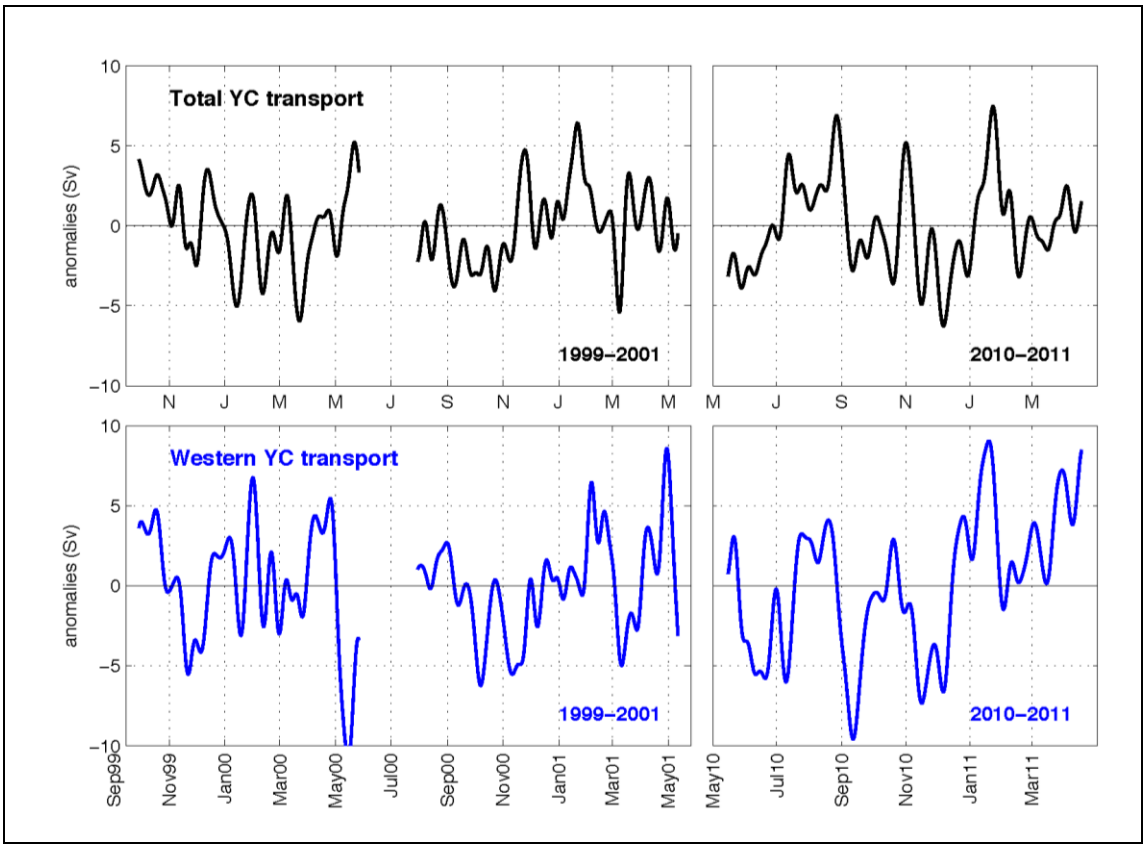

Figure 88. Time-evolution of YC transport anomalies considering the whole YC (black line) and the WYC (blue line), for the first period (1999–2001, left panels) and the second period (2010–2011, right panels) of Canek measurements.

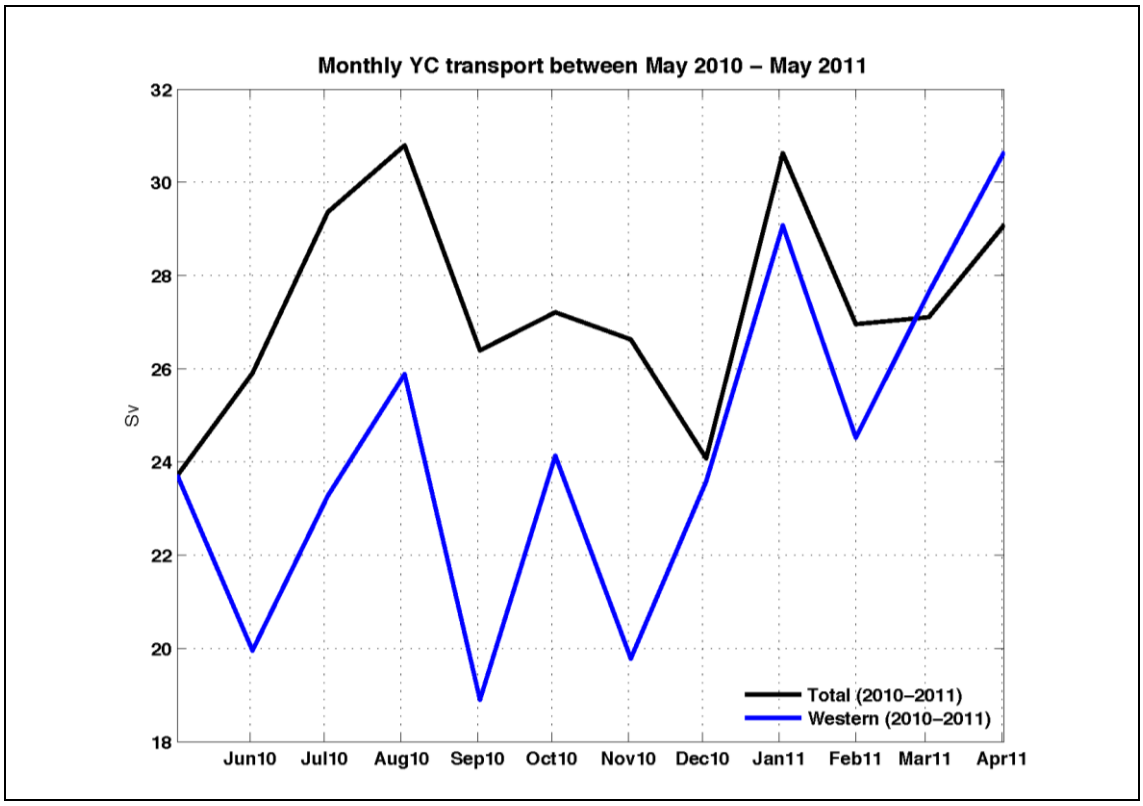

Figure 89. Monthly averaged time series of the total (black line) and western (blue line) YC transport between May 2010 and April 2011.

The suggestion of an asymmetric semi-annual cycle in the YC transport deduced from 20 years of numerical model simulations (Chang and Oey, 2012, 2013) is not clearly observed in all the Canek data. The period 2010-2011 does indicate such a cycle (Figure 89) and only a hint of it appears considering the western side of YC, but this is not always the case. The comparison between the two periods of Canek measurements (1999–2001 and 2008–2010) partially confirmed a Cayman wind-stress curl - WYC transport connection, with a time-lag of 1 month, as suggested by Chang and Oey (2012) but again, such a relation is not always present. Monthly-averaged series of $\nabla \times \bar{\tau}$ and WYC transport, revealed the global maxima of both series in winter rather than summer during the analysis periods, but time-series of both variables also show periods of non-connection. This suggests interannual variability modulates the plausible seasonal relation between winds over the Cayman Sea and YC transport, but remote forcing must play also a role since transport variations are not always in agreement with local (Cayman Sea) forcing variations.

Between May 2010 and May 2011 the whole YC was measured, yielding a total transport of 27 Sv, which is 4 Sv higher than between 1999 and 2001 (23 Sv) Between 2008–2011, considering only the western side of the channel, the yearly-means transports were rather

constant (~24 Sv). This western transport alone is 2 Sv higher than in 1999–2001. For the western transport alone, the standard deviation estimated during the five available years is 3.5 Sv. This suggests a significant interannual variability of currents through this channel. One important result is the importance of the western-eastern YC dynamics and the connection between the YCu and LC dynamics, which is complex and changes over time, varying its dynamics in seasonal, but also at interannual time-scales.

Topography determines also the basic characteristics of the flow. Throughout the slope of the Yucatan Peninsula, variability is oriented along the topography (from YUC2 to YUC5, from PE1 to PE3 and from PN1 to PN4) with some reversals of the current. Vectors time series shows southward current episodes near the surface during July–September 2009 and April–October 2010, corresponding to the offshore shift of the current core. Over the slope, particularly at PN section, high-frequency variability is observed, particularly in winter, between January and May 2010.

7. REFERENCES

Abascal, A. J., J. Sheinbaum, J. Candela, J. Ochoa, and A. Badan. 2003. Analysis of flow variability in the Yucatan Channel, J. Geophys. Res., 108 (C12), 3381, doi: 10.1029/2003JC001922.

Athie G., J. Candela, J. Ochoa and J. Sheinbaum. 2012. Impact of Caribbean cyclones on the detachment of Loop Current anticyclones, J. Geophys. Res., 117, C03018, doi: 10.1029/2011JC007090.

Atkinson, L. P., T. Berger, P. Hamilton, E. Waddell, K. Leaman and T. N. Lee. 1995. Current meter observations in the Old Bahama Channel, J. Geophys. Res., 100, 8555–8560.

Baringer, M. O., and J. C. Larsen. 2001. Sixteen years of Florida Current transport at 27°N, Geophys. Res. Lett., 28: 3179–3182.

Bunge, L., J. Ochoa, A. Badan, J. Candela and J. Sheinbaum. 2002. Deep flows in the Yucatan Channel and their relation to changes in the Loop Current extension, J. Geophys. Res., 107(C12), 3233, doi: 10.1029/2001JC001256.

Candela, J., J. Sheinbaum, J. Ochoa, and A. Badan. 2002. Potential vorticity flux through the Yucatán Channel and the Loop Current in the Gulf of Mexico, Geophys. Res. Lett., 29, 2059, doi:10.1029/2002GL015587.

Candela, J., S. Tanahara, M. Crepon, B. Barnier and J. Sheinbaum. 2003. Yucatan Channel flow: Observations versus CLIPPER ATL6 and MERCATOR PAM models, J. Geophys. Res., 108(C12), 3385, doi: 10.1029/2003JC001961.

Chang Y. L. and L. Y. Oey. 2010. Why can wind delay the shedding of Loop Current eddies?, J. Phys. Oceanogr., 40(11), doi: 10.1175/ 2010JPO4460.1.

Chang, Y.-L. and L.-Y, Oey. 2012. Why does the Loop Current tend to shed more eddies in summer and winter?, J. Geophys. Res., 39, L05605, doi: 10.1029/2011GL050773.

Chang, Yu-Lin, L.-Y. Oey. 2013. Loop Current Growth and Eddy Shedding Using Models and Observations: Numerical Process Experiments and Satellite Altimetry Data. J. Phys. Oceanogr., 43, doi: 10.1175/JPO-D-12-0139.1

Chelton, D.B. 1983. Effects of sampling errors in statistical estimation. Deep-Sea Res., 30, 1083-1101.

Chérubin, L. M., Y. Morel and E. P. Chassignet. 2006. Loop Current ring shedding: The Formation of Cyclones and the Effect of Topography, J. Phys. Oceanogr., 36(4): 569-591.

Cochrane, J. D. 1969. Currents and waters of the eastern Gulf of Mexico and western Caribbean, of the western tropical Atlantic, and of the eastern tropical Pacific Ocean. Tech. Rep., pp.29-31, Texas A& M Univ., Ref. 69-9T.

Cochrane, J. D. 1972. Separation of an anticyclone and subsequent developments in the Loop Current (1969), in Contributions on the Physical Oceanography of the Gulf of Mexico, Edited by L. R. A. Capurro and J. L. Reid, pp. 91-106, Texas A & M University Oceanographic Studies, Gulf Publishing Co., Houston.

Ezer, T., L.-Y. Oey, H.-C. Lee and W. Sturges. 2003. The Variability of Currents in the Yucatan Strait: Analysis of Results from a Numerical Ocean Model, J. Geophy. Res., 108(C1), 3012, doi: 10.1029/2002JC001509.

Fratantoni, P. S., T. N. Lee, G. P. Podesta and F. Muller-Karger. 1998. The influence of Loop Current perturbations on the formation and evolution of Tortugas eddies in the southern Strait of Florida, J. Geophys. Res., 103 (C11), 24,759-24,799.

Gordon, A. L. 1967. Circulation of the Caribbean Sea. J. Geophys. Res., 72, 6207-6223.

Hamilton, P. 1990. Deep currents in the Gulf of Mexico. J. Phys. Oceanogr., 20: 1087-1104.

Hamilton, P. 2007. Deep-current variability near the Sigsbee Escarpment in the Gulf of Mexico. J. Phys. Oceanogr. 37: 708-726.

Hurlburt, H. E. and J. D. Thompson. 1980. A numerical study of Loop Current intrusions and eddy shedding, J. Phys. Oceanogr., 10: 1611– 1651.

Hurlburt, H. E. 1986. Dynamic transfer of simulated altimeter data into subsurface information by a numerical ocean model, J. Geophys. Res., 91 (C2), 2372-2400.

Johns, W.E., T.L. Townsend, D.M. Fratantoni and W.D. Wilson. 2002. On the Atlantic inflow to the Caribbean Sea, Deep Sea res., 49, 211-243.

Kolodziejczyk, N., J. Ochoa, J. Candela and J. Sheinbaum. 2012. Observations of intermittent deep currents and eddies in the Gulf of Mexico, J. Geophys. Res., 117 (C9), doi: 10.1029/2012JC007890.

Larsen, J. 1992. Transport and heat flux of the Florida Current at 27N derived from cross-stream voltages and profiling data: theory and observations. Philos. Trans. Roy. Soc. London, A338, 169-236.

Leaman, P. S. Vertes, L. P. Atkinson, and T. N. Lee. 1995. Transport, potential vorticity, and current/ temperature structure across Northwest Providence and Santaren Channels and the Florida Current off Cay Sal Bank, J. Geophys. Res., 100: 8561–8569.

Leben, R. R. 2005. Satellite observations of Gulf of Mexico mesoscale circulation and variability, in Circulation in the Gulf of Mexico: Observations and Models, Vol. 161, edited by W. Sturges and A. Lugo-Fernandez pp. 181-201, Geophys. Monograph Ser., AGU, Washington.

Le Hennaf, M., V.H. Kourafalou, Y. Morel and A. Srinivasan. 2012. Simulating the dynamics and intensification of cyclonic Loop Current Frontal Eddies in the Gulf of Mexico, J. Geophys. Res., C2, doi: 10.1029/2011JC007279.

Maul, G. A., D. A. Mayer and S. R. Baig. 1985. Comparisons between a continuous 3-year current-meter observation at the sill of the Yucatan Strait, satellite measurements of Gulf Loop Current area, and regional sea level, J. Geophys. Res., 90: 9089– 9096.

Molinari, R. L., J. F. Festa and D. W. Behringer. 1978. The circulation in the Gulf of Mexico derived from estimated dynamic height fields. J. Phys. Oceanogr., 8, 987/996.

Ochoa, J., A. Badan, J. Sheinbaum and J. Candela. 2003. Canek: Measuring transports in the Yucatan Channel. In: Nonlinear Processes in Geophysical Fluid Dynamics: A tribute to the scientific work of Pedro Ripa (O.U. Velasco, J. Sheinbaum and J. Ochoa, Eds.), Kluwer, 275-286.

Oey, L-Y. 1996. Simulation of mesoscale variability in the Gulf of Mexico: Sensitivity studies, comparison with observations, and trapped wave propagation, Journal of Phys. Oceanog., 26(2): 145-175.

Oey, L.-Y., H.-C. Lee and W. J. Schmitz Jr. 2003. Effects of Winds and Caribbean Eddies on the Frequency of Loop Current Eddy Shedding: A Numerical Model Study, J. Geophy. Res., 108(C10), doi: 10.1029/2002JC001698.

Oey, L.-Y., T. Ezer, and H.-C. Lee. 2005. Loop Current, rings and related circulation in the Gulf of Mexico: A review of numerical models and future challenges, in Circulation in the Gulf of Mexico: Observations and Models, Vol. 161, edited by W. Sturges and A. Lugo-Fernandez pp. 31-56, Geophys. Monograph Ser., AGU, Washington.

Oey, L.-Y., T. Ezer, D.-P. Wang, X.-Q. Yin and S.-J. Fan, 2007. Hurricane-induced motions and interaction with ocean currents. Cont. Shelf Res., 27, 1249-1263, doi: 10.1016/j.csr.2007.01.008.

Pichevin, T. and D. Nof. 1997. The momentum imbalance paradox. Tellus A, 49, 298-319, doi: 10.1034/j.1600-0870.1997.t01-1-00009.x.

Rivas, D., A. Badan, and J. Ochoa. 2005. The ventilation of the deep Gulf of Mexico. J. Phys. Oceanogr., 35: 1763-1781.

Roemmich D. 1981. Circulation of the Caribbean Sea: A well-resolved inverse problem, J. Geophys. Res., 86, 7993-8005.

Rousset, C., L. M. Beal. 2010. Observations of the Florida and Yucatan Currents from a Caribbean Cruise Ship, J. Phys. Ocean., 40, doi: 10.1175/2010JPO4447.1.

Rousset, C. and L.M. Beal. 2011. On the seasonal variability of the currents in the Strait of Florida and Yucatan Channel, J. Geophys. Res., 116, C08004, doi:10.1029/2010JC006679.

Schmitz, W. J. Jr. 2005. Cyclones and westward propagation in the shedding of anticyclonic rings from the Loop Current, in Circulation in the Gulf of Mexico: Observations and Models, Vol. 161, edited by W. Sturges and A. Lugo-Fernandez pp. 241-262, Geophys. Monograph Ser., AGU, Washington.

Sheinbaum, J., J. Candela, A. Badan and J. Ochoa. 2002. Flow structure and transports in the Yucatan Channel, Geophys. Res. Lett., 29(3), doi: 10.1029/2001GL0139990.

Sturges, W., and J.C. Evans. 1983. On the variability of the Loop Current in the Gulf of Mexico, Journal of Marine Research, 41, 639-653.

Sturges, W. 2005. Deep-water exchange between the Atlantic, Caribbean and Gulf of Mexico, in Circulation in the Gulf of Mexico: Observations and Models, Vol. 161, edited by W. Sturges and A. Lugo-Fernandez pp. 263-278, Geophys. Monograph Ser., AGU, Washington.

Sturges, W., N. G. Hoffman and R. R. Leben. 2010. A trigger mechanism for Loop Current ring separations, J. Phys. Oceanogr., 40. doi: 10.1175/2009JPO4245.1.

Vukovich, F. M., B. W. Crissman, M. Bushnell and W. J. King. 1979. Some aspects of the Gulf of Mexico using satellite and in-situ Data, J. Geophys. Res., 84, 7749–7768.

Vukovich, F. M. 1988. Loop Current Boundary Variations, J. Geophys. Res., 93(C12): 15,585–15,591.

Zavala-Hidalgo, J., S. L., Morey and J. J. O'Brien. 2003. Cyclonic eddies northeast of the Campeche Bank from altimetry data, J. Phys. Oceanogr., 33, 623–629.

APPENDIX A. TABLES OF BASIC STATISTICS

APPENDIX A. TABLES OF BASIC STATISTICS

Table A- 1. Basic statistics for Mooring YUC2 during Canek 20

depth	mean_u	std_u	min_u	max_u	mean_v	std_v	min_v	max_v	MMS # of obs	sample interval
8	4.80	18.32	-92.06	80.50	37.96	45.41	-137.95	253.80	15245	30
12	4.90	17.51	-90.99	65.70	37.05	45.18	-135.37	257.90	15245	30
16	4.43	16.72	-85.40	63.38	36.13	44.30	-133.86	249.10	15245	30
20	3.59	16.06	-82.51	58.50	35.42	43.27	-129.00	230.90	15245	30
24	2.17	15.42	-86.58	55.40	33.98	42.20	-123.44	215.57	15245	30
28	0.31	14.82	-78.84	53.00	31.03	41.06	-120.56	211.35	15245	30
32	-1.39	14.48	-70.69	49.55	26.40	39.39	-114.59	198.96	15245	30
36	-2.70	14.34	-69.49	55.98	20.56	36.89	-110.24	181.17	15245	30
40	-3.34	14.31	-67.59	62.02	14.45	33.70	-108.13	165.78	15245	30
44	-3.25	14.34	-64.21	67.56	8.92	30.15	-99.81	151.19	15245	30
48	-2.44	14.49	-61.06	76.01	4.30	26.49	-90.60	134.54	15245	30
52	-1.11	14.71	-62.12	74.18	0.72	22.63	-84.79	118.18	15245	30

Table A- 2. Basic statistics for Mooring YUC2 during Canek 23

depth	mean_u	std_u	min_u	max_u	mean_v	std_v	min_v	max_v	MMS # of obs	sample interval
10	7.33	17.20	-88.60	84.80	46.56	47.40	-82.80	241.30	18612	30
18	5.40	15.54	-89.60	64.70	45.29	47.14	-78.00	233.70	18612	30
26	1.92	14.03	-86.70	66.20	40.99	44.96	-78.00	211.90	18612	30
34	-1.27	13.07	-76.60	54.50	30.23	39.83	-74.90	180.30	18612	30
42	-2.57	12.56	-67.10	51.10	16.42	31.77	-73.90	164.40	18612	30
50	-2.16	12.48	-55.00	49.50	5.69	23.72	-64.00	120.60	18612	30

Table A- 3. Basic statistics for Mooring YUC3 during Canek 20

depth	mean_u	std_u	min_u	max_u	mean_v	std_v	min_v	max_v	MMS # of obs	sample interval
14	10.44	19.35	-163.10	229.00	76.80	71.74	-129.80	318.40	15257	30
22	9.45	17.62	-84.10	77.30	74.37	69.56	-127.40	262.60	15257	30
30	7.57	16.52	-84.70	76.80	67.20	67.91	-131.90	258.90	15257	30
38	5.27	15.48	-81.30	72.40	55.57	65.54	-136.20	245.60	15257	30
46	3.25	14.43	-75.20	69.10	41.75	61.01	-140.10	237.30	15257	30
54	1.79	13.54	-70.70	65.50	28.07	53.81	-143.20	214.60	15257	30
62	0.44	12.87	-68.40	63.70	16.24	45.15	-138.20	183.20	15257	30
70	-0.80	12.26	-67.40	72.50	7.22	36.62	-119.30	166.60	15257	30
78	-1.89	11.47	-63.00	88.80	0.94	29.60	-95.50	139.80	15257	30
86	-2.53	10.63	-59.40	92.30	-3.06	24.45	-75.20	110.20	15257	30
94	-2.53	9.84	-61.20	89.90	-5.08	20.88	-71.90	91.00	15257	30
102	-1.89	9.23	-47.00	90.00	-5.53	18.43	-72.40	75.30	15257	30

Table A- 4. Basic statistics for Mooring YUC3 during Canek 23

depth	mean_u	std_u	min_u	max_u	mean_v	std_v	min_v	max_v	MMS # of obs	sample interval
8	-0.01	30.56	-326.20	376.58	71.36	59.72	-187.80	374.70	18618	30
16	-0.82	33.43	-254.60	440.50	82.93	70.92	-197.20	342.10	18618	30
24	-1.60	30.41	-223.00	290.80	76.36	68.68	-161.90	297.50	18618	30
32	-1.32	26.89	-106.80	189.30	65.34	65.62	-76.10	232.30	18618	30
40	-0.44	23.37	-90.70	86.30	51.20	59.81	-70.40	217.20	18618	30
48	0.03	19.60	-90.30	69.20	36.46	51.62	-62.00	193.90	18618	30
56	-0.34	16.14	-76.70	59.80	23.74	43.21	-57.80	164.10	18618	30
64	-0.99	13.73	-58.80	49.50	14.12	36.20	-59.40	139.90	18618	30
72	-1.50	12.25	-54.40	47.80	7.34	30.91	-60.40	128.80	18618	30
80	-1.52	11.16	-48.90	47.50	2.82	27.08	-63.00	115.80	18618	30
88	-1.08	10.20	-43.10	52.50	0.12	23.76	-63.80	104.40	18618	30
96	-0.50	9.49	-44.60	61.30	-1.29	20.34	-67.20	87.10	18618	30
104	0.06	9.22	-36.20	63.90	-1.87	16.87	-56.70	67.50	18618	30

Table A- 5. Basic statistics for Mooring YUC4 Canek 20

depth	mean_u	std_u	min_u	max_u	mean_v	std_v	min_v	max_v	MMS # of obs	sample interval
53	21.91	21.42	-69.10	119.10	117.00	49.03	-32.40	238.60	15253	30
69	21.87	20.18	-49.40	129.20	111.58	56.61	-49.30	223.10	15253	30
85	18.16	19.00	-35.90	129.80	91.09	57.16	-64.90	199.90	15253	30
101	12.99	17.33	-38.10	132.10	73.60	53.05	-83.20	176.70	15253	30
117	7.03	14.48	-42.30	134.90	61.50	48.77	-84.60	165.90	15253	30
133	3.20	12.24	-53.90	117.50	55.20	46.61	-66.30	154.40	15253	30
149	2.94	11.66	-49.80	110.80	50.79	45.17	-58.00	148.90	15253	30
165	3.85	11.57	-37.60	97.40	45.40	43.61	-67.70	139.90	15253	30
181	4.35	11.04	-34.60	76.60	39.28	41.35	-70.40	131.10	15253	30
197	4.05	10.35	-40.60	55.90	33.10	38.25	-74.70	126.30	15253	30
213	3.51	9.92	-37.20	51.70	27.14	34.66	-73.20	120.90	15253	30
229	3.05	9.35	-40.40	37.40	21.66	30.77	-69.30	111.90	15253	30
245	2.50	8.83	-38.70	39.30	16.61	26.99	-65.80	103.60	15253	30
261	1.59	8.53	-42.50	33.70	12.29	23.73	-60.70	91.30	15253	30
277	0.57	7.88	-28.50	33.70	8.94	21.13	-56.10	77.20	15253	30
293	-0.23	7.18	-30.20	31.10	6.37	19.40	-45.80	66.30	15253	30
309	-0.57	6.73	-29.50	29.40	4.29	18.34	-52.50	61.10	15253	30
325	-0.53	6.47	-29.10	26.60	2.51	17.41	-44.10	59.10	15253	30
341	-0.39	6.22	-29.30	29.80	0.73	16.02	-46.60	50.30	15253	30
357	-0.43	6.00	-28.60	25.40	-0.74	14.36	-49.40	45.50	15253	30
373	-0.69	5.82	-24.20	25.80	-1.95	13.06	-42.50	41.10	15253	30
389	-0.88	5.74	-33.20	26.00	-2.72	12.16	-41.30	40.20	15253	30
405	-0.99	5.65	-30.40	29.50	-3.13	11.46	-44.30	39.50	15253	30
421	-1.11	5.54	-26.40	27.20	-3.22	10.78	-43.70	39.30	15253	30
437	-1.13	5.43	-24.30	24.40	-3.01	9.98	-38.50	40.90	15253	30
453	-1.14	5.24	-25.80	23.10	-2.40	9.00	-36.10	44.40	15253	30
469	-0.96	4.95	-21.40	23.10	-1.65	7.71	-30.20	34.30	15253	30
485	-0.88	4.66	-19.20	24.60	-0.97	6.24	-26.60	36.00	15253	30
501	-0.62	4.30	-19.00	22.30	-0.51	5.01	-24.10	31.00	15253	30

Table A- 6. Basic statistics for Mooring YUC5 Canek 20

depth	mean_u	std_u	min_u	max_u	mean_v	std_v	min_v	max_v	MMS # of obs	sample interval
53	21.76	27.86	-51.10	137.00	109.59	24.79	-2.00	193.10	14878	30
69	22.02	24.80	-46.90	115.50	108.65	23.63	6.00	200.90	14878	30
85	17.74	19.28	-37.40	86.40	98.78	23.74	2.10	185.30	14878	30
101	13.85	15.76	-40.60	72.40	90.51	23.44	-8.00	169.80	14878	30
117	11.85	14.31	-39.00	63.80	83.04	24.20	-24.70	160.50	14878	30
133	10.76	13.52	-33.20	56.30	75.92	25.81	-32.40	144.90	14878	30
149	9.94	12.91	-38.60	59.50	70.30	27.19	-38.80	146.30	14878	30
165	9.31	12.58	-43.20	62.20	66.17	28.00	-41.60	144.10	14878	30
181	8.63	12.45	-44.10	63.40	62.54	28.23	-42.40	133.80	14878	30
197	8.20	12.03	-47.60	60.30	59.06	27.88	-43.80	129.00	14878	30
213	7.94	11.60	-49.90	68.70	55.77	27.39	-47.50	146.40	14878	30
229	7.62	11.11	-49.40	55.50	52.72	26.80	-48.80	120.10	14878	30
245	7.11	10.72	-46.60	57.40	49.78	26.01	-59.40	116.30	14878	30
261	6.51	10.31	-42.00	59.90	47.03	25.08	-62.10	111.90	14878	30
277	6.01	10.09	-37.90	60.80	44.42	24.20	-60.00	110.50	14878	30
293	5.67	10.03	-38.00	53.80	41.85	23.45	-60.30	103.20	14878	30
309	5.39	9.94	-39.00	49.80	39.33	22.58	-56.40	94.20	14878	30
325	5.09	9.86	-43.40	51.90	36.78	21.74	-61.30	93.90	14878	30
341	4.60	9.57	-48.50	50.60	34.23	21.06	-58.90	85.40	14878	30
357	3.94	9.16	-46.40	51.20	31.85	20.65	-62.20	83.90	14878	30
373	3.39	8.84	-43.00	48.20	29.67	20.49	-59.90	81.30	14878	30
389	3.12	8.59	-36.00	41.40	27.76	20.15	-58.20	83.40	14878	30
405	2.81	8.36	-36.20	43.30	25.96	19.79	-59.10	82.00	14878	30
421	2.42	8.30	-37.70	41.10	24.16	19.43	-55.10	84.10	14878	30
437	2.09	8.35	-38.80	39.10	22.27	19.13	-61.70	83.00	14878	30
453	1.83	8.41	-38.00	35.60	20.37	18.94	-67.50	80.70	14878	30
469	1.51	8.23	-34.70	31.90	18.43	18.71	-69.30	79.20	14878	30
485	1.16	7.87	-32.70	35.50	16.50	18.40	-65.20	76.80	14878	30
501	0.89	7.61	-29.60	31.40	14.34	17.83	-67.60	72.60	14878	30
594	-0.02	4.74	-19.25	21.56	-2.61	10.44	-43.31	46.91	3718	120
715	1.42	3.32	-8.39	16.13	-1.62	4.58	-22.25	19.03	3718	120
972	-0.52	2.81	-10.21	8.96	-4.17	6.99	-25.78	17.16	3717	120
1074	0.20	5.62	-20.74	27.36	2.09	11.75	-54.26	52.73	3718	120
1189	-0.23	2.99	-11.65	12.57	-4.69	7.82	-33.72	25.50	3717	120

Table A- 7. Basic statistics for Mooring YUC5 during Canek 23

depth	mean_u	std_u	min_u	max_u	mean_v	std_v	min_v	max_v	MMS #obs	sample interval
65	22.84	29.03	-44.80	122.40	108.25	31.38	-41.40	205.60	18649	30
81	18.00	23.60	-33.90	102.40	95.89	32.03	-41.10	184.80	18649	30
97	12.97	18.61	-33.70	94.40	85.61	32.21	-53.90	163.00	18649	30
113	10.02	15.27	-34.00	76.00	78.21	31.86	-58.10	148.90	18649	30
129	8.77	13.68	-37.30	61.40	72.05	31.74	-55.90	143.10	18649	30
145	8.16	13.16	-34.10	56.50	66.40	31.76	-56.40	141.80	18649	30
161	7.68	12.92	-33.60	58.40	61.68	31.67	-56.00	128.90	18649	30
177	7.16	12.27	-35.20	59.00	57.77	31.42	-50.80	130.20	18649	30
193	6.55	11.53	-42.10	67.10	54.25	30.73	-43.80	131.70	18649	30
209	6.00	11.02	-41.50	68.40	50.95	29.73	-44.10	129.40	18649	30
225	5.56	10.69	-41.20	64.80	47.93	28.72	-44.90	123.60	18649	30
241	5.16	10.56	-36.30	66.20	45.07	27.71	-38.90	123.50	18649	30
257	4.80	10.43	-32.90	69.00	42.26	26.59	-38.20	121.00	18649	30
273	4.42	10.27	-31.50	61.30	39.51	25.41	-39.70	122.10	18649	30
289	4.06	10.02	-32.60	52.00	36.91	24.35	-41.70	114.90	18649	30
305	3.63	9.70	-30.90	53.30	34.58	23.42	-41.60	104.70	18649	30
321	3.20	9.41	-30.60	47.20	32.38	22.53	-39.80	101.00	18649	30
337	2.78	9.13	-29.70	48.50	30.24	21.74	-43.80	97.30	18649	30
353	2.43	8.84	-28.00	44.70	28.31	21.13	-44.30	98.60	18649	30
369	2.08	8.49	-28.60	41.60	26.46	20.65	-42.40	98.00	18649	30
385	1.67	8.27	-27.50	35.00	24.65	20.10	-39.20	97.30	18649	30
401	1.32	8.05	-30.00	32.80	22.90	19.61	-41.60	102.10	18649	30
417	0.99	7.82	-29.50	34.60	21.34	19.25	-42.30	100.20	18649	30
433	0.67	7.69	-28.40	39.00	19.87	18.89	-44.20	97.10	18649	30
449	0.37	7.60	-28.20	42.00	18.37	18.53	-47.20	95.10	18649	30
465	0.07	7.56	-26.80	38.50	16.88	18.23	-50.00	93.90	18649	30
481	-0.12	7.33	-26.20	33.60	15.43	17.92	-49.90	91.20	18649	30
497	-0.27	7.10	-24.00	35.20	13.97	17.55	-55.10	85.60	18649	30
513	-0.35	7.01	-24.60	32.90	12.52	17.20	-57.10	82.00	18649	30
529	-0.40	7.00	-26.40	34.10	11.04	16.84	-54.40	79.70	18649	30
545	-0.42	6.89	-24.00	34.10	9.70	16.25	-51.10	79.30	18649	30
561	-0.35	6.69	-23.00	30.60	8.31	15.47	-47.60	79.70	18649	30
577	-0.26	6.39	-22.60	31.50	6.86	14.50	-39.70	80.50	18649	30
600	-0.43	5.71	-21.80	24.30	-0.32	10.59	-33.80	49.10	37290	15
722	-0.84	4.97	-23.50	23.30	-4.50	9.64	-39.40	29.90	37291	15
979	-0.73	3.82	-18.60	15.80	-5.32	7.86	-28.00	25.90	37291	15
1080	0.01	3.04	-15.00	16.40	-2.47	5.38	-23.20	19.00	37290	15
1190	0.68	3.11	-10.10	19.50	-1.07	3.04	-15.00	17.20	37289	15

Table A- 8. Basic statistics for Mooring YUC6 during Canek 20

depth	mean_u	std_u	min_u	max_u	mean_v	std_v	min_v	max_v	MMS # of obs	sample interval
63	13.72	21.52	-43.00	118.70	96.30	19.03	23.10	167.70	15224	30
79	12.87	20.39	-41.40	108.30	93.33	17.53	24.60	159.50	15224	30
95	11.67	18.58	-38.10	95.00	89.47	16.48	7.50	152.70	15224	30
111	10.22	16.69	-35.60	77.70	84.20	15.89	14.60	138.40	15224	30
127	8.78	15.30	-35.70	67.80	78.60	14.97	23.10	139.20	15224	30
143	7.54	14.31	-31.10	61.20	73.05	13.93	16.30	129.80	15224	30
159	6.83	13.62	-36.80	61.20	68.00	13.45	5.20	115.00	15224	30
175	6.47	13.18	-35.80	60.10	63.52	13.49	-5.50	113.20	15224	30
191	6.08	12.77	-35.80	56.30	59.89	13.53	-10.60	112.40	15224	30
207	5.72	12.30	-31.10	60.60	56.73	13.64	-17.40	111.30	15224	30
223	5.18	11.72	-30.70	56.90	54.15	13.82	-20.70	109.30	15224	30
239	4.81	11.36	-35.10	50.50	52.21	14.02	-19.40	108.40	15224	30
255	4.74	11.07	-32.70	52.00	50.78	14.01	-22.10	105.20	15224	30
271	4.66	10.69	-33.80	47.60	49.46	14.18	-23.50	105.20	15224	30
287	4.52	10.40	-31.20	46.80	48.04	14.26	-18.90	97.70	15224	30
303	4.17	10.23	-30.90	44.90	46.64	14.38	-19.50	99.30	15224	30
319	3.78	10.24	-34.20	48.00	45.28	14.58	-25.80	93.50	15224	30
335	3.54	10.13	-38.50	46.10	43.94	14.76	-33.20	90.70	15224	30
351	3.36	10.02	-39.70	43.80	42.59	14.86	-37.50	97.10	15224	30
367	3.12	10.02	-37.50	47.70	41.25	14.91	-39.00	93.50	15224	30
383	2.78	9.93	-36.70	46.60	40.00	15.00	-43.00	91.30	15224	30
399	2.62	9.87	-36.00	43.80	39.03	15.15	-41.50	94.70	15224	30
415	2.50	9.93	-35.80	39.70	38.20	15.11	-39.80	98.00	15224	30
431	2.35	9.99	-36.20	42.20	37.25	14.96	-39.70	99.30	15224	30
447	2.14	9.98	-37.60	48.40	36.40	14.79	-36.10	101.40	15224	30
463	1.97	9.92	-33.40	44.70	35.17	14.60	-35.00	101.40	15224	30
498	-2.55	8.54	-27.10	33.50	33.14	14.04	-18.90	99.00	15223	30
506	-2.47	8.65	-29.00	33.70	33.38	14.30	-20.90	98.40	15223	30
514	-2.46	8.66	-29.10	33.40	33.14	14.34	-21.40	96.00	15223	30
522	-2.45	8.69	-28.90	33.10	32.81	14.32	-22.00	95.40	15223	30
530	-2.46	8.73	-28.80	32.90	32.42	14.25	-24.20	93.70	15223	30
538	-2.50	8.69	-29.70	32.90	32.00	14.13	-23.30	92.50	15223	30
546	-2.56	8.64	-30.60	33.10	31.56	13.99	-24.10	91.50	15223	30
554	-2.59	8.55	-31.10	33.20	31.09	13.84	-23.90	88.70	15223	30
562	-2.61	8.47	-31.90	35.20	30.61	13.69	-25.10	86.00	15223	30
570	-2.64	8.43	-32.10	33.90	30.16	13.52	-24.30	82.50	15223	30

Table A- 8. Basic statistics for Mooring YUC6 during Canek 20 (continued)

depth	mean_u	std_u	min_u	max_u	mean_v	std_v	min_v	max_v	MMS # of obs	sample interval
578	-2.62	8.45	-34.00	33.60	29.71	13.45	-24.80	76.40	15223	30
586	-2.48	8.62	-38.00	40.30	29.15	13.45	-25.60	75.60	15223	30
594	-2.25	8.81	-43.50	41.30	28.24	13.47	-40.70	75.40	15223	30
602	-2.01	8.65	-45.70	40.90	26.36	12.67	-38.40	70.90	15223	30
666	2.11	8.83	-29.20	44.20	24.42	11.99	-41.90	57.00	13300	30
674	2.02	8.59	-24.00	44.90	23.48	11.76	-41.60	56.70	13300	30
682	1.92	8.37	-22.50	44.00	22.47	11.55	-40.60	56.40	13300	30
690	1.80	8.17	-22.00	44.00	21.44	11.35	-34.70	56.60	13300	30
698	1.67	7.97	-23.60	43.30	20.49	11.13	-34.40	55.30	13300	30
706	1.54	7.79	-24.70	41.40	19.66	10.87	-34.50	54.20	13300	30
714	1.46	7.69	-24.70	39.50	19.04	10.61	-34.50	53.10	13300	30
722	1.40	7.63	-24.40	37.60	18.53	10.43	-34.30	49.90	13300	30
730	1.33	7.44	-23.60	35.80	17.64	10.03	-33.80	46.70	13300	30
741	-0.68	3.44	-11.73	10.62	-1.04	5.51	-18.33	17.95	3805	120
848	-0.52	3.21	-11.17	11.07	-0.98	4.50	-16.16	14.65	3805	120
1050	-0.42	3.62	-14.32	11.85	0.85	4.43	-16.27	21.66	3805	120
1257	0.23	5.90	-19.88	28.12	8.41	6.96	-20.70	32.00	3805	120
1870	1.11	6.75	-19.74	32.83	14.27	8.25	-30.12	38.24	3805	120

Table A- 9. Basic statistics for Mooring YUC6 during Canek 23

depth	mean_u	std_u	min_u	max_u	mean_v	std_v	min_v	max_v	MMS # of obs	sample interval
56	7.73	25.78	-48.00	139.70	95.55	23.56	18.30	186.80	18663	30
72	6.55	23.23	-44.50	120.70	90.52	22.15	17.30	187.40	18663	30
88	5.24	20.66	-40.10	100.30	84.62	21.08	9.90	169.90	18663	30
104	4.15	18.59	-38.10	96.00	78.51	19.98	7.10	154.30	18663	30
120	3.24	16.74	-41.40	75.70	73.00	19.36	-2.30	144.90	18663	30
136	2.82	15.93	-36.40	74.20	68.32	19.07	-10.20	127.80	18663	30
152	2.55	15.67	-37.20	78.00	64.30	19.14	-29.20	117.80	18663	30
168	2.18	15.24	-38.40	71.10	61.08	19.05	-35.10	115.30	18663	30
184	1.83	14.61	-38.20	63.80	58.33	19.02	-34.70	114.10	18663	30
200	1.62	14.18	-39.80	56.70	55.82	19.07	-35.70	110.90	18663	30
216	1.59	13.67	-39.70	58.20	53.61	19.07	-34.30	109.40	18663	30
232	1.58	12.95	-40.60	63.10	51.65	19.08	-33.90	112.30	18663	30
248	1.55	12.36	-38.00	58.40	49.84	19.15	-32.30	110.10	18663	30
264	1.31	11.83	-37.00	54.70	48.31	19.03	-30.20	106.80	18663	30
280	1.02	11.31	-36.50	50.40	46.85	18.90	-27.50	102.10	18663	30
296	0.87	10.92	-33.70	49.90	45.38	18.79	-28.40	100.40	18663	30
312	0.78	10.63	-31.60	52.20	43.87	18.66	-32.50	98.30	18663	30
328	0.65	10.44	-33.10	51.70	42.41	18.58	-33.70	101.80	18663	30
344	0.49	10.34	-32.10	53.40	41.00	18.61	-34.10	105.70	18663	30
360	0.28	10.27	-33.70	48.90	39.71	18.51	-33.20	110.40	18663	30
376	0.05	10.26	-36.60	51.60	38.59	18.50	-35.80	108.80	18663	30
392	-0.10	10.22	-37.80	52.10	37.52	18.60	-37.70	111.80	18663	30
408	-0.25	10.18	-39.60	54.90	36.47	18.67	-43.90	110.30	18663	30
424	-0.44	10.01	-42.90	54.10	35.47	18.61	-41.10	106.30	18663	30
440	-0.66	9.71	-47.30	53.90	34.33	18.52	-38.90	103.60	18663	30
456	-0.74	9.39	-46.80	50.80	32.79	18.21	-34.70	99.40	18663	30
491	4.86	10.19	-43.80	49.50	29.70	17.10	-38.20	87.40	18663	30
499	5.11	10.22	-42.40	49.50	29.69	17.37	-41.00	88.70	18663	30
507	5.01	10.17	-42.20	46.20	29.42	17.38	-41.70	86.30	18663	30
515	4.88	10.17	-44.70	43.30	29.17	17.36	-40.00	84.70	18663	30
523	4.77	10.19	-45.60	42.60	28.89	17.34	-41.60	83.40	18663	30
531	4.70	10.16	-42.40	43.20	28.54	17.32	-42.30	83.50	18663	30
539	4.64	10.09	-43.80	42.30	28.17	17.25	-43.10	81.00	18663	30
547	4.57	10.03	-43.70	39.40	27.74	17.16	-43.90	78.50	18663	30
555	4.46	9.98	-44.10	40.10	27.28	17.03	-45.70	75.10	18663	30
563	4.35	9.92	-43.90	41.60	26.82	16.87	-44.00	72.70	18663	30
571	4.26	9.87	-43.00	42.80	26.33	16.72	-44.00	73.70	18663	30

Table A- 9.Basic statistics for Mooring YUC6 during Canek 23 (continued)

depth	mean_u	std_u	min_u	max_u	mean_v	std_v	min_v	max_v	MMS # of obs	sample interval
579	4.21	9.90	-41.55	47.00	25.72	16.70	-45.50	131.90	18663	30
587	4.22	9.86	-39.49	108.50	25.00	16.62	-86.60	128.88	18663	30
595	4.25	9.60	-37.30	103.39	24.13	16.20	-83.78	124.57	18663	30
626	1.49	8.14	-50.27	41.96	22.45	13.69	-48.86	95.41	18663	30
634	1.51	9.35	-58.60	48.50	22.49	15.07	-56.30	103.11	18663	30
642	1.32	9.50	-61.40	43.20	22.34	15.22	-56.00	104.76	18663	30
650	1.41	9.33	-44.50	44.43	21.89	14.93	-39.50	104.35	18663	30
658	1.34	8.83	-40.10	44.60	21.41	14.47	-37.30	103.50	18663	30
666	1.28	8.45	-32.40	31.60	20.74	13.99	-36.90	70.30	18663	30
674	1.18	8.19	-28.10	31.20	19.90	13.58	-36.10	64.70	18663	30
682	1.11	7.94	-27.50	32.80	19.02	13.21	-34.00	62.70	18663	30
690	1.07	7.73	-25.70	31.80	18.17	12.82	-34.50	60.70	18663	30
698	1.02	7.57	-23.50	32.70	17.33	12.40	-33.60	59.30	18663	30
706	0.98	7.42	-25.00	32.40	16.53	12.03	-31.30	56.10	18663	30
714	0.93	7.28	-24.60	32.00	15.89	11.76	-29.20	53.80	18663	30
722	0.80	7.12	-24.40	31.30	15.35	11.53	-28.20	52.10	18663	30
730	0.62	6.91	-25.40	29.60	14.73	11.16	-28.60	50.10	18663	30
741	-0.08	6.20	-23.10	21.36	12.65	9.28	-28.46	38.01	18660	30
847	0.39	6.02	-20.90	27.00	6.57	8.65	-40.40	36.00	37322	15
1050	-0.54	4.84	-19.56	19.73	0.26	6.06	-21.07	20.95	18662	30
1256	-1.21	3.58	-18.70	15.20	-2.41	5.71	-25.10	16.80	37320	45
1870	-0.37	4.07	-14.98	14.24	-1.73	6.51	-21.93	15.94	18661	30

Table A- 10. Basic statistics for Mooring YUC7 during Canek 20

depth	mean_u	std_u	min_u	max_u	mean_v	std_v	min_v	max_v	MMS # obs	sample interv
63	8.76	15.78	-45.50	68.10	54.32	19.60	4.60	140.40	15251	30
79	9.10	15.49	-35.60	64.50	55.48	18.80	-0.30	131.30	15251	30
95	8.61	14.94	-34.90	62.20	54.33	18.02	3.70	113.70	15251	30
111	8.07	14.28	-38.30	59.10	52.40	17.03	-2.20	107.70	15251	30
127	7.32	13.61	-36.40	62.10	49.38	15.78	-5.40	102.40	15251	30
143	6.40	12.90	-33.00	57.10	46.04	14.84	-7.90	95.90	15251	30
159	5.53	12.23	-33.20	51.70	42.54	14.01	-11.30	87.20	15251	30
175	5.01	11.62	-33.90	51.10	39.54	13.08	-9.10	81.50	15251	30
191	4.84	11.16	-29.60	58.50	37.09	12.39	-11.80	75.80	15251	30
207	4.31	10.91	-32.30	52.70	35.00	11.95	-12.90	74.40	15251	30
223	3.82	10.53	-30.80	52.20	33.11	11.56	-11.30	76.60	15251	30
239	3.60	10.30	-32.20	52.90	31.54	11.24	-8.50	75.80	15251	30
255	3.62	10.17	-32.00	51.20	30.28	11.10	-12.70	74.80	15251	30
271	3.51	10.05	-32.60	51.90	29.18	11.16	-16.20	73.20	15251	30
287	3.41	9.92	-33.60	48.20	28.29	11.04	-14.80	71.50	15251	30
303	3.27	9.68	-29.10	48.10	27.49	10.81	-11.40	68.80	15251	30
319	3.02	9.32	-30.40	42.60	26.59	10.60	-12.10	63.30	15251	30
335	2.62	8.97	-29.60	40.80	25.66	10.53	-8.20	62.80	15251	30
351	2.62	8.70	-28.30	39.20	24.70	10.36	-9.40	63.20	15251	30
367	2.50	8.52	-28.80	37.10	23.84	10.11	-13.30	62.60	15251	30
383	2.40	8.42	-25.80	39.70	23.03	9.98	-14.80	58.20	15251	30
399	2.26	8.42	-28.40	40.20	22.20	10.01	-17.30	57.20	15251	30
415	2.08	8.36	-30.30	41.40	21.39	9.96	-19.80	56.50	15251	30
431	1.89	8.36	-30.60	36.80	20.67	9.92	-18.40	55.00	15251	30
447	1.79	8.34	-34.20	36.60	19.95	9.91	-16.50	58.30	15251	30
463	1.77	8.30	-38.50	37.40	19.24	9.92	-16.60	53.00	15251	30
479	1.77	8.35	-31.80	33.20	18.27	9.89	-16.70	54.40	15251	30
514	3.60	8.62	-32.20	34.00	15.78	9.47	-20.70	46.00	15252	30
522	3.70	8.70	-32.60	35.20	15.68	9.67	-19.40	47.00	15252	30
530	3.63	8.68	-32.00	33.70	15.53	9.77	-17.90	47.60	15252	30
538	3.58	8.62	-30.60	32.30	15.38	9.82	-18.90	49.40	15252	30
546	3.55	8.53	-30.30	30.70	15.21	9.87	-17.20	50.60	15252	30
554	3.51	8.49	-29.60	30.20	15.02	9.89	-17.00	51.30	15252	30
562	3.48	8.44	-28.80	30.40	14.78	9.93	-17.00	52.20	15252	30
570	3.47	8.39	-28.90	31.00	14.54	9.97	-17.60	50.90	15252	30
578	3.41	8.38	-29.00	32.80	14.32	10.07	-17.00	48.70	15252	30
586	3.36	8.60	-32.00	38.90	14.10	10.30	-20.50	55.60	15252	30

Table A- 10. Basic statistics for Mooring YUC7 during Canek 20 (continued)

depth	mean_u	std_u	min_u	max_u	mean_v	std_v	min_v	max_v	MMS # of obs	sample interval
704	1.57	6.64	-20.85	25.74	10.03	9.31	-16.35	38.07	3811	120
961	0.55	5.39	-19.97	18.60	2.77	6.24	-16.53	26.90	3811	120
1520	-1.35	3.46	-19.98	8.38	0.91	8.06	-27.46	27.15	3811	120
1903	0.87	4.87	-17.85	19.34	4.88	12.21	-32.62	43.69	3811	120
2018	0.19	4.64	-21.20	17.07	4.50	10.74	-25.53	35.17	3811	120

Table A- 11. Basic statistics for Mooring YUC7 during Canek 23

depth	mean_u	std_u	min_u	max_u	mean_v	std_v	min_v	max_v	MMS # of obs	sample interval
59	19.10	27.90	-41.90	130.20	59.19	20.80	-1.70	139.50	18634	30
75	19.00	27.31	-37.90	121.20	58.70	20.24	0.10	134.00	18634	30
91	17.79	25.77	-34.20	108.80	57.09	19.26	1.80	135.00	18634	30
107	16.34	23.99	-36.20	98.50	54.57	18.20	5.70	131.20	18634	30
123	14.83	22.11	-38.10	94.20	51.07	17.10	-2.20	122.90	18634	30
139	13.34	20.21	-40.00	85.30	47.15	15.96	-7.10	119.10	18634	30
155	12.14	18.54	-35.60	78.10	43.67	15.19	-6.00	112.30	18634	30
171	11.37	17.31	-30.20	72.80	40.68	14.72	-6.40	100.40	18634	30
187	10.76	16.58	-28.70	71.80	38.36	14.37	-8.80	89.20	18634	30
203	10.23	16.11	-30.80	71.20	36.26	13.98	-3.40	90.30	18634	30
219	9.77	15.46	-29.30	70.80	34.26	13.57	-8.70	83.20	18634	30
235	9.36	14.99	-29.10	70.90	32.60	13.48	-13.20	80.10	18634	30
251	9.04	14.65	-30.00	70.70	31.15	13.44	-15.60	82.90	18634	30
267	8.82	14.31	-31.70	70.00	29.94	13.34	-17.50	83.10	18634	30
283	8.58	13.90	-34.90	65.60	28.93	13.25	-19.70	82.70	18634	30
299	8.28	13.50	-36.30	62.60	28.10	13.09	-18.00	78.20	18634	30
315	7.88	13.19	-37.10	61.10	27.27	12.91	-19.60	77.60	18634	30
331	7.58	12.86	-37.00	57.20	26.41	12.76	-20.30	74.90	18634	30
347	7.37	12.53	-35.90	53.40	25.49	12.66	-21.40	72.30	18634	30
363	7.20	12.36	-34.20	52.10	24.56	12.50	-24.80	67.70	18634	30
379	6.90	12.16	-35.80	53.00	23.59	12.41	-26.20	66.20	18634	30
395	6.58	12.00	-32.00	55.90	22.60	12.25	-23.50	62.90	18634	30
411	6.40	11.89	-34.50	56.10	21.77	12.12	-21.40	60.90	18634	30
427	6.19	11.70	-32.80	55.00	20.96	12.04	-21.70	58.60	18634	30
443	6.10	11.48	-34.00	52.30	20.23	11.96	-22.40	59.50	18634	30
459	5.99	11.30	-35.40	52.60	19.52	11.95	-23.60	58.30	18634	30
475	5.86	11.23	-37.70	52.80	18.71	11.94	-24.60	57.80	18634	30
491	5.65	11.04	-36.00	53.80	17.71	11.89	-29.00	58.10	18634	30
503	5.60	8.69	-24.80	46.00	17.35	11.32	-24.00	64.10	18634	30
511	5.70	8.84	-24.20	48.40	17.22	11.52	-25.10	64.30	18634	30
519	5.63	8.91	-24.20	45.80	17.03	11.62	-25.10	60.40	18634	30
527	5.60	8.94	-24.20	43.90	16.85	11.69	-26.10	57.80	18634	30
535	5.58	9.00	-24.00	47.10	16.68	11.75	-27.60	54.80	18634	30
543	5.58	9.02	-23.80	47.20	16.51	11.77	-28.10	55.60	18634	30
551	5.56	9.05	-25.10	45.70	16.31	11.76	-27.70	56.00	18634	30
559	5.51	9.05	-25.20	46.90	16.04	11.77	-27.20	56.90	18634	30
567	5.47	9.02	-25.60	48.70	15.76	11.79	-26.50	57.70	18634	30

Table A- 11. Basic statistics for Mooring YUC7 during Canek 23 (continued)

depth	mean_u	std_u	min_u	max_u	mean_v	std_v	min_v	max_v	MMS # of obs	sample interval
575	5.43	9.00	-28.40	48.40	15.51	11.83	-25.40	58.80	18634	30
583	5.36	9.00	-28.00	46.10	15.25	11.91	-26.40	58.80	18634	30
591	5.29	9.13	-28.80	43.30	14.96	12.11	-38.10	61.50	18634	30
599	5.12	9.36	-42.70	50.80	14.58	12.33	-37.89	60.90	18634	30
600	-0.43	5.71	-21.80	24.30	-0.32	10.59	-33.80	49.10	37290	15
607	5.34	9.10	-45.60	50.30	14.08	12.40	-39.80	64.00	18634	30
696	2.77	8.69	-32.93	38.98	11.12	11.42	-24.14	49.35	18632	30
953	0.52	6.45	-22.80	23.50	4.95	6.64	-18.30	33.40	37260	45
1155	0.02	3.94	-14.15	13.92	3.16	5.87	-14.54	28.82	9313	60
1512	-1.49	4.41	-22.10	16.10	3.38	8.95	-23.80	37.30	37260	45
1895	-0.45	5.40	-23.44	17.20	6.99	13.21	-26.43	49.45	18632	30
2010	-0.38	4.53	-23.30	16.20	6.27	10.90	-19.80	45.20	37263	15

Table A- 12. Basic statistics for Mooring PE1 during Canek 20

depth	mean_u	std_u	min_u	max_u	mean_v	std_v	min_v	max_v	MMS # of obs	sample interval
28	-5.52	15.17	-45.90	41.00	-10.14	11.53	-51.10	21.30	2500	30
36	-4.08	14.41	-46.00	41.80	-9.94	13.16	-50.60	26.60	2500	30
44	-2.67	12.59	-41.50	35.10	-8.18	13.94	-51.40	32.80	2500	30
52	-1.62	10.97	-46.30	29.00	-6.04	14.20	-51.80	37.60	2500	30
60	-0.78	10.12	-34.80	26.90	-4.08	14.09	-47.60	40.60	2500	30
68	-0.14	9.74	-29.30	26.70	-2.63	13.54	-47.70	44.70	2500	30
76	0.19	9.66	-29.60	28.80	-1.61	13.20	-46.80	45.90	2500	30
84	0.24	9.75	-27.00	29.40	-0.97	13.04	-44.30	42.70	2500	30
92	0.32	9.91	-29.20	29.10	-0.83	13.20	-42.50	42.40	2500	30
100	0.99	9.78	-30.20	35.00	-1.33	13.23	-38.30	41.40	2500	30
108	2.68	9.37	-26.00	40.60	-2.16	13.10	-38.30	39.60	2500	30

Table A- 13. Basic statistics for Mooring PE1 during Canek 23

depth	mean_u	std_u	min_u	max_u	mean_v	std_v	min_v	max_v	MMS # of obs	sample interval
11	-13.98	17.02	-80.70	59.40	-2.22	16.86	-88.40	104.90	18192	30
19	-5.49	18.06	-84.70	57.30	-8.12	16.25	-89.40	56.20	18192	30
27	-4.82	16.25	-74.30	56.90	-9.13	15.49	-76.30	47.50	18192	30
35	-3.19	14.65	-66.70	54.20	-8.77	15.17	-74.30	57.30	18192	30
43	-1.97	13.57	-62.30	61.40	-7.96	15.27	-79.50	54.70	18192	30
51	-1.10	12.72	-59.50	56.10	-6.81	15.38	-85.70	51.10	18192	30
59	-0.57	11.80	-53.20	47.60	-5.48	15.28	-83.70	47.90	18192	30
67	-0.44	10.99	-44.30	50.50	-4.08	14.86	-85.50	44.90	18192	30
75	-0.38	10.33	-40.20	50.20	-2.96	14.32	-89.20	53.20	18192	30
83	-0.22	9.84	-35.70	52.70	-2.29	13.78	-86.80	52.60	18192	30
91	0.18	9.37	-37.80	47.90	-2.17	13.28	-78.40	62.20	18192	30
99	0.77	8.90	-33.20	45.60	-2.47	12.82	-70.40	52.80	18192	30
107	1.61	8.56	-36.00	43.30	-2.99	12.35	-64.10	47.30	18192	30

Table A- 14. Basic statistics for Mooring PE2 during Canek 20

depth	mean_u	std_u	min_u	max_u	mean_v	std_v	min_v	max_v	MMS # of obs	sample interval
58	-25.43	37.71	-127.40	65.60	54.37	74.79	-75.70	217.40	15694	30
74	-23.11	35.69	-117.90	79.40	49.45	70.29	-79.10	204.50	15694	30
90	-20.58	33.64	-116.90	85.00	44.05	64.81	-80.60	182.90	15694	30
106	-18.20	31.31	-110.60	89.30	38.96	59.47	-81.30	161.50	15694	30
122	-16.10	29.01	-105.70	95.00	34.79	55.04	-79.90	151.90	15694	30
138	-14.18	27.07	-88.60	83.20	31.43	51.35	-79.50	143.00	15694	30
154	-12.73	25.32	-87.40	82.10	28.81	47.88	-70.60	141.10	15694	30
170	-11.55	23.98	-77.30	76.40	26.70	44.86	-70.00	137.80	15694	30
186	-10.48	22.91	-74.00	63.50	24.93	42.37	-71.70	131.30	15694	30
202	-9.59	22.01	-73.70	58.90	23.24	40.21	-61.80	129.40	15694	30
218	-8.72	21.06	-69.20	59.70	21.54	38.17	-54.20	126.80	15694	30
234	-8.06	20.09	-70.30	62.10	19.95	36.17	-56.60	114.90	15694	30
250	-7.44	19.28	-71.00	63.50	18.37	34.24	-56.00	107.80	15694	30
266	-6.83	18.62	-73.20	59.20	16.89	32.45	-53.50	104.30	15694	30
282	-6.15	17.94	-67.00	59.60	15.60	30.97	-51.00	100.80	15694	30
298	-5.43	17.09	-61.20	59.30	14.32	29.68	-51.50	99.40	15694	30
314	-4.87	16.37	-55.60	49.90	13.18	28.46	-55.90	95.20	15694	30
330	-4.43	15.76	-54.20	45.20	11.99	27.25	-53.90	96.20	15694	30
346	-4.13	15.20	-54.00	45.10	10.87	26.15	-56.80	85.60	15694	30
362	-3.69	14.65	-48.70	44.00	9.81	25.38	-52.40	88.10	15694	30
378	-3.12	14.10	-51.40	40.10	8.93	24.68	-53.40	90.50	15694	30
394	-2.50	13.58	-54.90	43.20	7.88	23.82	-49.20	85.90	15694	30
410	-1.98	13.20	-49.20	43.10	6.75	22.97	-52.00	73.00	15694	30
426	-1.48	12.92	-52.90	43.90	5.61	22.24	-51.20	69.70	15694	30
442	-0.87	12.52	-51.60	40.90	4.57	21.47	-50.80	69.90	15694	30
458	-0.11	12.09	-48.70	42.80	3.40	20.24	-48.10	69.00	15694	30
474	0.90	11.70	-50.50	42.30	1.87	17.98	-47.20	68.40	15694	30

Table A- 15. Basic statistics for Mooring PE2 during Canek 23

depth	mean_u	std_u	min_u	max_u	mean_v	std_v	min_v	max_v	MMS # of obs	sample interval
46	-23.48	25.86	-117.70	41.00	43.26	53.14	-54.30	183.30	18146	30
62	-25.47	32.44	-146.60	49.00	55.92	68.55	-70.10	206.20	18146	30
78	-23.43	30.17	-138.30	50.10	49.06	62.88	-69.80	179.10	18146	30
94	-21.38	28.39	-120.90	54.80	43.08	57.29	-64.90	164.70	18146	30
110	-19.10	26.65	-105.80	54.70	38.19	52.65	-66.60	149.60	18146	30
126	-16.95	24.69	-99.80	50.80	34.24	48.69	-63.20	139.40	18146	30
142	-15.11	23.04	-93.20	44.70	30.95	45.36	-61.10	137.60	18146	30
158	-13.67	21.84	-88.40	43.40	28.17	42.38	-57.40	135.20	18146	30
174	-12.54	20.78	-76.90	42.50	25.79	39.99	-54.00	129.70	18146	30
190	-11.57	19.99	-74.20	43.30	23.69	37.70	-52.90	124.20	18146	30
206	-10.67	19.38	-70.80	42.50	21.75	35.70	-52.40	118.60	18146	30
222	-9.83	18.63	-67.90	38.50	20.08	34.07	-52.50	111.60	18146	30
238	-8.83	17.82	-62.10	40.90	18.68	32.47	-50.00	98.20	18146	30
254	-7.77	17.08	-59.80	42.00	17.35	30.88	-51.10	89.70	18146	30
270	-6.99	16.35	-57.00	43.10	16.01	29.51	-52.00	90.00	18146	30
286	-6.41	15.73	-57.00	45.40	14.64	28.23	-50.20	92.40	18146	30
302	-5.84	15.28	-55.00	49.90	13.35	27.00	-50.20	84.00	18146	30
318	-5.30	14.81	-52.00	57.00	12.16	25.90	-52.50	84.20	18146	30
334	-4.76	14.30	-61.20	53.50	11.13	25.08	-54.10	80.20	18146	30
350	-4.08	13.71	-60.80	54.70	10.16	24.28	-51.90	79.70	18146	30
366	-3.48	13.26	-49.50	57.10	8.95	23.39	-52.80	75.70	18146	30
382	-2.88	12.90	-47.80	54.80	7.61	22.61	-53.00	78.60	18146	30
398	-2.27	12.58	-43.80	49.70	6.20	21.91	-52.90	77.10	18146	30
414	-1.52	12.22	-43.80	52.30	4.79	21.27	-54.40	70.40	18146	30
430	-0.83	11.92	-46.40	52.20	3.39	20.58	-57.80	71.10	18146	30
446	-0.23	11.55	-38.90	48.80	2.02	19.71	-58.20	67.40	18146	30
462	0.43	11.03	-37.80	48.30	0.66	18.35	-51.30	64.90	18146	30
478	1.14	10.29	-36.90	43.70	-0.46	15.99	-47.30	53.50	18146	30

Table A- 16. Basic statistics for Mooring PE3 during Canek 20

depth	mean_u	std_u	min_u	max_u	mean_v	std_v	min_v	max_v	MMS # of obs	sample interval
56	-18.68	32.72	-112.30	77.00	50.07	47.80	-73.50	173.50	15692	30
72	-20.57	32.98	-100.10	74.40	52.34	48.47	-68.70	169.50	15692	30
88	-20.42	31.67	-92.40	72.20	50.67	46.74	-61.80	161.90	15692	30
104	-19.63	30.37	-93.80	72.40	48.07	44.80	-57.70	154.20	15692	30
120	-18.40	28.91	-86.80	67.30	44.80	42.22	-57.90	149.80	15692	30
136	-17.11	27.65	-81.40	65.10	41.70	39.82	-48.40	144.70	15692	30
152	-15.81	26.43	-79.70	65.20	38.79	37.76	-52.30	130.60	15692	30
168	-14.47	25.02	-79.50	67.40	36.22	35.90	-53.50	125.20	15692	30
184	-13.55	24.00	-80.30	70.20	34.22	34.43	-48.80	122.80	15692	30
200	-12.79	23.25	-80.30	71.40	32.71	33.31	-45.10	115.60	15692	30
216	-11.96	22.52	-76.00	78.00	31.38	32.18	-42.70	107.20	15692	30
232	-11.39	21.79	-73.20	86.20	30.08	31.27	-41.10	104.80	15692	30
248	-10.98	21.24	-77.80	82.20	29.12	30.51	-37.70	101.10	15692	30
264	-10.56	20.61	-73.00	80.10	28.21	29.79	-36.60	99.30	15692	30
280	-10.27	20.23	-74.90	77.40	27.23	29.03	-38.50	100.60	15692	30
296	-9.97	19.92	-74.50	68.50	26.39	28.47	-44.30	97.40	15692	30
312	-9.72	19.52	-73.90	65.20	25.63	27.98	-43.90	95.80	15692	30
328	-9.39	18.98	-76.20	56.80	24.73	27.57	-42.40	98.00	15692	30
344	-9.07	18.58	-70.80	57.10	23.85	27.18	-45.00	95.10	15692	30
360	-8.75	18.13	-67.40	51.50	23.10	26.62	-43.10	93.40	15692	30
376	-8.48	17.65	-67.20	51.30	22.29	26.10	-36.90	88.00	15692	30
392	-8.25	17.17	-65.30	51.40	21.56	25.53	-34.80	84.10	15692	30
408	-7.89	16.76	-59.00	52.90	20.85	25.06	-36.80	85.80	15692	30
424	-7.53	16.39	-62.40	51.20	20.19	24.62	-35.50	88.60	15692	30
440	-7.21	15.98	-58.30	51.40	19.47	24.21	-36.60	89.00	15692	30
456	-6.87	15.61	-61.20	52.90	18.81	23.68	-34.00	89.10	15692	30
472	-6.46	14.98	-59.50	53.70	17.90	22.92	-35.90	89.00	15692	30
589	-3.47	11.97	-45.90	42.80	14.63	19.59	-38.50	76.20	31384	15
794	-2.38	8.77	-29.80	32.40	7.11	14.13	-32.90	59.00	31325	15
989	0.56	8.38	-32.70	30.00	0.63	9.77	-31.90	31.60	31385	15

Table A- 17. Basic statistics for Mooring PE3 during Canek 23

depth	mean_u	std_u	min_u	max_u	mean_v	std_v	min_v	max_v	MMS # of obs	sample interval
57	-20.21	27.58	-128.40	75.30	54.22	49.15	-70.50	219.20	16826	30
73	-21.19	27.44	-128.70	63.40	61.18	52.31	-70.60	191.50	16826	30
89	-20.36	26.21	-125.40	58.40	56.79	49.75	-68.30	174.30	16826	30
105	-19.27	24.87	-111.70	54.90	52.16	47.05	-68.40	159.40	16826	30
121	-17.96	23.49	-110.60	51.70	47.76	44.34	-65.60	147.60	16826	30
137	-16.50	22.13	-103.10	51.30	43.73	41.60	-62.90	138.00	16826	30
153	-15.27	21.05	-83.70	52.50	40.62	39.43	-57.60	128.60	16826	30
169	-14.24	20.19	-81.80	56.00	38.22	37.72	-56.30	120.40	16826	30
185	-13.30	19.30	-69.80	57.40	36.11	36.13	-58.70	112.30	16826	30
201	-12.33	18.50	-61.50	56.90	34.18	34.58	-56.10	111.80	16826	30
217	-11.68	17.94	-60.90	54.80	32.37	33.12	-51.30	109.80	16826	30
233	-11.21	17.48	-61.20	52.90	30.88	31.98	-47.00	106.40	16826	30
249	-10.68	17.08	-61.30	51.00	29.51	31.01	-46.70	104.70	16826	30
265	-10.27	16.60	-59.00	48.80	28.43	30.11	-47.80	103.50	16826	30
281	-9.80	16.06	-58.40	46.00	27.42	29.28	-45.30	104.10	16826	30
297	-9.32	15.65	-59.10	42.90	26.42	28.57	-47.30	104.30	16826	30
313	-8.86	15.32	-55.70	41.60	25.39	27.91	-46.80	103.10	16826	30
329	-8.38	14.91	-53.20	42.60	24.34	27.23	-46.40	104.80	16826	30
345	-7.92	14.46	-55.70	40.70	23.28	26.50	-46.00	106.40	16826	30
361	-7.66	14.06	-55.50	40.80	22.31	25.81	-43.40	107.90	16826	30
377	-7.38	13.75	-56.90	39.10	21.36	25.16	-41.70	107.90	16826	30
393	-6.97	13.49	-59.20	37.90	20.49	24.61	-41.90	109.80	16826	30
409	-6.62	13.18	-59.00	39.30	19.61	24.03	-41.80	108.30	16826	30
425	-6.35	12.81	-55.70	38.40	18.80	23.51	-41.50	106.90	16826	30
441	-6.00	12.52	-50.50	38.70	18.01	23.03	-38.70	105.10	16826	30
457	-5.64	12.22	-47.80	37.40	17.16	22.56	-40.00	103.90	16826	30
473	-5.33	11.80	-41.30	33.70	16.27	21.96	-43.40	103.60	16826	30
489	-4.97	11.27	-38.90	32.60	15.31	21.05	-39.90	100.10	16826	30
591	-3.69	9.27	-39.48	27.42	10.72	17.38	-34.77	84.11	9051	60
795	-1.02	6.94	-25.56	23.42	2.99	12.22	-31.36	58.66	9051	60
991	0.58	6.52	-23.04	20.81	-0.91	7.79	-29.03	26.86	9051	60

Table A- 18. Basic statistics for Mooring PE4 during Canek 20

depth	mean_u	std_u	min_u	max_u	mean_v	std_v	min_v	max_v	MMS # of obs	sample interval
47	-4.10	28.29	-112.00	96.00	41.38	36.69	-56.30	184.70	11258	30
63	-2.44	28.81	-111.70	89.00	45.62	38.13	-54.00	156.70	11258	30
79	-2.27	27.56	-104.10	79.60	43.50	35.44	-53.00	129.10	11258	30
95	-2.15	26.34	-93.10	74.50	40.92	32.91	-51.80	126.90	11258	30
111	-2.15	24.93	-77.80	65.90	38.30	30.83	-52.70	115.40	11258	30
127	-1.56	23.55	-66.50	58.30	35.96	29.00	-45.00	109.40	11258	30
143	-1.07	22.19	-65.30	59.50	33.71	27.54	-38.20	105.20	11258	30
159	-0.72	21.11	-62.70	64.60	31.77	26.34	-42.00	102.30	11258	30
175	-0.41	20.27	-63.60	63.30	30.14	25.30	-36.40	100.10	11258	30
191	-0.02	19.71	-63.90	62.20	28.62	24.33	-33.80	93.60	11258	30
207	0.11	19.26	-60.60	60.70	27.29	23.65	-31.00	93.60	11258	30
223	0.27	18.88	-58.80	63.70	26.10	23.06	-32.50	89.30	11258	30
239	0.27	18.42	-54.60	62.90	24.94	22.62	-31.70	86.30	11258	30
255	0.32	18.02	-59.10	63.00	23.99	22.18	-33.60	88.80	11258	30
271	0.50	17.57	-55.60	58.20	23.04	21.55	-30.80	87.50	11258	30
287	0.61	17.24	-55.60	64.20	22.03	21.07	-31.30	85.70	11258	30
303	0.67	16.83	-51.50	61.00	21.15	20.62	-30.30	85.60	11258	30
319	0.57	16.51	-53.90	59.30	20.23	20.05	-31.80	90.30	11258	30
335	0.41	16.13	-50.60	58.30	19.54	19.61	-29.70	83.50	11258	30
351	0.39	15.72	-49.50	59.10	18.74	19.15	-31.10	79.70	11258	30
367	0.38	15.41	-48.60	58.10	17.95	18.73	-30.10	75.40	11258	30
383	0.44	15.06	-47.30	57.40	17.07	18.44	-29.90	76.20	11258	30
399	0.47	14.63	-47.50	59.00	16.30	18.05	-31.00	74.50	11258	30
415	0.51	14.34	-46.20	56.50	15.60	17.51	-31.30	72.10	11258	30
418	-7.70	17.07	-54.32	62.60	15.31	15.47	-30.70	81.41	15715	30
431	0.41	14.10	-48.60	57.10	14.79	17.04	-32.30	72.80	11258	30
434	-7.90	16.84	-55.06	63.21	14.73	15.11	-31.00	81.19	15715	30
447	0.43	13.60	-45.60	57.20	13.82	16.34	-33.00	72.70	11258	30
450	-7.55	16.39	-54.50	63.10	14.04	14.76	-30.90	80.61	15715	30
466	-7.21	15.94	-54.10	60.00	13.36	14.45	-34.60	80.30	15715	30
482	-6.94	15.52	-55.10	56.60	12.74	14.09	-30.40	70.50	15715	30
498	-6.65	15.04	-54.00	56.30	12.17	13.78	-31.40	68.10	15715	30
514	-6.38	14.64	-53.90	53.10	11.69	13.52	-33.70	66.00	15715	30
530	-6.26	14.23	-51.50	54.40	11.32	13.29	-34.10	64.60	15715	30
546	-6.08	14.01	-49.30	53.20	10.97	13.04	-39.60	63.90	15715	30
562	-5.91	13.88	-49.40	57.50	10.59	12.84	-39.00	63.50	15715	30
578	-5.74	13.69	-49.10	54.70	10.23	12.69	-40.00	64.20	15715	30

Table A- 18. Basic statistics for Mooring PE4 during Canek 20 (continued)

depth	mean_u	std_u	min_u	max_u	mean_v	std_v	min_v	max_v	MMS # of obs	sample interval
594	-5.50	13.50	-50.20	56.30	9.90	12.51	-38.80	66.20	15715	30
610	-5.27	13.17	-51.30	53.60	9.64	12.26	-37.30	66.20	15715	30
626	-5.08	12.92	-50.70	51.60	9.21	12.04	-39.20	62.40	15715	30
642	-4.93	12.67	-50.30	51.50	8.75	11.80	-42.30	63.60	15715	30
658	-4.88	12.35	-48.00	51.00	8.49	11.60	-40.80	64.50	15715	30
674	-4.76	12.01	-46.10	50.10	8.32	11.41	-40.30	63.30	15715	30
690	-4.62	11.73	-41.60	45.60	8.09	11.18	-42.10	61.90	15715	30
706	-4.39	11.46	-39.30	43.70	7.71	10.99	-40.00	60.10	15715	30
722	-4.14	11.13	-39.00	42.90	7.33	10.79	-40.30	58.00	15715	30
738	-3.95	10.87	-36.60	41.20	6.95	10.48	-41.40	53.90	15715	30
754	-3.87	10.67	-34.90	43.00	6.50	10.29	-39.30	56.80	15715	30
770	-3.69	10.47	-35.90	40.20	6.13	10.18	-41.50	55.90	15715	30
786	-3.50	10.18	-34.90	38.70	5.90	10.01	-38.80	57.10	15715	30
802	-3.31	9.93	-33.30	38.40	5.64	9.85	-38.00	56.40	15715	30
818	-3.05	9.75	-32.30	36.50	5.25	9.53	-41.10	55.00	15715	30
834	-2.84	9.56	-31.90	37.20	4.85	9.24	-37.50	44.60	15715	30
850	-2.65	9.34	-29.40	38.50	4.53	8.87	-36.80	42.90	15715	30
866	-2.51	9.15	-30.90	42.30	4.17	8.49	-29.00	44.50	15715	30
882	-2.37	8.88	-31.30	41.50	3.80	8.17	-26.80	39.10	15715	30
898	-2.17	8.52	-27.30	41.30	3.48	7.87	-24.30	38.00	15715	30
914	-1.94	8.19	-30.00	41.10	3.12	7.53	-23.60	36.60	15715	30
930	-1.79	7.86	-26.40	40.40	2.55	7.18	-25.30	36.20	15715	30
946	-1.61	7.33	-27.00	37.90	2.13	6.69	-29.10	36.10	15715	30
962	-0.69	9.13	-30.10	41.00	4.20	8.83	-27.30	46.80	15715	30
1239	0.86	5.75	-17.50	25.60	-1.81	6.22	-22.30	21.80	31430	45
1495	0.68	5.42	-17.00	21.30	-1.53	6.22	-27.70	17.50	31430	45
1989	0.16	5.45	-21.00	27.00	-0.90	4.88	-21.10	18.40	31431	45

Table A- 19. Basic statistics for Mooring PE4 during Canek 23

depth	mean_u	std_u	min_u	max_u	mean_v	std_v	min_v	max_v	MMS # of obs	sample interval
36	-30.73	22.33	-101.20	65.60	19.64	32.44	-116.40	168.10	18112	30
52	-11.12	26.82	-129.20	89.10	59.35	45.47	-79.10	193.00	18112	30
68	-11.37	25.24	-120.40	78.80	56.42	42.12	-74.50	170.20	18112	30
84	-11.40	23.95	-119.10	63.70	53.55	39.24	-63.70	167.20	18112	30
100	-11.00	22.52	-122.60	62.20	50.26	36.36	-65.20	154.50	18112	30
116	-10.43	21.17	-114.30	60.40	46.66	33.64	-64.00	127.80	18112	30
132	-9.92	20.13	-100.20	57.80	43.38	31.32	-62.70	117.70	18112	30
148	-9.34	19.15	-81.20	52.40	40.56	29.40	-54.50	116.80	18112	30
164	-8.68	18.33	-78.10	53.00	38.41	28.05	-51.10	109.40	18112	30
180	-8.18	17.66	-78.80	54.60	36.58	27.02	-47.90	109.10	18112	30
196	-7.89	17.09	-66.30	52.40	34.91	26.29	-48.50	101.50	18112	30
212	-7.35	16.61	-63.30	50.50	33.20	25.49	-46.10	95.40	18112	30
228	-6.97	16.22	-57.20	49.30	31.75	24.76	-43.00	93.60	18112	30
244	-6.58	15.73	-54.80	48.50	30.48	24.03	-47.40	94.90	18112	30
260	-6.07	15.19	-56.90	46.90	29.26	23.39	-47.20	96.50	18112	30
276	-5.77	14.75	-52.20	47.40	28.31	22.91	-43.00	93.60	18112	30
292	-5.53	14.40	-51.50	47.30	27.39	22.40	-42.80	93.70	18112	30
308	-5.32	14.14	-47.60	48.30	26.53	21.83	-42.50	89.90	18112	30
324	-5.16	13.92	-45.90	46.50	25.72	21.28	-39.00	85.50	18112	30
340	-5.03	13.58	-45.10	45.40	24.93	20.86	-43.10	79.90	18112	30
356	-4.84	13.30	-44.40	43.90	24.00	20.44	-48.80	81.70	18112	30
372	-4.76	13.01	-42.90	42.60	23.08	19.84	-49.30	81.00	18112	30
388	-4.62	12.72	-44.70	41.60	22.19	19.23	-52.50	74.70	18112	30
404	-4.44	12.50	-47.10	39.70	21.43	18.79	-49.50	77.20	18112	30
420	-4.19	12.25	-50.70	41.00	20.62	18.42	-48.30	74.60	18112	30
436	-4.07	11.96	-50.80	39.60	19.81	18.00	-51.60	72.50	18112	30
441	-6.67	12.58	-57.50	40.40	19.16	17.83	-54.90	70.50	18112	30
452	-3.92	11.66	-49.00	38.00	19.01	17.51	-52.00	71.20	18112	30
457	-6.46	12.20	-55.60	38.10	18.35	17.32	-53.00	68.60	18112	30
468	-3.73	11.18	-48.40	36.60	17.99	16.81	-48.00	68.70	18112	30
473	-6.22	11.82	-57.10	38.80	17.55	16.81	-49.60	70.60	18112	30
489	-5.96	11.50	-54.80	37.70	16.80	16.37	-48.90	72.20	18112	30
505	-5.76	11.17	-51.50	38.70	16.09	15.93	-50.20	69.40	18112	30
521	-5.54	10.88	-50.40	37.10	15.39	15.46	-49.50	67.30	18112	30
537	-5.26	10.73	-51.00	36.10	14.81	15.08	-49.70	65.50	18112	30
553	-5.09	10.59	-46.80	36.90	14.18	14.77	-46.20	65.10	18112	30
569	-4.97	10.45	-45.00	35.90	13.57	14.51	-42.40	64.80	18112	30

Table A- 19. Basic statistics for Mooring PE4 during Canek 23 (continued)

depth	mean_u	std_u	min_u	max_u	mean_v	std_v	min_v	max_v	MMS # of obs	sample interval
585	-4.83	10.27	-41.10	35.20	13.04	14.18	-38.70	64.60	18112	30
601	-4.69	10.00	-39.60	36.50	12.54	13.80	-39.30	64.00	18112	30
617	-4.58	9.77	-39.20	38.80	11.93	13.46	-36.80	63.80	18112	30
633	-4.42	9.62	-41.40	34.40	11.27	13.12	-35.00	63.50	18112	30
649	-4.20	9.46	-44.10	33.50	10.67	12.81	-34.50	61.70	18112	30
665	-4.01	9.30	-44.80	33.10	10.11	12.49	-34.90	60.40	18112	30
681	-3.89	9.06	-40.10	34.00	9.56	12.14	-33.80	52.70	18112	30
697	-3.78	8.91	-40.50	35.20	9.01	11.85	-33.10	48.30	18112	30
713	-3.65	8.75	-37.90	34.50	8.41	11.56	-34.30	49.50	18112	30
729	-3.49	8.60	-36.50	32.70	7.83	11.26	-34.80	48.60	18112	30
745	-3.43	8.44	-37.10	32.40	7.36	10.96	-34.10	47.50	18112	30
761	-3.22	8.28	-36.90	32.70	6.86	10.71	-34.50	44.40	18112	30
777	-3.04	8.07	-36.70	33.50	6.37	10.53	-35.10	45.50	18112	30
793	-2.92	7.75	-35.40	30.50	5.96	10.24	-34.20	47.20	18112	30
809	-2.74	7.54	-34.80	29.60	5.46	9.88	-34.90	45.90	18112	30
825	-2.48	7.34	-35.40	28.60	4.98	9.61	-35.30	39.80	18112	30
841	-2.25	7.18	-34.90	30.10	4.61	9.41	-33.30	40.30	18112	30
857	-2.10	7.08	-34.70	31.40	4.22	9.23	-31.40	39.20	18112	30
873	-1.91	6.99	-34.40	32.40	3.84	9.00	-26.70	39.10	18112	30
889	-1.70	6.84	-34.20	32.10	3.48	8.73	-27.70	42.70	18112	30
905	-1.53	6.67	-32.70	29.40	3.15	8.45	-25.10	42.00	18112	30
921	-1.31	6.51	-30.60	27.50	2.88	8.17	-25.30	36.50	18112	30
937	-1.14	6.33	-29.40	25.70	2.56	7.81	-24.40	36.20	18112	30
953	-1.04	6.03	-29.50	24.20	2.11	7.27	-23.10	46.50	18112	30
969	-0.73	5.38	-28.80	23.40	1.55	6.09	-20.10	30.60	18112	30
1245	0.46	4.49	-13.62	20.39	-1.26	5.57	-21.67	17.61	9049	60
1499	0.68	3.37	-10.83	15.42	-1.43	5.14	-25.41	20.70	9051	60
1990	1.35	3.06	-15.19	18.77	-1.41	4.48	-22.12	13.64	9053	60

Table A- 20. Basic statistics for Mooring PE5 during Canek 20

depth	mean_u	std_u	min_u	max_u	mean_v	std_v	min_v	max_v	MMS # of obs	sample interval
59	-0.40	31.45	-113.90	111.70	29.16	44.92	-119.90	162.00	15681	30
75	0.90	32.14	-107.10	111.30	30.94	45.77	-112.80	150.90	15681	30
91	0.34	30.13	-88.20	101.20	29.04	42.25	-106.10	135.50	15681	30
107	-0.19	28.35	-74.20	98.50	27.27	39.04	-93.70	126.20	15681	30
123	-0.59	26.66	-67.80	92.10	25.62	35.99	-87.80	116.80	15681	30
139	-0.55	25.42	-61.80	89.60	24.35	33.42	-80.90	105.40	15681	30
155	-0.39	24.05	-55.50	84.90	23.04	31.30	-75.60	103.60	15681	30
171	0.05	22.62	-61.50	81.90	21.79	29.67	-72.90	104.00	15681	30
187	0.48	21.54	-53.40	79.90	20.68	28.61	-73.80	100.00	15681	30
203	0.61	20.80	-46.10	79.10	19.95	27.61	-75.80	99.20	15681	30
219	0.71	20.11	-49.30	78.70	19.23	26.60	-73.20	102.00	15681	30
235	0.81	19.47	-49.30	72.00	18.54	25.84	-73.40	96.30	15681	30
251	0.79	18.97	-48.10	67.70	17.77	25.15	-74.40	96.90	15681	30
267	0.88	18.54	-51.80	64.60	17.06	24.41	-72.60	91.70	15681	30
283	0.88	18.09	-54.90	65.30	16.51	23.64	-72.40	90.00	15681	30
299	0.77	17.66	-52.30	67.60	15.99	22.99	-74.20	89.20	15681	30
315	0.58	17.28	-52.70	71.10	15.44	22.42	-73.10	87.00	15681	30
331	0.36	16.82	-50.50	67.70	14.90	21.80	-69.90	82.60	15681	30
347	0.28	16.39	-49.80	62.80	14.36	21.13	-70.90	81.00	15681	30
363	0.22	16.09	-45.30	64.70	13.86	20.55	-68.00	76.40	15681	30
379	0.02	15.85	-43.30	64.90	13.32	20.02	-64.50	74.00	15681	30
395	-0.19	15.56	-46.00	62.90	12.79	19.50	-64.50	71.10	15681	30
411	-0.36	15.21	-42.50	59.80	12.28	18.89	-67.40	71.70	15681	30
427	-0.48	14.89	-41.50	56.80	11.85	18.31	-66.00	68.30	15681	30
443	-0.57	14.65	-45.50	55.10	11.44	17.91	-61.60	66.30	15681	30
459	-0.69	14.47	-42.70	57.50	10.91	17.59	-59.90	62.90	15681	30
475	-0.82	14.34	-45.40	53.40	10.39	17.06	-56.60	61.50	15681	30
482	-0.21	14.08	-54.10	56.40	10.38	16.75	-55.98	63.60	15679	30
491	-0.96	14.14	-44.90	51.20	9.91	16.67	-60.60	60.90	15681	30
498	-0.30	13.97	-47.10	50.70	9.98	16.44	-56.60	57.80	15679	30
507	-1.04	13.91	-45.50	49.20	9.40	16.23	-59.00	56.60	15681	30
514	-0.41	13.87	-43.90	49.60	9.51	16.20	-56.30	60.60	15679	30
523	-1.08	13.54	-44.60	44.90	8.85	15.73	-54.50	55.30	15681	30
530	-0.49	13.77	-45.30	45.10	9.24	16.01	-54.60	54.90	15679	30
546	-0.52	13.61	-45.30	44.20	8.89	15.70	-58.20	51.80	15679	30
562	-0.50	13.43	-50.20	44.90	8.45	15.33	-57.00	51.00	15679	30
578	-0.56	13.16	-51.70	43.50	8.10	14.97	-56.80	48.10	15679	30

Table A- 20. Basic statistics for Mooring PE5 during Canek 20 (continued)

depth	mean_u	std_u	min_u	max_u	mean_v	std_v	min_v	max_v	MMS # of obs	sample interval
594	-0.73	12.97	-48.40	39.40	7.81	14.60	-56.70	51.90	15679	30
610	-0.82	12.88	-47.60	37.50	7.58	14.26	-58.30	54.00	15679	30
626	-0.82	12.82	-52.00	36.60	7.39	13.87	-57.40	55.60	15679	30
642	-0.87	12.75	-51.60	38.70	7.21	13.47	-56.40	55.80	15679	30
658	-0.94	12.53	-51.00	38.30	7.11	13.11	-55.40	54.20	15679	30
674	-0.98	12.35	-49.70	37.00	6.83	12.77	-53.60	51.30	15679	30
690	-1.08	12.21	-49.60	36.60	6.52	12.50	-49.50	49.70	15679	30
706	-1.11	12.02	-46.70	36.50	6.27	12.23	-50.90	49.10	15679	30
722	-1.14	11.81	-44.00	34.90	5.99	11.83	-45.60	46.00	15679	30
738	-1.12	11.41	-41.70	36.60	5.72	11.48	-46.50	45.20	15679	30
754	-1.14	11.10	-41.70	37.80	5.47	11.10	-42.20	48.60	15679	30
770	-1.12	10.84	-43.70	38.10	5.17	10.76	-40.90	46.20	15679	30
786	-1.15	10.54	-42.50	39.10	4.94	10.50	-39.10	46.20	15679	30
802	-1.24	10.17	-39.10	34.70	4.76	10.20	-36.20	40.40	15679	30
818	-1.21	9.84	-35.90	33.80	4.55	9.94	-35.10	40.90	15679	30
834	-1.17	9.49	-38.70	32.40	4.27	9.72	-34.10	42.00	15679	30
850	-1.23	9.21	-36.60	30.30	3.93	9.41	-30.70	38.30	15679	30
866	-1.33	9.06	-33.70	30.00	3.65	9.15	-31.80	38.00	15679	30
882	-1.35	8.90	-34.90	29.00	3.35	8.94	-34.80	37.50	15679	30
898	-1.31	8.63	-34.00	31.70	3.08	8.67	-31.90	35.50	15679	30
914	-1.28	8.40	-32.60	29.10	2.90	8.43	-29.40	33.60	15679	30
930	-1.21	8.18	-31.20	28.00	2.72	8.18	-27.30	34.50	15679	30
946	-1.30	7.96	-30.40	27.20	2.44	7.96	-29.60	33.90	15679	30
962	-1.37	7.75	-31.30	26.60	2.18	7.79	-27.80	33.50	15679	30
978	-1.38	7.48	-28.10	27.90	1.86	7.58	-28.10	33.90	15679	30
994	-1.40	7.20	-27.90	27.00	1.59	7.41	-29.40	33.60	15679	30
1010	-1.38	6.83	-26.50	29.20	1.37	7.05	-23.40	30.50	15679	30
1026	-1.32	6.46	-25.20	23.90	1.05	6.67	-28.60	33.00	15679	30
1209	-1.41	5.58	-22.70	17.80	0.28	5.01	-19.80	19.60	31358	15
1465	-0.92	4.95	-20.20	15.90	-0.30	4.16	-15.80	15.80	31359	15
1751	-1.19	5.12	-15.60	15.90	-0.13	4.11	-13.90	16.80	31359	15
2259	-2.06	5.42	-19.20	15.30	0.02	4.82	-19.50	18.30	31360	15
2767	-2.18	5.43	-18.80	13.00	0.02	5.12	-21.50	17.90	31359	15
3288	-1.90	5.03	-20.80	15.70	-0.17	4.81	-16.70	18.40	31361	45

Table A- 21. Basic statistics for Mooring PE5 during Canek 23

depth	mean_u	std_u	min_u	max_u	mean_v	std_v	min_v	max_v	MMS # of obs	sample interval
59	11.71	33.70	-122.30	134.90	34.12	49.54	-96.10	178.60	18175	30
75	11.09	32.14	-107.50	133.40	32.17	45.91	-88.80	213.70	18175	30
91	10.41	30.03	-105.50	118.00	30.34	41.90	-84.60	218.70	18175	30
107	9.66	27.96	-109.80	106.60	28.48	38.35	-82.00	193.20	18175	30
123	8.89	26.23	-101.00	98.10	26.73	35.64	-80.60	214.00	18175	30
139	8.33	24.70	-112.70	88.70	25.11	33.50	-77.60	199.70	18175	30
155	7.77	23.53	-119.10	83.80	23.62	31.76	-75.10	224.10	18175	30
171	7.34	22.54	-113.30	75.80	22.28	30.29	-66.80	232.90	18175	30
187	7.31	21.77	-120.10	73.30	21.08	29.00	-60.40	224.90	18175	30
203	7.29	20.89	-136.70	66.60	20.07	28.04	-60.10	224.70	18175	30
219	7.19	20.10	-146.70	69.20	19.25	27.07	-56.20	224.10	18175	30
235	7.21	19.47	-120.40	68.10	18.50	26.12	-56.40	206.10	18175	30
251	7.09	18.98	-119.30	63.00	17.69	25.29	-54.00	222.00	18175	30
267	6.96	18.34	-109.80	58.70	16.98	24.60	-55.40	242.60	18175	30
283	6.82	17.71	-92.20	61.60	16.31	24.02	-56.00	236.60	18175	30
299	6.64	17.15	-94.10	59.20	15.86	23.34	-59.90	178.10	18175	30
315	6.31	16.73	-79.80	56.90	15.48	22.74	-51.60	170.30	18175	30
331	6.00	16.30	-68.60	54.50	15.06	22.14	-48.10	171.50	18175	30
347	5.71	15.77	-63.80	52.50	14.63	21.47	-49.60	172.60	18175	30
363	5.40	15.25	-63.60	55.00	14.23	20.85	-47.90	161.20	18175	30
379	5.04	14.80	-65.10	57.70	13.86	20.36	-43.90	102.00	18175	30
395	4.81	14.38	-63.30	59.40	13.38	19.88	-39.20	107.50	18175	30
402	5.62	14.71	-83.40	62.80	12.49	19.90	-37.50	253.60	18176	30
411	4.59	14.04	-64.80	58.50	12.90	19.39	-35.90	75.80	18175	30
418	5.40	14.34	-73.00	61.70	12.04	19.34	-34.10	252.70	18176	30
427	4.43	13.76	-64.40	55.80	12.47	18.94	-34.40	73.70	18175	30
434	5.11	13.94	-72.50	57.40	11.61	18.78	-40.10	227.60	18176	30
443	4.22	13.36	-64.70	52.90	12.06	18.43	-39.90	72.90	18175	30
450	4.86	13.61	-70.10	54.00	11.22	18.25	-38.60	211.40	18176	30
459	3.95	12.93	-64.60	51.00	11.41	17.78	-37.60	68.70	18175	30
466	4.66	13.29	-69.20	53.30	10.85	17.79	-35.70	164.00	18176	30
482	4.43	12.94	-65.90	53.90	10.46	17.33	-32.10	147.50	18176	30
498	4.28	12.66	-66.20	53.30	10.15	16.92	-29.40	145.80	18176	30
514	4.20	12.42	-63.00	51.60	9.81	16.54	-29.70	140.10	18176	30
530	3.97	12.16	-63.60	49.70	9.54	16.20	-29.30	151.90	18176	30
546	3.71	11.85	-64.30	48.90	9.29	15.85	-26.90	135.90	18176	30
562	3.48	11.55	-65.90	49.30	9.06	15.45	-25.70	129.20	18176	30

Table A-21. Basic statistics for Mooring PE5 during Canek 23 (continued)

depth	mean_u	std_u	min_u	max_u	mean_v	std_v	min_v	max_v	MMS # of obs	sample interval
578	3.29	11.30	-71.10	51.40	8.77	15.11	-27.80	123.00	18176	30
594	3.14	11.06	-58.90	50.60	8.47	14.73	-28.60	149.30	18176	30
610	2.93	10.81	-65.20	47.90	8.22	14.32	-26.10	139.70	18176	30
626	2.69	10.60	-59.10	46.50	8.03	13.96	-27.50	152.00	18176	30
642	2.50	10.32	-54.60	47.00	7.76	13.52	-24.60	117.50	18176	30
658	2.34	10.07	-52.40	44.20	7.53	13.12	-23.90	111.10	18176	30
674	2.19	9.80	-60.50	44.00	7.27	12.72	-24.90	139.30	18176	30
690	2.00	9.51	-58.10	40.50	7.07	12.28	-23.70	135.90	18176	30
706	1.71	9.24	-57.30	40.20	6.77	11.88	-23.70	111.80	18176	30
722	1.51	8.99	-41.80	38.20	6.50	11.49	-23.90	106.50	18176	30
738	1.38	8.71	-35.60	37.40	6.23	11.12	-23.70	99.10	18176	30
754	1.25	8.50	-33.60	36.70	5.93	10.80	-25.30	73.10	18176	30
770	1.09	8.33	-33.30	36.90	5.69	10.48	-24.60	72.10	18176	30
786	0.91	8.13	-28.60	35.90	5.43	10.18	-23.10	59.10	18176	30
802	0.80	7.94	-29.40	32.90	5.15	9.89	-22.80	47.20	18176	30
818	0.69	7.79	-30.70	32.60	4.85	9.62	-22.60	47.10	18176	30
834	0.59	7.63	-28.10	32.80	4.71	9.48	-19.70	45.60	18176	30
850	0.54	7.44	-26.70	32.10	4.58	9.26	-19.80	40.70	18176	30
866	0.43	7.31	-27.50	30.60	4.42	9.07	-20.60	44.20	18176	30
882	0.36	7.15	-26.20	28.20	4.15	8.74	-19.70	42.30	18176	30
898	0.32	6.82	-22.90	26.90	3.86	8.28	-20.70	39.50	18176	30
914	0.26	6.49	-24.00	25.90	3.62	7.83	-19.00	43.80	18176	30
930	0.14	6.01	-24.00	24.30	3.22	7.22	-17.70	49.40	18176	30
946	0.11	4.90	-21.60	23.30	2.50	6.08	-15.70	51.90	18176	30
1161	-0.52	5.07	-21.98	22.30	1.00	5.40	-16.31	34.96	9085	60
1416	-0.79	4.17	-13.82	15.21	-0.16	3.73	-12.67	13.34	9083	60
1772	-1.35	4.73	-16.69	11.97	-0.31	4.39	-14.25	16.25	9085	60
2279	-2.65	6.60	-21.70	16.50	-0.54	6.01	-19.90	19.10	36351	15
2835	-3.03	6.14	-19.25	15.49	-0.68	5.74	-25.33	17.22	9085	60
3446	-3.15	6.99	-29.40	21.80	-0.64	6.02	-27.50	18.50	36348	15

Table A- 22. Basic statistics for Mooring PEN during Canek 20

depth	mean_u	std_u	min_u	max_u	mean_v	std_v	min_v	max_v	MMS # of obs	sample interval
55	-33.14	44.20	-145.90	75.10	44.22	73.87	-90.10	211.40	15753	30
71	-30.39	41.50	-131.80	81.40	40.35	69.40	-80.20	197.60	15753	30
87	-27.46	38.74	-115.90	83.00	36.28	64.15	-83.10	176.60	15753	30
103	-24.42	36.06	-107.40	79.40	32.40	58.64	-89.20	157.60	15753	30
119	-21.70	33.54	-101.50	84.90	28.85	53.95	-92.40	139.80	15753	30
135	-19.35	31.23	-103.20	85.90	25.95	50.07	-94.70	141.80	15753	30
151	-17.34	29.34	-96.70	91.60	23.71	46.71	-94.10	133.50	15753	30
167	-15.73	27.75	-95.60	89.80	21.93	44.03	-97.70	133.10	15753	30
183	-14.52	26.24	-93.90	88.10	20.53	41.77	-99.70	130.30	15753	30
199	-13.48	24.85	-94.70	88.70	19.26	39.53	-97.10	119.00	15753	30
215	-12.49	23.48	-86.30	84.20	18.17	37.42	-84.10	109.30	15753	30
231	-11.62	22.23	-79.90	77.00	16.95	35.53	-75.80	100.90	15753	30
247	-10.82	21.25	-78.30	68.00	15.78	33.64	-72.20	100.80	15753	30
263	-10.06	20.35	-73.60	61.00	14.75	31.84	-72.10	101.30	15753	30
279	-9.23	19.46	-71.40	58.00	13.68	30.15	-73.00	100.50	15753	30
295	-8.40	18.43	-62.10	54.20	12.82	28.68	-75.00	90.40	15753	30
311	-7.50	17.46	-59.60	52.70	11.80	27.15	-78.40	84.70	15753	30
327	-6.56	16.59	-56.60	53.60	10.56	25.67	-76.00	86.50	15753	30
343	-5.69	15.80	-54.20	54.50	9.43	24.45	-65.60	75.40	15753	30
359	-4.87	15.09	-54.60	49.70	8.36	23.30	-67.40	72.80	15753	30
375	-4.15	14.44	-49.60	44.40	7.22	22.35	-59.00	71.50	15753	30
391	-3.45	13.76	-47.00	44.20	6.16	21.44	-54.80	72.40	15753	30
407	-2.66	13.33	-50.70	43.10	5.15	20.59	-50.80	77.00	15753	30
423	-1.83	13.21	-49.50	44.50	4.12	19.69	-51.80	71.80	15753	30
439	-0.96	13.17	-51.30	42.30	3.04	18.98	-51.00	68.60	15753	30
455	-0.10	13.00	-45.90	42.80	2.16	18.07	-46.80	67.30	15753	30
471	0.91	12.33	-50.70	40.30	1.12	16.43	-46.20	60.30	15753	30

Table A- 23. Basic statistics for Mooring PEN during Canek 23

depth	mean_u	std_u	min_u	max_u	mean_v	std_v	min_v	max_v	MMS # of obs	sample interval
52	-20.34	32.79	-109.10	39.80	6.75	53.23	-68.40	177.40	6066	30
68	-18.37	32.66	-96.40	41.50	7.09	52.37	-69.30	165.70	6066	30
84	-15.99	31.63	-99.40	41.00	6.47	50.23	-68.80	153.50	6066	30
100	-13.81	30.51	-91.10	48.70	5.80	48.00	-67.80	145.10	6066	30
116	-11.59	28.65	-83.00	56.20	4.91	45.46	-66.30	130.20	6066	30
132	-9.68	26.45	-79.60	54.50	3.92	42.56	-65.20	120.00	6066	30
148	-8.16	24.89	-75.00	47.60	2.98	39.85	-67.40	107.00	6066	30
164	-6.90	23.94	-67.30	49.40	2.43	38.02	-67.70	100.90	6066	30
180	-5.72	22.75	-58.80	47.70	2.10	36.33	-61.40	100.80	6066	30
196	-4.83	21.65	-55.90	47.40	1.64	34.45	-56.40	103.60	6066	30
212	-4.33	20.80	-54.30	49.00	1.18	32.67	-55.20	93.10	6066	30
228	-3.70	19.74	-53.80	52.70	1.04	31.09	-50.30	82.40	6066	30
244	-2.95	18.59	-58.10	52.50	1.09	29.80	-49.50	79.20	6066	30
260	-2.46	17.42	-53.80	52.60	0.97	28.71	-53.70	77.10	6066	30
276	-2.20	16.87	-52.50	54.30	0.88	27.63	-53.90	75.10	6066	30
292	-2.06	16.30	-49.80	52.20	0.90	26.75	-56.10	74.30	6066	30
308	-1.89	15.40	-51.50	49.80	0.84	26.21	-58.60	73.60	6066	30
324	-1.68	14.50	-56.50	46.20	0.62	25.43	-57.10	68.00	6066	30
340	-1.47	13.60	-47.50	40.70	0.34	24.34	-56.40	65.70	6066	30
356	-1.30	12.92	-46.10	34.30	0.04	23.70	-54.10	66.40	6066	30
372	-0.81	12.47	-38.30	33.20	-0.12	23.13	-51.30	66.70	6066	30
388	-0.33	12.20	-35.30	37.80	-0.45	22.69	-49.30	64.60	6066	30
404	0.19	11.98	-38.20	35.00	-0.97	22.40	-50.30	60.40	6066	30
420	0.74	11.83	-39.50	33.40	-1.66	22.01	-51.10	56.00	6066	30
436	1.53	11.82	-39.70	41.40	-2.66	21.52	-52.70	55.60	6066	30
452	2.67	11.99	-38.70	44.90	-3.61	20.50	-51.80	51.50	6066	30
468	4.04	11.71	-38.30	39.70	-4.35	18.39	-44.20	50.20	6066	30

Table A- 24. Basic statistics for Mooring PN1 during Canek 20

depth	mean_u	std_u	min_u	max_u	mean_v	std_v	min_v	max_v	MMS # obs	Sample interval
38	-0.08	38.72	-148.00	86.50	-2.72	25.81	-69.30	101.00	15280	30
46	0.29	38.04	-145.60	67.70	-3.10	25.42	-62.30	101.00	15280	30
54	1.39	37.58	-144.20	76.50	-3.57	25.12	-55.50	100.40	15280	30
62	3.04	37.18	-133.00	83.10	-3.76	24.85	-59.00	102.30	15280	30
70	5.13	36.68	-128.50	93.00	-3.54	24.34	-62.30	102.50	15280	30
78	7.25	35.47	-117.10	100.50	-3.60	23.92	-58.20	106.70	15280	30
86	9.20	32.90	-103.10	105.80	-3.93	23.44	-60.20	103.10	15280	30
94	10.53	29.35	-87.20	101.40	-4.03	22.67	-60.20	100.60	15280	30
102	10.93	25.34	-79.90	82.40	-3.39	21.34	-53.10	101.60	15280	30
110	10.68	21.36	-56.60	71.10	-2.29	19.46	-47.50	93.10	15280	30
124	6.63	13.93	-34.88	49.14	0.14	14.23	-30.81	51.52	3820	120

Table A- 25. Basic statistics for Mooring PN1 during Canek 23

depth	mean_u	std_u	min_u	max_u	mean_v	std_v	min_v	max_v	MMS # of obs	sample interval
14	-6.91	31.76	-168.38	75.17	4.05	27.61	-109.25	158.93	8905	60
22	-7.40	32.23	-134.83	70.90	3.01	28.05	-62.00	140.23	8905	60
30	-7.03	31.07	-129.30	63.75	2.02	27.12	-56.65	122.85	8905	60
38	-6.06	29.77	-124.63	59.43	1.31	26.27	-56.10	117.83	8905	60
46	-4.88	28.82	-120.78	62.43	0.75	25.29	-55.35	117.50	8905	60
54	-3.55	28.35	-120.65	66.00	0.18	24.25	-54.40	113.43	8905	60
62	-1.87	27.91	-119.45	70.63	-0.51	22.99	-50.45	104.80	8905	60
70	0.19	26.97	-112.50	66.85	-1.12	21.82	-51.35	88.95	8905	60
78	2.03	25.58	-99.90	62.53	-1.69	20.62	-49.55	86.33	8905	60
86	3.53	23.70	-91.33	61.83	-2.02	19.62	-48.45	87.48	8905	60
94	4.91	21.43	-87.70	59.73	-2.01	18.82	-49.08	82.33	8905	60
102	6.02	19.21	-82.23	53.30	-1.63	17.81	-48.23	76.53	8905	60
110	6.74	17.32	-69.43	55.45	-1.24	16.74	-42.88	71.40	8905	60
124	3.84	11.25	-31.04	38.10	0.38	11.91	-27.55	53.08	4652	120

Table A- 26. Basic statistics for Mooring PN2 during Canek 20

depth	mean_u	std_u	min_u	max_u	mean_v	std_v	min_v	max_v	MMS # of obs	sample interval
53	-24.10	51.31	-177.80	79.30	30.94	63.98	-111.20	190.20	15267	30
69	-24.21	51.00	-167.80	73.40	28.23	60.31	-107.70	178.00	15267	30
85	-22.57	48.81	-157.20	66.40	25.42	55.75	-98.90	156.30	15267	30
101	-20.66	46.14	-138.90	60.40	22.98	51.03	-86.30	141.90	15267	30
117	-18.75	43.20	-127.00	57.10	20.94	46.63	-73.50	132.90	15267	30
133	-16.67	40.19	-114.90	64.20	19.02	42.91	-75.60	128.50	15267	30
149	-14.58	37.58	-111.30	69.10	17.28	39.49	-62.30	123.90	15267	30
165	-12.90	35.59	-103.30	71.50	15.80	36.85	-56.50	108.60	15267	30
181	-11.24	33.72	-106.90	75.20	14.26	34.40	-55.50	100.50	15267	30
197	-9.57	31.53	-99.80	72.60	12.66	31.62	-50.50	96.00	15267	30
213	-8.12	29.61	-91.40	67.10	11.23	29.02	-47.70	90.30	15267	30
229	-6.79	28.28	-95.70	69.50	9.96	27.15	-42.90	90.10	15267	30
245	-5.66	27.61	-93.70	67.60	8.60	26.03	-42.20	85.70	15267	30
261	-4.53	26.89	-88.60	76.00	7.31	25.15	-45.20	84.80	15267	30
277	-3.18	25.77	-86.60	76.50	5.99	23.72	-48.30	84.80	15267	30
293	-1.76	24.73	-82.20	76.90	4.59	22.17	-48.40	81.40	15267	30
309	-0.41	23.83	-79.40	75.10	3.17	20.94	-48.50	75.80	15267	30
325	0.72	23.05	-78.00	71.20	1.93	19.96	-49.00	71.60	15267	30
341	1.79	22.45	-72.20	74.90	0.87	19.04	-46.20	67.60	15267	30
357	2.67	21.75	-62.90	75.30	-0.17	18.26	-47.10	62.70	15267	30
373	3.31	20.97	-60.70	74.20	-1.05	17.48	-50.60	60.50	15267	30
389	3.69	20.00	-60.20	77.70	-1.72	16.84	-50.20	62.90	15267	30
405	3.85	19.06	-61.50	76.80	-2.18	16.19	-49.90	63.00	15267	30
421	3.71	18.32	-60.30	70.40	-2.34	15.57	-49.40	56.30	15267	30
437	3.47	17.41	-58.90	72.20	-2.13	14.97	-51.20	47.80	15267	30
453	3.40	15.95	-55.30	70.20	-1.82	14.12	-48.50	46.10	15267	30
469	3.12	14.30	-45.80	71.00	-1.47	12.56	-46.60	39.10	15267	30

Table A- 27. Basic statistics for Mooring PN2 during Canek 23

depth	mean_u	std_u	min_u	max_u	mean_v	std_v	min_v	max_v	MMS # of obs	sample interval
48	-37.43	27.80	-126.30	37.00	25.00	43.91	-79.20	147.10	18614	30
64	-43.17	35.20	-150.10	49.90	31.67	57.53	-97.40	178.30	18614	30
80	-40.91	34.58	-142.00	49.20	28.95	54.77	-98.90	157.20	18614	30
96	-38.40	34.08	-130.90	45.00	26.91	51.61	-83.40	149.70	18614	30
112	-35.37	32.99	-119.90	44.50	25.42	48.27	-79.10	151.20	18614	30
128	-32.08	31.56	-111.10	38.10	24.06	44.91	-69.90	138.90	18614	30
144	-29.02	30.12	-107.60	37.30	22.68	41.74	-62.40	125.60	18614	30
160	-26.57	29.08	-108.70	38.60	21.31	38.81	-59.60	127.10	18614	30
176	-24.48	28.23	-97.60	39.60	20.10	36.46	-59.00	128.40	18614	30
192	-22.57	27.48	-99.10	37.20	19.18	34.69	-56.80	122.00	18614	30
208	-20.55	26.62	-97.30	38.30	18.30	33.13	-53.70	116.60	18614	30
224	-18.67	25.64	-91.90	39.80	17.18	31.48	-52.00	113.60	18614	30
240	-16.80	24.67	-93.60	41.00	15.99	29.71	-48.30	110.40	18614	30
256	-15.11	23.71	-93.10	42.30	14.94	28.13	-43.50	106.60	18614	30
272	-13.57	23.07	-96.60	40.50	13.94	26.93	-44.00	101.00	18614	30
288	-11.93	22.44	-92.00	41.80	12.87	25.63	-45.10	96.80	18614	30
304	-10.32	21.81	-92.10	41.00	11.47	24.04	-45.90	90.00	18614	30
320	-9.00	21.28	-92.30	46.00	10.01	22.56	-50.60	81.30	18614	30
336	-7.75	20.67	-82.40	43.70	8.75	21.34	-49.90	77.60	18614	30
352	-6.69	20.04	-73.50	45.90	7.57	20.31	-48.30	79.10	18614	30
368	-5.76	19.47	-66.30	47.80	6.40	19.58	-51.60	75.40	18614	30
384	-4.90	18.98	-59.50	50.70	5.38	19.05	-53.30	63.90	18614	30
400	-4.06	18.48	-60.90	49.60	4.27	18.60	-54.60	62.00	18614	30
416	-3.29	17.99	-57.90	47.90	3.31	18.04	-52.40	56.90	18614	30
432	-2.53	17.37	-60.40	50.30	2.45	17.53	-50.40	51.70	18614	30
448	-1.49	16.30	-50.10	52.10	1.69	16.81	-47.70	53.90	18614	30
464	-0.43	14.90	-46.10	48.90	1.06	15.46	-43.80	51.80	18614	30
480	0.44	13.12	-41.60	43.50	0.36	13.27	-38.70	49.60	18614	30

Table A- 28. Basic statistics for Mooring PN3 during Canek 20

depth	mean_u	std_u	min_u	max_u	mean_v	std_v	min_v	max_v	MMS # of obs	sample interval
51	-19.99	40.81	-157.80	87.00	34.54	63.69	-116.70	197.90	15243	30
67	-22.15	43.10	-144.80	87.20	39.40	68.35	-122.00	191.70	15243	30
83	-21.87	42.08	-144.60	70.00	37.71	65.43	-118.40	174.10	15243	30
99	-21.28	41.06	-140.20	57.50	35.78	62.10	-102.50	166.80	15243	30
115	-20.26	39.75	-132.80	56.70	33.81	58.43	-95.00	159.70	15243	30
131	-19.05	37.98	-126.00	61.00	31.84	54.87	-90.40	154.60	15243	30
147	-17.64	36.33	-119.50	60.20	30.02	51.68	-83.30	150.40	15243	30
163	-16.28	34.55	-112.80	50.00	28.56	49.02	-72.90	143.10	15243	30
179	-15.16	33.07	-105.90	53.60	27.40	46.74	-70.30	132.50	15243	30
195	-14.31	31.96	-99.40	53.20	26.27	44.98	-72.90	136.20	15243	30
211	-13.47	31.03	-100.00	60.70	25.21	43.12	-68.20	134.50	15243	30
227	-12.63	30.04	-92.70	60.70	24.22	41.47	-63.40	125.50	15243	30
243	-11.84	28.96	-86.40	64.80	23.13	39.93	-64.50	122.40	15243	30
259	-11.24	28.16	-83.90	66.10	22.10	38.50	-60.70	116.50	15243	30
275	-10.79	27.58	-82.40	65.00	21.30	37.15	-58.00	107.60	15243	30
291	-10.21	26.91	-77.40	64.90	20.43	35.81	-56.30	103.20	15243	30
307	-9.59	26.23	-74.40	63.70	19.42	34.47	-51.40	100.90	15243	30
323	-9.07	25.63	-71.50	64.80	18.50	33.25	-52.20	98.80	15243	30
339	-8.47	25.13	-72.80	62.30	17.69	32.03	-49.50	98.80	15243	30
355	-7.96	24.67	-72.70	63.90	16.81	30.86	-51.60	97.20	15243	30
371	-7.39	24.08	-68.00	61.60	15.95	29.81	-49.10	94.20	15243	30
387	-6.82	23.45	-62.10	63.10	15.13	28.74	-43.50	95.10	15243	30
403	-6.33	22.99	-60.60	55.70	14.42	27.75	-39.00	95.20	15243	30
419	-5.76	22.56	-61.40	53.50	13.67	26.88	-39.00	90.90	15243	30
435	-5.35	22.20	-62.30	56.90	12.92	26.07	-39.60	88.00	15243	30
451	-4.83	21.74	-61.20	55.30	12.22	25.17	-38.70	83.00	15243	30
467	-4.42	21.24	-62.10	54.00	11.49	24.26	-35.90	86.50	15243	30
483	-4.06	20.51	-61.50	49.00	10.59	23.06	-33.50	82.70	15243	30
994	2.63	8.08	-24.90	29.30	-1.15	5.86	-28.50	23.50	30482	15
1190	1.58	6.48	-25.70	21.50	-0.59	4.46	-18.10	20.20	30483	15

Table A- 29. Basic statistics for Mooring PN3 during Canek 23

depth	mean_u	std_u	min_u	max_u	mean_v	std_v	min_v	max_v	MMS # of obs	sample interval
45	-40.58	27.98	-145.30	138.70	28.34	53.07	-131.60	178.50	18613	30
61	-36.20	29.21	-122.50	48.80	23.52	53.22	-103.30	174.70	18613	30
77	-39.34	33.66	-145.90	55.10	30.19	62.52	-108.50	174.80	18613	30
93	-37.98	32.33	-132.30	45.50	28.64	58.81	-92.00	160.90	18613	30
109	-36.13	31.01	-128.70	44.70	27.30	54.98	-82.90	155.20	18613	30
125	-33.87	29.65	-123.20	39.10	26.12	51.49	-76.20	151.00	18613	30
141	-31.34	28.02	-119.30	37.50	24.68	47.87	-71.20	146.90	18613	30
157	-29.13	26.82	-112.20	33.30	23.54	44.70	-67.20	137.80	18613	30
173	-27.10	25.90	-111.50	37.10	22.50	41.87	-68.10	126.70	18613	30
189	-25.36	24.96	-104.40	35.00	21.76	39.79	-63.80	119.90	18613	30
205	-23.75	24.13	-99.90	35.00	20.88	37.81	-57.30	118.50	18613	30
221	-22.62	23.57	-99.60	38.40	20.13	36.12	-50.60	114.50	18613	30
237	-21.46	23.01	-96.50	39.30	19.42	34.65	-49.00	112.40	18613	30
253	-20.31	22.41	-93.00	36.10	18.80	33.43	-46.30	104.90	18613	30
269	-19.40	21.87	-90.40	37.10	18.27	32.40	-43.60	98.00	18613	30
285	-18.56	21.48	-85.00	36.50	17.87	31.40	-42.00	95.90	18613	30
301	-17.80	21.05	-82.30	36.70	17.40	30.38	-39.50	96.90	18613	30
317	-17.17	20.65	-83.40	42.30	16.92	29.38	-43.30	92.20	18613	30
333	-16.44	20.31	-77.80	44.70	16.43	28.52	-39.50	88.00	18613	30
349	-15.69	20.01	-73.40	46.60	15.97	27.68	-41.80	89.60	18613	30
365	-14.97	19.62	-70.70	45.90	15.49	26.95	-42.40	86.50	18613	30
381	-14.35	19.28	-70.20	48.30	15.02	26.18	-44.20	81.90	18613	30
397	-13.84	18.94	-66.00	46.90	14.57	25.39	-42.20	81.60	18613	30
413	-13.34	18.67	-65.00	48.10	14.24	24.70	-42.30	82.00	18613	30
429	-12.80	18.44	-65.30	48.20	13.93	24.16	-43.70	85.30	18613	30
445	-12.31	18.15	-62.00	46.50	13.60	23.67	-44.80	87.60	18613	30
461	-11.85	17.88	-59.40	41.80	13.24	23.12	-43.10	86.50	18613	30
477	-11.35	17.54	-56.30	38.70	12.87	22.51	-43.10	82.70	18613	30
493	-10.74	17.01	-52.80	40.70	12.41	21.80	-43.60	73.90	18613	30
995	1.93	7.08	-25.50	26.00	-0.85	5.51	-22.10	24.20	37217	15
1190	1.49	5.65	-23.40	18.56	-0.22	4.86	-20.86	18.31	18612	30

Table A- 30. Basic statistics for Mooring PN4 during Canek 20

depth	mean_u	std_u	min_u	max_u	mean_v	std_v	min_v	max_v	MMS # of obs	sample interval
94	-20.88	7.19	-44.50	-2.80	50.36	13.60	16.10	79.7	769	30
110	-20.93	6.94	-41.40	0.50	50.75	13.62	14.60	79.4	769	30
126	-20.56	8.39	-42.60	7.40	50.58	13.53	10.50	79.2	769	30
142	-20.09	10.25	-45.10	17.40	48.89	13.59	10.60	81	769	30
158	-19.71	10.03	-46.20	15.40	47.29	13.71	10.80	81.4	769	30
174	-20.02	9.70	-52.60	12.30	45.36	13.84	14.40	87.6	769	30
190	-18.58	9.21	-53.50	4.10	43.15	12.76	13.00	84.3	769	30
206	-16.96	8.26	-48.50	5.10	40.30	11.23	11.90	79.5	769	30
222	-16.94	8.48	-45.30	3.30	37.56	10.09	10.50	65.9	769	30
238	-16.74	8.20	-43.00	2.80	34.67	9.25	5.90	54.7	769	30
254	-15.49	8.00	-35.80	6.30	33.03	8.40	8.20	54.4	769	30
270	-14.58	7.93	-37.30	8.00	30.81	7.65	13.30	51.8	769	30
286	-13.58	7.73	-33.80	6.80	29.72	6.64	13.10	47.5	769	30
302	-13.47	7.52	-30.80	7.30	28.41	6.51	10.00	46.6	769	30
318	-13.44	7.43	-31.00	7.90	27.90	7.16	5.60	47.7	769	30
334	-13.25	7.41	-31.50	9.50	27.31	6.59	7.20	45.3	769	30
350	-12.81	6.81	-30.10	7.00	26.04	6.50	7.90	44.6	769	30
366	-12.37	6.55	-32.40	7.90	25.27	6.76	4.30	45.9	769	30
382	-12.40	6.31	-28.50	9.00	24.59	6.52	-1.60	43.4	769	30
398	-12.74	6.36	-30.00	4.60	24.29	6.46	-2.40	40	769	30
414	-12.21	5.81	-30.30	3.50	23.75	6.37	2.80	39	769	30
430	-11.75	5.71	-33.90	4.60	22.99	6.36	3.70	40.6	769	30
446	-11.68	5.52	-30.30	3.30	22.41	6.19	3.10	37	769	30
462	-11.62	5.63	-28.60	2.40	21.91	6.06	1.50	36.1	769	30
478	-11.57	5.83	-27.80	4.40	21.06	6.44	-2.40	38.2	769	30
494	-11.63	6.19	-27.80	6.50	20.51	6.58	-0.30	41	769	30
510	-11.55	6.25	-30.60	8.40	19.70	6.32	-3.60	38.7	769	30
517	-11.70	4.45	-51.40	34.50	11.14	19.30	-33.10	76.3	15187	30
533	-11.50	4.29	-51.60	32.50	10.91	18.96	-34.30	80.2	15187	30
549	-11.26	4.11	-50.00	33.70	10.69	18.64	-32.50	78.1	15187	30
565	-11.08	3.95	-45.30	32.70	10.50	18.27	-33.20	80	15187	30
581	-11.01	3.82	-45.80	34.70	10.23	17.89	-36.00	75.4	15187	30
597	-10.95	3.77	-49.50	37.00	9.96	17.49	-35.50	68.5	15187	30
613	-10.85	3.68	-46.20	35.90	9.79	17.14	-36.10	65.4	15187	30

Table A- 30. Basic statistics for Mooring PN4 during Canek 20 (continued)

depth	mean_u	std_u	min_u	max_u	mean_v	std_v	min_v	max_v	MMS # of obs	sample interval
629	-3.57	10.65	-39.60	34.60	9.61	16.82	-40.90	65.6	15187	30
645	-3.41	10.46	-37.30	32.40	9.40	16.47	-38.70	68.7	15187	30
661	-3.25	10.34	-37.20	35.60	9.12	16.00	-36.80	65.4	15187	30
677	-3.22	10.25	-34.40	36.60	8.83	15.60	-38.70	61.9	15187	30
693	-3.12	10.22	-36.10	38.30	8.60	15.19	-37.60	63.2	15187	30
709	-3.06	10.13	-35.40	39.80	8.37	14.90	-37.90	62.1	15187	30
725	-2.95	10.01	-33.40	36.50	8.20	14.57	-38.40	60.6	15187	30
741	-2.77	9.85	-36.80	36.70	7.95	14.27	-35.50	58.3	15187	30
757	-2.53	9.74	-35.10	36.90	7.70	13.87	-34.60	62.6	15187	30
773	-2.40	9.63	-39.30	33.10	7.40	13.41	-30.50	60.2	15187	30
789	-2.30	9.53	-37.00	35.00	7.16	12.96	-27.80	53.8	15187	30
805	-2.21	9.43	-33.50	34.20	6.97	12.57	-24.90	47.8	15187	30
821	-2.18	9.37	-31.70	34.80	6.70	12.24	-24.50	48.5	15187	30
837	-2.11	9.34	-28.70	34.20	6.38	11.96	-22.50	53.3	15187	30
853	-1.91	9.26	-29.00	38.90	6.08	11.67	-24.70	51.5	15187	30
869	-1.71	9.28	-29.40	38.20	5.72	11.35	-23.90	56	15187	30
885	-1.57	9.38	-36.40	39.50	5.39	11.01	-24.90	59	15187	30
901	-1.50	9.42	-38.30	36.30	4.98	10.64	-27.70	57.3	15187	30
917	-1.41	9.38	-35.00	34.80	4.58	10.23	-30.60	59.6	15187	30
933	-1.25	9.35	-36.30	36.20	4.15	9.78	-30.20	51.5	15187	30
949	-1.04	9.36	-34.10	35.90	3.78	9.37	-33.00	40.6	15187	30
965	-0.86	9.26	-30.60	37.40	3.45	8.94	-30.80	37.7	15187	30
981	-0.71	9.09	-31.10	39.30	3.12	8.47	-32.40	34.4	15187	30
997	-0.55	8.83	-32.80	39.70	2.89	7.96	-28.90	34.3	15187	30
1013	-0.39	8.69	-36.40	42.40	2.59	7.52	-28.70	30.4	15187	30
1215	0.72	10.35	-25.00	38.30	0.68	6.54	-21.40	20.5	30371	45
1470	1.81	10.79	-27.50	41.60	-0.10	5.76	-18.60	15.9	30373	45
1756	1.67	11.32	-28.80	43.50	-0.12	6.02	-21.10	16.9	30369	45
2262	1.57	11.52	-29.80	41.50	-0.25	6.46	-24.90	25.7	30370	45
2768	1.57	12.04	-30.00	39.10	0.37	6.67	-20.60	27.3	30371	45
3288	0.97	11.73	-31.90	38.50	1.29	6.13	-16.30	28	30371	45

Table A- 31. Basic statistics for Mooring PN4 during Canek 23

depth	mean_u	std_u	min_u	max_u	mean_v	std_v	min_v	max_v	MMS # of obs	sample interval
50	-20.02	41.39	-163.90	77.00	-6.34	46.66	-133.90	147.70	18620	30
66	-19.94	40.89	-158.30	80.10	-5.68	46.87	-135.70	142.70	18620	30
82	-19.99	39.70	-154.40	79.30	-5.04	45.79	-131.30	132.20	18620	30
98	-19.74	37.68	-151.80	80.80	-4.31	43.53	-121.20	116.60	18620	30
114	-19.11	34.97	-143.40	73.60	-3.55	40.91	-114.70	108.60	18620	30
130	-18.27	32.07	-159.60	63.60	-2.70	38.49	-113.80	100.80	18620	30
146	-17.34	29.80	-150.20	55.20	-2.09	36.32	-111.00	93.20	18620	30
162	-16.36	28.01	-146.30	53.40	-1.73	34.42	-107.30	95.90	18620	30
178	-15.35	26.46	-156.30	51.20	-1.61	32.87	-100.20	97.30	18620	30
194	-14.59	25.18	-163.70	50.40	-1.45	31.43	-97.20	94.90	18620	30
210	-13.97	24.02	-180.00	51.90	-1.37	30.13	-92.00	92.20	18620	30
226	-13.36	23.05	-161.50	54.30	-1.31	28.92	-87.20	88.40	18620	30
242	-12.77	22.15	-163.40	53.60	-1.33	27.84	-88.10	88.00	18620	30
258	-12.20	21.27	-166.70	51.30	-1.32	26.91	-86.40	83.00	18620	30
274	-11.68	20.55	-170.40	48.80	-1.24	26.06	-88.10	80.30	18620	30
290	-11.25	19.94	-167.80	45.70	-1.11	25.30	-83.30	78.70	18620	30
306	-10.92	19.32	-159.70	43.30	-0.95	24.48	-81.00	70.10	18620	30
322	-10.58	18.66	-159.90	39.50	-0.81	23.68	-76.90	71.00	18620	30
338	-10.28	17.90	-136.40	40.70	-0.70	22.99	-71.10	69.60	18620	30
354	-9.96	17.24	-116.10	40.60	-0.56	22.37	-66.30	69.90	18620	30
370	-9.66	16.76	-105.80	40.40	-0.45	21.74	-66.30	71.50	18620	30
386	-9.45	16.33	-109.60	38.40	-0.47	21.10	-66.00	68.00	18620	30
402	-9.24	15.91	-88.20	39.10	-0.47	20.51	-63.00	66.10	18620	30
418	-8.88	15.44	-56.70	38.00	-0.36	20.00	-63.30	66.70	18620	30
426	-7.41	16.08	-234.40	47.60	-0.32	19.78	-99.20	195.10	18620	30
434	-8.52	14.96	-55.00	36.70	-0.25	19.59	-61.10	64.50	18620	30
442	-7.08	15.40	-191.60	37.60	-0.39	18.97	-65.70	147.80	18620	30
450	-8.14	14.56	-55.30	34.70	-0.27	19.06	-60.90	61.20	18620	30
458	-6.80	14.85	-158.60	38.30	-0.49	18.34	-53.70	145.00	18620	30
466	-7.88	14.10	-54.00	33.50	-0.41	18.37	-57.60	60.10	18620	30
474	-6.54	14.44	-149.90	37.20	-0.53	17.85	-52.10	147.40	18620	30
482	-7.59	13.60	-54.70	34.30	-0.50	17.73	-53.30	56.40	18620	30
490	-6.32	14.08	-205.00	36.30	-0.55	17.39	-50.10	148.20	18620	30
498	-7.20	13.00	-52.50	33.80	-0.45	16.91	-51.80	57.40	18620	30
506	-6.13	13.72	-167.30	34.60	-0.57	17.00	-48.50	152.30	18620	30
522	-5.94	13.40	-162.50	34.50	-0.56	16.55	-47.70	140.30	18620	30
538	-5.65	13.01	-155.20	33.20	-0.64	16.05	-45.80	140.80	18620	30

Table A- 31. Basic statistics for Mooring PN4 during Canek 23 (continued)

depth	mean_u	std_u	min_u	max_u	mean_v	std_v	min_v	max_v	MMS # of obs	sample interval
554	-5.47	12.76	-148.80	31.20	-0.72	15.64	-43.60	145.80	18620	30
570	-5.31	12.48	-154.70	30.30	-0.77	15.18	-42.40	112.40	18620	30
586	-5.04	12.19	-160.80	29.20	-0.82	14.73	-46.90	107.60	18620	30
602	-4.82	11.96	-139.50	26.10	-0.86	14.33	-39.80	105.70	18620	30
618	-4.66	11.69	-125.30	28.40	-0.89	13.98	-37.80	98.20	18620	30
634	-4.50	11.46	-117.90	29.90	-0.92	13.67	-37.50	105.80	18620	30
650	-4.27	11.19	-128.20	30.00	-0.96	13.29	-36.80	81.90	18620	30
666	-4.10	11.00	-130.80	28.50	-1.03	12.96	-37.10	82.60	18620	30
682	-3.95	10.86	-99.70	30.00	-1.17	12.65	-37.20	92.30	18620	30
698	-3.76	10.71	-108.10	32.10	-1.29	12.41	-39.30	85.20	18620	30
714	-3.57	10.55	-101.50	31.90	-1.38	12.14	-37.00	76.30	18620	30
730	-3.38	10.36	-87.50	31.90	-1.44	11.86	-34.90	54.80	18620	30
746	-3.22	10.21	-90.10	31.30	-1.48	11.57	-33.60	45.50	18620	30
762	-3.06	10.03	-76.60	30.60	-1.58	11.32	-33.40	57.40	18620	30
778	-2.91	9.84	-89.70	33.30	-1.70	11.13	-35.30	57.00	18620	30
794	-2.70	9.63	-86.80	31.80	-1.77	10.94	-33.50	70.10	18620	30
810	-2.53	9.46	-87.50	31.30	-1.81	10.76	-33.20	70.70	18620	30
826	-2.32	9.38	-64.20	32.70	-1.86	10.57	-34.20	73.80	18620	30
842	-2.14	9.29	-72.90	33.50	-1.92	10.45	-35.80	81.00	18620	30
858	-1.95	9.21	-61.00	34.20	-1.98	10.34	-39.90	76.30	18620	30
874	-1.77	9.12	-52.50	34.10	-2.08	10.10	-39.90	64.00	18620	30
890	-1.57	8.97	-40.40	36.40	-2.15	9.91	-39.50	70.20	18620	30
906	-1.37	8.91	-32.70	36.10	-2.20	9.74	-40.30	61.60	18620	30
922	-1.15	8.84	-35.00	35.00	-2.32	9.62	-41.30	54.80	18620	30
938	-0.97	8.75	-40.70	34.30	-2.34	9.42	-43.00	41.60	18620	30
954	-0.81	8.62	-31.40	37.30	-2.35	9.19	-40.50	28.80	18620	30
970	-0.64	8.44	-33.30	34.60	-2.32	8.97	-42.10	26.30	18620	30
986	-0.46	8.07	-24.40	34.90	-2.35	8.55	-40.30	24.00	18620	30
1002	-2.47	16.75	-51.90	55.30	2.08	15.05	-45.20	51.50	18620	30
1218	1.50	9.00	-23.50	37.60	-2.83	7.75	-30.60	18.80	33313	45
1473	1.52	7.60	-18.39	36.17	-2.61	6.80	-30.98	15.17	9307	60
1758	1.90	9.33	-24.90	39.60	-3.10	7.36	-30.00	19.20	37236	45
2284	1.13	8.77	-23.58	33.25	-3.51	7.78	-28.93	19.96	18619	30
2811	1.13	7.95	-21.22	32.25	-2.77	6.88	-22.28	17.96	9301	60
3340	1.38	10.02	-31.70	38.40	-2.66	6.98	-25.70	22.70	37237	45

The Department of the Interior Mission

As the Nation's principal conservation agency, the Department of the Interior has responsibility for most of our nationally owned public lands and natural resources. This includes fostering the sound use of our land and water resources; protecting our fish, wildlife, and biological diversity; preserving the environmental and cultural values of our national parks and historical places; and providing for the enjoyment of life through outdoor recreation. The Department assesses our energy and mineral resources and works to ensure that their development is in the best interests of all our people by encouraging stewardship and citizen participation in their care. The Department also has a major responsibility for American Indian reservation communities and for people who live in island communities.

The Bureau of Ocean Energy Management Mission

The Bureau of Ocean Energy Management (BOEM) works to manage the exploration and development of the nation's offshore resources in a way that appropriately balances economic development, energy independence, and environmental protection through oil and gas leases, renewable energy development and environmental reviews and studies.